The Analysis of Homologous Recombination Pathways in *Saccharomyces Cerevisiae*

Ye Dee TAY

A thesis submitted to the University of Oxford for the degree of Doctor of Philosophy in Medical Oncology



Wolfson College
University of Oxford

March 2010

Abstract

Ye Dee Tay
Wolfson College

Submitted for D.Phil.
Hilary term 2010

The Analysis of Homologous Recombination Pathways in *Saccharomyces Cerevisiae*

Homologous recombination (HR) is essential for the repair of DNA double-strand breaks (DSBs) and damaged replication forks. However, HR can also cause gross chromosomal rearrangements (GCRs) by producing crossovers (COs), resulting in the reciprocal exchange of sequences between non-sister chromatids. Therefore, HR-mediated GCRs are suppressed via the promotion of HR pathways that favour noncrossover (NCO) formation, such as the synthesis-dependent strand annealing (SDSA) and dissolution pathways, which are modulated by Mph1 and Sgs1 helicases, respectively. The mismatch repair (MMR) pathway is intricately associated with HR via its roles in repairing mismatches on heteroduplex DNA that can arise during HR and in preventing homeologous recombination. Using a plasmid break-repair assay, we have revealed a novel, MMR-independent role of MutSα in promoting the formation of a subset of COs that is specifically supressible by Mph1, during HR between two completely homologous sequences. In contrast, the MMR-dependent function of MutSα, together with Mph1 and Sgs1, was shown to be required for the suppression of CO formation during homeologous recombination. These data indicate that Mph1 can both antagonise and promote the functions of MutSα during DSB repair, depending on the levels of homology between the two recombining sequences.

COs are generated by the resolution of Holliday junction (HJ) intermediates formed at the terminal stages of HR. Several *S.cerevisiae* proteins such as Yen1, Mus81, Slx1 and Rad1 have been implicated in HJ resolution. However, the *in vivo* roles of these proteins in HJ resolution remain to be confirmed. To directly and quantitatively monitor *in vivo* HJ resolution in *S.cerevisiae*, a transformation-based HJ resolution assay using a plasmid-borne HJ substrate has been developed. Using this system, we have demonstrated an *in vivo* HJ resolution function of Yen1, which acts redundantly with Mus81. Moreover, these redundant activities of Yen1 and Mus81 are essential for survival during replication stress, but are dispensable for DSB repair. An Slx4 and Rad1-dependent *in vivo* HJ resolution activity was also observed in the absence of Yen1 and Mus81 that was suppressed by presence of Slx1. Models describing how the nucleases interact to process HJs *in vivo* will be discussed.

Acknowledgements

Time flies. I can hardly believe that I am indeed on the verge of completing my four-year D.Phil. study. But one thing that I do believe is that my D.Phil. study could not be completed without the help and support of many of my colleagues.

First and foremost, I would like to express my profound gratitude to Dr Leonard Wu, without whom I would not have the opportunity to study in this prestigious university. Leonard has been a perfect supervisor, not only for his patient guidance, valuable ideas and criticisms on my research and presentation skills, but also for his endless support and encouragement, particularly during my preparations for this thesis. Also, I would also like to thank Leonard for his great efforts in publishing our findings in quick succession in the past few months. It is with great regret to know that Leonard has decided to pursue a career outside of academia. But I sincerely wish him a smooth career transition and all the best in the future career.

I am also very grateful to Julie Sidebotham, for her great organization of the laboratory as well as her work on setting up the plasmid gap repair assay and initiating the pilot study on Mph1. I am indebted to my colleagues, Gusia, Jacqueline and Mika, who have provided much technical support and useful discussions on my projects, as well as tips on how to live through a postdoctoral career.

All members of Ian Hickson's and Peter McHugh's groups have also provided many helpful discussions and technical assistance over the years. Special thanks are due to Dr Katsuhiro Hanada who has given lots of inspiration and criticisms on the Holliday Junction projects, and Thomas Ashton, who provided me the first *mph1Δ sgs1Δ* double mutant strain. I am also grateful to the ladies in the kitchen, who provided labware and growth medium in excellent condition. I would also like to thank Cancer Research UK and Clarendon Scholarship for their financial support throughout my entire D.Phil. study.

Last but not least, I owe my deepest gratitude to my family: to my fiancée, Karen, who supported me throughout my D.Phil. and took care of all the house work while tolerating my boring lifestyle during thesis-writing; to my parents, for their endless encouragement and support, and for not urging me to go back to Malaysia, yet; and to my brother and sister, who support me and my family tirelessly.

Abbreviations

AIR	P-ribosylaminoimidazole
ARS	Autonomous replication sequence
ATP	Adenosine-5'-triphosphate
BIR	Break-induced replication
BER	Base Excision Repair
bp	base pair
BRCT	BRCA1(breast cancer 1 early onset) C-terminus
CAIR	P-ribosylaminoimidazole carboxylate
CCD	Conserved C-terminal domain
ChIP	Chromatin immuno-precipitation
CO	Crossover
CORE	Counterselectable reporter
CPT	Camptothecin
D-loop	Displacement-loop
dHJ	double HJ
DNA	Deoxyribonucleic acid
DSB	Double strand break
DSBR	Double-strand break repair
dsDNA	Double-stranded DNA
DTT	Dithiothreitol
ECL	Enhanced chemiluminescence
EDTA	ethylenediaminetetraacetic acid
FA	Fanconi Anaemia
FRET	Fluorescence resonance energy transfer
GC	Gene conversion
GCR	Gross chromosomal rearrangement
Gy	Gray
HhH	Helix-turn-helix domain
HJ	Holliday junction
HR	Homologous ecombination
HRP	Hourse radish peroxidase
HU	Hydroxyurea
ICL	Interstrand cross-link
IDL	Insertion/deletion loop
IP	Immunoprecipitation
IPTG	Isopropyl β- D-1-thiogalactopyranoside
IR	Ionizing radiation
IRO	Integrative recombinant oligonucleotides
JM	Joint molecule
kDA	kilo Dalton
KO	Knock-out
LB	Luria-Bertani
LOH	Loss of heterozygosity
MLR	MUS312/MEI interaction-like region
MMR	Mismatch repair
MMS	Methylmethane sulphonate

MRX	Mre11-Rad50-Xrs2
MS	Mass Spectrometry
MutSα	Msh2 and Msh6
MutSβ	Msh2 and Msh3
NER	Nucleotide excision repair
NHEJ	Non-homologous end-joining
NCO	Non-crossover
PBS	Phosphate buffered saline
PCNA	Proliferating-cell nuclear antigen
PCR	Polymerase chain reaction
PHD	Plant homeo-domain
PMS	Post-meiotic segregation
rDNA	Ribosomal DNA
RPA	Replication protein A
SAP	SAF-AB, Acinus and PIAS
SCE	Sister chromatid exchange
SD	Synthetic defined
SDS	Sodium dodecyl sulfate
SDSA	Synthesis-dependent strand annealing
SOC	Super Optimal broth with Catabolite repression
SSA	Single-strand annealing
ssDNA	single-stranded DNA
SUMO	Small ubiquitin-related modifier
TAE	Tris/Acetate/EDTA
TE	Tris/EDTA
Tris	tris(hydroxymethyl)aminomethane
UBZ4	ubiquitin-binding motif
UV	Ultra-violet
WCE	Whole cell extract
YPD	Yeast extract-peptone-dextrose
ZMM	Zip1-4, Mer3, Msh4 and Msh5

Table of Contents

Acknowledgements **3**
Abbreviations **4**

Chapter One
1. Introduction **11**
1.1. Homologous Recombination Pathways 12
1.1.1. Double Strand Break Repair (DSBR) 12
1.1.2. Synthesis-dependent Strand Annealing (SDSA) 15
1.1.3. Single-strand Annealing (SSA) 17
1.1.4. Break-Induced Replication (BIR) 18

1.2. DNA End Resection 20

1.3. Strand Invasion and Second-end Capture 22
1.3.1. Regulation of Rad51-mediated strand invasion 23
1.3.1.1. Srs2 (Suppressor of Rad Six) 25
1.3.1.2. Sgs1 (Slow Growth Suppressor of *top3Δ*) 27
1.3.1.3. Mph1 (Mutator Phenotype) 28

1.4. HJ Processing 29
1.4.1. The structure of a HJ 31
1.4.2. HJ Branch Migration 33
1.4.3. HJ Resolution in Prokaryotes, Bacteriophages and Archaea 34
1.4.4. HJ Resolution in Eukaryotes 37
1.4.4.1. Resolvase A (RAD51C-XRCC3 & Yen1/GEN1) 38
1.4.4.2. Mus81-Mms4/Eme1 Complex 41
1.4.4.3. Slx1-Slx4 Complex 46
1.4.4.4. Rad1-Rad10 Complex 49
1.4.4.5. Double Holliday Junction Dissolution 51

1.5. The Regulation of CO Formation 53

1.6. The Role of HR in Replication Fork Management 55

1.7. Mismatch Repair (MMR) Pathway 59
1.7.1. MMR proteins 59
1.7.2. The roles of MMR in HR 62
1.7.2.1. Mismatch correction of heteroduplex DNA 62
1.7.2.2. Suppression of recombination between divergent sequences 63
1.7.2.3. The removal of 3' non-homologous tail during DSB 65
1.7.2.4. Meiosis-specific Role of MMR 65

1.8. Aims of Study 66

Chapter Two
2. Materials and Methods **69**
2.1. Materials 70

2.1.1. *Escherichia coli* strains 70
2.1.2. *Saccharomyces cerevisiae* strains 70
2.1.3. Plasmids 71
2.1.4. Oligonucleotides 71
2.1.5. RusA purified proteins 71
2.1.6. Antibody....71

2.2. Methods....74
2.2.1. Bacterial assays 74
2.2.1.1. *E.coli* transformation....74
2.2.1.1.1. Chemically competent cells (Preparation)....74
2.2.1.1.2. Transformation for chemically competent cells 74
2.2.1.1.3. Electrically competent cells (Preparation)....75
2.2.1.1.4. Electroporation 75
2.2.1.2. Small-scale isolation of plasmid DNA (Miniprep) 76
2.2.1.3. Large-scale isolation of plasmid (Maxi- & Gigaprep)....76
2.2.1.4. Cloning of pADE2(400/400) & pADE2(1bp/mis)....76
2.2.1.5. Cloning of P1 & P2 77
2.2.1.6. Cloning of JM 77

2.2.2. Yeast assays 79
2.2.2.1. *S.cerevisiae* transformation 79
2.2.2.2. *Delitto perfetto*: site-directed mutagenesis....79
2.2.2.3. Gene knock-out in *S.cerevisiae*....80
2.2.2.4. *S.cerevisiae* genomic DNA extraction 81
2.2.2.5. Plasmid Break Repair Assay 81

2.2.3. Biochemistry....82
2.2.3.1.Restriction endonuclease reaction....82
2.2.3.2.Annealing and ligation 82
2.2.3.3.Holliday junction cleavage assay 83
2.2.3.4.Caesium Chloride density gradient centrifugation....83
2.2.3.5.DNA gel purification....84
2.2.3.6.Polymerase Chain Reaction (PCR) 84
2.2.3.7.Southern blotting and hybridisation 85
2.2.3.8.Western blotting 85
2.2.3.9.DNA sequencing 86
2.2.3.10.Immunoprecipitation 86

2.2.4. Statistics....86

Chapter Three
3. Mph1 requires mismatch repair-independent and -dependent functions of MutSα to regulate crossover formation during homologous recombination repair..... 88
3.1. Introduction 89

3.2. Results..... 90
3.2.1. Validation of a Plasmid Break Repair Assay to study DSBR..... 90

3.2.2. Mph1, but not Sgs1, specifically suppresses a subset of crossovers that are generated in a MutSα-dependent manner 94
3.2.3. The MutSα-dependent suppression of crossovers by Mph1 does not require the mismatch recognition function of MutSα. 98
3.2.4. Analysis of a potential interaction between Mph1 and MutSα 99
3.2.5. Modification of pADE2(400/400) to analyse homeologous recombination 100
3.2.6. Mph1 acts redundantly with Sgs1 to effect MutSα-dependent suppression of crossovers during homeologous recombination 104
3.2.7. *mph1Δ sgs1Δ* cells are proficient for gene conversion during homeologous recombination 106
3.2.8. Non-crossover products that arise during homeologous recombination are processed differently in the absence of both Mph1 and Sgs1 110

3.3. Discussion 114

Chapter Four

4. Development of a system for the analysis of *in vivo* Holliday Junction resolution in *Saccharomyces cerevisiae* 123

4.1. Introduction 124

4.2. Results 126
4.2.1. Development of a system for the analysis of *in vivo* HJ resolution in *S.cerevisiae* 126
4.2.2. The design of the HJ-containing plasmid substrate, X-JM 128
4.2.3. Construction of X-JM 131
4.2.4. Confirmation of X-JM substrate 135
4.2.5. *In vivo* HJ resolution of X-JM in *S.cerevisiae* 141
4.2.6. Physical Analysis of X-JM Resolution Products 144
4.2.7. P1-P2 dimer was generated by resolution of HJ in X-JM rather than inter-plasmid recombination 147
4.2.8. Sequence Analysis of X-JM Resolution Products 150

4.3. Discussion 153

Chapter Five

5. The analysis of putative Holliday Junction Resolvases in *Saccharomyces cerevisiae* 155

5.1. Introduction 156

5.2. Results 157
5.2.1. Exploitation of XerC/D site-specific recombination to generate a synthetic HJ for introduction into *S.cerevisiae* 157
5.2.2. Induction of JM-HJ 161
5.2.3. Purification of JM-HJ 162
5.2.4. Verification of the Structure of JM-HJ Molecules 164
5.2.5. JM-HJ is Resolved by Bacterial HJ Resolvase, RusA 168
5.2.6. *In vivo* Resolution of HJ on JM-HJ 170

5.2.7. Analysis of JM-HJ resolution products.....174
5.2.8. Analysis of the ability of putative HJ resolvase mutants to resolve JM-HJ *in vivo* 176
5.2.9. Yen1 and Mus81 are required for replication fork restart..... 181
5.2.10. Analysis of Yen1 and Mus81-independent HJ Resolution Activity... 184

5.3. Discussion 187

6. General Discussion 195

7. Bibliography 206

8. Appendix 228

9. Publications.....232

Chapter One

1. Introduction

1. Introduction

The maintenance of genomic integrity is vital for the survival and propagation of genetic information of an organism as they are constantly challenged by genotoxic stresses from both endogenous and exogenous sources. DNA double-strand breaks (DSBs), in which both DNA strands are broken, is regarded as one of the most harmful among all DNA lesions because a single unrepaired DSB is sufficient to cause cell death (Rich et al., 2000). Failure to repair a DSB may result in genomic instability via chromosomal rearrangements, including deletions, inversions or translocations, which in turn can promote carcinogenesis. DSBs can be induced endogenously during DNA synthesis when replication forks encounter a damaged DNA template. They can also be generated by exogenous genotoxic challenges such as ionizing radiation (IR), Ultraviolet (UV) rays, topoisomerase poisons or other radiomimetic drugs. In addition to these "accidental" DSBs, programmed DSBs are also generated by eukaryotic cells by the expression of specific endonucleases. For instance, a single DSB is generated by the HO endonuclease for mating-type switching in yeast (Paques and Haber, 1999) or by Spo11 for the initiation of meiotic recombination which is essential for gene "reshuffling" and proper segregation of chromosomes during meiotic I division (Keeney, 2001). In vertebrates, programmed DSBs are also generated for the production of the diverse repertoire of molecules of the immune system via V(D)J recombination and class-switch recombination (Soulas-Sprauel et al., 2007). Two major pathways have evolved to repair DSBs: non-homologous end-joining (NHEJ) and homologous recombination (HR). NHEJ restores continuity to broken DNA by directly joining the two ends of DSBs largely independently of homology. NHEJ

mediates either accurate or error-prone repair depending on the sequence and any chemical modifications present at the ends of DSBs (Lieber et al., 2003). In contrast, HR is generally regarded as an error-free repair pathway as it involves the "copying" of sequences from a homologous template which is usually the sister chromatid, to repair the DSB while preventing the loss of genetic information.

1.1. Homologous Recombination Pathways

Several models have been proposed to explain the molecular mechanisms of HR-mediated DSB repair pathways, which are thought to be executed under different circumstances. These pathways will be introduced below:

1.1.1. Double Strand Break Repair (DSBR)

In 1983, Szostak and coworkers proposed a model to describe how recombination could mediate DSB repair (Szostak et al., 1983) (Figure 1.1 (i)). This model was formulated based on an earlier conception by Holliday and by Meselson and Radding (Holliday, 1964; Meselson and Radding, 1975). The experimental support for Szostak's model came initially from studies on plasmid-chromosome recombination in yeast, which established the recombinogenic nature of DSBs and demonstrated the occurrence of gene conversion (GC) during DSB repair (Orr-Weaver and Szostak, 1983; Orr-Weaver et al., 1981, 1983). Szostak's model suggested that recombination is initiated by the introduction of a DSB into the recipient chromatid by an endonuclease (Szostak et al., 1983). Both ends of the DSB are resected by exonucleases to form 3' single-stranded DNA. Invasion of one

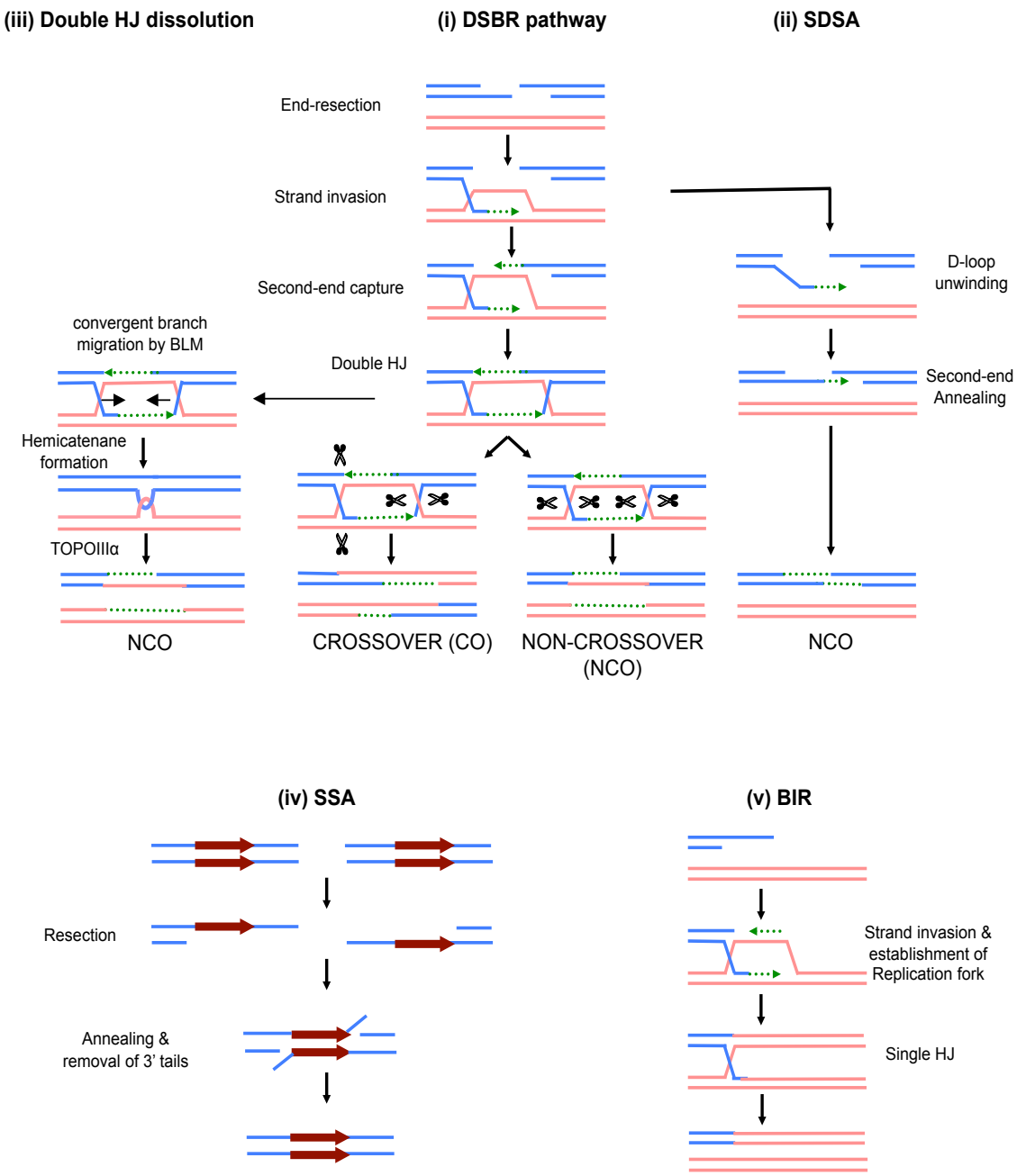

(iii) Double HJ dissolution
(i) DSBR pathway
(ii) SDSA
End-resection
Strand invasion
Second-end capture
Double HJ
convergent branch migration by BLM
Hemicatenane formation
TOPOIIIα
NCO
CROSSOVER (CO)
NON-CROSSOVER (NCO)
D-loop unwinding
Second-end Annealing
NCO
(iv) SSA
Resection
Annealing & removal of 3' tails
(v) BIR
Strand invasion & establishment of Replication fork
Single HJ

Figure 1.1. Homologous Recombination pathways. (i) Double Strand Break Repair (DSBR) pathway. DSB is processed to form 3' single-stranded ends, which in turn invade into a homologous template to prime DNA synthesis. Upon second-end capture, a double Holliday Junction (dHJ) is formed. The two HJs of a dHJ can either be resolved in opposite orientations to form crossovers (COs), or in the same orientation to form non-crossovers (NCOs). (ii) SDSA pathway. Invading 3' ssDNA can be dissociated from the template after DNA synthesis. Annealing and religation to the other end of the DSB produce exclusively NCO products. (iii) Double HJ (dHJ) dissolution pathway. A dHJ is collapsed into a hemicatenane via convergent branch migration catalysed by the BLM helicase, followed by TOPOIIIα-mediated strand passage activity to "dissolve" the hemicatenane. NCO products are generated exclusively. (iv) SSA pathway. If DSB is flanked by direct repeats, repair can be carried out by the annealing of the two single-stranded repeats once resection has proceeded past the repeat sequences. (iv) BIR pathway. If only one DSB is available, the processed DSB can invade into a homologous template and establish a replication fork. The lost sequences on the other DSB end will thus be replaced by complete replication of the homologous sequences. (DNA synthesis is indicated by dotted green line).

of the ends into a homologous duplex, forms a D-loop that can be extended by DNA synthesis. In a process known as "second-end capture", the extended D-loop anneals to complementary single-stranded sequences at the other end of the DSB. Subsequent gap filling and ligation result in the formation of two Holliday Junctions (HJs), physically linking the two DNA duplexes. These dHJ intermediates can be resolved in different orientations to form either crossovers (COs), in which the sequences flanking the HJ are exchanged, or non-crossovers (NCOs), in which the flanking sequences remain the same. If the heteroduplex DNA formed during strand invasion contains a mismatch, repair of the mismatch can result in GC on both CO and NCO products.

1.1.2. Synthesis-dependent Strand Annealing (SDSA)

Szostak's DSBR model proposed 50% of the recombination products should be COs assuming that HJ resolution orientation is unbiased. However, many mitotic recombination events are frequently not associated with a CO event. To explain this, a modified version of Szostak's recombination model was proposed based on the studies of homothallic switching of yeast mating type in *S.cerevisiae* (Hastings, 1988; McGill et al., 1989; Nasmyth, 1982; Thaler and Stahl, 1988). The main feature of this modified model is that, instead of forming dHJs, the newly synthesized DNA strand is displaced from the homologous template and then anneals to the other end of the DSB thereby restoring continuity of the DNA duplex (Figure 1.1 (ii)). This model was first named Synthesis-dependent strand annealing (SDSA) by Nassif et al. (Nassif et al. 1994). The SDSA model of recombination is consistent with results obtained from other organisms such as *Drosophila* (Engels et

al., 1990; Gloor et al., 1991; Nassif et al., 1994), mammals (Belmaaza et al., 1994), *Ustaligo* (Ferguson and Holloman, 1996) and *E.coli* (Kreuzer et al., 1995).

The SDSA model was proposed to explain several observations that are not consistent with the model proposed by Szostak et al. (Szostak et al., 1983). Firstly, the Szostak model predicts the formation of two heteroduplex regions and that these should segregate to different chromatids (Figure 1.1). However, using alleles that form heteroduplex DNA that is poorly corrected by mismatch repair (MMR) in *S.cerevisiae*, two independent studies showed that both heteroduplex regions are retained on the same chromatid (Gilbertson and Stahl, 1996; Porter et al., 1993). Secondly, in both mitotic (Nelson et al., 1996) and meiotic (Gilbertson and Stahl, 1996; Porter et al., 1993) cells, DSB-induced GCs were found to be unidirectional. These results are consistent with the SDSA model in which only one 3' end of the DSB necessarily forms a D-loop to initiate DNA synthesis, thus resulting in GC on only one side of the DSB. Thirdly, two independent groups demonstrated that GC could occur using two templates located at two different loci (Paques et al., 1998; Silberman and Kupiec, 1994). These results support the SDSA model in that the only way for these repair events to occur is by unwinding the newly synthesized DNA from the two templates on different loci before returning to the donor molecule. More recently, it was discovered that NCOs are formed at least 30 minutes earlier than COs during meiotic DSB repair, suggesting that NCOs and COs are generated by different pathways (Allers and Lichten, 2001). This notion is reinforced in *ndt80Δ* mutant cells. Ndt80 is a meiosis-specific transcription factor essential for the completion of meiosis I prophase (Chu et al., 1998). In the absence of *Ndt80*, high levels of branched DNA structures correlate with the suppression of COs whereas NCOs are formed with normal timing and levels (Allers and Lichten,

2001). These observations indicate that COs are predominantly derived from the branched DNA structures while NCOs arise in a different pathway, independently of these branched recombination intermediates. Hence, these data support the SDSA model as the main pathway of generating NCO products, whereas COs are formed by HJ resolution.

1.1.3. Single-strand Annealing (SSA)

When a DSB occurs between direct repeats, a form of DSB repair known as SSA can arise, which results in deletion of one copy of the two repeats and any intervening sequences (Elliott et al., 2005; Liang et al., 1998; Paques and Haber, 1999) (Figure 1.1 (iv)). This repair model was first suggested by Lin and coworkers for mammalian DNA repair (Lin et al., 1984). In SSA, the repair begins with resection of the ends of the DSB by exonucleases to generate a long single-stranded stretch of DNA. If resection proceeds past the repeat sequences the complementary strands of the repeated sequences can anneal. Finally, any 3' ssDNA ends that are nonhomologous are removed by nucleolytic cleavage followed by new DNA synthesis to fill the gap and ligation to restore the two continuous strands. The Rad1-Rad10 heterodimeric endonuclease and the Msh2-Msh3 mismatch recognition complex are essential for the cleavage of 3' single-stranded non-homologous tails on either side of the annealed regions (Bardwell et al., 1994; Fishman-Lobell et al., 1992; Ivanov and Haber, 1995; Sugawara et al., 1997).

In yeast, the efficiency of SSA is nearly 100% when the repeat sequences flanking the DSB are at least 400bp long (Sugawara and Haber, 1992). Repair is also efficient even if the repeats are separated by as much as 15kb (Paques and

Haber, 1999). Recent studies suggested that SSA not only results in deletion between flanking repeats, but also contributes to inverted repeat recombination, gene targeting, chromosomal translocation and fusions (VanHulle et al., 2007; Wang and Baumann, 2008). SSA is likely to play a more significant role in the repair of genomes in higher eukaryotes, which contain significant amounts of repetitive DNA.

1.1.4. Break-Induced Replication (BIR)

BIR is thought to occur when only one end of the DSB is available (Figure 1.1 (v)). The BIR model involves the invasion of the donor template by a single DSB end, followed by the re-establishment of a replication fork and DNA synthesis that can proceed to the end of the donor template. The experimental support for this repair model initially came from Morrow et al. (Morrow et al., 1997). They showed that a chromosome fragmentation vector containing a selectable auxotrophic marker, a centromere, origin of replication and a targeting sequence homologous to a unique, endogenous sequence on yeast chromosome III could be repaired to yield an independently segregating chromosome. Consistent with the BIR model, Morrow and co-workers showed that the repaired chromosome fragment contained all sequences centromere-distal to the targeted endogenous chromosomal locus and still retained the endogenous targeted chromosome III (Morrow et al., 1997). The BIR repair pathway requires Rad51 and Rad52, which are both essential for the strand-invasion step (see below) during DSBR (Davis and Symington, 2004; Llorente et al., 2008). The fact that BIR shares similar genetic requirements to the DSBR pathway suggests a common strand invasion intermediate in these two

recombinational repair processes. Rad51-independent BIR has also been reported previously but was shown to occur much less efficiently than Rad51-dependent BIR (Malkova et al., 1996; Malkova et al., 2005). The initiation of BIR pathway is inherently slow and triggers the DNA damage checkpoint (Malkova et al., 2005). This explains why Rad51-dependent BIR is strongly out-competed by DSBR or SDSA in wild type cells during the repair of a two-ended DSB (Llorente et al., 2008). Recent experiments have shown that both leading and lagging strand DNA synthesis machineries are required for BIR, in contrast to the SDSA pathway that utilizes only the leading strand DNA synthesis apparatus (Lydeard et al., 2007; Wang et al., 2004). Therefore, Lagging strand synthesis is considered to be the defining feature of BIR (Llorente et al., 2008).

The BIR repair pathway is thought to be essential for telomere maintenance in the absence of telomerase or when a telomere becomes uncapped (Davis and Symington, 2004; Garvik et al., 1995; Hackett and Greider, 2003; Le et al., 1999; Lundblad and Blackburn, 1993; Teng et al., 2000). BIR has also been suggested to be vital for the restart of a stalled/collapsed replication fork (Llorente et al., 2008). One-ended DSBs may occur naturally during replication as a consequence of impairment of replication-fork progression (Branzei and Foiani, 2005; Michel et al., 2001). This type of DSB can arise when replication forks hit a single-strand break/gap on either the leading or lagging template strand (see below) (Kuzminov, 1999).

From a mechanistic point of view, Szostak's DSB repair model involves DSB end-resection, strand invasion, D-loop formation and resolution of recombination intermediates. Some of these steps are common between SDSA, SSA, BIR and dHJ dissolution models. The genetic and biochemical studies of the

enzymes known to be responsible for these processes will be discussed in the following sections.

1.2.DNA End Resection

To initiate HR from a DSB, ends must be nucleolytically processed. Following DSB formation, DSB ends are resected to form 3' ssDNA tails (Figure 1.1(i)). In *S.cerevisiae*, 3' ssDNA that can extend hundreds to a few thousand nucleotides have been shown to form following DSB formation (Sun et al., 1991; Wang and Haber, 2004; White and Haber, 1990). DSB end-resection has been proposed to occur in a two-step mechanism (Figure 1.2) (Mimitou and Symington, 2008). In the first step, the Mre11 nuclease as part of the Mre11-Rad50-Xrs2 (MRX) complex, together with the nuclease Sae2, trims DSB ends to create relatively short 3' ssDNA overhangs (Figure 1.2). This initial processing step also acts to remove terminal adducts at DSB ends. Extensive resection is catalysed by the 5'-3' exonuclease, Exo1, or a parallel mechanism that requires the concerted action of the 3'-5' helicase, Sgs1 and the 5'-3' exonuclease, Dna2 (Figure 1.2) (Mimitou and Symington, 2008; Zhu et al., 2008).

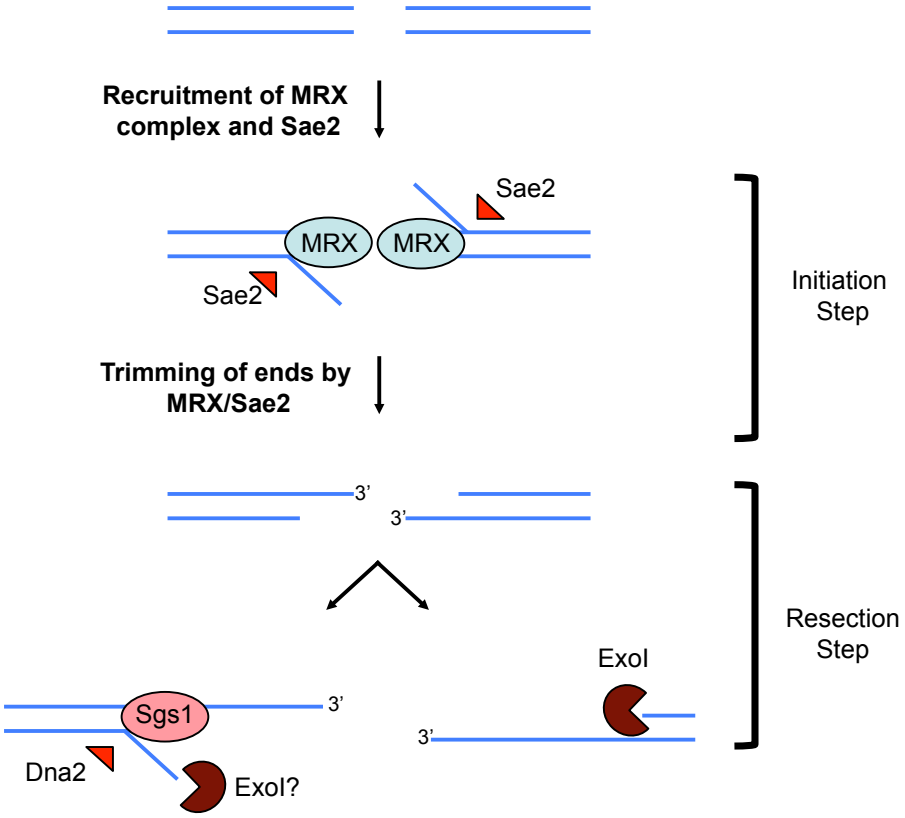


Figure 1.2. DSB end-resection model. The MRX complex and Sae2 trim the DSB ends to create a minimally resected intermediate that is the preferred substrates of subsequent DNA resection factors. The minimally resected intermediates can then be subjected to extensive resection catalysed by Exo1 or in a parallel pathway the combined action of Sgs1 and Dna2. (Adapted from Mimitou and Symington, 2008)

1.3.Strand Invasion and Second-end Capture

Resection of a DSB generates a 3' ssDNA tail that is the substrate for the recruitment of HR factors and cell cycle checkpoint activators (Mimitou and Symington, 2009). The ssDNA tail facilitates the search for homologous DNA sequences, normally the sister chromatid, followed by ssDNA invasion into the homologous template to form a D-loop. This process is known as strand invasion, which is catalysed by Rad51 in eukaryotes.

In yeast, the *RAD51* gene, which is a member of the *RAD52* epistasis group, encodes the orthologue of the bacterial recombinase enzyme RecA (Aboussekhra et al., 1992; Basile et al., 1992; Krogh and Symington, 2004; Ogawa et al., 1993; Shinohara et al., 1992). Similar to RecA, Rad51 catalyses the base pairing of the ssDNA to a homologous DNA template. *S.cerevisiae* Rad51 is a 43kDa protein with 30% identity to the catalytic domain of RecA covering the Walker A and B domains for nucleotide binding and/or hydrolysis, known as the ATPase domain (Aboussekhra et al., 1992; Basile et al., 1992; Shinohara et al., 1992). These domains are essential for the proper functioning of Rad51 as evidenced by the mutation of the conserved lysine residue within the Walker A domain to alanine (Rad51-K191A) which abolishes DNA binding and ATPase activities of ScRad51 (Sung and Stratton, 1996). ScRad51 binds to ssDNA to form right-handed helical filaments, similar to those generated by RecA, to facilitate strand invasion (Ogawa et al., 1993; Sung and Robberson, 1995).

The BIR pathway occurs with one-ended DSBs or when only one end of a two-ended DSB is available for HR. When two ends of a DSB are present, however,

the second end of the DSB that has been processed to form 3' ssDNA can anneal to the single-stranded D-loop generated as a result of the first-end strand invasion event (Figure 1.1 (i)). This process is known as second-end capture. Second-end capture allows initiation of DNA synthesis to duplicate the lost sequences from the template, thereby facilitating the formation of a stable dHJ intermediate that links two homologous sequences covalently.

1.3.1. Regulation of Rad51-mediated strand invasion

Replication protein A (RPA), a heterotrimeric ssDNA binding protein, promotes the binding of Rad51 to 3' ssDNA tails to form a presynaptic filament (Sung et al., 2003). RPA functions by binding to long ssDNA, thereby minimizing the secondary structures formed on the ssDNA. This facilitates the loading of Rad51 onto the ssDNA and hence the formation of a continuous Rad51-ssDNA presynaptic filament (Sung et al., 2003). Paradoxically, as an ssDNA-binding protein complex, RPA also competes with Rad51 for ssDNA binding sites. Because RPA has a higher affinity for ssDNA than Rad51, RPA can inhibit the formation of a Rad51-bound presynaptic filament *in vitro* when RPA is in excess (Sung, 1997a, b; Sung et al., 2003). Because of the *in vivo* abundance of RPA, most ssDNAs formed as a result of end resection presumably are immediately bound by RPA.

The inhibitory effect of RPA on RAD51 nucleoprotein filament formation can be overcome by mediator proteins that assist the replacement of RPA to Rad51 on ssDNA. Two such recombination mediators are Rad52 and the Rad55-57 heterodimeric complex (New et al., 1998; Sung, 1997a, b). Both Rad52 and the Rad55-57 heterodimeric complex interact with RPA and Rad51, and are thought to

mediate Rad51-ssDNA presynaptic filament formation by displacing RPA while recruiting Rad51 to ssDNA (Mortensen et al., 1996; Song and Sung, 2000; Sugiyama and Kowalczykowski, 2002; Sung, 1997b). The idea that Rad52 is essential for the loading of Rad51 onto RPA-coated ssDNA is consistent with the fact that Rad51 localization to the sites of DSBs *in vivo* occurs in a Rad52-dependent manner, as demonstrated by immunofluorescence and ChIP analysis (Bishop, 1994; Essers et al., 2002; Miyazaki et al., 2004; Sugawara et al., 2003; Wolner et al., 2003). Apart from its role in promoting presynaptic filament formation, Rad52 protein is also thought to facilitate second end capture because of its *in vitro* DNA annealing of the ssDNA strand that is displaced by DNA strand exchange by Rad51 and RPA, to a second ssDNA strand (Sugiyama et al., 2006).

Another recombination mediator that promotes the formation of D-loop from Rad51-ssDNA presynaptic filament is Rad54 (Krejci et al., 2003a; Petukhova et al., 1998; Symington, 2002). Rad54 is a bidirectional motor protein that can translocate along dsDNA at approximately 300bp/s powered by the free energy derived from ATP hydrolysis (Amitani et al., 2006). The translocation of Rad54 on duplex DNA generates positive supercoils ahead of the protein movement and negative supercoils trailing it (Sung et al., 2003). The negative supercoils produced by Rad54 result in the transient separation of the two strands of a DNA duplex, and therefore facilitates the binding of presynaptic filament to the template DNA duplex by base-pairing, forming a D-loop. When translocating on duplex DNA, Rad54 removes Rad51 from the post-synaptic filament. The removal of Rad51 may be important in providing access of DNA polymerases to the 3' invading ends for DNA synthesis as well as allowing the recycling of Rad51 proteins.

The reversal of strand invasion step in HR is crucial for the promotion of the SDSA pathway that can prevent the formation of dHJs and hence the canonical DSBR pathway. Negative regulation of the strand invasion step in *S.cerevisiae* is currently thought to be executed at least by three enzymes: Srs2, Sgs1 and Mph1.

1.3.1.1. Srs2 (Suppressor of Rad Six)

SRS2 encodes a protein that possesses ssDNA-dependent ATPase, DNA helicase and translocase activities (Rong and Klein, 1993; Van Komen et al., 2003). In *S.cerevisiae*, mutations in the *SRS2* gene lead to a hyper-recombination phenotype (Aboussekhra et al., 1992; Fabre et al., 2002). However, *SRS2* mutation suppresses the UV sensitivity of *rad6* and *rad18* mutant cells and this is thought to occur by channelling DNA lesions from an error-prone repair pathway into the RAD52-mediated recombinational repair pathway (Schiestl and Prakash, 1990). These observations suggest that Srs2 is an anti-recombinase.

Srs2 is thought to negatively regulate HR by efficiently disrupting the presynaptic filament formed by association of Rad51 to ssDNA (Krejci et al., 2003b; Veaute et al., 2003). It was shown that Srs2 dismantles Rad51-bound presynaptic filaments using its ATP-dependent translocase activity, as mutants that cannot bind or hydrolyze ATP fail to disrupt Rad51-bound presynaptic filaments (Krejci et al., 2004). Krejci and co-workers suggested that Srs2 activity might be recruited to the Rad51-bound presynaptic filament via the direct physical interaction between Srs2 and Rad51 since biochemical and two-hybrid analyses indicate that the two proteins can directly interact (Krejci et al., 2003b). Consistent with this view, Rad51 mutants that cannot interact with Srs2 are resistant to the

anti-recombination activity of Srs2 (Seong et al., 2009). Similarly, the Srs2 mutant that fails to interact with Rad51 but retains wild type levels of ATPase and helicase activities is compromised for its anti-recombination role (Colavito et al., 2009). Srs2 has also been shown to interact physically with the sumolyated form of proliferating-cell nuclear antigen (PCNA) (Papouli et al., 2005; Pfander et al., 2005). PCNA is a DNA polymerase processivity factor sumoylated specifically during S-phase (Hoege et al., 2002; Stelter and Ulrich, 2003). Sumolyated PCNA was shown to inhibit HR during S-phase (Pfander et al., 2005). Therefore, the sumolyation of PCNA is thought to recruit Srs2 to inhibit Rad51 nucleofilament formation, thereby preventing aberrant recombination during DNA replication (Macris and Sung, 2005). Furthermore, it has been shown RPA has a synergistic effect with Srs2 in preventing the ability of Rad51 to mediate strand exchange during HR (Krejci et al., 2003b; Veaute et al., 2003). RPA is thought to sequester ssDNA, released as a result of Srs2-mediated Rad51 dissociation from the presynaptic filament, from being re-nucleated by Rad51 to mediate strand exchange. The inhibitory action of Srs2 on presynaptic filament formation can be partially overcome by the addition of the recombination mediator Rad52 that facilitates Rad51 binding to RPA coated ssDNA template (Krejci et al., 2003b). This suggests that the cell can regulate the efficiency of presynaptic filament formation and thus the level of HR by altering the levels of the antagonistic functions of Srs2 and Rad52.

1.3.1.2. Sgs1 (Slow Growth Suppressor of *top3Δ*)

Apart from its pro-recombinogenic role in DSB end-resection, Sgs1 also plays a role in negatively regulating HR. Gangloff and colleagues demonstrated that in the absence of Srs2 and Sgs1, Rad51-mediated recombination can result in cell death in *S.cerevisiae* (Gangloff et al., 2000). This implies that Srs2 and Sgs1 redundantly acts to suppress HR. Consistent with this idea, Sgs1 overexpression can suppress the hyper-recombination and repair defect of *srs2Δ* cells (Ira et al., 2003; Mankouri et al., 2002). Furthermore the human helicase BLM, the orthologue of Sgs1 in *S.cerevisiae*, can also act as a DNA translocase to dislodge Rad51 from presynaptic filaments, thus functioning similarly to Srs2 to suppress strand exchange and therefore the initiation of HR (Bugreev et al., 2007).

DNA strand exchange activity mediated by human Rad51 is greatly stimulated by Ca^{2+} (Bugreev and Mazin, 2004). Ca^{2+} is thought to maintain the Rad51-bound presynaptic filament in an "active" state, which can readily mediate strand exchange, by reducing the ATP hydrolysis rate of Rad51 in a presynaptic filament. Bugreev et al. showed that BLM can disrupt only an "inactive" presynaptic filament in an ADP-bound form, suggesting a possible mechanism in HR regulation: until the cell is fully prepared for HR, the RAD51-ssDNA presynaptic filament remains "inactive" and susceptible to BLM dissociation to alleviate untimely HR events (Bugreev et al., 2007). Similarly, RECQ5β (also known as RECQL5), another human RecQ helicase, can also perform the same function of disrupting Rad51 presynaptic filaments and thus prevent inappropriate HR (Hu et al., 2007). Taken together, Bugreev et al. and Hu et al. established a role

for RecQ helicase family members in regulating HR by Rad51-ssDNA disruption function (Bugreev et al., 2007; Hu et al., 2007).

1.3.1.3. Mph1 (Mutator Phenotype)

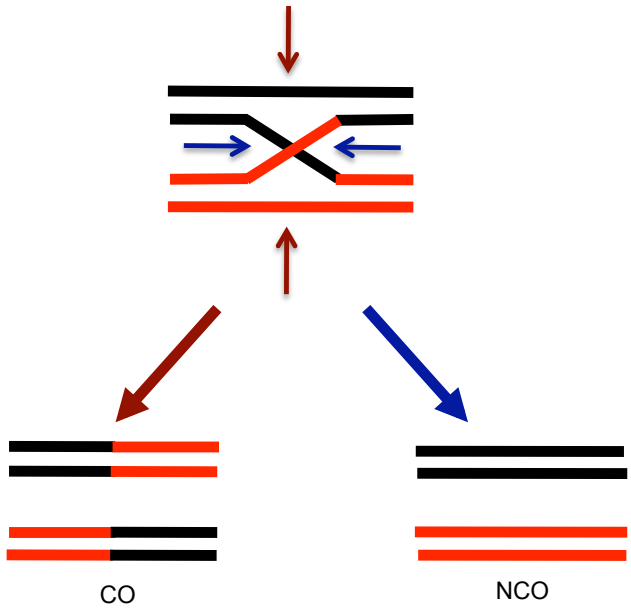
Mph1 was initially identified in a screen for *S.cerevisiae* mutants with increased spontaneous mutation rates as measured by the formation of canavanine resistant colonies (Entian et al., 1999). Based on the epistatic relationship of *MPH1* and *RAD51* with respect to spontaneous canavanine reversion rates and methylmethane sulphonate (MMS) sensitivity, Schurer and coworkers proposed that Mph1 functions in one of several HR pathways (Schurer et al., 2004). Mph1 protein is an ATP-dependent helicase with 3'-5' polarity (Prakash et al., 2005). The helicase activity of Mph1 is required to suppress spontaneous unequal SCEs and DSB- induced chromosome COs (Prakash et al., 2009). Mph1 is thought to channel repair intermediates into a NCO pathway since the efficiency and kinetics of HO-induced break repair are identical between wild type and *mph1Δ* cells (Prakash et al., 2009). Mph1 functions independently of Srs2 and Sgs1 (Prakash et al., 2009). Using ChIP, Prakash and coworkers showed that Mph1 is targeted to a DSB induced by the HO endonucleases (Prakash et al., 2009). They also showed that purified Mph1 binds and dissociates Rad51-bound D-loop structures, a reaction that requires the helicase activity of Mph1. Mph1 attenuates strand exchange by a different mechanism to that of Srs2. *In vitro*, Srs2 strongly attenuates the D-loop reaction when added with Rad51 to ssDNA but Srs2 is incapable of dissociating pre-formed D-loop product (Prakash et al., 2009). Mph1, in contrast, efficiently reduces the level of D-loop formation regardless of the order of the helicase

addition. However, Mph1 does not significantly affect the formation of Rad51-ssDNA presynaptic filament formation, as indicated by biochemical and electron microscopic analyses (Prakash et al., 2009). This led to the proposal that Mph1 specifically dissociates Rad51-made D-loops to channel HR intermediates into the SDSA pathway and thus limit CO formation. This mode of negative regulation of strand invasion is also conserved in *S.pombe*, because the *S.pombe* orthologue of *S.cerevisiae* Mph1, Fml1, has been shown to suppress CO formation by D-loop disruption (Sun et al., 2008).

1.4.HJ Processing

A four-way DNA intermediate known as a HJ, the existence of which has been predicted by Robin Holliday in 1964, is formed during HR and DSBR (Holliday, 1964). Physical evidence to support Holliday's proposal of such a four-way DNA intermediate was provided by electron-microscope studies (Bell and Byers, 1979; Benbow et al., 1975; Potter and Dressler, 1979) (Figure 1.3 (ii)). The resolution of such DNA intermediates is essential for the proper segregation of the two inter-linked duplexes. In HR, HJ resolution is achieved by dual-incisions across the branch point to release nicked duplexes that can be readily sealed by DNA ligase. One orientation of resolving a HJ generates NCO products, in which the DNA sequences flanking the DSB remain unchanged (Figure 1.3 (i)). In contrast, the opposite resolution orientation produces CO products that results in the exchange of DNA sequences that flank the DSB (Figure 1.3 (i)). The implications of CO and NCO formation for genome stability and cell survival will be discussed in a later section.

(i)



(ii)

This image has been removed due to copyrights reason. For reference please refer to the identical image present in Liu Y, West SC (2004). Happy Hollidays: 40th anniversary of the Holliday junction.*Nat Rev Mol Cell Biol.* (11):937-44.

Figure 1.3. HJ resolution. (i) Symmetrical, dual incisions indicated by the red arrows result in the exchanges of sequences flanking the HJ and hence the formation of a CO, while incisions indicated by the blue arrows generate NCO products. (ii) Electron micrograph showing a single HJ. Recombination intermediate between two homologous plasmids was cleaved by *Eco*RI to form a χ-structure. Adapted from Potter, H., and Dressler, D. (1979).

1.4.1. The structure of a HJ

Nucleic acids are polyelectrolytes and hence electrostatic interactions can influence their folding process and thus their structures (Lilley and White, 2001). Therefore, the structure of a HJ is highly dependent on the concentration and type of metal cations present (Lilley and White, 2001). It has been shown by gel-electrophoresis and Fluorescence Resonance Energy Transfer (FRET) analyses that a HJ can acquire two conformations (Clegg et al., 1994; Duckett et al., 1988). In the absence of metal cations, HJ can adopt a square-planar structure, in which the central region is open with each of the arms directed towards one of the four corners of a square (Figure 1.4 (i)) (Clegg et al., 1994). In contrast, in the presence of divalent metal cations such as Mg^{2+} (Figure 1.4 (i)), HJs undergo a folding process involving pair-wise coaxial stacking of helical arms, and a right-handed rotation of the axes, to give the stacked X-structure (Duckett et al., 1988). This is because the Mg^{2+} cations neutralise the electrostatic repulsions that are caused by the phosphate groups in the DNA backbone at the point of CO (Lilley and White, 2001). FRET analysis and three independent crystallography studies on HJ structures also showed that when a HJ adopts the stacked X-structure in the presence of Mg^{2+}, the two linked helices lie anti-parallel to each other (Clegg et al., 1994; Eichman et al., 2000; Nowakowski et al., 1999; Ortiz-Lombardia et al., 1999). The relevance of these different HJ conformations *in vivo* remains unclear because in a cell, a HJ will most probably be constrained by the overall nucleosome organisation, unlike artificial oligo-based HJs that are short and free to rotate in solution.

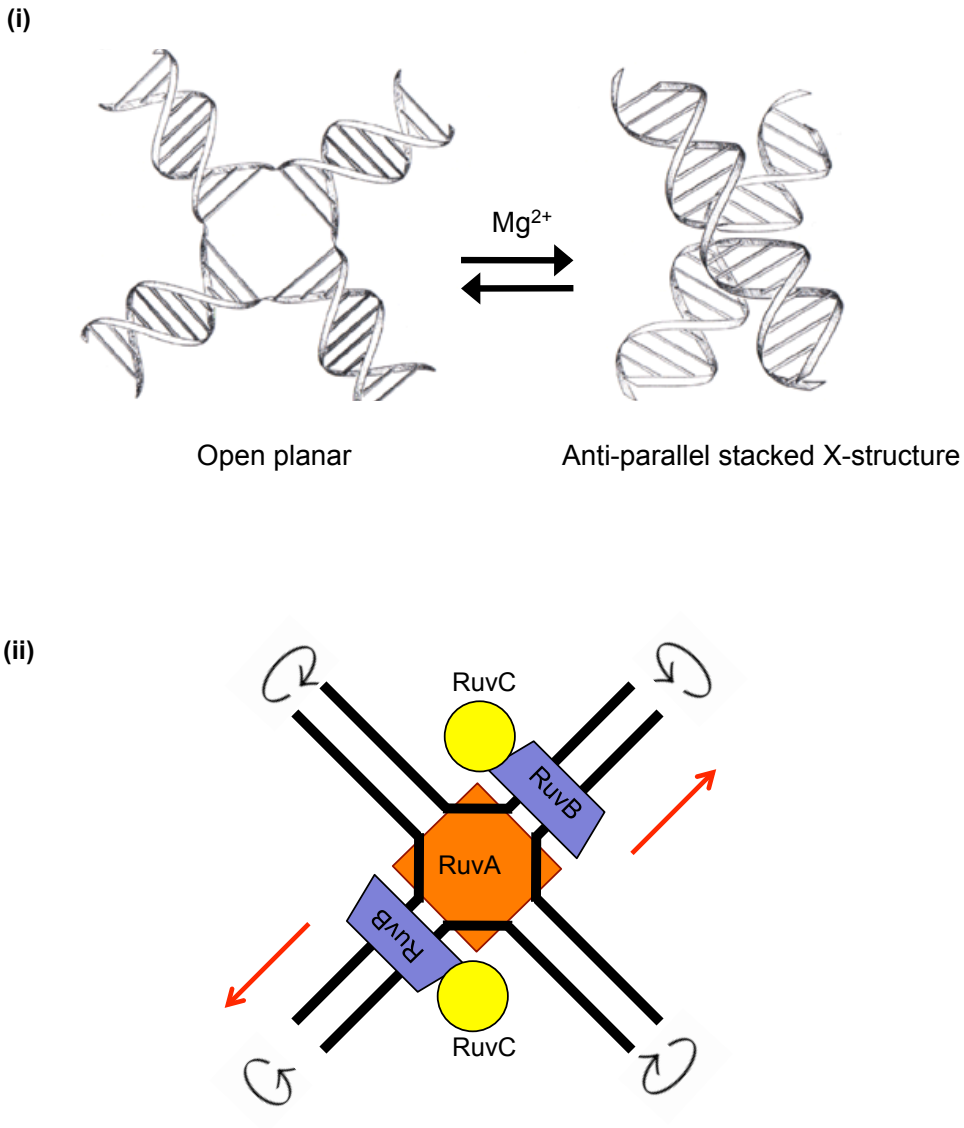


Figure 1.4. (i) The HJ structure shown in the anti-parallel stacked X (right), which forms in the presence of Mg^{2+}, and the open-planar configuration (left) (Adapted from Lilley and White (2001)), (ii) Mechanism of RuvABC-mediated HJ resolution. RuvA and RuvB helicases bind to the HJ, inducing the square-planar configuration allowing branch migration to occur in the direction indicated by the red arrows. RuvC dimer binds to the HJ and introduces symmetrical nicks at consensus sequences located at the HJ. The curved arrows represent the direction of rotation of the four arms of HJ due to the branch migration activity of the RuvAB complex.

1.4.2. HJ Branch Migration

Since HJs form between homologous sequences, branch migration of a HJ can occur by step-wise breakage and formation of hydrogen bonds between base pairs as one DNA strand is exchanged for another. HJ branch migration is an isoenergetic process that can occur spontaneously since it does not alter the overall number of hydrogen bonds (Panyutin and Hsieh, 1993). However, the rate of spontaneous branch migration is highly sensitive to the presence of metal ions, which can affect the structure of a HJ. HJ branch migration is inhibited in the presence of $MgCl_2$ (Panyutin and Hsieh, 1994). This is because in the presence of Mg^{2+}ions, the base stacking in HJ inhibits spontaneous branch migration (Panyutin et al., 1995). Panyutin and Hsieh also showed that a single base pair (bp) mismatch can impede spontaneous branch migration (Panyutin and Hsieh, 1993).

In bacteria, branch migration of HJ is actively promoted by the RuvAB complex in an ATP-dependent manner. RuvA tetramers bind to a HJ and result in a fourfold symmetric square-planner structure whereas RuvB catalyses branch migration using its helicase activity (Figure 1.4 (ii)). The HJ branch migration activity of RuvAB is thought to facilitate RuvC-mediated HJ resolution because branch migration allows RuvC to "screen" for consensus sequences and generate symmetrical incisions across these sequences (West, 1997). In humans, RecQ helicases such as BLM and WRN have also been shown to promote HJ branch migration. The HJ branch migration activity of BLM is crucial for its dHJ dissolution activity (see below), in which two HJs converge by branch migration, forming a hemicatenane that can be unlinked by topoisomerase (Figure 1.1 (iii))

(Wu and Hickson, 2003). The branch migration activities of BLM and WRN are also thought to be important in catalysing fork regression for the restart of stalled replication forks (Figure 1.8) (Karow et al., 2000; Machwe et al., 2006). Moreover, Rad54, which has no helicase activity, has been shown to catalyse branch migration of synthetic HJs as well as four-way junctions on joint molecule (JM) generated by human Rad51 (Bugreev et al., 2006). The branch migration activity of Rad54 is conserved between humans and *S.cerevisiae* (Bugreev et al., 2006). Rad54 branch migration activity is thought to be important for the extension of heteroduplex DNA, such that a D-loop intermediate can be stabilized and form a dHJ upon second-end capture. Rad54-mediated branch migration activity has also been proposed to play an anti-recombination role. It was suggested that Rad54-mediated branch migration may occur in the direction towards the invading strand, thereby disrupting a D-loop intermediates to facilitate SDSA (Bugreev et al., 2006).

1.4.3. HJ Resolution in Prokaryotes, Bacteriophages and Archaea

Enzymes that catalyse the resolution of HJ are homodimeric/heterodimeric endonucleases with high specificity for branched DNA. HJ resolvases use a metal-binding pocket to co-ordinate an activated water molecule for phosphodiester bond hydrolysis (Sharples, 2001). In *E.coli*, HJ resolution is carried out by the sequential action of RuvAB branch migration activity and RuvC HJ cleavage activity (West, 1997). *E.coli* strains with mutations at the *ruv* locus were originally isolated in two laboratories (Otsuji et al., 1974; Sharples et al., 1990). The *ruv* mutants exhibit increased sensitivity to UV, IR and mitomycin C. This led to the suggestions that the gene products of *ruv* genes are required for DNA recombinational repair. The first evidence for HJ structural modification by protein binding came from

experiments in which the RuvA protein was shown to bind a HJ as a tetramer which resulted in the HJ acquiring a fourfold symmetrical structure (Parsons et al., 1995). The RuvB proteins form hexameric rings around DNA and possess *in vitro* branch migration and ATP-dependent helicase activities (Stasiak et al., 1994). Experiments showed that RuvA specifically targets RuvB to HJs to promote HJ branch migration (Figure 1.4 (ii)) (Iwasaki et al., 1992; Parsons et al., 1992; Parsons and West, 1993).

The mechanism of RuvC-mediated HJ resolution can be divided into three experimentally separable steps: (i) structure-specific DNA binding, (ii) DNA structure modification and (iii) endonucleolytic cleavage (West, 1997). RuvC, on its own, exhibits specific binding and endonucleolytic activity on HJ but not other branched DNA structures (Dunderdale et al., 1991; Iwasaki et al., 1991). Like RuvA, purified RuvC can also modify a HJ structure by holding the HJ, but in a twofold symmetrical X-structure (Bennett and West, 1995). Once loaded onto the HJ held in a square-planner configuration by RuvAB, RuvC catalyses resolution of the HJ in the presence of divalent metal ions (Mg^{2+} or Mn^{2+}). This is achieved by the introduction of symmetrical nicks in a pair of strands of like polarity at or around the branch point of a HJ (Dunderdale et al., 1991; Shah et al., 1994). The nicks on both resolved duplexes can then be ligated without the need for further processing. The nuclease activity of RuvC preferentially cleaves the sequence 5'-(A/T)TT↓(G/C)-3' (Eggleston and West, 2000; Shah et al., 1994). It was shown that the efficiency of HJ resolution is maximal when this consensus sequence is located precisely at the branch point of the HJ (West, 1997). The frequency of this consensus sequence on a gene will affect the frequency of HJ resolution and thus the stability of this particular gene locus. Furthermore, the structural specificity shown by RuvC resolvase may be important to ensure its action is strictly executed

on four-way recombination intermediates rather than other substrate such as a three-way junction that arises through replication (West, 1997). As genetic studies showed that RuvAB branch migration activity is closely linked to the HJ resolution activity of RuvC, it was proposed that the RuvABC proteins function as a "resolvasome" complex that executes HJ resolution in *E.coli* during recombination (Eggleston and West, 2000).

In the absence of the *ruv* genes in *E.coli*, a spontaneous mutation that is capable of suppressing the DNA repair defect was identified (Mahdi et al., 1996; Mandal et al., 1993). The mutation is an insertion mutation upstream of the *rusA* coding regions, which activates transcription of the normally silent gene on the cryptic prophage DLP12 (Mahdi et al., 1996; Mandal et al., 1993). RusA is poorly expressed in *E.coli* and deletion mutations show no obvious effect on recombination or UV sensitivity (Mahdi et al., 1996). Purified RusA protein binds, distorts and resolves HJs *in vitro*, by a dual incision mechanism similar to that of RuvC (Chan et al., 1997; Giraud-Panis and Lilley, 1998). RusA prefers to cut 5' of a CC dinucleotide at the branch point of a HJ, a sequence specificity that is different from that of RuvC (Chan et al., 1997; Giraud-Panis and Lilley, 1998). RusA also displays less structural specificity than RuvC because it can bind and cleave other branched DNA structures such as replication fork structures but with less efficiency than that observed with a HJ (Bolt and Lloyd, 2002; Chan et al., 1998).

HJ resolution activities have also been isolated from organisms in different domains of life. T4 endonuclease VII and T7 endonuclease I can resolve a range of branched DNA molecules, including Y junctions, single-strand overhangs and HJs (Sharples, 2001). T4 endonuclease VII and T7 endonuclease I play important roles in debranching recombination intermediates before packaging the phage genome

(Kemper and Brown, 1976; Mizuuchi et al., 1982). HJ resolvases, Hjc (Holliday Junction Cleavage) and Hje (Holliday Junction Endonuclease), are also found in the hyperthermophile archae, i.e. *Pyrococcus furiosus* and *Sulfolobus solfataricus*, respectively (Komori et al., 1999; Kvaratskhelia and White, 2000). Furthermore, A22R from vaccinia virus has been shown to demonstrate HJ cleavage activities (Garcia et al., 2000). Despite the common selectivity for the specific four-way structure of a HJ, these HJ resolvases are unrelated at the primary sequence level. The only exception is that RuvC, Cce1 (see below) and A22R share a structural motif essential for their endonuclease functions (Garcia et al., 2000).

1.4.4. HJ Resolution in Eukaryotes

In *S.cerevisiae*, Cce1 (cruciform-cutting endonuclease) has been shown to resolve HJs (Whitby and Dixon, 1997). Cce1 protein is localized to the mitochondria and is required for the maintenance of the mitochondria genome (Kleff et al., 1992; Lockshon et al., 1995). Like RuvC, Cce1-mediated HJ resolution activity is sequence-specific. Cce1 prefers to cleave a tetranucleotide sequence with the consensus 5'-ACT↓A-3' (Schofield et al., 1998). The orthologue of Cce1 in *S.pombe,* Ydc2, also resolves HJs symmetrically, producing nicked duplexes that are readily ligatable, and also complements the DNA repair defects of *ruvC* mutants expressing Ydc2 (Oram et al., 1998; Whitby and Dixon, 1997).

While mitochondrial HJ resolvases have been identified in two eukaryotic model organisms, the identity of nuclear HJ resolvase in eukaryotes remains elusive. To date, several nuclear proteins identified from different model organisms,

have been proposed to act as a HJ resolvase. These proteins will be discussed individually as follows.

1.4.4.1. Resolvase A (RAD51C-XRCC3 & Yen1/GEN1)

A Nuclear HJ resolution activity, designated as Resolvase A, can be detected in mammalian cell-free extracts (Constantinou et al., 2002; Constantinou et al., 2001; Elborough and West, 1990; Hyde et al., 1994; Liu et al., 2004). After multiple fractionations of HeLa cell extracts, Rad51C and XRCC3, two of five paralogues of Rad51, were found to be closely associated with Resolvase A in fractions containing branch migration and HJ resolution activities (Liu et al., 2004). Indeed, extracts from hamster ovary cells with mutations in *RAD51C* or *XRCC3* or human cells depleted of RAD51C lack Resolvase A-mediated HJ resolution activity (Liu et al., 2004). However, HJ branch migration and resolution activities were not observed using purified recombinant RAD51C and XRCC3 proteins, suggesting that additional factors may be required for the HJ resolution mediated by Resolvase A (Liu et al., 2004).

Further analysis of the Resolvase A activity using a mass spectrometry (MS) approach led to the identification of human HJ resolvase GEN1 (Ip et al., 2008). The HJ resolution pattern of GEN1 was identical to that produced by Resolvase A, suggesting that GEN1 is most probably the active component of Resolvase A. In the same study, Yen1, the *S.cerevisiae* orthologue of GEN1, was independently identified by screening the extracts from clones of the yeast gene fusion (TAP-tag) library for HJ resolution activity (Ip et al., 2008). More importantly, Ip and coworkers demonstrated that both recombinant GEN1 and Yen1 resolve synthetic

HJ substrates by the introduction of symmetrical incisions across the HJ branch point, to produce nicked duplex products in which the nicks can be readily ligated (Figure 1.5). Like RuvC, both GEN1 and Yen1 display some sequence preferences (Ip et al., 2008). Contrary to the findings in Liu et al., the HJ resolution activity mediated by GEN1 is not directly associated with RAD51C-XRCC3 complex. This was evidenced by the absence of RAD51C and XRCC3 from the most purified GEN1 fraction from HeLa cells or in the affinity-purified GEN1-FLAG fractions that display HJ resolution activity (Ip et al., 2008). It is currently unknown if full-length GEN1 protein is functionally active because only the purified, truncated form of GEN1 (N-terminal fragment) was shown to display efficient HJ resolution (Ip et al., 2008). Hence it has been proposed that GEN1 resolvase might be subjected to regulation in which it is activated by proteolytic cleavage or by interaction with other factors such as RAD51C-XRCC3.

The identification of GEN1/Yen1 and the analysis of their mechanism of endonucleolytic action suggest that the RuvC HJ resolution model is indeed universal across the three domains of life. Despite displaying all the biochemical features of a canonical HJ resolvase, GEN1 and Yen1 do not show any sequence conservation to RuvC, Cce1, Hjc or other bacteriophage resolvases (Ip et al., 2008). Instead, Ip and colleagues suggest that GEN1/Yen1 represent a new subclass of the Rad2/XPG family of nucleases. Indeed, by mutating the two conserved glutamic acid residues in the nuclease motif analogous to Rad2/XPG family proteins, Yen1 nuclease function is inactivated. The mutation of *YEN1* in *S.cerevisiae* does not result in overt sensitivity to any DNA damaging agents (Lorenz et al., 2009). This indicates that Yen1 is not a core HR protein and that Yen1-mediated HJ resolution activity may possibly be effected by other factors with over-lapping

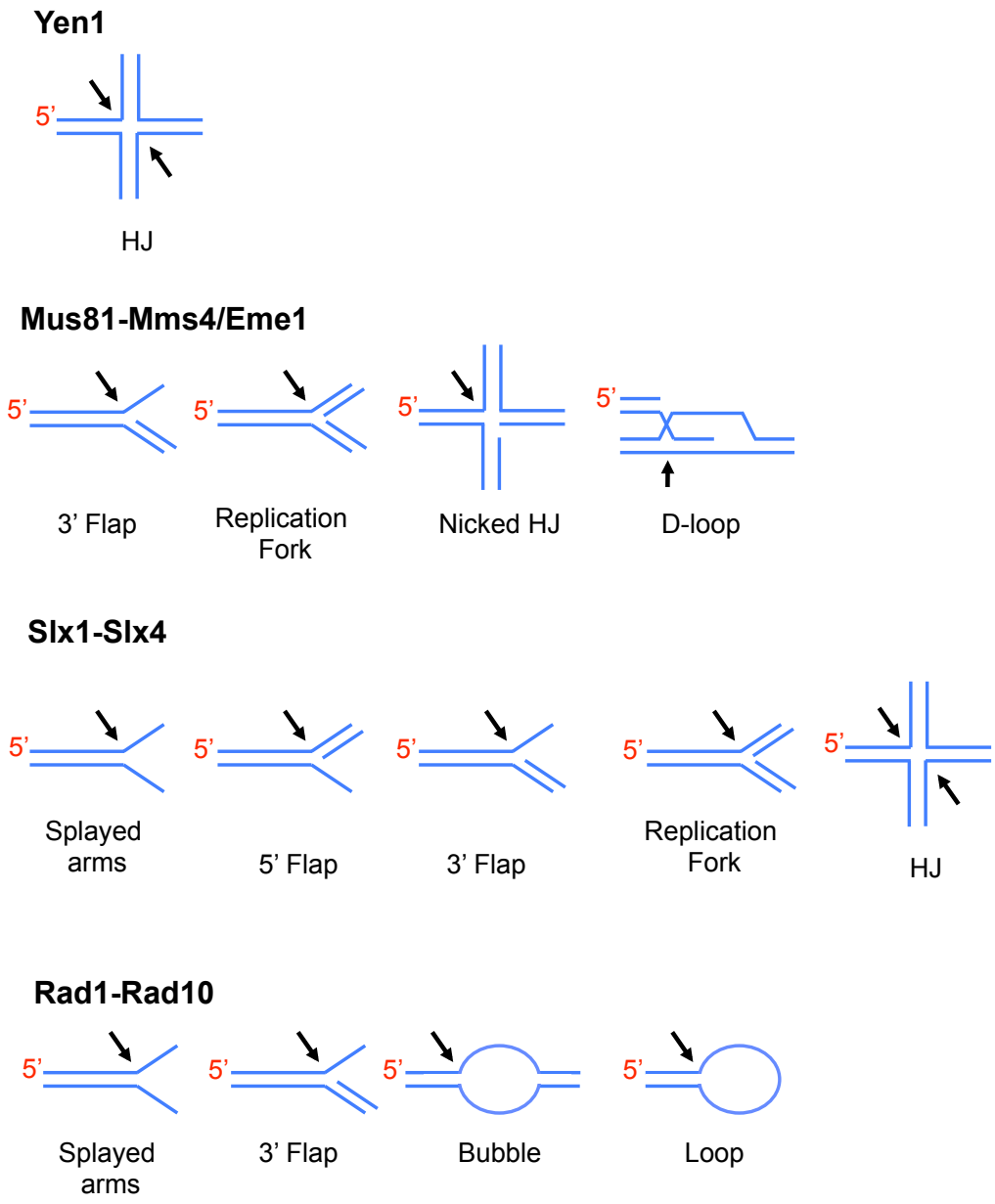


Figure 1.5. Summary of model DNA structures that are cleaved by Yen1, Mus81-Mms4/Eme1, Slx1-Slx4 and Rad1-Rad10 complexes. Black arrows indicate location of incisions made by the endonucleases. Adapted from Rouse, J. (2009).

functions. Interestingly, *YEN1* gene is absent from the *S.pombe* genome. This potentially explains why *mus81Δ* mutations in *S.pombe* displays a more severe meiotic recombination defect and reduced CO formation than *mus81Δ* mutation in *S.cerevisiae* since Yen1 may be able to functionally compensate for the loss of Mus81 (Blanco et al., 2010; Lorenz et al., 2009). It has also been shown that GEN1 may be linked with tumorigenesis, as evidenced by the identification of two breast cancer patients with deletion/frameshift mutations in GEN1 in a genome-wide study of all coding sequences in tumours derived from a cohort of breast cancer patients (Wood et al., 2007).

1.4.4.2. Mus81-Mms4/Eme1 Complex

Mus81 belongs to the XPF family of DNA structure-specific endonuclease and constitutes the catalytic subunit of a heterodimeric complex (Haber and Heyer, 2001). The binding partner of Mus81 is Mms4 in *S.cerevisiae* or Eme1 in *S.pombe*. Human MUS81 has two binding partners, EME1 and EME2 (Ciccia et al., 2007). Mus81 and Mms4/Eme1 were identified in several independent screens, i.e. a screen for mutations that cause synthetic lethality with *sgs1Δ*, a screen for interaction partners of Rad54 and checkpoint kinases, and a screen for mutants conferring MMS sensitivity (Boddy et al., 2001; Boddy et al., 2000; de los Santos et al., 2001; Interthal and Heyer, 2000; Mullen et al., 2001; Prakash and Prakash, 1977).

Mus81-Eme1 protein complexes purified from *S.pombe* and human cells were shown to display *in vitro* HJ resolution activities on model HJ substrates (Boddy et al., 2001; Chen et al., 2001; Ciccia et al., 2003). However, *S.cerevisiae*

Mus81-Mms4 resolves synthetic HJs poorly (Bastin-Shanower et al., 2003; Ehmsen and Heyer, 2008; Fricke et al., 2005). Interestingly, the cleavage activities of *S.pombe* Mus81-Eme1 and *S.cerevisiae* Mus81-Mms4 on HJs are enhanced greatly if the HJ contains a nick in the vicinity of the junction (Gaillard et al., 2003; Osman et al., 2003) (Figure 1.5). To explain the specific preference of Mus81-Mms4/Eme1 complexes of *S.cerevisiae* and *S.pombe* for nicked-HJs, Osman and colleagues proposed a model that accounts for the formation of CO products without the need to form an intact HJ (Osman et al., 2003). They proposed that Mus81-Eme1 cleaves meiotic strand invasion intermediates in two steps prior to the formation of an intact dHJ such that only CO products can be generated (Figure 1.6).

Although the Mus81 heterodimeric complex might be regarded as a eukaryotic HJ resolvase, the products of HJ resolution generated by Mus81 are different from other HJ resolvases such as the archael Hjc or bacterial RuvC. RuvC and Hjc incise symmetrically at the branch point of a HJ such that the nicks can be ligated direcly by a DNA ligase (Lilley and White, 2001; West, 1997). In contrast, Mus81-Mms4/Eme1 generates products containing gaps and flaps, implying an asymmetrical incision mechanism that differs from other HJ resolvases (Boddy et al., 2001). Recently, a truncated form of recombinant human MUS81-EME1 complex was shown to symmetrically cleave a HJ, which is in the form of a cruciform structure generated by extrusion of an inverted repeat sequence on a plasmid (Taylor and McGowan, 2008). The symmetrical nature of the bilateral cleavage was confirmed by the fact that the majority of the nicks generated by human Mus81/Eme1 complex are ligatable (Taylor and McGowan, 2008). This observation is consistent with the findings in *S.cerevisiae*, in which Mus81-Mms4 has been shown to catalyse *in vivo* resolution of cruciform structures formed on

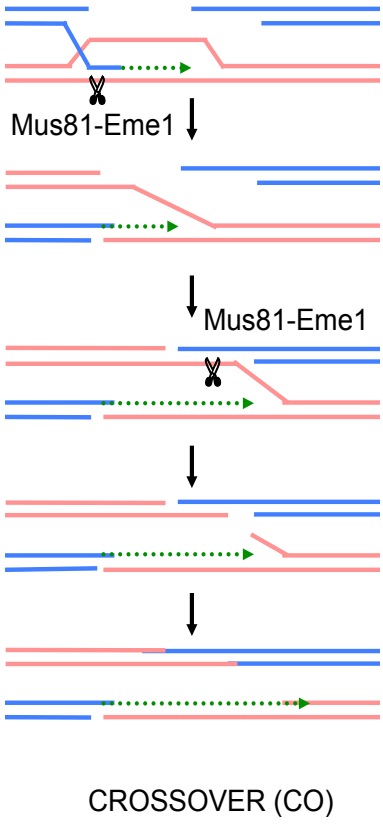


Figure 1.6. Two-step incision model by Mus81-Eme1 complex. Osman et al. (2003) proposed that the Mus81-Eme1 complex initially cleaves the D-loop prior to the formation of a stable HJ, followed by a second cleavage event on the resulting flap structure. Such a two-step incisions by Mus81-Eme1 complex forms exclusively CO products without the formation of an intact HJ.

plasmid-borne palindromes (Cote and Lewis, 2008). In the absence of Mus81, RusA HJ resolvase is able to substitute for the resolution of such cruciform substrate in *S.cerevisiae* (Cote and Lewis, 2008). These results suggest that under some circumstances Mus81 can indeed resolve an intact HJ in a symmetrical manner.

MUS81 mutations cause sporulation defects in both *S.cerevisiae* and *S.pombe* as a result of the failure in DNA segregation during meiotic HR (Boddy et al., 2001; de los Santos et al., 2003; de los Santos et al., 2001; Interthal and Heyer, 2000). In *S.pombe*, *mus81Δ* results in less than 1% spore viability compared to wild type cells, whereas 90-100% of *mus81Δ* or *mms4Δ* cells in *S.cerevisiae* undergo meiotic prophase arrest and the spore viability is 50% in the rare tetrads formed (Boddy et al., 2001; de los Santos et al., 2003; de los Santos et al., 2001; Interthal and Heyer, 2000). Interestingly, the spore viability of *mus81Δ* fission yeast can be restored by the expression of RusA HJ resolvase (Boddy et al., 2001). The suppression of meiotic defects in *mus81Δ* cells by RusA resolvase strongly suggests that Mus81 is responsible for the resolution of HJs. In contrast to *S.pombe*, overexpression of RusA does not suppress the meiotic defects in *S.cerevisiae* with mutations in *MUS81* (de los Santos et al., 2003). Meiotic HR results in obligate COs that are thought to be generated by HJ resolution. Meiotic CO formation in *S.pombe* is reduced 20-50 fold in *mus81Δ* diploids whereas NCO events occur at a normal frequency compared to wild type cells (Osman et al., 2003; Smith et al., 2003). In contrast, genetic and physical studies in *mus81* mutants of *S.cerevisiae* have shown only a two-fold decrease in meiotic CO frequency relative to wild type cells (de los Santos et al., 2003; de los Santos et al., 2001). This indicates that Mus81 is essential for meiotic CO formation in *S.pombe*, possibly for its HJ

resolution activity, while Mus81 is required to a lesser degree in *S.cerevisiae* for generating meiotic CO products.

Both *mus81Δ* or *mms4Δ* mutations result in synthetic lethality with mutations in *SGS1, TOP3* or *RMI1* (Boddy et al., 2000; Fabre et al., 2002; Mullen et al., 2001). Since Sgs1-Top3-Rmi1 is essential for the dissolution of dHJ intermediates that form in the later stage of HR, this implies that Mus81-Mms4 complex acts late in the HR pathway. Consistent with this idea is the fact that elimination of HR by mutating *RAD52, RAD51, RAD55 or RAD57* suppresses the synthetic lethality of *mus81Δ/mms4Δ* and *sgs1Δ/top3Δ/rmi1Δ* mutations (Fabre et al., 2002). Furthermore, it was shown that in the absence of Sgs1 and Mus81 during meiosis in *S.cerevisiae*, unresolved recombination intermediates accumulate (Jessop and Lichten, 2008; Oh et al., 2008). These observations are consistent with the proposal that Mus81-Mms4 acts in parallel with Sgs1-Top3-Rmi1 complex to promote the resolution of HJs.

One common feature between the purified Mus81-Mms4/Eme1 complexes of *S.pombe, S.cerevisiae* and human cells is that they all cleave 3' flap and three-way junctions more efficiently than a HJ substrate (Figure 1.5) (Chen et al., 2001; Ciccia et al., 2003; Constantinou et al., 2001; Kaliraman et al., 2001; Whitby et al., 2003). Moreover, *MUS81* mutant cells in *S.cerevisiae* and *S.pombe* display overt sensitivity to agents that lead to replication fork stalling or collapse, for example MMS, UV, camptothecin (CPT), the DNA synthesis inhibitor, HU, and the DNA crosslinking agent, Cisplatin (Boddy et al., 2001; Doe et al., 2002; Interthal and Heyer, 2000; Mullen et al., 2001; Vance and Wilson, 2002). Taken together, Mus81-Mms4/Eme1 complex has also been proposed to cleave the "Y-shaped" stalled replication forks to restart replication fork via BIR pathway (Haber and

Heyer, 2001; Kaliraman et al., 2001). Since replication forks stall when they encounter DNA lesions such as DNA interstrand crosslinks, Mus81 is essential for the cleavage of such stalled replication forks to form DSB, which in turn can be used to initiate BIR and thus restore the replication fork, while allowing the repair of the DNA lesion (Hanada et al., 2007; Hanada et al., 2006).

1.4.4.3. Slx1-Slx4 Complex

SLX stands for Synthetic Lethality of unknown (X) functions and six such genes were identified in a screen for factors required for viability in the absence of Sgs1 (Mullen et al., 2001). Six of the SLX genes form three separate heterodimeric complexes: Slx3-Slx2, Slx5-Slx8 and Slx1-Slx4 (Rouse, 2009). Slx3-Slx2 complex is Mus81-Mms4. Slx5-Slx8 is a SUMO (small ubiquitin-related modifier)-targeted ubiquitin ligase, which is important in the regulation of targeted protein degradation. Slx1-Slx4 complex has been demonstrated to co-operate with Sgs1 in enabling the completion of ribosomal DNA (rDNA), and this may be responsible for the synthetic lethality of *slx1Δ* or *slx4Δ* with *sgs1Δ* in *S.cerevisiae* (Rouse, 2009). Like Mus81-Mms4, biochemical analysis shows that *S.cerevisiae* Slx1-Slx4 complex is also a heterodimeric endonuclease with a marked preference for branched DNA structures such as 5' flaps, 3' flaps, simple Y-structures and full replication fork-like structures (Fricke and Brill, 2003) (Figure 1.5). Slx1-Slx4 will also resolve HJs but does so by making asymmetrical nicks. *slx1Δ* or *slx4Δ* mutant cells also do not have any obvious meiotic defects raising questions about the physiological relevance of the HJ resolution activity of Slx1-Slx4 (Fricke and Brill, 2003).

The SLX4 orthologs in humans and *Drosophila* are known as BTBD12 and MUS312, respectively (Andersen et al., 2009; Fekairi et al., 2009; Munoz et al., 2009; Svendsen et al., 2009). Mammalian SLX4 interacts with a number of proteins including XPF (Rad1 in *S.cerevisiae*), MUS81, SLX1, the MSH2/MSH3 MMR complex, the telomere binding complex TRF2-RAP1, protein kinase PLK1 and an uncharacterised protein, C20orf94 (Rouse, 2009). Interestingly, the Gaillard, Harper and Rouse groups revealed that human SLX1-SLX4 resolve migrating and static HJs by making symmetrical incisions (Fekairi et al., 2009; Munoz et al., 2009; Svendsen et al., 2009) (Figure 1.5). Hence, SLX1-SLX4 may yet be another HJ resolvase functioning in human cells, in parallel to MUS81-EME1 and GEN1.

Human SLX4 consists of several domains that are essential for its interactions with other proteins (Figure 1.7) (Fekairi et al., 2009; Munoz et al., 2009; Svendsen et al., 2009). At the carboxyl terminus of SLX4, CCD (conserved C-terminal domain) and SAP (named after SAF-AB, Acinus and PIAS) domains can be found. CCD domain is essential for the conserved interaction of SLX4 and SLX1, whereas the putative DNA-binding SAP domain mediates the binding of MUS81 to SLX4 (Aravind and Koonin, 2000; Fekairi et al., 2009). XPF binding to SLX4 is mediated through the N-terminal section of SLX4. The N-terminal region of human SLX4 contains at least two additional functional domains: UBZ4, a ubiquitin-binding motifs and BTB/POZ, a protein-protein interaction domain, which is not found in yeast (Fekairi et al., 2009). The interactions of SLX4 with XPF in humans is consistent with the functional interaction of Slx4 and Rad1/Rad10 in *S.cerevisiae*, in which Slx4 is essential for 3'-flap cleavage by Rad1-Rad10 endonuclease during SSA and GC when the DSB is flanked by non-homologous sequences (Flott et al., 2007; Li et al., 2008). Moreover, Slx4,

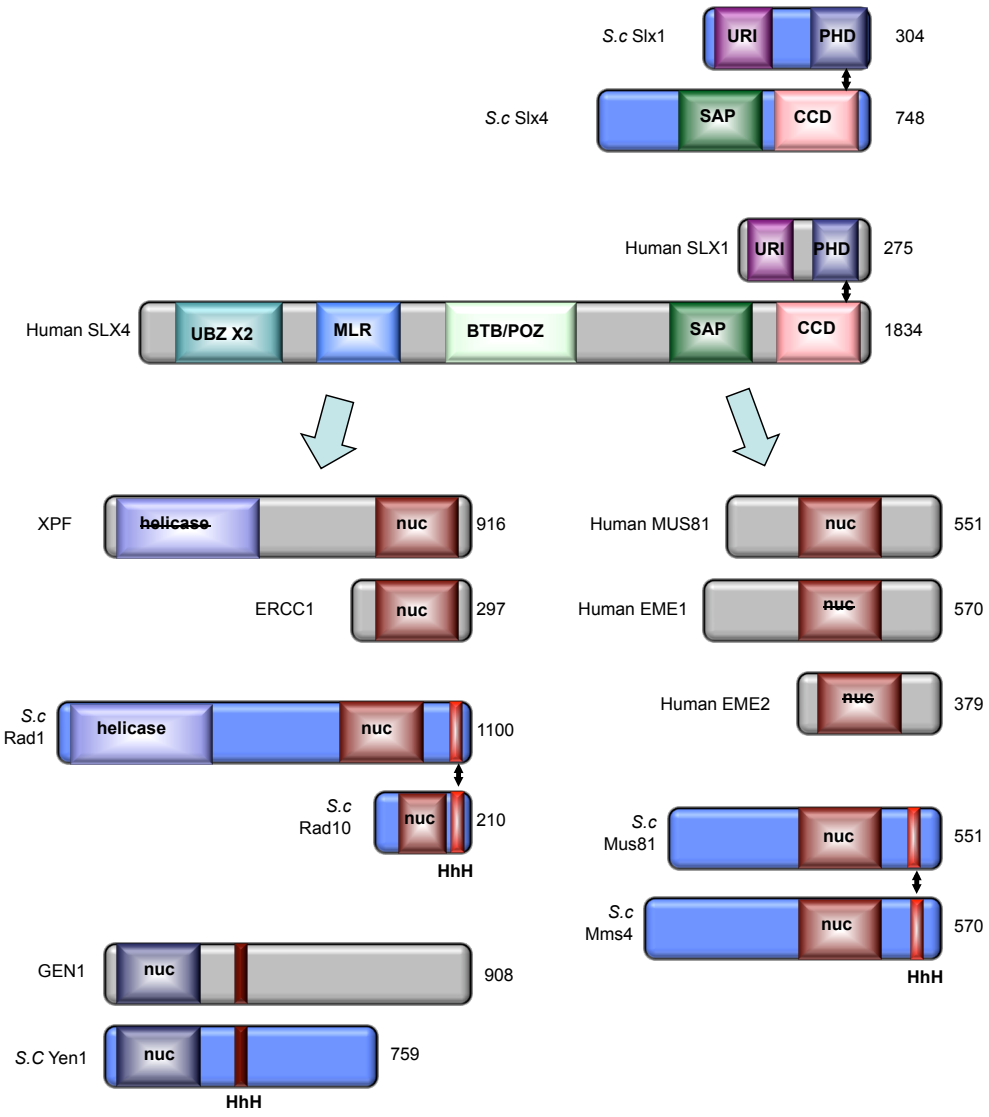


Figure 1.7. Nucleases together with their obligate binding partners that have been implicated in the resolution of HJs. *S.cerevisiae* endonucleases are in blue. The length of each protein is represented by the number of amino acids designated to the right of each protein. Blue arrows indicate the two motifs of human SLX4 that interacts physically with XPF and MUS81. Small double arrows represent the interaction domains between the components of heterodimeric endonucleases. URI: UvrC and intron-encoded endonuclease; PHD: Plant-homeo domain; CCD: conserved C-terminal domain; SAP: DNA-binding domain; MLR: MUS312/MEI9 interaction-like Region; UBZ: ubiquitin-binding motif; BTB/POZ: protein-protein interaction domain; HhH: helix-turn-helix domain; Nuc: endonuclease domain.

independently of Slx1, is also required for the recovery of stalled replication forks induced by MMS (Rouse, 2009). Slx4 is thought to co-operate with the BRCT [BRCA1 (breast cancer 1 early onset) C-terminus] domain-containing protein Esc4 in promoting the recovery from MMS-induced replisome stalling (Roberts et al., 2006; Rouse, 2004, 2009).

Based on the multiple interactions of human SLX4 with other proteins, including structure-specific endonucleases such as SLX1, MUS81 and XPF, it has been proposed that SLX4 acts as a platform for other catalytic interacting partners to mediate HJ resolution, DNA repair and interstrand crosslink repair (Fekairi et al., 2009; Munoz et al., 2009; Svendsen et al., 2009). The importance of other interactions of human SLX4 with other partners is yet to be revealed. This hypothesis is also in agreement with the notion in *S.cerevisiae* that Slx4 has multiple, independent functions involving different interaction partners: Slx4-Slx1 interaction for the processing of rDNA replication, Slx4-Esc4 interaction for the recovery from replisome stalling and Slx4-Rad1-Rad10 interaction for 3'-flap cleavage.

1.4.4.4. Rad1-Rad10 Complex

Rad1 and Rad10 form a heterodimeric complex involved in the nucleotide excision repair (NER) pathway (Miller et al., 1982; Paques and Haber, 1999; Wilcox and Prakash, 1981). *RAD1/RAD10* and the *RAD2* gene products of *S.cerevisiae* are required for the incision step of NER. Purified Rad1 and Rad10 interact with synthetic bubble structure and incise the DNA at the 5' end of the centrally unpaired region (Davies et al., 1995) (Figure 1.5). Unlike other NER

factors, Rad1 and Rad10 are also required for DNA interstrand crosslink repair, the removal of non-homologous 3'-flaps that arise during SSA, (Paques and Haber, 1999) (Figure 1.5), for the repair of topoisomerase-I-mediated replicative damage (Vance and Wilson, 2002), and for the meiotic MMR of long insertion/deletion DNA loops (Kearney et al., 2001).

Rad1 was also proposed to act at a late stage of HR following the observation that integration of linear DNA fragments into a homologous sequence in the yeast genome was reduced by deletion of *RAD1* (Schiestl and Prakash, 1988). It was also shown that purified Rad1 binds specifically to HJs and, in the presence of Magnesium, catalyses cleavage of HJ (Habraken et al., 1994). Habraken and coworkers also identified Rad1 as the catalytic subunit of Rad1-Rad10 complex because HJ cleavage can occur without Rad10 (Habraken et al., 1994). Nevertheless, this finding was contested by Davies et al. because using Rad1-Rad10 complex that was purified independently, they were unable to show any HJ cleavage on synthetic HJs (Davies et al., 1995). They claimed that Rad1-Rad10 mediated HJ cleavage demonstrated by Habraken et al. (Habraken et al.,1994) is likely to be caused by the 3' flap cleavage activity of Rad1/Rad10 on the bubble structure that forms on the homologous core of synthetic X12 structure during base-pair "breathing" (West, 1995). To form CO products, according to the canonical DSB repair model, HJ resolution is obligatory. The fact that purified Rad1-Rad10 complex cannot resolve synthetic HJ as demonstrated in Davies et al. (1995) is more consistent with the genetic observation that no apparent meiotic CO defect was observed in the absence of Rad1-Rad10 (*S.cerevisiae*) or Rad16-Swi10 (*S.pombe*) (Heyer et al., 2003). Therefore, Rad1 is unlikely to function as the main HJ resolvase, at least in budding and fission yeast.

In mammalian cells, *XPF* and *ERCC1* encode the Rad1 and Rad10 homologues respectively (de Laat et al., 1999). *ercc1*$^{-/-}$ mice are infertile and display meiotic defects which are considered to be unrelated to meiotic CO formation (Hsia et al., 2003). Surprisingly, mouse *ercc1*$^{-/-}$ embryonic stem cells display deficiency in gene targeting, but are as resistant to IR as wild type cells (Niedernhofer et al., 2001). Mouse *ercc1*$^{-/-}$ embryonic stem cells also display wild type frequency of spontaneous and induced SCEs, the CO event requiring the resolution of HJs formed between sister chromatids (Niedernhofer et al., 2001). Hence, this suggests that mouse ERCC1 is unlikely to be a component of HJ resolvase in mice. The homologue of XPF in *D.melanogaster* is MEI-9. Genetic analysis in *D.melanogster* showed that *mei-9* mutants result in a ten-fold decrease in meiotic COs compared to wild type flies. This effect seems to affect the later stages of recombination as the early steps of recombination such as heteroduplex DNA formation is unaffected in *mei-9* mutants (McKim et al., 2002). Like XPF, MEI-9 also interacts physically with ERCC1. Furthermore, MEI-9 has also been shown to interact with MUS312, which is the *S.cerevisiae* homologue of Slx4 (see below), and HDM, which belongs to a protein superfamily with ssDNA-binding activity (Joyce et al., 2009). It was proposed that MEI-9, ERCC1, MUS312 and HDM form a functional complex with endonuclease activity to process late meiotic recombination intermediates to form CO products (Joyce et al., 2009).

1.4.4.5. Double Holliday Junction Dissolution

An alternative mechanism to resolve HJs is a process termed dHJ dissolution. In humans dHJ dissolution is mediated by the concerted actions of

BLM and hTOPOIIIα, which are the human orthologues of *S.cerevisiae* Sgs1 and Top3, respectively (Wu and Hickson, 2003) (Figure 1.1 (iii)). As a typeIA topoisomerase, hTOPOIIIα can relax negatively supercoiled DNA. In the dHJ dissolution pathway, the two HJs converge as a result of the branch migration activity of BLM to form a hemicatenane, which is subsequently unlinked by the strand passage activity of TOPOIIIα to form exclusively NCO products (Wu and Hickson, 2003) (Figure 1.1 (iii)).

The dHJ dissolution model is distinct from classical HJ resolution because it prevents the exchange of flanking sequences, thereby limiting the formation of CO products such as sister chromatid exchange (SCE). This is consistent with findings showing that in the absence of BLM or its TOPIIIα interaction domain, very high levels of SCE occur (Hu et al., 2001; Wu et al., 2000). Indeed, the inability of cells lacking BLM to execute dHJ dissolution may explain the typical increase in SCE frequency, which is a diagnostic marker of Bloom's syndrome (Hickson, 2003). Moreover, this model is consistent with the genetic and physical evidence in *S.cerevisiae*, in which Sgs1 helicase, together with its interaction with Top3, was shown to suppress CO formation (Ira et al., 2003). More recently, it has been discovered that the activity of BLM and hTOPOIIIα on dHJ substrate can be stimulated by a protein known as RMI1 (Raynard et al., 2006; Wu et al., 2006). RMI1 is thought to promote the resolution of dHJs by recruiting hTOPOIIIα to the dHJ.

1.5. The Regulation of CO Formation

The resolution of HJs results in CO or NCO formation. NCO formation restores the continuity of broken DNA without exchanging sequences that flank the DSB. In contrast, CO formation involves the reciprocal exchange of flanking sequences of a DSB between two recombining duplexes following recombination. The implications of CO formation can be very different in meiotic and mitotic recombination. In meiosis, COs are crucial for the faithful segregation of chromosomes because they provide the physical linkage, which ensures the correct orientation of the homologous chromosomes on the meiotic spindle during the first meiotic division. Human aneuploidy has been attributed to the alteration in the number/or distribution of COs (Lamb et al., 2005). COs are also important for creating genetic diversity during meiosis. In mitosis, COs between sister chromatids are genetically silent. However, COs derived from recombination between homologous chromosomes can result in loss of heterozygosity (LOH). If recombination occurs between non-allelic loci, CO formation can result in gross chromosomal rearrangement (GCR) that is deleterious to genome stability. In summary, COs are actively promoted in meiosis whereas COs are suppressed in mitosis during HR-mediated DSB repair.

Meiotic CO formation is mediated by two different pathways. The major CO pathway is dependent on the ZMM complex, which includes at least seven structurally diverse proteins, i.e. Zip1-4, Mer3, Msh4 and Msh5 (Lynn et al., 2007). Zip1 is a component of the synaptonaemal complex and mediates stable homologue juxtaposition through its polymerization. Zip2 and Zip3 are required for the initiation of Zip1 polymerization along the homologous chromosomes while Mer3,

Msh4 and Msh5 are directly involved in the DNA recombination process (Lynn et al., 2007; Perry et al., 2005). This ZMM-dependent pathway is subjected to CO interference, which is a phenomenon that prevents COs from being close together and ensures each pair of homologues forms at least one CO (an obligate CO) (Lorenz and Whitby, 2006). The ZMM-independent pathway, in contrast, is dependent on the Mus81-Mms4/Eme1 complex for the promotion of CO formation, presumably via the model shown in Figure 1.6. COs are not distributed evenly across the genome. It has been shown that COs are actively suppressed in the centromeric regions as CO in this region may result in segregation defects (Rockmill et al., 2006). It has also been proposed that the regulation of COs events involves the higher order of chromosome structure (Mets and Meyer, 2009). Mets and Meyer proposed that in *C.elegans,* condensins I and II, which are responsible for compacting chromosome structures during meiosis, regulates the number and distribution of DSBs and hence CO levels (Mets and Meyer, 2009).

Mitotic COs are actively suppressed because of their potentially deleterious consequences to genome stability. COs are associated with only 5-20% of spontaneous or DSB-induced mitotic GC events in *S.cerevisiae* (Ira et al., 2003; Malkova et al., 1996). The current models suggest that COs can either be generated via HJ resolution in DSBR or the Mus81-dependent CO pathway (Figure 1.1 (i) and 1.6). Hence it has been proposed that COs are suppressed by channeling recombination intermediates into repair pathways that only generate NCO products, i.e. SDSA and dHJ dissolution pathways (Figure 1.1 (ii)) (Ira et al., 2003; Paques and Haber, 1999; Wu and Hickson, 2003).

1.6. The Role of HR in Replication Fork Management

DNA is potentially vulnerable to damage during S-phase when the two strands of duplex DNA are unwound to allow DNA replication. The replication of a DNA lesion-containing template can result in replication fork stalling or collapse, depending on the nature of the lesions. HR has been intricately linked to the repair of damaged replication forks (Cox et al., 2000; Kowalczykowski, 2000; Marians, 2000; Rothstein et al., 2000). For instance, when a replication fork runs into a single strand nick on the template strand, a one-ended DSB can be generated and this can result in the collapse of the replication fork (Figure 1.8). The recovery of collapsed replication forks is highly dependent on the BIR pathway (Llorente et al., 2008). The one-ended DSB can be processed to form a 3' single stranded DNA tail, which will mediate Rad51-dependent strand invasion into the intact homologous duplex, forming a D-loop. DNA replication can then be primed from the invading strand thus restoring a replication fork (Figure 1.8, step (a)). The HJ that forms as a result of strand exchange event must be resolved to ensure proper segregation of the fully replicated, but linked DNAs (Figure 1.8).

Lesions in the form of DNA-adducts may stall the progression of replication forks without necessarily causing fork breakage and thus a DSB (Figure 1.8). The mechanisms of restarting a stalled replication fork are different, depending on whether the DNA lesion is present on the lagging or the leading strand template. Due to the discontinuous nature of lagging strand synthesis, DNA lesions on the lagging strand template may not necessarily cause replication forks to stall but can be bypassed by re-priming a nascent Okazaki fragment synthesis downstream of the lesion. The DNA lesion and the single-stranded gap left behind can then be repaired

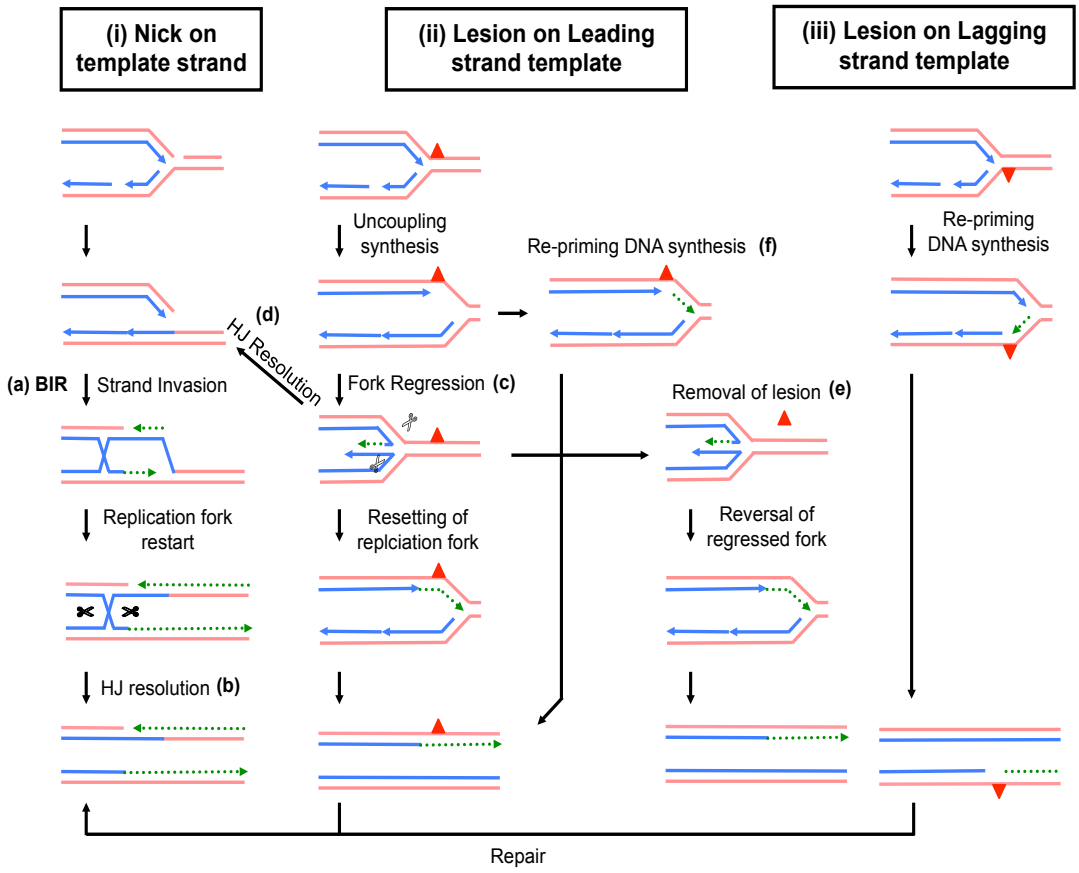


Figure 1.8. Models for the restoration of stalled/collapsed replication forks. A replication fork that runs into a nick on a template strand results in the formation of a DSB, which can initiate a BIR event (a) and restart a replication fork. The HJ formed during the single-ended strand invasion has to be resolved (b) prior to/after replication fork restart. DNA lesions on the leading strand template result in stalled replication forks and thus uncoupling of leading and lagging polymerases. Regression of the stalled replication fork (c) allows DNA synthesis using the nascent lagging strand as a template. Resetting of the fork thus allows lesion bypass and restoration of replication fork progression. Alternatively, a regressed fork can also be resolved by a HJ resolvase (d) to form a one-ended DSB and thus restore a replication fork by BIR (a). Fork regression also provides more access for the recognition/repair of DNA lesions (e) to allow replication to restart following resetting the fork. A replication fork stalled by lesions on the leading strand template can also be bypassed by re-priming DNA synthesis (f) at sequences downstream of the lesions. Similarly, lesions on lagging template can be bypassed by re-priming DNA synthesis downstream of the DNA lesions, but without fork stalling.

by HR, post-replicatively (Figure 1.8). In contrast, DNA lesions on the leading strand template will cause a replication fork to stall and potentially lead to the uncoupling of leading and lagging strand polymerases (Higuchi et al., 2003; McInerney and O'Donnell, 2004; Pages and Fuchs, 2003). The continued progression of lagging strand DNA synthesis will result in the formation of a single strand gap ahead of the nascent leading strand.

Replication forks stalled at leading strand template lesions have also been proposed to undergo a process known as fork regression (Figure 1.8, step (c)) (Atkinson and McGlynn, 2009; McGlynn and Lloyd, 2000). Fork regression is achieved by re-annealing of the parental strands in the stalled replication fork resulting in the annealing of the released nascent strands, forming a structure commonly known as a "chicken foot" (Figure 1.8, step (c)). The primary role of fork regression is to facilitate replication fork restart via several potential mechanisms discussed below. Fork regression allows replication template switching to occur, in which bypass of the lesion can be effected by the extension of the leading strand using the nascent lagging stand as a template, followed by the reversal of the "chicken foot" structure (Figure 1.8, step (c)). Fork regression and reversal will therefore allow the bypass of the blocking lesion, which can be repaired post-replicatively. Moreover, replication fork regression will reposition the blocking lesion back into the parental duplex, thereby facilitating the access of repair enzymes to the blocking lesion, assuming that access to the lesion may be restricted by the large replication machinery (Figure 1.8, step (e)). Replication fork restart via fork regression can also be achieved by resolving the "chicken foot" structure that resembles a four-way HJ. The "resolution" of a regressed fork will

result in the formation a one-ended DSB and a homologous template, which can be used to restore a replication fork using BIR (Figure 1.8, step (d)).

In *E.coli,* fork regression can be catalysed by the DNA helicase RecG (McGlynn and Lloyd, 2000). RecG helicase promotes fork regression by simultaneously translocating along the leading and lagging strand template DNA, thus resulting in a coupled unwinding and annealing of the nascent strands (McGlynn and Lloyd, 2000, 2001; McGlynn et al., 2001). In humans, RecQ helicases BLM, WRN and RECQ5β have been shown to catalyse regression of model fork substrates *in vitro* (Kanagaraj et al., 2006; Machwe et al., 2006; Machwe et al., 2007; Ralf et al., 2006). FANCM is another human helicase that can also catalyse regression of model forks *in vitro* (Gari et al., 2008b). Because Fanconi Anaemia (FA) cells are especially sensitive to DNA cross-linking agents, the role of fork regression by FANCM has been proposed to counter the movement of replisomes towards interstrand crosslinks, thus providing access for the repair enzymes to the lesion. Consistent with this, Fml1, the FANCM orthologue in *S.pombe*, was shown to promote regression of model fork substrate *in vitro* (Sun et al., 2008). This finding led Sun and co-workers to propose that Fml1 uses its fork regression activity to promote Rad51-dependent recombination at stalled replication forks (Sun et al., 2008). In *S.cerevisiae*, Rad5, which functions in a post-replication repair pathway for the repair of UV damaged DNA, can also catalyse *in vitro* fork regression via concerted unwinding of the daughter strands of the fork substrate, despite having no detectable helicase activity on linear DNA structures (Blastyak et al., 2007; Johnson et al., 1994). Despite the increasing number of enzymes identified to catalyse replication fork *in vitro*, there is still no direct evidence that

these enzymes catalyse fork regression *in vivo*. This is largely due to the technical difficulties in the direct detection of regressed forks *in vivo.*

It has also been shown *in vitro* using the *E.coli* replication machinery, that leading strand synthesis can be re-initiated *de novo* downstream of the lesion, hence restoring the replication fork while bypassing the DNA damage (Figure 1.8, step (f)) (Heller and Marians, 2006). However, it is unknown if such leading strand re-priming event does occur *in vivo* in *E.coli* or in eukaryotic organisms.

1.7.Mismatch Repair (MMR) Pathway

1.7.1. MMR proteins

The MMR pathway, which is highly conserved from bacteria to humans, plays an important role in the maintenance of genome stability. The primary role of the MMR pathway is to repair mismatches generated during DNA replication. In the absence of a functional MMR pathway, DNA mismatches in the form of base-base mismatch or insertion/deletion loops (IDLs) can lead to deletion, substitution or frameshift mutations.

The major understanding of the mechanistic steps of MMR have been analysed in *E.coli*, in which an *in vitro* MMR reaction was reconstituted from purified components (Constantin et al., 2005; Lahue et al., 1989). In *E.coli*, MMR is initiated by the binding of a MutS homodimer to mismatch DNA, thereby facilitating an ATP-dependent recruitment of MutL. MutL then relays the recognition by MutS to both the MutH endonuclease and UvrD helicase. MutH incises the unmethylated strand (nascent strand) whereas UvrD helicase unwids the ends of the nicked mismatch containing strand from the template, thereby providing

an entry of single strand exonuclease for the exonucleolytic degradation until the mismatch is removed. The resulting gap is finally filled by the replicative DNA polymerase.

S.cerevisiae contains six MutS homologs (MSH1-6) and four MutL homologs (MLH1-3, PMS1) (Surtees et al., 2004). The members of MSH and MLH proteins form heterodimers, respectively, which display specialized functions with respect to the types of DNA substrates on which they act (Schofield and Hsieh, 2003). The Msh2-Msh6 (MutSα) complex targets base-base mismatches and small IDLs while the Msh2-Msh3 (MutSβ) complex recognizes IDLs up to 12 nucleotides in length (Figure 1.9 (i)). The early stages in MMR pathway can be separated into distinct steps: mismatch recognition, stable binding and MMR factor recruitment. The conserved domain I in Msh2 contributes to a non-specific DNA binding activity and is critical for Msh2-Msh3-dependent MMR but not for MMR function of Msh2-Msh6 (Figure 1.9 (ii)). Domain I of Msh3 is also essential for DNA mismatch binding specificity (Figure 1.9 (ii)) (Lee et al., 2007). Similarly, Msh6 possesses a mismatch recognition domain that is essential for the stable binding of Msh2-Msh6 complex to DNA mismatches, as evidenced by the failure of Msh2-Msh6-340 (with mutations in the Msh6 recognition domain) in recognizing DNA mismatches (Figure 1.9 (ii)) (Bowers et al., 2000). In addition, all Msh proteins contain Walker A and Walker B motifs and have been shown to bind and catalyse ATP hydrolysis (Figure 1.9 (ii)) (Alani, 1996; Blackwell et al., 2001; Junop et al., 2001; Owen et al., 2005). The ATPase activity of Msh2-Msh6 heterodimeric complex is modulated by DNA mismatches and is essential for conformational changes of the complex which are required for the recruitment of downstream repair factors (Bowers et al., 2000). The importance of the ATPase activity of

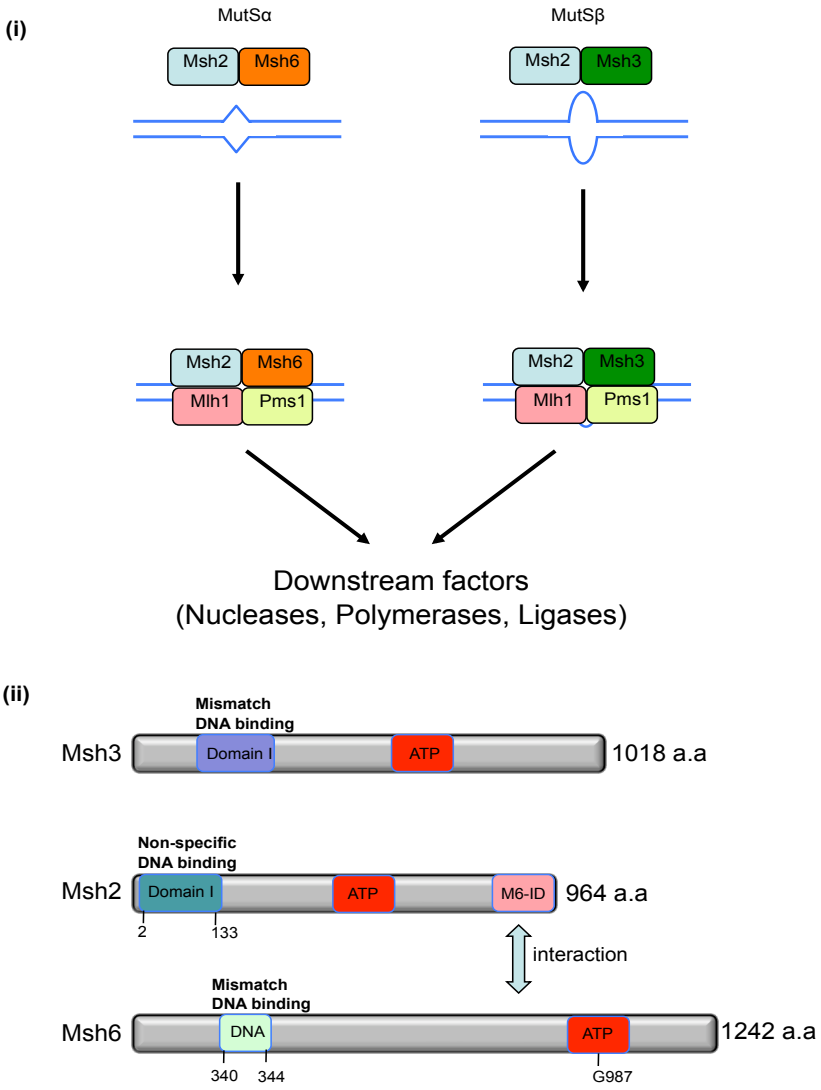


Figure 1.9. MMR proteins. (i) Substrate specificities of MSH and MLH proteins in eukaryotic MMR. Msh2-Msh6 (MutSα) complex recognises a single bp mismatch substrate, whereas Msh2-msh3 (MutSβ) complex recognises an IDL substrate. Mlh1-Pms1 (MutLα) complex forms a complex with either MutSα or MutSβ to recruit downstream MMR factors. (ii) The protein domains of *S.cerevisiae* Msh2, Msh3 and Msh6. The length of each protein is represented by the number of amino acids designated to the right of each protein. Domain I of Msh3 and DNA-binding domain of Msh6 (340-344) are required for the binding to DNA mismatches. Domain I of Msh2 binds DNA non-specifically, irrespective of the presence of mismatches. All Msh proteins possess ATP-binding domains. Mutation at G987 position of ATP-binding domain of Msh6 abolishes its ATP hydrolysis activity and thus its MMR activity. Msh2 interacts with Msh6 via its C-terminal domain. DNA: mismatch DNA-binding domain; ATP: ATP-binding domain; M6-ID: Msh6-interaction domain.

Msh2-Msh6 complex is highlighted by the fact that although Msh2-Msh6 can bind to palindromic insertion substrate, which can form stem-loop structures, with high affinity *in vitro*, palindromes do not stimulate the ATPase activity of Msh2-Msh6 heterodimeric complex and therefore such substrates cannot be repaired by Msh2-Msh6-mediated MMR (Bowers et al., 2000).

1.7.2. The roles of MMR in HR

Apart from repairing mismatches arising from DNA replication errors, the MMR pathway is closely associated with the HR pathway. Components of the MMR pathway are responsible for the mismatch correction of heteroduplex DNA formed during meiotic HR, the suppression of recombination between divergent sequences and the removal of 3' non-homologous tail during DSB repair (Schofield and Hsieh, 2003).

1.7.2.1. Mismatch correction of heteroduplex DNA

Heteroduplex DNA, in the form of single bp mismatches or IDLs, are formed during recombination between sequences that are not completely identical. Similar to mismatch correction during post-replication repair, the recognition of single bp mismatch and IDLs are dependent on Msh2-Msh6 and Msh2-Msh3 complexes, respectively. In meiotic cells of yeast, the repair of mismatches on heteroduplex DNAs can lead to different outcomes. Mismatches can undergo repair and produce a non-Mendelian segregation of alleles in tetrad spores (e.g. 2:6 or 6:2 segregation), more commonly known as GC. The mismatches can also be repaired to give a Mendelian (2:2) ratio of alleles, which is termed restoration. If the

mismatches escape MMR during meiosis, postmeiotic segregation (PMS) of alleles in the ratio of 5:3 will occur. Indeed, mutations in MMR genes result in the elevation in the frequency of PMS (Paques and Haber, 1999; Schofield and Hsieh, 2003).

1.7.2.2. Suppression of recombination between divergent sequences

The MMR machinery also plays an essential anti-recombination role that limits recombination between similar but non-identical sequences. This function of MMR is critical for the prevention of potentially lethal genome rearrangements mediated by HR between dispersed repetitive elements in eukaryotic genomes. In *E.coli*, biochemical studies showed that the rate and extent of heteroduplex DNA formation catalyzed by RecA between diverged sequences is reduced by MutS and MutL (Fabisiewicz and Worth, 2001; Worth et al., 1994). Similarly, it was shown in a study using an inverted repeat assay system, that the presence of even a single mismatch within an otherwise completely homologous sequences could inhibit mitotic recombination in budding yeast and this inhibition is dependent on an intact MMR pathway (Datta et al., 1997). Additional mismatches have a cumulative negative effect on the recombination rate (Datta et al., 1997). In the absence of both Msh2 and Msh3, budding yeast displays GC tract lengths that are about 50% longer than in wild type cells (Chen and Jinks-Robertson, 1998). Meiotic heteroduplex DNA formed in the absence of MMR machinery is also 65% longer than those formed in wild type cells (Chen and Jinks-Robertson, 1999). These observations suggest that the MMR machinery actively inhibits recombination by blocking

heteroduplex extension in the presence of mismatches. In budding yeast, it has been shown that *sgs1Δ* cells have increased recombination rates between homeologous sequences that are 91% identical (Myung et al., 2001). This effect of *sgs1Δ* is synergistic with the effect of an *msh2Δ* mutation (13-fold increase), which results in a 96-fold increase homeologous recombination in the *sgs1Δmsh2Δ* double mutant (Myung et al., 2001). Consistently, using an HO-induced DSB system to study SSA between homeologous repeats, Sugawara et al. found that Msh2 and Msh6, but not other MMR proteins, are required for heteroduplex rejection together with Sgs1 helicase (Sugawara et al., 2004). This led to the proposal that during homeologous recombination, mismatches on heteroduplex DNAs are recognized by Msh2-Msh6 complex, which recruits Sgs1 to effect heteroduplex rejection using its DNA unwinding activity, in order to suppress homeologous recombination (Sugawara et al., 2004).

The anti-recombination role of MMR pathway is also important in the suppression of telomeric recombination, as shown by the finding that loss of the MMR pathway promotes alternative lengthening of telomeres and hence cellular proliferation in the absence of telomerase (Rizki and Lundblad, 2001). Telomeres in *S.cerevisiae* are composed of irregular $G_{1\text{-}3}T$ repeats and hence mismatches are often produced when telomeric sequences recombine. In the absence of the MMR machinery, homeologous recombination between telomeric sequences is no longer suppressed and hence alternative lengthening of telomeres can occur.

1.7.2.3. The removal of 3' non-homologous tail during DSB

Msh2 and Msh3, but not other MMR pathway components, are also essential for the processing of non-homologous ends during mitotic recombination (Harfe and Jinks-Robertson, 2000; Paques and Haber, 1999). Msh2-Msh3 complex is required for the recognition of the branched DNA structures with 3' non-homologous tail and concertedly act with the Rad1-Rad10 complex which is required for the cleavage of such 3' flap structures (Sugawara et al., 1997). This 3' non-homologous tail removal function is essential during the repair of diverged sequences, when homeology at the invading 3' single-stranded end prevents the priming of DNA synthesis (Sugawara et al., 1997). This function is also vital during SSA-mediated DSB repair, in which the 3' tails generated from the sequences between two direct repeats have to be removed (Figure 1.1(iii)) (Sugawara et al., 1997).

1.7.2.4. Meiosis-specific Role of MMR

Some MMR proteins also have meiosis-specific functions. Msh4 and Msh5 form a heterodimeric complex that has no MMR activity, but instead has been implicated in promoting a subset of meiotic COs (Hoffmann and Borts, 2004; Hollingsworth et al., 1995; Ross-Macdonald and Roeder, 1994). *S.cerevisiae* Msh4-Msh5 promotes meiotic CO formation in a pathway that is non-epistatic with Mus81-Mms4 (Abdullah et al., 2004; de los Santos et al., 2003). In addition, purified human MSH4-MSH5 complex has been shown to bind specifically to HJs and can translocate away from the HJ in an ATP-dependent manner (Snowden et al., 2004). Based on these genetic and biochemical observations, Msh4-Msh5

complex has been proposed to form a sliding clamp that can embrace homologous chromosomes, thereby stabilizing the D-loop and leading to the formation of a dHJ structure, which can be resolved into CO products (Snowden et al., 2004). Other MMR proteins that have meiotic-specific functions are Mlh1 and Mlh3. Using two-hybrid and co-immunoprecipitation (IP) approaches, it was shown that Mlh1 and Mlh3 form a heterodimeric complex (Wang et al., 1999). Mlh1-Mlh3 complex has been implicated in promoting meiotic COs, because in the absence of Mlh3, the meiotic CO level is decreased to only 70% of the wild type levels while the cells maintain normal level of MMR activity (Wang et al., 1999). This phenotype is also accompanied by increased chromosome non-disjunction during meiosis I and reduced spore viability in *mlh1Δ* mutant cells (Hoffmann et al., 2003). This led to the suggestion that Mlh1 may also have a solely structural role during meiotic CO (Hoffmann and Borts, 2004). It is unknown if Msh4-Msh5 and Mlh1-Mlh3 function co-ordinately in meiotic CO promotion, because direct interaction between the two complexes could not be detected using co-IP (Hoffmann and Borts, 2004). Rather, Mlh1-Mlh3 complex has been shown to form a "supercomplex" with Sgs1-Top3 complex (Wang and Kung, 2002). It was suggested that Mlh1-Mlh3 may promote CO formation indirectly by sequestering the dHJ dissolution activity of Sgs1-Top3.

1.8. Aims of Study

HR-mediated DSB repair can be accomplished via different pathways, giving rise to either NCO or CO products. CO formation is vital during meiosis but it can as well be detrimental if it occurs between non-allelic loci during mitotic recombination. My thesis focuses on the investigation of the regulation of mitotic

CO suppression in the HR of *S.cerevisiae*. The roles of Mph1 and Sgs1 helicases on HR pathway choice during DSB repair were investigated. As MMR pathway is closely associated with HR and has previously been shown to affect CO frequency during DSB repair, the interaction of MMR pathway with these helicases, in the context of CO suppression, was also examined.

CO products are generated primarily by the resolution of HJ intermediates formed during DSBR. In bacteria, HJ resolution is carried out by the RuvABC resolvasome. RuvABC is classified as the HJ resolvase in *E.coli* based largely on the fact that RuvABC can catalyse *in vitro* HJ resolution by introducing two symmetrical nicks on opposite strands of model HJ substrate. Several eukaryotic enzymes have been shown to display *in vitro* HJ resolution activity similar to the bacterial RuvC resolvase. However, the activities of some of these eukaryotic enzymes are slightly different to the RuvC resolvase activity, in that they resolve synthetic HJ asymmetrically or in some cases they resolve other branched DNA structures more efficiently than model HJs. These inconsistencies have raised the question of whether these eukaryotic nucleases indeed resolve HJs *in vivo*.

Conventional genetic assays are not ideal for the direct analysis of HJ resolution step, which is the terminal stage, of the multi-step and multi-pathway HR. While CO formation can be inferred as a successful HJ resolution event, the failure of CO formation may be caused by defects in any stages of the HR pathway. The fact that some factors, e.g. Sgs1, can act in multiple stages in HR complicates the interpretation of a failure of CO formation even further. Therefore, in order to study the *in vivo* HJ resolution step directly and quantitatively, a transformation-based HJ resolution system, performed using a plasmid-borne HJ substrate, has been developed. The details of the HJ resolution system and the over-lapping roles

of some of the eukaryotic "HJ resolvases" *in vivo* will be discussed in the results section.

Chapter Two

2. Materials and Methods

2.1.Materials

All media was sterilised by autoclaving, with the exception of galactose, which was filter-sterilised to prevent isomerisation. Standard sterile techniques were employed.

2.1.1. *Escherichia coli* strains

E.coli were utilised for the cloning and amplification of plasmids. Cells were grown in Luria-Bertani (LB) agar plates or liquid medium (Formedium). Agar plates and liquid LB media were supplemented with 100mg/l ampicillin (Sigma) to select for plasmid retention. All strains were grown at 37°C.

***E.coli* Strains**	**Genotype**	**Source**
DH5α	F^- endA1 glnV44 thi-1 recA1 relA1 gyrA96 deoR nupG Φ80d*lacZ*ΔM15 Δ(*lacZYA-argF*)U169, hsdR17(r_K^- m_K^+), λ–	Invitrogen
JW2861-2	*ΔxerD745::kan*	Coli Genetic Stock Center, Yale
RM40	*lac*PO-*xerC*	McCulloch *et al.* (1994)

Table 1. *E.coli* strains used in this thesis.

2.1.2. *Saccharomyces cerevisiae* strains

Cells were grown on yeast extract-peptone-dextrose (YPD) liquid media or agar plates. For prototroph selection, cells were grown on Synthetic Defined (SD) liquid or solid media with appropriate amino acids omitted. YPD, SD media and all amino acids were supplied by Formedium. Induction media for the expression of genes from the *GAL1* promoter was YP media with 2% raffinose and 2% galactose as the combined carbon sources in place of glucose. All

strains were grown at 30°C. Refer to Table 2 for all *S.cerevisiae* strain used in this thesis.

2.1.3. Plasmids

Refer to Table 3 for all plasmids used in this thesis. Refer to the respective chapters for plasmids constructed for this thesis.

2.1.4. Oligonucleotides

All oligonucleotides used in this thesis were manufactured by Sigma-aldrich custom oligo services. Please refer to Appendices for sequences of specific oligonucleotides indicated in the text.

2.1.5. RusA purified proteins

Purified RusA protein was kindly supplied by Professor Robert Lloyd.

2.1.6. Antibody

Antibodies used in this thesis are as follow:-

- M2 monoclonal anti-FLAG mouse antibody (Sigma)
- Monoclonal anti-HA mouse antibody (Roche)
- Monoclonal anti-mouse antibody HRP conjugate (Sigma)

Strains	Genotype	Source
BY4741	*Mat a*; *his3Δ1*; *leu2Δ0*; *met15Δ0*; *ura3Δ0*	a
BY4741 *ade2Δ*	BY4741 (*ADE2::KanMX4*)	a
mph1Δ	BY4741(*MPH1::KanMX4*)	a
sgs1Δ	BY4741 (*SGS1::KanMX4*)	a
msh2Δ	BY4741 (*MSH2::KanMX4*)	a
msh3Δ	BY4741 (*MSH3::KanMX4*)	a
msh6Δ	BY4741 (*MSH6::KanMX4*)	a
rad51Δ	BY4741 (*RAD51::KanMX4*)	a
dnl4Δ	BY4741 (*DNL4::KanMX4*)	a
rad1Δ	BY4741 (*RAD1::KanMX4*)	a
msh2Δ mph1Δ	BY4741 (*MSH2::KanMX4 MPH1::Hyg*)	b
msh2Δ sgs1Δ	BY4741 (*MSH2::KanMX4 SGS1::Hyg*)	b
msh3Δ mph1Δ	BY4741 (*MSH3::KanMX4 MPH1::Hyg*)	b
msh6Δ mph1Δ	BY4741 (*MSH6::KanMX4 MPH1::Hyg*)	b
rad1Δ mph1Δ	BY4741 (*RAD1::KanMX4 MPH1::Hyg*)	b
msh2Δ1	BY4741 (*MSH2::MSH2(Δ2-133))*	b
msh2Δ1 mph1Δ	BY4741 (*MSH2(Δ2-133) MPH1::Hyg)*	b
msh6-340	BY4741 (*MSH6::msh6-340* (LYEK➔CFAE))	b
msh6-340 mph1Δ	BY4741 (*MSH6::msh6-340* (LYEK➔CFAE) *MPH1::Hyg*)	b
msh6-G987D	BY4741 (*MSH6::msh6-G987D)*	b
msh6-G987D mph1Δ	BY4741 (*MSH6::msh6-G987D MPH1::Hyg*)	b
mph1Δ sgs1Δ	BY4741 (*MPH1::KanMX4 SGS1::KanMX4*)	b
YDM01	BY4741 (*MPH1::FLAG-MPH1*)	b
YDM02	BY4741 (*FLAG-MPH1 HA-MSH2*)	b
YDM03	BY4741 (*FLAG-MPH1 MSH6-HA*)	b
yen1Δ	BY4741 (*YEN1::KanMX4*)	a
yen1::natR	BY4741 (*YEN1::NatR*)	b
mus81Δ	BY4741 (*MUS81::KanMX4*)	a
slx1Δ	BY4741 (*SLX1::KanMX4*)	a
mus81Δ yen1Δ	BY4741 (*MUS81::KanMX4 YEN1::NatR*)	b
mus81Δ rad1Δ	BY4741 (*MUS81::KanMX4 RAD1::NatR*)	b
mus81Δ slx4Δ	BY4741 (*MUS81::KanMX4 SLX4::NatR*)	b
slx1Δ yen1Δ	BY4741 (*SLX1::Hyg YEN1::NatR*)	b
slx4Δ yen1Δ	BY4741 (*SLX4::Hyg YEN1::NatR*)	b
rad1Δ yen1Δ	BY4741 (*RAD1::Hyg YEN1::NatR*)	b
mus81Δ yen1Δ slx1Δ	BY4741 (*MUS81::KanMX4 YEN1::NatR SLX1::Hyg*)	b
mus81Δ yen1Δ rad1Δ	BY4741 (*MUS81::KanMX4 YEN1::NatR RAD1::Hyg*)	b
mus81Δ yen1Δ slx4Δ	BY4741 (*MUS81::KanMX4 YEN1::NatR SLX4::Hyg*)	b
mus81Δ yen1Δ rad1Δ slx1Δ	BY4741 (*MUS81::KanMX4 YEN1::NatR RAD1::KlURA3 SLX1::Hyg*)	b
mus81Δ yen1Δ slx4Δ slx1Δ	BY4741 (*MUS81::KanMX4 YEN1::NatR SLX4::KlURA3 SLX1::Hyg*)	b
$yen1^{EE}$	BY4741 (*YEN1::yen1-(E193A, E195A))*	b
$mus81^{DD}$	BY4741 (*MUS81::mus81-(D414A, D415A))*	b
$mus81^{DD}yen1^{EE}$	BY4741 (*YEN1::yen1-(E193A, E195A) MUS81:: mus81-(D414A, D415A))*	b

a Open Biosystems
b Constructed in this study

Table 2. *S.cerevisiae* strains used in this thesis.

Plasmid	***Source***
pRS401	American Type Culture Collection (ATCC)
pRS412	ATCC
P1	this study
P2	this study
JM (*cer*-containing)	this study
pADE2(400/400)	this study
pADE2(1bp/mis)	this study
pGSHU	Storici and Resnick (2006).
pGSKU	Storici and Resnick (2006).
pEAE129 (*GAL10-msh6-340*)	Bowers, J *et al.* (2000)
pEAE216 (*GAL10-msh6-G987D*)	Bowers, J *et al.* (2000)
p4339 (TA::MX4-natR switcher cassette)	(Tong and Boone, 2006)
pSD115	McCulloch *et al.* (1994)
pYES	ATCC
pYES-RusA	Hocine Mankori
pYES-RusA(D70N)	Hocine Mankori
pRS415	ATCC
pRS313	ATCC

Table 3. Plasmids used in this thesis.

2.2.Methods

2.2.1. Bacterial assays

2.2.1.1. *E.coli* transformation

2.2.1.1.1. Chemically competent cells (Preparation)

A single colony of cells was inoculated into 10ml LB medium and cultured overnight at 37° with agitation. The pre-culture was then added into 200ml of pre-warmed LB medium and incubated at 37°C with agitation until the culture reach an OD_{600}=0.4. The culture was chilled for 15minutes in an ice bath and poured into chilled 50ml falcon tubes. Cells were harvested by centrifugation at 3000rpm for 10minutes at 4°C. The cell pellet was resuspended in 100ml of ice-cold Solution A (100mM RbCl, 50mM $MnCl_2.4H_2O$, 30mM KOAc, 10mM $CaCl_2$, 15% glycerol, pH5.8). After 5 minutes incubation on ice, the cell suspension was pelleted at 1500rpm for 5 minutes at 4°C. The pellet was resuspended in 20ml ice-cold solution B (10mM MOPS, 10mM RbCl, 75mM $CaCl_2$, 15% glycerol). Aliquots (50µl) of competent cells were transferred into pre-chilled 1.5ml Eppendorf tubes, which were then flash-frozen and stored at -80°C.

2.2.1.1.2. Transformation for chemically competent cells

A 50µl aliquot of chemically competent cells was used per plasmid transformation. Cells were slowly thawed on ice. Ligation mixture or purified plasmids in a volume of no more than 5µl was added. The transformation mix

was incubated on ice for 30 minutes, followed by a heat-shock at 42°C for 60s. 750μl of pre-warmed SOC medium was then added and the cells were incubated at 37°C for 1 hour. The transformation mix was diluted as necessary and plated on LB agar plate with appropriate antibiotic. Plates were incubated at 37°C overnight.

2.2.1.1.3. Electrically competent cells (Preparation)

A single colony of *E.coli* was inoculated into 50ml of LB medium overnight at 37°C. The overnight cultured is inoculated into 500ml of pre-warmed LB medium and was incubated at 37°C with agitation. Cultures with an OD_{600}=0.4 were rapidly harvested by centrifugation at 1000g for 15 minutes at 4°C. The cell pellet was resuspended in 500ml of ice-cold distilled water. The pellet was washed and spun down for another five times using ice-cold distilled water before finally being resuspended in 2ml of ice-cold 10% glycerol. The cell suspension was then aliquoted into 40 ice-cold 1.5ml eppendorf tubes, which were then flash-frozen in dry ice before storage in -80°C.

2.2.1.1.4. Electroporation

A 50μl aliquot of electrically competent cells was thawed out on ice. Cells were transferred to a pre-chilled 2mm electroporation cuvette (Equibio). DNA in a volume of no more than 5μl was added. Electroporation was carried out using Bio-rad Gene pulser II with setting at 1.8kV, 200Ω and 25μF. The cells were then added to pre-warmed SOC buffer and were incubated at 37°C for 90 minutes before plating on LB agar plate (supplemented with 100μg/ml Ampicillin) with appropriate dilution.

2.2.1.2. Small-scale isolation of plasmid DNA (Miniprep)

Single colony isolated from an *E.coli* transformation was cultured in a 1.5 ml liquid LB media supplemented with 100mg/l ampicillin overnight. Plasmid DNA was isolated from pelleted cells using QIAprep® Spin miniprep kit (Qiagen) according to the manufacturer's instructions.

2.2.1.3. Large-scale isolation of plasmid (Maxi- & Gigaprep)

For maxiprep, a single bacterial colony was inoculated into 5ml LB medium containing Ampicillin at 37°C for 8 hours. 500µl of starter culture was added to 250ml of LB medium containing ampicillin and this was incubated at 37°C overnight in an orbital incubator. Cells were harvested by centrifugation at 6000 x *g* (JA10.500 rotor, Beckman Avanti J-25 centrifuge) for 15 min at 4°C. Preparation of plasmid DNA was performed using the Qiagen plasmid maxi kit according to manufacturer's instructions. Giga-prep of the JM-HJ cell pellet was performed using Qiagen Giga kit according to the manufacturer's instructions.

2.2.1.4. Cloning of pADE2(400/400) & pADE2(1bp/mis)

pADE2(400/400) was constructed by the following modifications to plasmid pRS401: ARS209 was amplified by PCR using primers A1 and A2 using plasmid pRS412 as a template. The resulting fragment was cloned into pRS401 via AatII sites introduced into the ARS-containing fragment by PCR to generate pRS401/ARS. A fragment containing nucleotides 200-999, of the *Saccharomyces cerevisiae ADE2* ORF was amplified by PCR using BY4741

genomic DNA as a template and cloned into pRS401/ARS via PCR-introduced BamHI sites to generate pADE2(400/400). The homeologous *ADE2* sequence used to generate pADE2(1bp/mis) was synthesized by Genscript and cloned into pRS401/ARS via Xma1 and Spe1 sites to generate pADE2(1bp/mis). The orientation and sequences of inserts of all clones were confirmed by sequencing. The sequences of the *ADE2*-derived fragments in the plasmids used in this study are shown in Appendices.

2.2.1.5. Cloning of P1 & P2

Refer to Chapter 4.

2.2.1.6. Cloning of JM

A single *cer* sequence was amplified from plasmid pSD115 using primers A and B (Figure 2.1) to generate PCR-cer1 that was cloned directionally into pRS411 via Kpn1 and XhoI restriction sites to create pRS411-cer1. The *HIS3* marker was amplified by PCR using primers C and D and plasmid pRS313 as a template to generate fragment PCR-HIS3 (Figure 2.1). A second *cer* sequence was amplified by PCR using primers E and F and plasmid pSD115 as a template to generate fragment PCR-cer2 (Figure 2.1). pRS411-cer1 that had been linearised by XhoI was co-transformed with PCR-HIS3 and PCR-cer2 fragments into *dnl4Δ* cells. HR-mediated Recombineering was used to link the three linear DNA fragments, which contain overlapping regions of homologies. The JM product was selected for by screening for both methionine and histidine prototrophy (Figure 2.1). *dnl4Δ* cells were chosen as a host for "recombineering" such that high fidelity HR system, and not NHEJ, would be

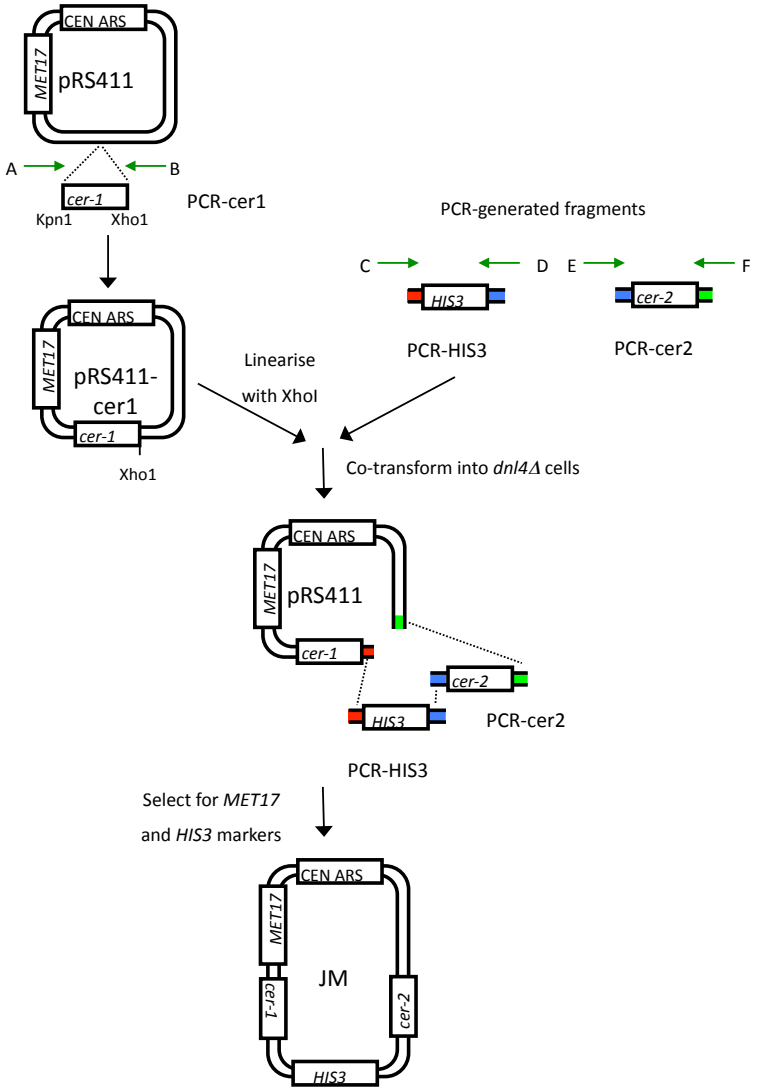


Figure 2.1 Schematic diagram outlining the construction of JM. PCR-cer1, PCR-HIS3 and PCR-cer2 were amplified from their respective plasmid vectors by PCR (see text for details). PCR-cer1 was cloned directionally into pRS411, forming pRS411-cer1. Xho1-linearised pRS411-cer1, PCR-HIS3 and PCR-cer-2 fragments were co-transformed into *dnl4Δ* cells for linking by recombineering. Yeast clones with JM were selected by screening for methionine and histidine prototrophy. Coloured boxes indicate regions of homology that facilitate recombination-mediated circularisation of pRS411-cer1 to form JM. Green arrows indicate primers used in PCR.

used to assemble the three DNA fragments. Plasmid DNA from independent clones was transformed into an *xerD*$^-$ strain of *E.coli* (JW2861-2) and the construction of JM confirmed using a combination of restriction digestion and sequence analysis.

2.2.2. Yeast assays

2.2.2.1. *S.cerevisiae* transformation

All yeast transformation in this study was carried out using Frozen-EZ Yeast Transformation II™ Kit (Zymo Research). Briefly, 10ml of yeast culture at OD_{600}=0.8~1.0 was harvested by centrifugation at 500*g* for 4 minutes. The cell pellet was washed with 10ml of EZ 1 solution and re-pelleted by centrifugation. The cell pellet was then re-suspended in 1ml of EZ 2 solution. 50µl of competent cells was mixed with 0.2-1µg of DNA and 500µl of EZ3 solution was added. The mixture was then incubated at 30°C for 45 minutes with agitation. Finally, the cell mixture was appropriately diluted and plated on selective solid media. The plates were incubated at 30°C for 2-4 days.

2.2.2.2. *Delitto perfetto*: site-directed mutagenesis

Site-directed mutagenesis throughout this thesis was performed using the *delitto perfetto* approach as described by (Storici and Resnick, 2006). Briefly, a COunterselectable REporter (*CORE*) cassette, consisting of both hygromycin/Geneticin resistance marker and *KlURA3* auxotrophic marker flanked by 50 nucleotides homologous to the appropriate flanking regions of the genomic target locus, was amplified by PCR using *Takara Ex Taq*™

polymerase (Lonza) and either pGSHU (*hyg*) or pGSKU (*KanMX4*) as template. The *CORE* cassette was inserted by standard DNA targeting procedures at the desired genomic locus. The *CORE* cassette was then removed by counter-selecting against the *KlURA3* marker on 5-FOA media after transforming the cells with Integrative Recombinant Oligonucleotides (IROs) containing the desired mutation sequences. Positive clones, which were 5-FOA resistant and hygromycin/geneticin sensitive, were identified by PCR and sequencing at the desired genomic locus. *S.cerevisiae* mutants that have been constructed using this technique and the respective IROs used are shown in Table 4.

***S.cerevisiae* mutant strains**	**IROs**
msh6-340	XhoI fragment of pEAE129
msh6-G987D	XhoI fragment of pEAE216
msh2Δ1	Genscript custom-made sequences
$yen1^{EE}$	Oligos EE-forward & reverse
$mus81^{DD}$	Oligos DD-forward & reverse
FLAG-Mph1	Genscript custom-made sequences
HA-Msh2	Genscript custom-made sequences
Msh6-HA	Genscript custom-made sequences

Table 4. Mutants generated by *delitto perfetto* and their respective IROs.

2.2.2.3. Gene knock-out in *S.cerevisiae*

S. cerevisiae gene knock-out (KO) in this thesis was performed by conventional gene replacement strategy as described in (Burke et al., 2000). In summary, a KO cassette consisting of either hygromycin or geneticin resistance cassette flanked by 50 nucleotides homologous to the flanking regions of the genomic

target locus was amplified from pGSHU or pGSKU, respectively. The KO cassette was then transformed into the appropriate strain using the standard yeast transformation protocol. Positive clones were selected by appropriate antibiotic resistance and were confirmed by PCR and sequencing. *yen1Δ* drug-resistance cassette switch from *KanMX4* to *NatMX* was performed by transforming the *NatMX*-containing EcoRI fragment of p4339 plasmid into *yen1Δ*.

2.2.2.4. *S.cerevisiae* genomic DNA extraction

5ml yeast cultures were grown to saturation in the appropriate liquid media at 30ºC. Cells were pelleted by centrifugation and resuspended in 100µl of lysis buffer (2% Triton X-100, 1% SDS, 100mM NaCl, 10mM Tris-Cl (pH8), 1mM EDTA) and 100µl of phenol:chloroform:isoamyl alcohol (25:24:1). 0.3g of acid-washed glass beads was added and cells were lysed in a FastPrep FP120 bead beater (Thermo Electron Corporation). DNA in the aqueous phase was used directly in PCR or *E.coli* tranformation. For Southern blot analysis, DNA in the aqueous phase was first ethanol precipitated, resuspended in 400µl of TE plus 3µl of a 10mg/ml solution of RNase A and incubated at 37°C for 5 minutes. The RNase treated genomic DNA was finally ethanol precipitated and resuspended in 50µl of TE for Southern blot analysis.

2.2.2.5. Plasmid Break Repair Assay

Repair substrates, i.e. pADE2(400/400) and pADE2(1mis/bp), were linearized by digestion with Hpa1 (New England BioLabs) and gel purified using a Qiagen Gel extraction kit. Cells were transformed with 400ng cut DNA using the

Frozen-EZ yeast transformation II™ kit (Zymo Research) following the manufacturer's recommendations. The cut plasmid was also co-transformed with pYES plasmid to control for variations in inter-sample transformation efficiencies in order to calculate absolute repair efficiencies. Following transformation, cells were plated onto the appropriate media to select for repair events (SD-met) or pYES transformants (SD-ura) and plates were incubated at 30°C for 3 days. In repair assays, transformants arising as red or white colonies were counted and scored as CO and NCO repair events, respectively. Repair assays were performed a minimum of three times.

2.2.3. Biochemistry

2.2.3.1. Restriction endonuclease reaction

All restriction endonucleases used in this thesis were purchased from New England Biolabs and standard restriction reaction (i.e. 20µl unless otherwise stated) were performed according to manufacturer's recommendation.

2.2.3.2. Annealing and ligation

For the generation of "flapped" molecules, five times molar excess of Flap1 and Flap2 were incubated with P1-Gap and P2-Gap respectively in annealing buffer (10mM $MgCl_2$ and 50mM Tris-HCl pH 8.0) at 80°C. The mixtures were cooled down gradually in thermostable container overnight to allow efficient base pairing between the complementary regions of the Flap1 and Flap2 to the gapped regions of the plasmids. Subsequent ligation reaction between the oligonucleotides and gapped plasmids were carried out in the annealing buffer

at 14°C for 18 hours using approximately 400 units of T4 DNA ligase (NEB) with the addition of 1mM ATP and 5mM dithiothreitol (DTT). Excess oligonucleotides which are not ligated to the "gapped" molecules were removed by Gel Extraction kit (Qiagen). Equimolar P1-Flap and P2-Flap were used in the annealing and ligation reaction for the generation of X-JM. The annealing and ligation conditions were as described above.

2.2.3.3. Holliday junction cleavage assay

Cleavage of 30ng of JM by 100nM RusA was assayed at 37°C in buffer SCB (25mM Tris-HCl, pH 8.0, 1mM DTT, 100 µg/ml bovine serum albumin, 10% (v/v) glycerol) 1mM $MgCl_2$. Reactions (20µl final volume) were terminated by adding 5µl of stop mixture (25% SDS, 200mM EDTA, 10mg/ml proteinase K) and incubated for a further 10 min at 37°C to deproteinize the mixture. The reaction products were separated in a 0.7% agarose gel and were visualized by ethidium bromide staining.

2.2.3.4. Caesium Chloride density gradient centrifugation

500-600µg DNA, 200µl Ethidium bromide and 4.3g of Caesium chloride were dissolved in TE (pH8.0) to a final volume of 4.5ml. The mixture underwent ultracentrifugation at 65,000 rpm for 17-18 hours at 4°C using Beckman ultracentrifuge Beckman L8-80M. The "supercoiled" DNA fraction was extracted using syringe and needle. Isoamyl alcohol was added to the DNA solution, mixed and centrifuged. The top layer of isoamyl alcohol containing Ethidium bromide was extracted. This organic extraction process was repeated at least 4 times until the aqueous phase was completely clear. The Caesium

chloride in the clear DNA solution was dialysed out twice in 2L of 10mM Tris-Cl (pH7.5). DNA was finally ethanol precipitated and resuspended in TE (pH8.0).

2.2.3.5. DNA gel purification

Plasmid DNA was separated by gel electrophoresis on 0.7% TAE agarose gel. DNA stained with Ethidium Bromide was then visualized under a UV transluminator (FotodyneUV model 3-3000). Small gel slices were excised and DNA was purified using Qiagen gel purification kit. DNA in larger gel slices was purified by electro-elution into 1 X TAE at 100V for 2hrs or 30V for overnight using dialysis cassette (Novagen) or dialysis tube (Pierce). Electro-eluant was then concentrated by standard ethanol precipitation.

2.2.3.6. Polymerase Chain Reaction (PCR)

TaKaRa Ex Taq™ polymerase was used throughout this study. General reaction mixture (50μl) containing 1.25 unit *TaKaRa Ex Taq*™ polymerase, 1X *Ex Taq* buffer, 2.5mM of each dNTP, 0.2-1.0μM of forward and reverse primers, DNA template <500ng, and distilled water was prepared. PCR was run in Eppendorf mastercycle gradient machine using general programme as stated below: -

94°C	2min	
94°C	30sec	⎡
55°C	30sec	⎢ 25-30 cycles
72°C	~1min/ 1kb DNA amplification	⎣
72°C	5min	

PCR products were either cleaned up with QIAquick® PCR purification kit (Qiagen) according to the manufacturers instructions for sequencing, or concentrated by ethanol precipitation for yeast transformation reaction.

2.2.3.7. Southern blotting and hybridisation

Southern blots in this study were carried out by upward capillary transfer of DNA from agarose gels according to standard protocols (Sambrook et al., 1989). Restriction fragment or PCR products were used to prepare the probe for Southern hybridisation. The probes were prepared using Amersham Rediprime II Random Prime Labelling system and dCTP[α-^{32}P]- 3000Ci/mmol (Perkin Elmer) as radio-labelled deoxynucloetides.

2.2.3.8. Western blotting

S. cerevisiae cells were lysed in lysis buffer (150mM NaCl, 10% glycerol, 1mM DTT, 1mM EDTA, protease inhibitor cocktail (Roche)), by vortexing the mixture using glass-beads in a bead-beater (Thermo scientific). Clear whole cell lysate was obtained after 15 min centrifugation at 13,200 rpm on a tabletop microcentrifuge, followed by 1 hour of 45,000 rpm ultracentrifugation at 4°C. Whole cell lysates were separated on 7% SDS-polyacrylamide gels. The proteins were transferred to Hybond-C extra membrane (Amersham Pharmacia Biotech) in a protein transfer buffer (25mM Tris, 192mM glycine, 20% methanol) using a wet transfer unit (Bio-rad). The membrane was incubated with blocking buffer (5% (w/v) semi-skimmed powered milk, 0.1% TWEEN-20 in 1X PBS) for 1 hour. The membrane was incubated with the primary antibody (diluted 1:1000 in blocking buffer) for 2 hours at room temperature. The membrane was then washed 3 times in wash buffer (0.1% TWEEN-20 in 1X PBS), with each wash lasting for 15 minutes. The membrane was then incubated with a secondary antibody conjugated to horse-radish peroxidase (HRP) at a dilution of 1:1000 for 1 hour at room temperature. After 3 times washing as

described before, the protein was detected using an Enhanced Chemiluminescence (ECL) kit (Amersham Pharmacia Biotech).

2.2.3.9. DNA sequencing

All DNA sequencing in this study was carried out by DNA sequencing service in the Weatherall Institute of Molecular Medicine.

2.2.3.10. Immunoprecipitation

IP of proteins tagged with either HA or FLAG epitopes was performed according to manufacturer's instruction, using anti-HA antibody and Protein A-sepharose or agarose conjugate of anti-FLAG antibody (Sigma) respectively. Briefly, cell lysates were first incubated with anti-HA antibody for 1.5 hours with constant agitation at 4°C. The cell lysate was then incubated with Protein A-sepharose for 1.5 hours with constant mixing at 4°C. The lysate-sepharose mixture was spun down at 3000xg for 2 mins, washed for at least 5 times, before elution in 100ul of PBS at 95°C for 5 minutes. For FLAG IP, the cell lysate was added directly to the anti-FLAG agarose conjugate for 1.5 hours, washed for at least 5 times, before elution using 3XFLAG peptides at 150ng/µl.

2.2.4. Statistics

Statistical analyses for the CO frequencies of plasmid break-repair assay (Chapter three) and the relative HJ resolution efficiencies (Chapter Five) were performed in Excel (Microsoft Office) and on http://www.physics.csbsju.edu/stats/KS-test.html. Each data set was tested for normal distribution using Kolmogorov–Smirnov goodness-to-fit test, rejecting

the null hypothesis (H_0; 'data fits a normal distribution') at the level of $P < 0.05$. All the data were consistent with a normal distribution and were compared with the appropriate control experiment using a two-tailed, unpaired, two-sample Student's *t*-test.

Chapter Three

3. Mph1 requires mismatch repair-independent and -dependent functions of MutSα to regulate crossover formation during homologous recombination repair

3.1.Introduction

HR is essential for the repair of both "accidental" and "programmed' DSBs. As described in Chapter 1, several HR models have been proposed to act under different circumstances and produce different outcomes (Paques and Haber, 1999). The DSBR pathway gives rise to both COs and NCOs, whereas SDSA and dissolution pathways generate exclusively NCOs. CO suppression is of particular importance during mitotic HR to prevent deleterious genome rearrangements, such as chromosome translocations and LOH, when sister chromatid or homologous chromosomes are not available to be used as templates for HR repair. Two helicases, Mph1, which dismantles D-loops to prevent strand invasion, and Sgs1, which catalyzes dHJ dissolution together with Top3 and Rmi1, have been proposed to suppress CO formation during HR (Ira et al., 2003; Prakash et al., 2009).

Apart from recognizing and repairing DNA mismatches that arise during replication, the MMR pathway also plays a key role in regulating homeologous recombination (Bailis and Rothstein, 1990; Datta et al., 1996; Selva et al., 1995). Together with the Rad1-Rad10 complex, MutSβ acts to regulate a subset of COs during HR (Nicholson et al., 2006; Saparbaev et al., 1996; Symington et al., 2000). MutSα has also been shown to function together with Sgs1 in heteroduplex rejection to prevent homeologous recombination during SSA (Goldfarb and Alani, 2005; Sugawara et al., 2004). Such interactions between components of HR and MMR pathways led us to raise the question if the anti-recombination function of Mph1 is also associated with the MMR machinery during DSB repair.

To address this question, a plasmid break repair assay was used in our study. A plasmid containing a DSB is efficiently repaired by HR when introduced into

S.cerevisiae cells, provided that the DSB occurs within sequence that is homologous to the yeast chromosomal sequences. This assay was chosen because the HR-mediated repair of a linearised plasmid transformed into yeast parallels many aspects of the repair of a single genomic DSB as both processes require and are modulated by many of the same genetic factors (Bartsch et al., 2000; Ira et al., 2003; Paques and Haber, 1999; Symington, 2002; Szostak et al., 1983; Welz-Voegele and Jinks-Robertson, 2008). In this chapter, the roles of the Mph1 and Sgs1 helicases and the MMR MutSα complex, in the context of CO suppression during plasmid-borne DSB repair, will be discussed.

3.2. Results

3.2.1. Validation of a Plasmid Break Repair Assay to study DSBR

The plasmid pADE2 (400/400), which carries an autonomous replicating sequence (ARS) and the *MET17* auxotrophic marker, was used as a substrate in a plasmid break repair assay. In addition, pADE2 (400/400) contains 800bp sequences corresponding to residues 200-999 of the endogenous *ADE2* ORF in *S.cerevisiae* (Figure 3.1). The recognition sequence of the HpaI restriction enzyme, which forms blunt-ended breaks, is present in the middle of the 800bp *ADE2* homologous sequence of pADE2 (400/400). When linearised by HpaI, the two 400bp terminal homologies can be used to target the endogenous *ADE2* gene for repair following transformation. Blunt-end DSB is generated in order to prevent recircularisation of the linearised plasmid *in vivo* by end joining (Boulton and Jackson, 1996; Milne et al., 1996). By selecting for the *MET17* auxotrophic marker after transformation with linear pADE2 (400/400), two classes of repair products are expected to form,

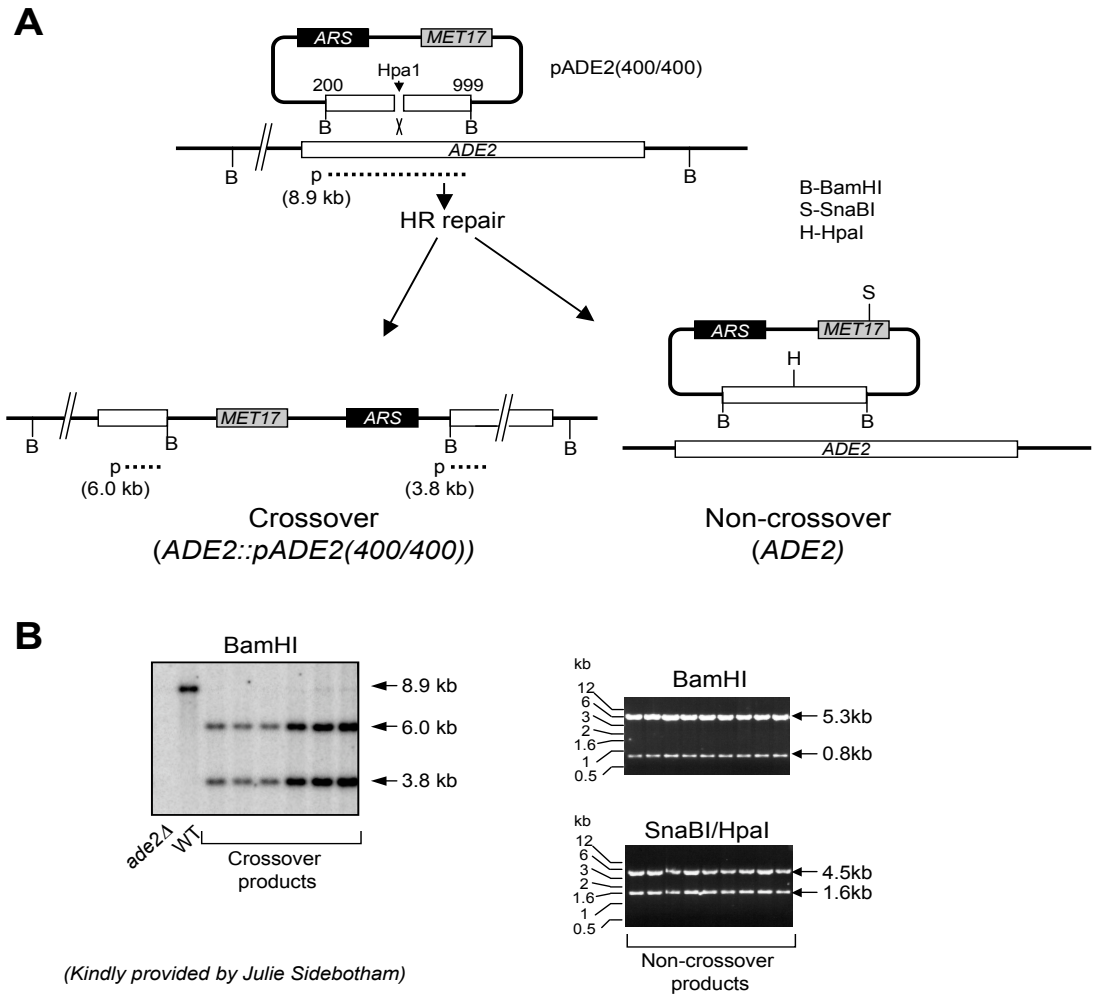


Figure 3.1 Plasmid-break Repair Assay. (A) Schematic diagram showing plasmid-break repair assay in which pADE2(400/400) is repaired using the endogenous *ADE2* locus. HR repair of pADE2(400/400) is mediated via a 800p fragment comprising residues 200-999 of the *ADE2* open reading frame. pADE2(400/400) is linearized at a unique Hpa1 site which bisects the *ADE2* fragment into two 400bp regions of homology to *ADE2*. The structures of CO and NCO repair products are shown. (B) Confirmation of repair products. Left panel: Integration of pADE2(400/400) into the *ADE2* locus in CO events was confirmed by Southern analysis; dotted line labeled p in (A) indicates the sequence used as a probe and the sizes in parentheses indicate the predicted BamHI fragments detected in wild-type (lane 2) and six independent CO products (lanes 3–8). Shown also is genomic DNA from *ade2Δ* cells (lane 1). *Right panels*: Intact circular pADE2(400/400) plasmid was recovered from NCO products and analyzed by BamHI or SnaBI and HpaI digestion, as indicated. Predicted sizes of restriction fragments are shown on the right of each panel.

i.e. CO and NCO products (Figure 3.1A). CO formation results in the integration of the pADE2 (400/400) into the endogenous *ADE2* locus, thus inactivating the *ADE2* gene. The *ADE2* gene is required for purine biosynthesis to convert P-ribosylaminoimidazole (AIR) to P-ribosylaminoimidazolecarboxylate (CAIR) (Xiao, 2006). CO formation that inactivates *ADE2* causes the accumulation of AIR, which is a red pigment, and hence results in a red cell phenotype. In contrast, NCO formation following DSB repair results in the recircularisation of pADE(400/400) without disrupting the endogenous *ADE2* locus and consequently the cells that form NCO products are white. Therefore, the frequency of CO formation following DSB repair can be visually determined by measuring the percentage of red colonies formed as a total of repair events.

To confirm further that the repair of pADE2 (400/400) is mediated by HR but not NHEJ DSB repair, the requirement for a homologous template and Rad51 for pADE2 (400/400) DSB repair was tested. In order to determine the absolute total repair efficiencies, repair substrates were co-transformed with an unrelated plasmid, pYES, which contains a different auxotrophic marker to pADE2 (400/400), to control for differences in transformation efficiencies. In the absence of the *ADE2* gene or Rad51, the repair efficiencies of pADE2 (400/400) DSB was less than 10% of that seen in wild type cells (Figure 3.2A). In contrast, repair efficiency in the absence of Dnl4, an enzyme essential for catalysing the ligation step of NHEJ, is approximately 80% relative to the wild type strain (Figure 3.2A). These results confirm that the DSB of pADE2 (400/400) is repaired by HR.

To ensure that the repair products are generated by HR using the *ADE2* locus as a repair template, CO products were analysed by Southern hybridisation whereas NCO products were recovered and transformed into *E.coli*. Plasmids were

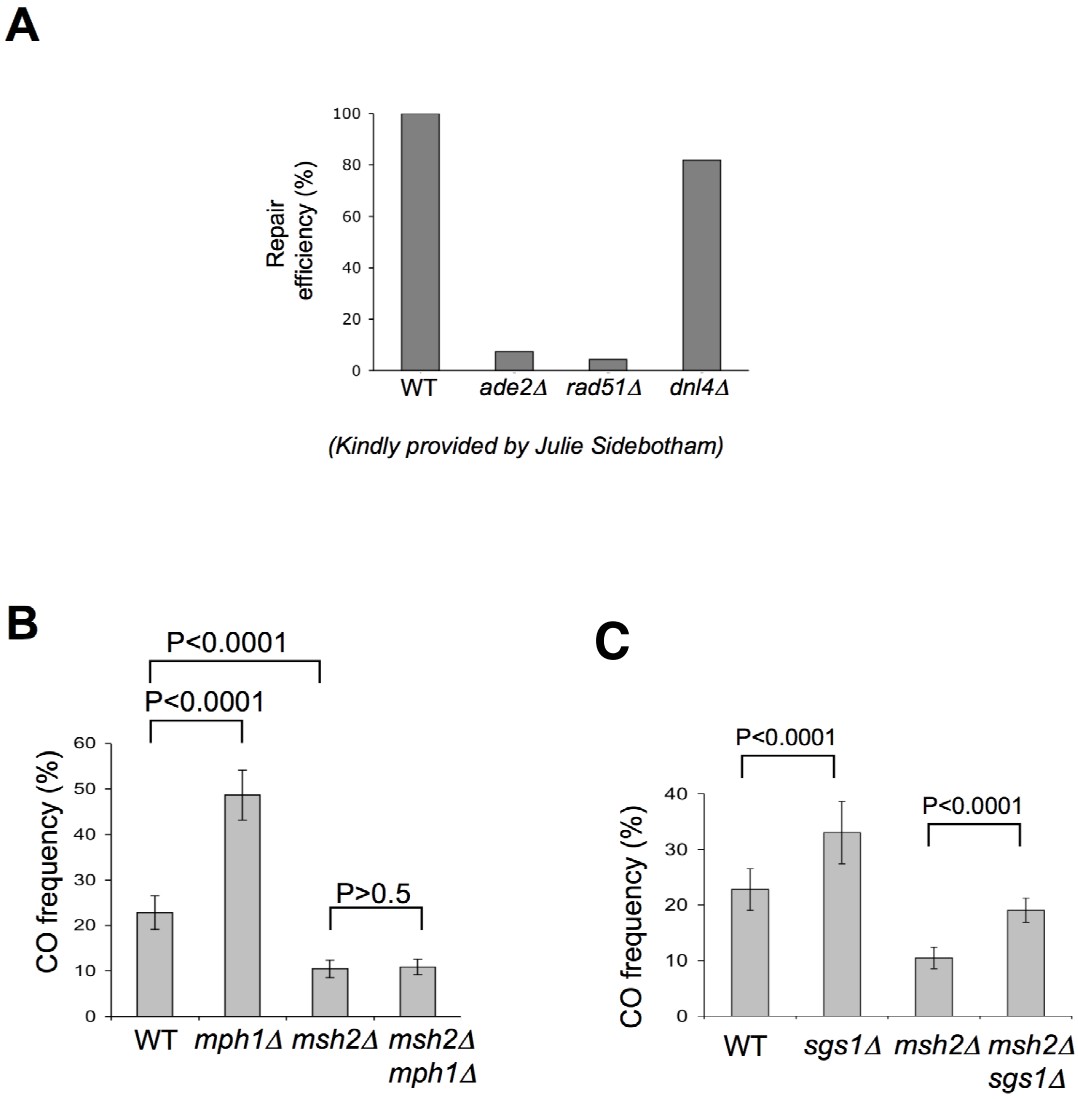


Figure 3.2 pADE2(400/400) is repaired by HR and the anti-CO function of Mph1, but not Sgs1, requires Msh2. (A) The repair efficiencies of HpaI-linearized pADE2(400/400) in wild type and mutant backgrounds as indicated. (B-C) CO frequency following repair of pADE2(400/400) in various genetic backgrounds, as indicated. Bars are means with standard deviations.

then prepared and subjected to restriction digestion analysis. To distinguish CO products from the wild type *ADE2* locus, genomic DNA was digested with BamHI and was probed with the 800bp *ADE2* targeting fragment (Figure 3.1B). As predicted, the genomic DNA prepared from red colonies (CO) that had been digested with BamHI produced two shorter DNA fragments, of 6.0kb and 3.8kb, as compared to the 8.9kb fragment detected in wild type cells (Figure 3.1B, left panel). This indicates that pADE(400/400) plasmid had integrated into the endogenous *ADE2* locus but not other ectopic sites. BamHI restriction digestion of the NCO products generated the predicted 5.3kb and 0.8kb fragments (Figure 3.1B, upper right panel). SnaBI and HpaI double digestions also converted NCO repair products into 1.6kb and 4.5kb fragments (Figure 3.1B, lower right panel). The reconstitution of the HpaI site in the 800bp homology thus indicates that the DSB was accurately repaired, consistent with error-free HR-mediated DSB repair.

3.2.2. Mph1, but not Sgs1, specifically suppresses a subset of crossovers that are generated in a MutSα-dependent manner

In wild type cells, the CO frequency for the repair of pADE2(400/400) was found to be ~20% (Figure 3.2B). This frequency is increased ~2-fold in *mph1Δ* cells (Figure 3.2B). This figure is comparable to the 3-fold increase in CO formation observed during the repair of an HO endonuclease-induced genomic DSB (Prakash et al., 2009). This result suggests that Mph1 functions to suppress COs during extra-chromosomal, as well as chromosomal DSB repair. To gain insight into the mechanism by which Mph1 influences CO formation, potential genetic interactions

between Mph1 and other factors known to influence CO frequency, such as MMR factors and Sgs1, were investigated.

In an *msh2Δ* background, repair of pADE2(400/400) results in a CO frequency of ~10%, which is approximately half of that of the wild type strain (Figure 3.2B). This suggests that a subset of COs is generated in an Msh2-dependent manner. However, in contrast to wild type cells, the loss of Mph1 in an *msh2Δ* background did not result in an increase in CO frequency (Figure 3.2B). This indicates that Mph1 normally suppresses a subset of COs that are generated in an Msh2-dependent manner. Like Mph1, Sgs1 has also been shown to suppress COs during inter-chromosomal and plasmid gap HR repair (Ira et al., 2003; Welz-Voegele and Jinks-Robertson, 2008). This is confirmed by the observation that in the absence of *SGS1*, CO frequency following pADE2 (400/400) repair is increased by approximately 1.5 fold as compared to wild type cells (Figure 3.2C). However, in contrast to Mph1, loss of *SGS1* still results in a ~two-fold increase in CO frequency in the absence of *MSH2* (Figure 3.2C). This suggests that COs that are suppressed by Sgs1 are generated in an Msh2-independent manner. In summary, Mph1 and Sgs1 suppress distinct classes of COs that differ in their dependence on Msh2. This is consistent with the suggestion that Mph1 acts non-epistatically with Sgs1 in attenuating CO formation during DSB repair (Prakash et al., 2009).

As described in Chapter 1, Msh2 binds to Msh3 and Msh6 to form MutSβ and MutSα of the MMR pathway, respectively, for the recognition of different classes of mismatch substrates. Apart from its mismatch recognition role in the MMR pathway, Msh2 has also been implicated in mitotic recombination. Msh2-Msh3, together with the Rad1-Rad10 endonuclease, is required for the removal of non-homologous DNA ends during GC and SSA repair (Saparbaev et al., 1996;

Sugawara et al., 1997). This raised the question of which of these functions of Msh2 are required to generate COs that are suppressible by Mph1. To address this question, potential interactions between Mph1 and Msh3, Msh6 and Rad1 were investigated. The loss of *MPH1* resulted in a two- to three-fold increase in CO formation in *msh3Δ* and *rad1Δ* cells (Figure 3.3A). This indicates that the ability of Mph1 to suppress CO does not require the Msh3- and Rad1-dependent functions of Msh2 (Sugawara et al., 1997). However, the loss of *MPH1* does not affect the CO frequency in an *msh6Δ* background (Figure 3.3A). These observations suggest that Mph1 suppresses COs that are specifically generated in a MutSα-dependent manner.

To confirm these observations, endogenous *MSH2* was mutated to form *msh2Δ1,* a separation-of-function allele of *MSH2* that contains an in-frame deletion of residues 2-133 of Msh2 (Lee et al., 2007). The gene product encoded by the *msh2Δ1* allele lacks the entire mismatch recognition-binding domain I of Msh2. As described in the introduction, domain I of Msh2 is essential for the MMR function of Msh2-Msh3 complex, but not for the MMR function of Msh2-Msh6 (Lee et al., 2007). Therefore cells carrying the *msh2Δ1* allele are effectively *msh3Δ* cell with respect to its MMR function, despite the physical presence of wild type Msh3 protein. Repair of pADE2(400/400) in *msh2Δ1* cells resulted in a CO frequency that was reduced compared to wild type cells but comparable to *msh2Δ* or *msh3Δ* cells, consistent with the *msh2Δ1* cells lacking Msh3-dependent functions of Msh2 (Figure 3.3B). However, the loss of *MPH1* from an *msh2Δ1* background resulted in a ~2-fold increase in CO frequency, in contrast to the *msh2Δ* mutant background (Figure 3.3B). This observation confirms the notion that Mph1 specifically suppress a subset of COs generated in a MutSα-dependent, but MutSβ-independent manner.

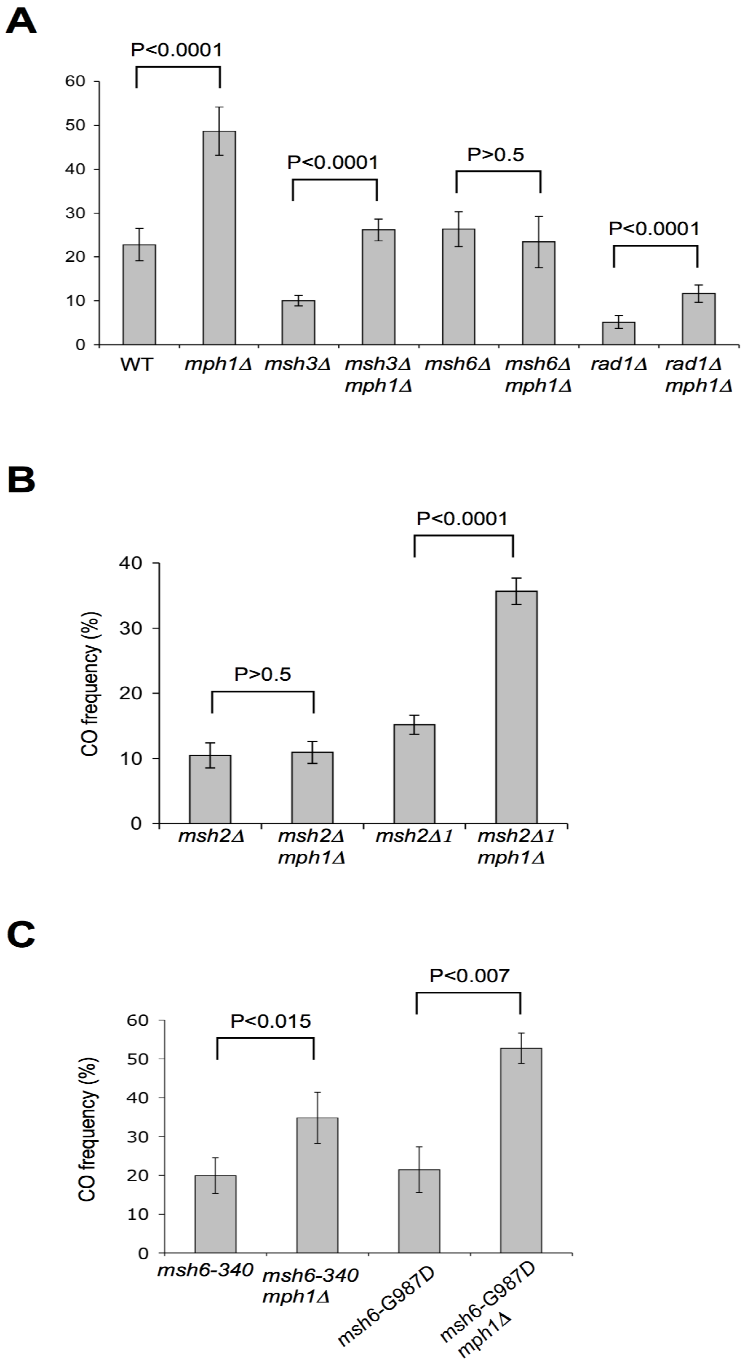


Figure 3.3 The anti-CO function of Mph1 is dependent on MutSα but independent of MutSβ (A) CO frequency during repair of pADE2(400/400) in various genetic backgrounds, as indicated. (B) CO frequency during repair of pADE2(400/400) in the presence of various *msh2* alleles in the presence or absence of Mph1. (C) CO frequency during repair of pADE2(400/400) in the presence of various *msh6* alleles in the presence or absence of Mph1. Bars are means with standard deviations.

3.2.3. The MutSα-dependent suppression of crossovers by Mph1 does not require the mismatch recognition function of MutSα.

The 800bp targeting sequence on pADE2(400/400) is completely homologous to the corresponding sequence of the endogenous *ADE2* gene in *S.cerevisiae*. Hence, Rad51-mediated strand invasion is not expected to generate single base-pair mismatches that could be recognized by the MutSα. Therefore, the observation that COs, which are normally suppressed by Mph1, are generated in a MutSα-dependent manner was somewhat unexpected. This led to the question as to whether the mismatch-recognition function of MutSα is required for the generation of this specific subset of COs. To answer this question, the endogenous *MSH6* allele was replaced with either of two different *MSH6* mutant alleles: *msh6-340* or *msh6-G987D*. The *msh6-340* allele encodes a form of Msh6 containing 4 amino acid substitutions in its mismatch recognition domain (Bowers et al., 2000). Msh2-Msh6-340 complex is incapable of recognizing mismatches but is able to bind homo-duplexes with affinity equal to that of the wild type Msh2-Msh6 complex (Bowers et al., 2000). Msh6-G987D, which has a mutation in the ATP binding domain and thus has a severely reduced ATPase activity when in a complex with Msh2, is able to recognize DNA mismatches but remains stably bound to DNA mismatches (Bowers et al., 1999; Bowers et al., 2000). The ATPase activity of MutSα modulates the conformational change of the complex that affects the subsequent recruitment/activation of downstream MMR factors to perform MMR (Surtees et al., 2004). The *msh6-340* and *msh6-G987D* alleles resulted in a reduced ability or complete inability of the cells, respectively, to recognize base-base

mismatches during HR (see below). However, the loss of *MPH1* from cells carrying either *msh6-340* or *msh-G987D* alleles resulted in a ~2-fold increase in CO frequency (Figure 3.3C). This suggests that the mismatch recognition or processing function of MutSα is not essential for formation of COs that are suppressible by Mph1.

3.2.4. Analysis of a potential interaction between Mph1 and MutSα

The antagonistic genetic interaction of Mph1 and MutSα complex with respect to CO formation raised the question of whether Mph1 physically interacts with the MutSα complex. To address this question, co-IP was performed to see if an Mph1- MutSα complex could be detected. Endogenous Mph1 and Msh2 were tagged with triple-FLAG and triple-HA, respectively, at the N-terminus of each protein in BY4741 cells, forming the YDM02 strain. A strain with a triple-FLAG tagged Mph1 (YDM01) was also constructed as a negative control for the HA-IP. The 110kDa HA-Msh2 protein, which could only be detected in the whole cell extract (WCE) of YDM02, was precipitated by HA-IP (Figure 3.4A, right upper panel). As expected, the 113kDa FLAG-tagged Mph1 (Prakash et al., 2005), was detectable by anti-FLAG antibody in the WCE of YDM01 and YDM02 (Figure 3.4A, left lower panel). However, there was no evidence that FLAG-Mph1 could be detected in the HA-IP of WCE of the YDM02 strain (Figure 3.4A, right lower panel).

To analyse if an interaction between Mph1 and Msh6 could be detected, a triple-HA tag was fused to the C-terminus of Msh6 in YDM01, forming YDM03 strain that expresses both FLAG-Mph1 and Msh6-HA. HA-IPs were performed

with WCEs of wild type, YDM01 and YDM03 strains (Figure 3.4B, Lane 4-6 in both right panels). Msh6-HA of 141kDa was precipitated by HA-IP of YDM03 (Figure 3.4B, Lane 6 in right upper panel). However, FLAG-Mph1 was not detectable in the HA-IP of the WCE of YDM03 (Figure 3.4B, Lane 6 in right lower panel). These results indicate that a physical interaction between Mph1 and Msh6 was not detectable using co-IP.

3.2.5. Modification of pADE2(400/400) to analyse homeologous recombination

The suppression of recombination between homeologous sequences has been shown to be dependent on the MMR pathway (Bailis and Rothstein, 1990; Chen and Jinks-Robertson, 1998). Having revealed an antagonistic interaction between Mph1 and MutSα complex in the regulation of CO formation using a completely homologous substrate, the roles of Mph1 and MutSα in regulating homeologous recombination were also examined. To address this question, a homeologous recombination substrate that is 98.8% homologous to the 200-999 residues of *ADE2* gene was designed. Ten single base changes (labelled 0-9), dispersed approximately every 50-60bp, was introduced into the *ADE2* targeting fragment of pADE(400/400) to form pADE2(1bp/mis) (Figure 3.5A). The position of the HpaI site, which is the site of DSB, remains unchanged in pADE2(1bp/mis). Therefore, HpaI-digested pADE2(400/400) and pADE2(1bp/mis) are identical apart from the 10 base substitutions (Figure 3.5A). Following strand invasion into the endogenous *ADE2* gene, homeology of the pADE2(1bp/mis) substrate is expected to generate base-base mismatches, which would be recognized by MutSα complex

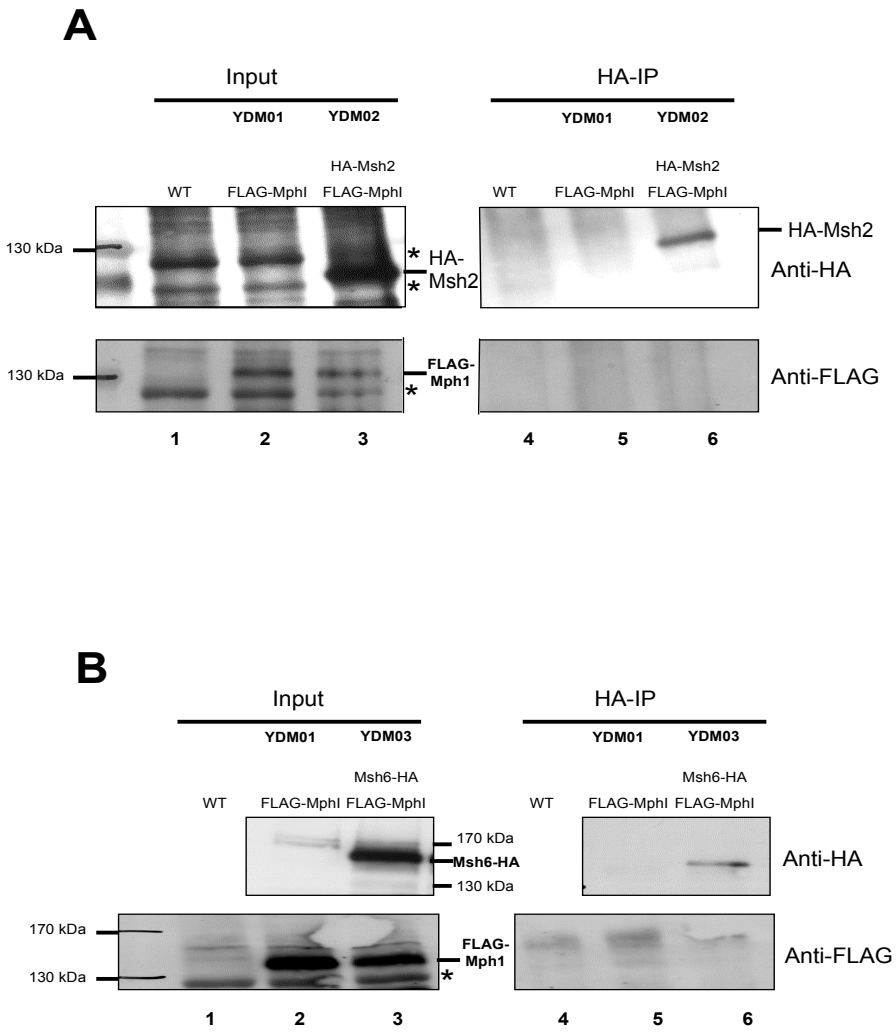


Figure 3.4 Mph1 does not co-IP with Msh2 or Msh6. (A) *Left panels*: WCEs of wild type, YDM01 (FLAg-Mph1), and YDM02 (FLAG-Mph1 & HA-Msh2) strains. *Right panels:* IP of HA-epitope from WCE of wild type, YDM01 and YDM02 strains. Western blots were probed with anti-HA or anti-FLAG, as indicated. (B) *Left panel:* WCE of wild type, YDM01 (FLAG-Mph1) and YDM03 (FLAG-Mph1 & Msh6-HA). *Right panel:* IP of HA epitope from WCE of wild type, YDM01 and YDM03 strains. HA and FLAG epitopes were probed with monoclonal mouse anti-HA (Roche) and anti-FLAG (Sigma) antibodies, respectively. Asterisks represent non-specific detection of proteins in WCE.

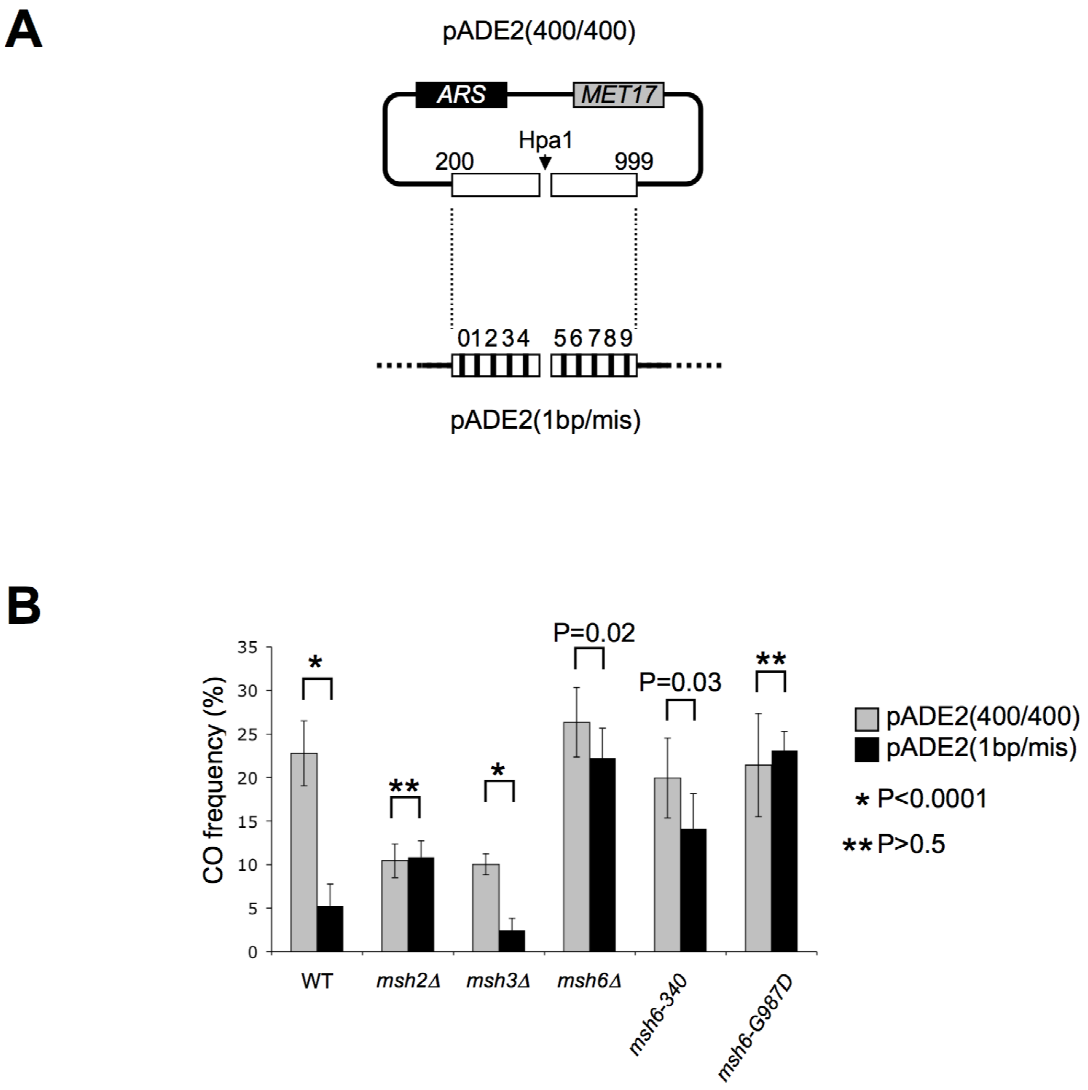


Figure 3.5 Validation of the pADE2(1bp/mis) homeologous substrate (A) Schematic diagram showing the derivation of pADE2(1bp/mis) in which the *ADE2* targeting fragment of pADE2(400/400) has been replaced with a modified version containing 10 single base substitutions as indicated by vertical black bars. The unique HpaI site present in pADE2(400/400) is present in pADE2(1bp/mis). (B) Comparison of CO frequencies arising from the repair of pADE2(400/400) versus pADE2(1bp/mis) in various genetic backgrounds, as indicated. Bars are means with standard deviations.

but not MutSβ of the MMR pathway. To confirm this prediction, plasmid break repair assays using pADE2(1bp/mis) were carried out in MMR mutants. In wild type cells, the CO frequency arising from pADE2(1bp/mis) repair was found to be four-fold lower than that observed during pADE2(400/400) repair (Figure 3.5B). A similar fold reduction was also seen in an *msh3Δ* mutant background (Figure 3.5B). This suggests that COs generated by repair using the homeologous substrate, pADE2(1bp/mis), are suppressed in wild type cells and that Msh3 is not essential for the efficient suppression of CO formation by homeologous recombination. In contrast, *msh2Δ, msh6Δ, msh6-340* or *msh6-G987D* cells have a reduced or complete inability to suppress CO formation by homeologous recombination, as shown by the unchanged/slightly reduced CO frequency when repairing pADE2(1bp/mis) (Figure 3.5B). These observations indicate that the base-base mismatch recognition function of MutSα is essential for the homeology-mediated suppression of COs generated during the repair of pADE(1bp/mis). As shown by the slight reduction in CO frequency when repairing the homeologous substrate, some residual suppression of CO formation was still observed in *msh6Δ* and *msh6-340* mutant cells (Figure 3.5B). This is presumably due to the minor suppression activity of MutSβ on the DSB repair of homeologous substrate, as MutSβ has been shown to demonstrate some overlapping/redundant roles with MutSα in human and yeast cells (Habraken et al., 1996; Umar et al., 1998). A similar minor reduction was not observed in *msh6-G987D* cells possibly because Msh6-G987D exerts a dominant negative effect by binding to the single base mismatch formed during heteroduplex formation, thereby preventing the overlapping suppression activity of MutSβ complex. In summary, pADE2(1bp/mis) is a suitable substrate for the investigation of interaction between Mph1 and MutSα in CO regulation of

homeologous recombination because DSB repair using pADE2(1bp/mis) occurs in a MutSα-dependent, but MutSβ-independent manner.

3.2.6. Mph1 acts redundantly with Sgs1 to effect MutSα-dependent suppression of crossovers during homeologous recombination

In the absence of Mph1, CO frequency of repair using the homeologous substrate was reduced by two-fold. This level of CO suppression is intermediate to that of wild type and *msh2Δ* or *msh6Δ* cells (Figure 3.6A, Lower panel). This indicates that Mph1 is required to efficiently effect MutSα-dependent suppression of COs during the repair of pADE2(1bp/mis). Given the non-epistatic relationship between Mph1 and Sgs1 in suppressing COs during HR (Prakash et al., 2009), and that Sgs1 has previously been implicated in heteroduplex rejection during SSA (Sugawara et al., 2004), the potential role of Sgs1 in CO suppression during homeologous recombination was also examined. In the absence of Sgs1, cells also have a two-fold reduced ability to effect MutSα-dependent suppression of CO formed during the repair of the homeologous substrate as compared to wild type cells (Figure 3.6A). Together, this suggests that Mph1 and Sgs1 may have overlapping functions in suppressing CO formation during homeologous recombination. Indeed, the CO frequencies of pADE2(400/400) and pADE2(1bp/mis) repair were identical in *mph1Δsgs1Δ* double mutant cells (Figure 3.6A, upper panel), indicating that in the absence of Mph1 and Sgs1, *mph1Δsgs1Δ* double mutant cells completely fail to discriminate homeologous and homologous sequences with respect to CO formation.

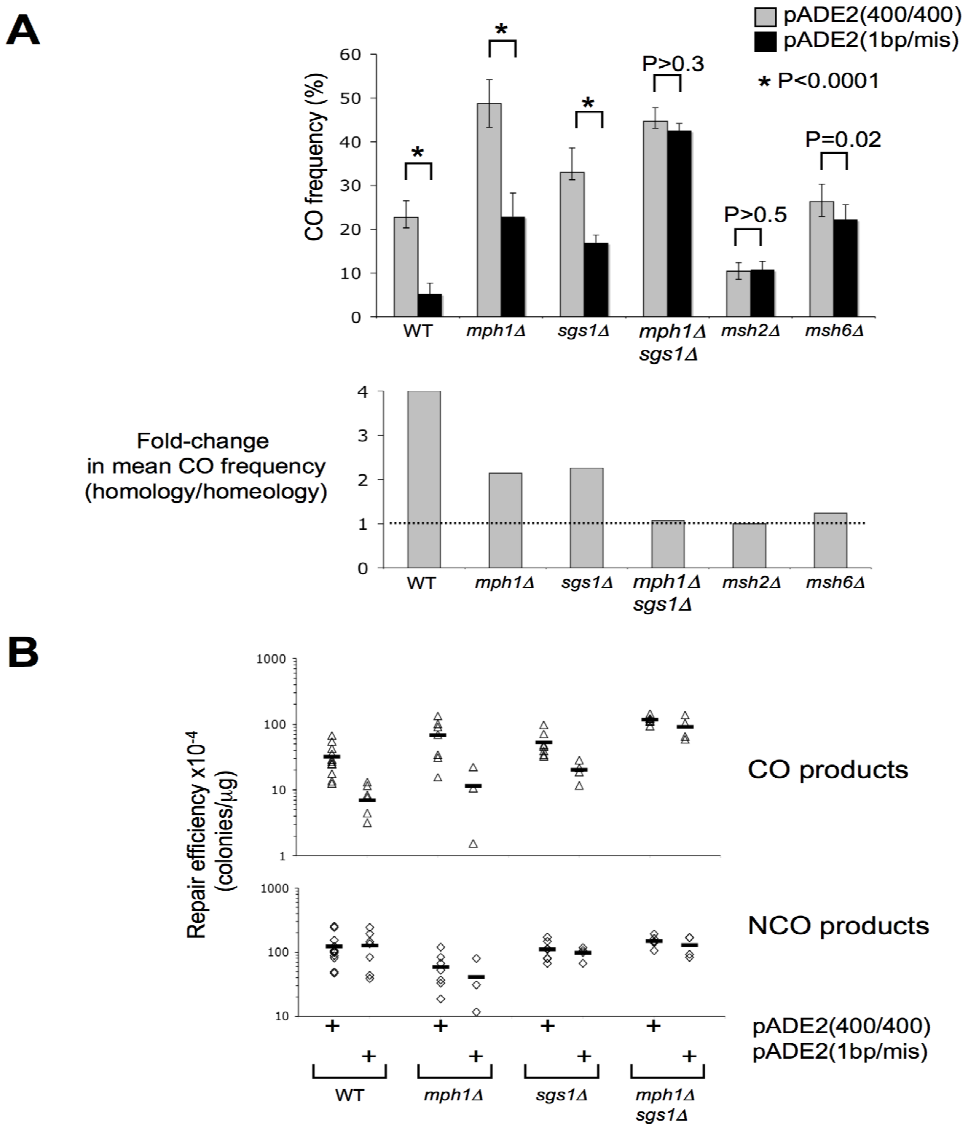


Figure 3.6 Homeology-mediated suppression of COs is defective in *mph1Δ sgs1Δ* cells. (A) Upper panel: Comparison of CO frequencies arising from the repair of pADE2(400/400) versus pADE2(1bp/mis) in various genetic backgrounds, as indicated. Lower panel: Fold-change in mean CO frequencies from upper panel comparing homologous (pADE2(400/400)) and homeologous (pADE2(1bp/mis)) repair substrates. Level indicative of no-change (1-fold) is shown by a dotted line. (B) Absolute CO and NCO repair efficiencies following correction for transformation efficiency for repair of either pADE2(400/400) or pADE2(1 bp/mis) in different genetic backgrounds, as indicated. * indicates those datasets that share common *P*–values.

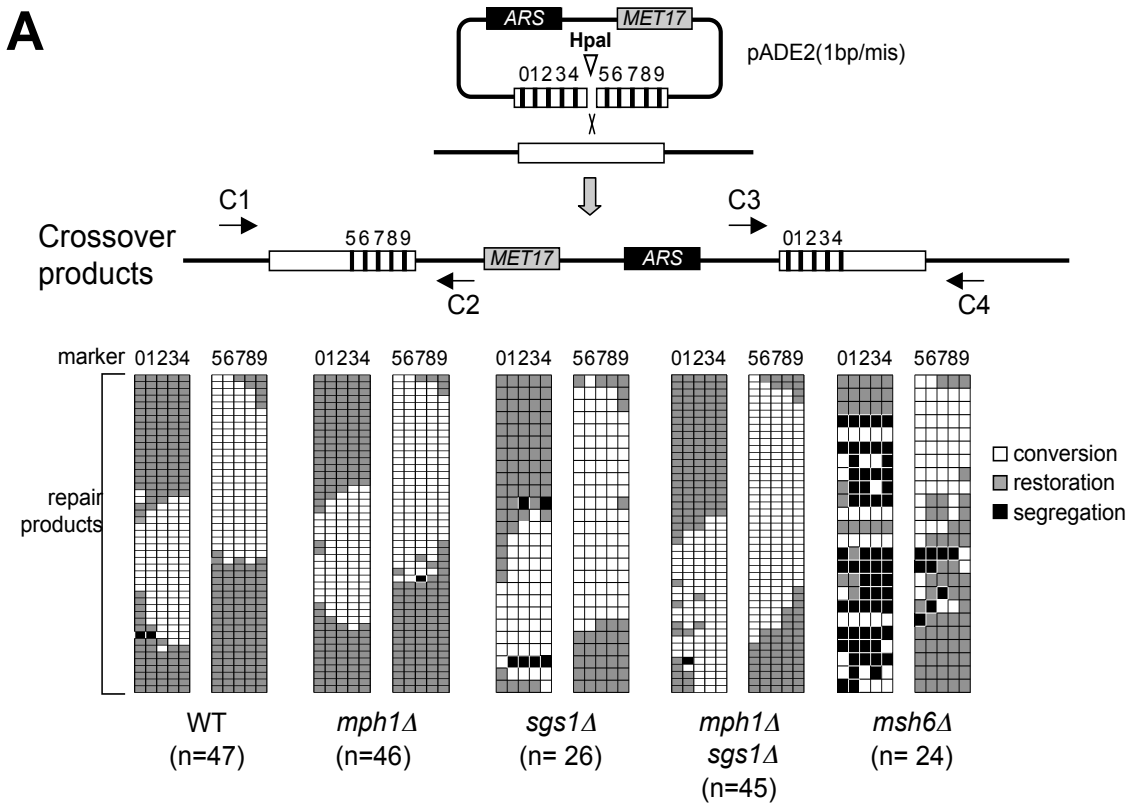
CO frequency is scored as the ratio of COs per total repair events. Therefore, a decrease in CO could arise through a reduction in the absolute CO frequency and/or an increase in the absolute NCO frequency. In order to establish if the changes in CO frequency in response to the presence of homeology are a result of a change in the absolute CO levels, the absolute CO and NCO efficiencies were determined by co-transformation of pYES with the repair substrates and normalization of transformation efficiencies between the mutant strains, as described above. Greater variations in the inter-experimental absolute repair efficiencies as compared to the CO frequencies were observed in all strains tested (Figure 3.6B). However, the differences in CO frequency between the repair of homologous and homeologous substrates were found to be a result of changes in absolute CO frequency and not the absolute NCO frequency, the levels of which were unaffected in the presence of homeology (Figure 3.6B). This observation is consistent with previous findings showing that the presence of homeology impedes CO formation to a much greater extent than NCO formation (Welz-Voegele and Jinks-Robertson, 2008). Together, these findings suggest that during DSB repair using homeologous sequences, Mph1 and Sgs1 are both required for MutSα to efficiently suppress the formation of COs.

3.2.7. *mph1Δ sgs1Δ* cells are proficient for gene conversion during homeologous recombination

The failure of *mph1Δ sgs1Δ* double mutants to discriminate homeologous from HR substrates with regards to CO suppression mimics the phenotype of *msh2Δ* and *msh6Δ* mutant cells, which are defective in the recognition and repair of base-

base mismatches. This raised the question of whether *mph1Δ sgs1Δ* mutant cells are also defective in the MMR pathway. To analyze this possibility, the plasmid-derived *ADE2* sequences of CO and NCO products arising from the repair of pADE2(1bp/mis) in wild type, *mph1Δ*, *sgs1Δ*, *mph1Δ sgs1Δ* and *msh6Δ* strains were amplified by PCR. PCR products were sequenced to determine the frequency of three classes of products predicted to occur at each of the 10 single bp heterology markers on the pADE2(1bp/mis) homeologous substrate: restoration, GC or marker segregation. Marker restoration occurs if the marker retains the original plasmid sequence while GC involves the marker conversion to the corresponding bases of the endogenous *ADE2* sequence. Marker segregation occurs when the two strands of an un-repaired mismatch are segregated into daughter molecules following DNA replication, resulting in the presence of both sequences in the same cell (White et al., 1985).

Consistent with previous findings, in all genetic backgrounds, GC occurred more frequently in CO products than in NCOs (Figure 3.7A and B) (Paques and Haber, 1999). Marker segregation was seen in only 6% (8/140) of all wild type repair products (CO + NCO), indicating that base-base mismatch-containing DNA was efficiently disrupted by either reverse branch migration or subjected to GC. In contrast, 57% (27/47) of all repair products in *msh6Δ* mutant cells, which is ten-fold higher than that seen in wild type cells, showed marker segregation (Figure 3.7A and B). Tracts of marker segregation in individual CO products from *msh6Δ* cells were also longer than those from wild type cells (Figure 3.7A). Marker segregation tended to occur for markers 0-4 of the CO products in *msh6Δ*, suggesting an asymmetry in the processing of the two DSB ends (Figure 3.7A). Despite a lack of the MutSα complex, *msh6Δ* cells still have significant levels of GC in both CO and


A
ARS
MET17
HpaI
01234 56789
pADE2(1bp/mis)
C1
C3
Crossover products
56789
MET17
ARS
01234
C2
C4
marker 01234 56789
repair products
conversion
restoration
segregation
WT (n=47)
mph1Δ (n=46)
sgs1Δ (n= 26)
mph1Δ sgs1Δ (n=45)
msh6Δ (n= 24)

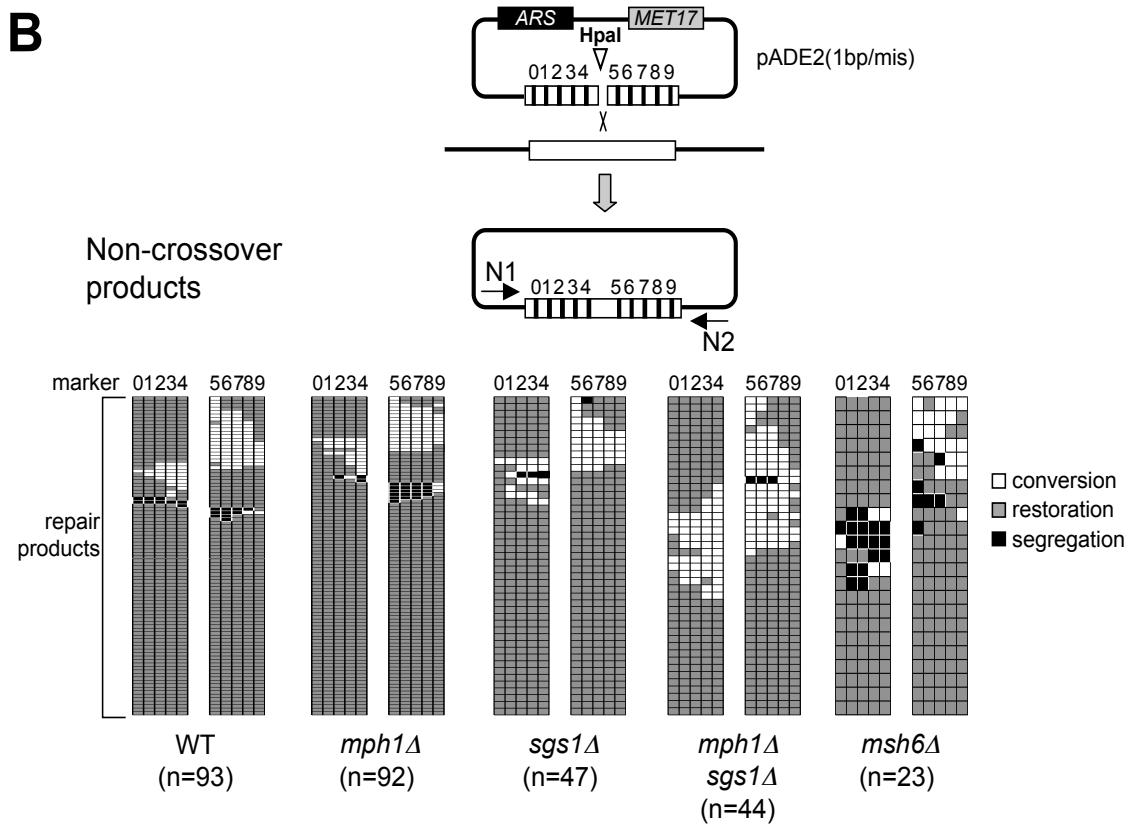

B
ARS
MET17
HpaI
01234 56789
pADE2(1bp/mis)
Non-crossover products
N1
01234 56789
N2
marker 01234 56789
repair products
conversion
restoration
segregation
WT (n=93)
mph1Δ (n=92)
sgs1Δ (n=47)
mph1Δ sgs1Δ (n=44)
msh6Δ (n=23)

Figure 3.7 *mph1Δ sgs1Δ* cells do not have an overt defect in mismatch recognition but display altered processing of non-crossover products (A) Upper panel: Schematic diagram showing the formation of CO products resulting from the repair of pADE2(1bp/mis). The positions of single bases (labeled 0-9) differing from the wild type *ADE2* sequence are indicated by vertical black lines. The location of the HpaI-induced break is indicated by an open arrowhead. Black arrows indicate primers used to amplify by PCR the indicated fragments from CO products for marker analysis. Lower panel: Status of each of the markers 0-9 in individual repair products from different genetic backgrounds, as indicated. Number of individual repair products analyzed from each genetic background is shown in parentheses. (B) Upper panel: Schematic diagram showing the formation of NCO products resulting from the repair of pADE2(1bp/mis). Lower panel: Status of each of the markers 0-9 in individual repair products from different genetic backgrounds, as indicated. Number of individual repair products analyzed from each genetic background is shown in parentheses. To aid comparison between strains in (A) and (B), the data for each strain has been proportionally scaled in order that the total number of repair products occupy the same area.

NCO products. This likely indicates that a subset of base-base mismatches may be recognized and subsequently repaired by MutSβ, which has partially overlapping functions with MutSα in recognizing base-base mismatches (Habraken et al., 1996). Nonetheless, inactivation of MutSα is strongly correlated with increased levels of marker segregation during the repair of pADE2 (1bp/mis). Marker segregation levels observed in both CO and NCO products of *mph1Δ sgs1Δ* double mutants were comparable to the levels seen in wild type cells. This suggests that the failure of *mph1Δ sgs1Δ* double mutants to discriminate homeology from homology during HR repair was not a result of an overt defect in the MMR pathway during homeologous recombination.

3.2.8. Non-crossover products that arise during homeologous recombination are processed differently in the absence of both Mph1 and Sgs1

Figure 3.8 shows the comparison of GC frequencies of all ten markers in all products from all genetic backgrounds tested. Markers that are closer to the DSB ends generally have higher GC conversion rates in both CO and NCO products, consistent with GC tracts initiating from the ends of DSBs. Among CO products, the loss of Mph1 had no effect on GC frequencies of all ten markers whereas the loss of Sgs1 resulted in higher GC frequencies as has previously been shown (Lo et al., 2006). Consistent with the observation in *msh6Δ* cells that the two ends of the DSB are processed asymmetrically, the increase in GC frequencies in the COs of *sgs1Δ* mutant cells were only observed for markers 5-9 (Figure 3.8, upper panel). *mph1Δ sgs1Δ* mutant cells also displayed elevated GC frequencies of markers 5-9

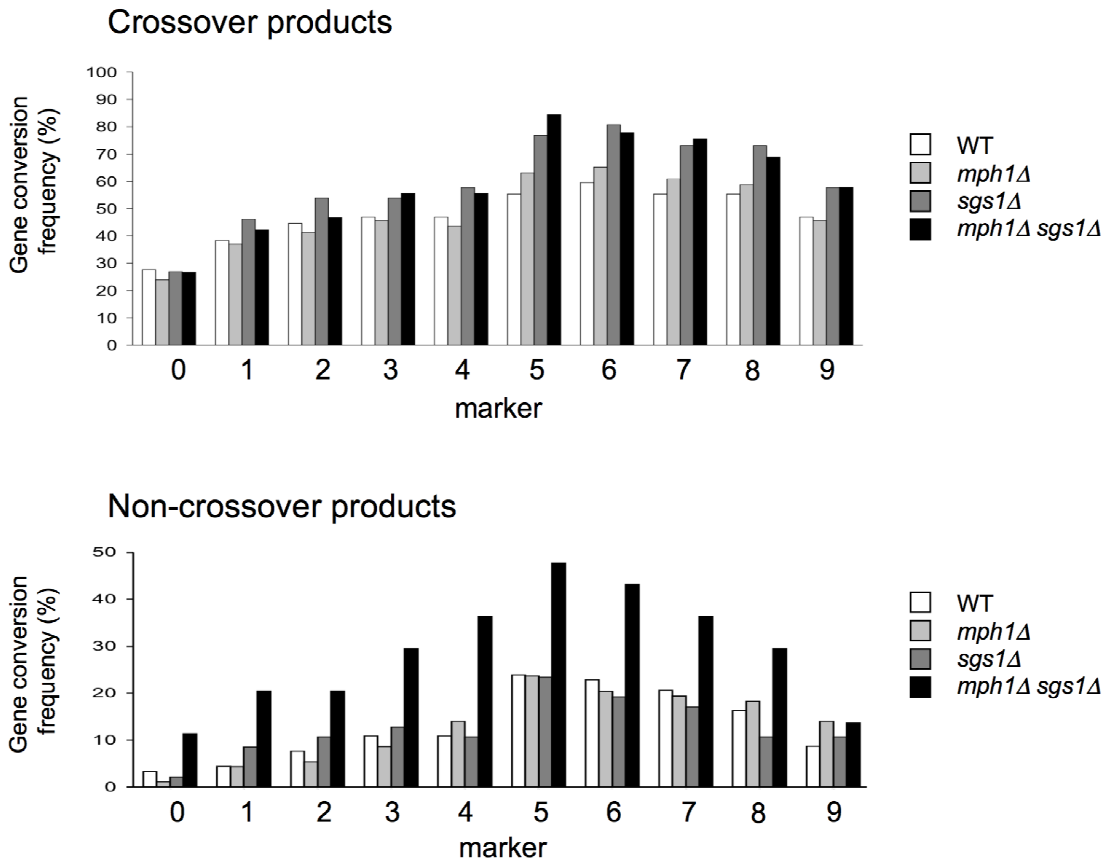


Figure 3.8 NCO products from *mph1Δ sgs1Δ* cells have elevated frequencies of gene conversion. Upper panel: GC frequencies for individual markers 0-9 in CO products resulting from the repair of pADE2(1bp/mis) in various genetic backgrounds, as determined from Figure 3.7A. Lower panel: GC frequencies for individual markers 0-9 in NCO products resulting from the repair of pADE2(1bp/mis) in various genetic backgrounds, as determined from Figure 3.7B.

of CO products, to a level comparable to those of *sgs1Δ* cells (Figure 3.8, upper panel).

The NCO products from *mph1Δ* and *sgs1Δ* single mutants displayed GC frequencies for all ten markers that are comparable to the wild type strain (Figure 3.8, lower panel). Surprisingly, *mph1Δ sgs1Δ* double mutant cells had significantly elevated levels of GC in NCO products for 9 out of 10 markers (marker 0-8) compared to wild type NCOs (Figure 3.8, lower panel). Together, these results suggest that Sgs1 suppresses GC in both CO and NCO products. In contrast, Mph1 suppresses GC specifically in NCO products and does so in a manner that is redundant with Sgs1.

As shown in Figure 3.7, GC events can occur on either one side (uni-directional) or both sides (bi-directional) of the DSB. The profile of GC tract directionality was altered in *mph1Δsgs1Δ* double mutant cells compared to wild type cells. In the absence of Mph1, uni- and bi-directional GC conversion in CO products occurred at a level similar to wild type cells (Figure 3.9, upper panel). In contrast, the frequency of bi-directional GC events in *sgs1Δ* and *sgs1Δ mph1Δ* CO products was elevated (Figure 3.9, upper panel). The proportion of repair products containing uni- and bi-directional GC tracts in NCOs was similar between wild type, single *mph1Δ* and *sgs1Δ* mutant cells (Figure 3.9, lower panel). However, there was a ten-fold increase in bi-directional GC tracts in NCOs of *mph1Δ sgs1Δ* double mutant cells compared to wild type cells, *mph1Δ* or *sgs1Δ* single mutant cells, at the expense of repair events showing no GC (Figure 3.9, lower panel).

In summary, consistent with previous findings, CO products that form in the absence of Sgs1 have increased bi-directional GC tracts and an asymmetrical increase in GC frequency (Lo et al., 2006). On the contrary, this study revealed that

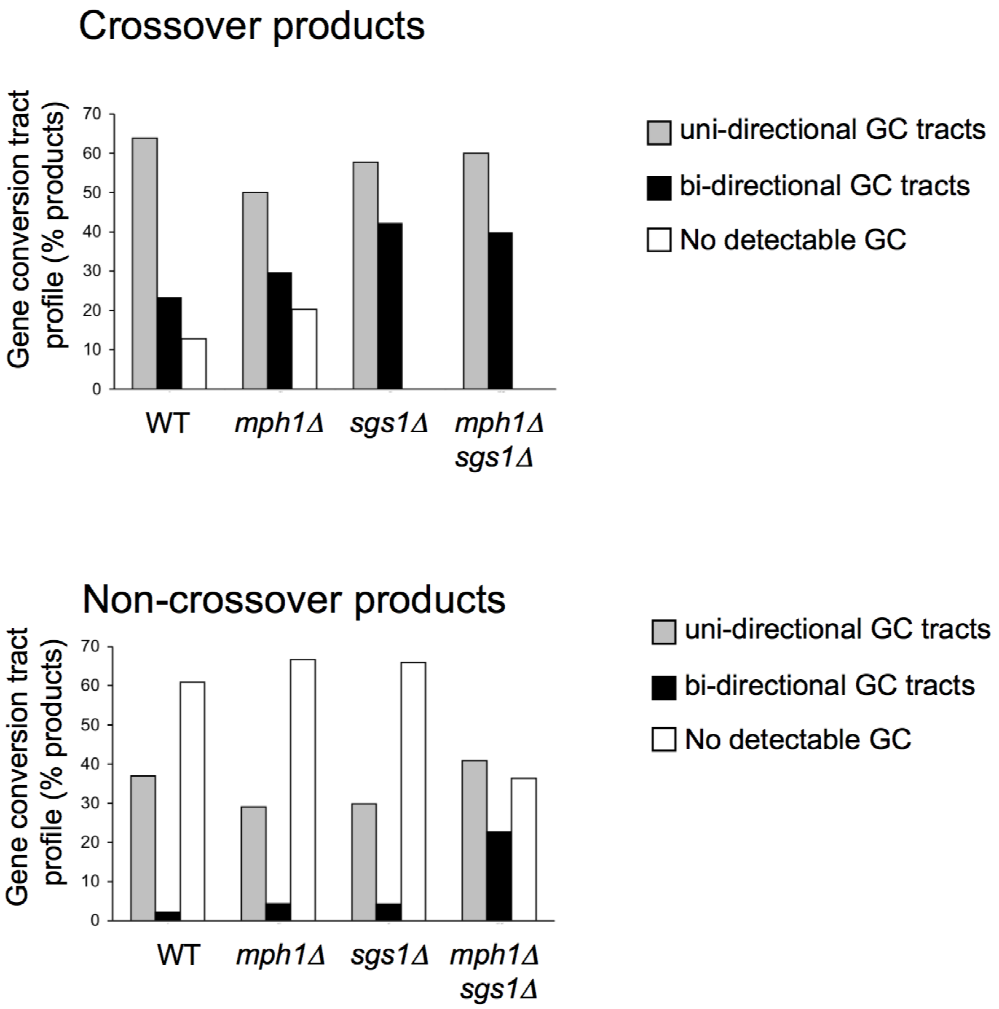


Figure 3.9 NCO products from *mph1Δ sgs1Δ* cells have elevated frequencies of bi-directional gene conversion tracts. Upper panel: GC tract directionality of CO products resulting from the repair of pADE2(1bp/mis) in various genetic backgrounds, as determined from Figure 3.7A. Lower panel: GC tract directionality of NCO products resulting from the repair of pADE2(1bp/mis) in various genetic backgrounds, as determined from Figure 3.7.

the GC frequency and bi-directional GC events in NCO products are only increased when both Mph1 and Sgs1 are absent. These findings suggest that during homeologous recombination, NCOs are processed differently in the absence of both Mph1 and Sgs1.

3.3. Discussion

CO formation during HR between non-sister chromatids can lead to deleterious GCR. To suppress such events, eukaryotic cells have evolved several mechanisms, which require helicases such as Sgs1, Srs2 and Mph1, to negatively regulate the HR pathway. In this chapter, the CO-suppression role of Mph1 has been confirmed using a plasmid break repair assay. This is consistent with the findings that Fml1, the *S.pombe* orthologue of *S.cerevisiae* Mph1, also suppress CO formation in a plasmid break-repair assay (Prakash et al., 2009; Sun et al., 2008). Furthermore, both antagonistic and synergistic genetic interactions, in the context of CO formation, between Mph1 and MutSα complex were observed when either a completely homologous or homeologous sequence was used to target DSB repair.

Previous studies have implicated MutSβ, but not MutSα, in the formation of COs during inter-chromosomal recombination (Nicholson et al., 2006; Saparbaev et al., 1996). However in this study, it was shown that the formation of a subset of CO is absolutely dependent on MutSα, when a completely homologous sequence was used to target repair. This subset of MutSα-dependent COs is normally suppressed by the Mph1 helicase, but not by Sgs1. However, Sgs1 has previously been linked to MutSα in rejecting heteroduplex DNA during SSA repair (Sugawara et al., 2004). It was proposed that Sgs1 may be recruited to the heteroduplex DNA by

MutSα to unwind heteroduplex DNA using its helicase activity (Sugawara et al., 2004). The difference between the observations of our plasmid break-repair assay and SSA assay by Sugawara et al. suggests that the interactions between Mph1, Sgs1 and MutSα in CO regulation are HR pathway-specific (Sugawara et al., 2004). The antagonistic relationship between Mph1 and MutSα does not depend on the mismatch recognition function of MutSα nor the presence of sequence divergence. This suggests that Mph1 may be recruited to HR intermediates through a constitutive function of MutSα and is consistent with the high-throughput interaction studies using MS approach, which detected an interaction between Mph1 and Msh6 (Gavin et al., 2002). This interaction between Mph1 and MutSα however could not be detected using a co-IP approach suggesting that the discrepancy in results of the second approach may be an issue of sensitivity.

Why is MutSα required for CO formation during recombination between completely homologous sequences? In addition to having a binding preference for mismatch-containing DNA, purified *S.cerevisiae* Msh2-Msh6 complex has been shown to bind specifically to HJs (Alani et al., 1997; Marsischky et al., 1999). It was shown, by electron micrographs and gel mobility shift assays, that yeast MutSα binds to the core of HJs and has an affinity and specificity at least as high as it has for mismatches (Marsischky et al., 1999). In addition, structural analysis showed that Msh2 and Msh6 form an asymmetric oval disc, which is "pierced" by two channels termed θ structure (Warren et al., 2007). Based on observations by single-molecule unzipping force analysis, *S.cerevisiae* MutSα was shown to form a clamp that can slide along DNA duplexes in an ATP-dependent manner (Jiang et al., 2005). Taken together, we propose that MutSα complexes are probably loaded onto a D-loop via binding to the HJ-like early strand invasion intermediates (Figure

3.10). The increasing loadings of MutSα complexes stabilize the D-loop structure, thus increasing the probability of second-end capture that leads to the formation of a dHJ (Figure 3.10). The resolution of the two HJs in opposite orientations results in the formation of COs. To suppress such MutSα-mediated COs, the D-loop structure can be disrupted by the DNA unwinding activity of Mph1 helicase (Figure 3.10). Mph1 may disrupt the D-loop structure while dissociating the MutSα sliding clamps that stabilize the structure, thus indirectly suppressing the COs mediated by MutSα. This model explains why the helicase activity of Mph1 is essential for its CO suppression activity, as evidenced by the observation that Mph1 with point mutations in the conserved helicase motifs are completely deficient in suppressing CO formation (Prakash et al., 2009). Since Sgs1 is predicted to suppress CO formation by dHJ dissolution, which occurs following the strand invasion and dHJ formation steps, the CO suppression activity of Sgs1 can be effected independently of MutSα. This is also consistent with the model proposed in Figure 3.10. It remains unknown whether the CO suppression mediated by Srs2 helicase is dependent on MutSα. However, based on our model and judging by the fact that Srs2 suppress recombination by disrupting Rad51-ssDNA presynaptic filament rather than D-loop structure (Krejci et al., 2003b; Prakash et al., 2009; Veaute et al., 2003), it is likely that Srs2-mediated CO suppression may be independent of MutSα.

Marsischy et al. (1999) has also shown that the MutSα complex facilitates the cleavage of HJs by phage HJ resolvases. It was proposed that the interaction between MutSα and a HJ enhances the accessibility of the HJ structure to T4 and T7 endonucleases. Therefore it is possible that MutSα can bind to HJs and effect a biased resolution of HJ that generates exclusively COs (Figure 3.10). An observation, which indirectly supports this hypothesis, is that MutSα binds

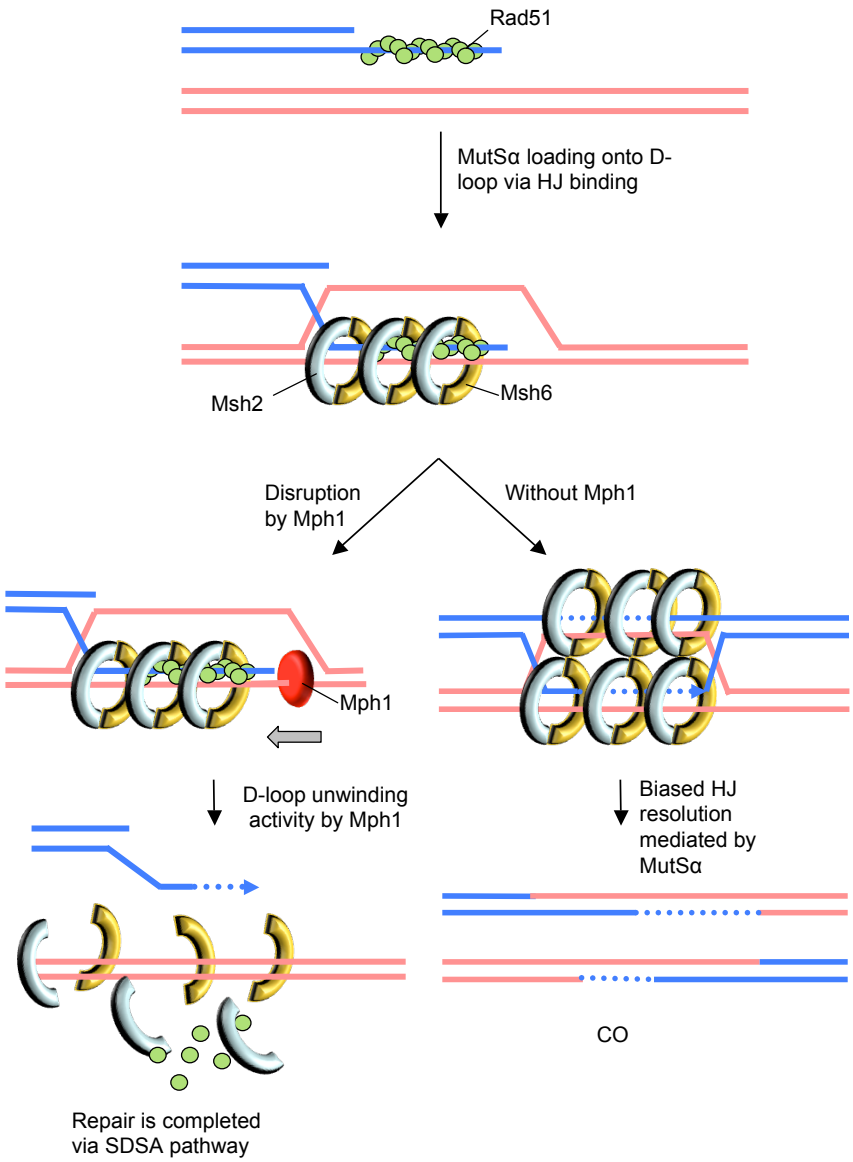


Figure 3.10 Mechanistic model showing how Mph1 may suppress COs promoted by MutSα. MutSα is loaded onto D-loop structures via bindings to HJs. MutSα forms a sliding clamp, which stabilizes the D-loop structure and increases the probability of second-end capture, and thus dHJ formation. Mph1 helicase unwinds the D-loop and displacing MutSα from the D-loop and thus suppresses the MutSα-dependent CO formation. In the absence of Mph1, D-loops stabilized by MutSα form dHJ. The asymmetrical binding of MutSα to HJs may confer directionality to the HJ resolution, thereby forming predominantly COs.

asymmetrically to mismatch DNA substrates (Gradia et al., 1997; Jiang et al., 2005; Kijas et al., 2003). If MutSα also binds asymmetrically to a HJ, the orientation-specific binding of MutSα may confer directionality to the HJ resolution by exposing specific strands on the HJ to the HJ resolvases for cleavage into CO products. It will be of interest to determine if MutSα affects the efficiency and orientation of HJ resolution catalysed by the potential eukaryotic HJ resolvases GEN1/Yen1, MUS81-EME1 and SLX1-SLX4.

Rather than antagonizing the MutSα-dependent CO formation during recombination between two completely homologous sequences, Mph1, together with Sgs1, was required for the efficient MutSα-dependent suppression of COs during homeologous recombination. This observation is consistent with recent findings in Putnam et al. (2009). Using an assay that analyses the GCR rate of natural DNA sequences without involving any artificial induction of DSBs, Putnam et al. found that dispersed repetitive elements in the genome resembling segmental duplications are prone to causing GCR and that the two helicases, Mph1 and Sgs1, are essential for the suppression of GCR presumably via the prevention of aberrant HR between these non-allelic/homeologous loci (Putnam et al., 2009). The MMR function of MutSα is required for the suppression of CO using pADE2 (1bp/mis) repair substrate, which is predicted to form base-base mismatches when it recombines with the endogenous *ADE2* loci. In the absence of MutSα, the cells lack the ability to distinguish pADE2(400/400) and pADE2(1bp/mis) repair substrates. Interestingly, *mph1Δ sgs1Δ* mutant cells that also seem to lack the ability to discriminate completely homologous and homeologous repair substrates, are not defective in MMR (Figure 3.7A and B). Instead, the analysis of GC events revealed

that NCOs are generated differently in *mph1Δ sgs1Δ* double mutant cells, as compared to the wild type or single mutant cells (Figure 3.8 and 3.9).

NCO products can be generated by SDSA, dHJ dissolution or HJ resolution pathways. SDSA and dHJ dissolution pathways form exclusively NCO products via D-loop disruption and convergent dHJ branch migration, respectively. Both mechanisms reduce the length of heteroduplex DNA and hence reduce the probability of GC events in the NCO products formed. In contrast, HJ resolution does not involve either of those processes to limit the length of heteroduplex DNA. Instead, NCO and CO products are generated by alternative orientations of HJ resolution. Therefore the GC frequencies of CO and NCO products formed via HJ resolution are expected to be similar and greater than those of NCO products formed via SDSA and dissolution pathways.

The fact that the GC profile of NCO products of *mph1Δ* and *sgs1Δ* single mutant cells was similar to the wild type level (Figure 3.8 and 3.9) supports the notion that in the absence of either Mph1 or Sgs1, which results in compromised SDSA or dissolution, respectively, the majority of NCOs are generated by the remaining, intact NCO pathway. When the cells are compromised in both SDSA and dissolution pathways, as in *mph1Δ sgs1Δ* mutant cells, elevated GC frequency and bidirectional GC tracts of the NCO products were observed. Such GC profile was consistent with the predicted GC profile of NCOs generated via HJ resolution. The loss of Mph1 did not affect the GC profile of CO products. However the absence of Sgs1 gave rise to a slight increase in GC frequency and of bi-directional GC events in CO products, as has previously been reported (Lo et al., 2006). This observation is wholly consistent with a role of Mph1 in SDSA, because, in the absence of SDSA the channelling of intermediates into dissolution/resolution

pathways of HR would be expected to affect the quantity of COs (Figure 3.6B, upper panel) but not the GC profile of COs (Figure 3.8). Together, these results provide *in vivo* evidence to support the proposed roles for Mph1 and Sgs1 in SDSA and dHJ dissolution, respectively. These results also support the notion that SDSA and dHJ dissolution pathways are the predominant pathways in DSB processing. Although HJ resolution can act as a "back-up" pathway when SDSA and dissolution pathways are impaired, HJ resolution may result in the formation of COs. Therefore, our findings support the view that CO formation can be suppressed, during mitotic HR, by channeling DSB repair intermediates into SDSA and dissolution pathways that produce exclusively NCOs.

A model outlining how Mph1, Sgs1 and MutSα may interact during homologous and homeologous recombination is shown in Figure 3.11. During HR, MutSα has a pro-CO formation role, independently of its MMR function, which is specifically suppressed by Mph1 but not Sgs1 (Figure 3.11, Green box). The fact that MutSα has multiple, separable functions in MMR and HR pathways is not unprecedented as a similar situation exists for MutSβ whereby mutant alleles of *MSH2* indicate that the removal of non-homologous tails and heteroduplex rejection during SSA are separable functions of MutSβ (Goldfarb and Alani, 2005).

We propose that MutSα suppresses COs, during homeologous recombination by acting on the tracts of mismatches that are generated through Rad51-mediated D-loop extension and second-end capture (Figure 3.11, yellow box). Mph1 may thus promote MutSα-dependent suppression of dHJ formation by its ability to disrupt D-loops, thus circumventing the generation of mismatches. This explains why Mph1 is required for MutSα-dependent homeology-mediated

suppression of CO without itself being a core component of the HR machinery (Prakash et al., 2009; Scheller et al., 2000).

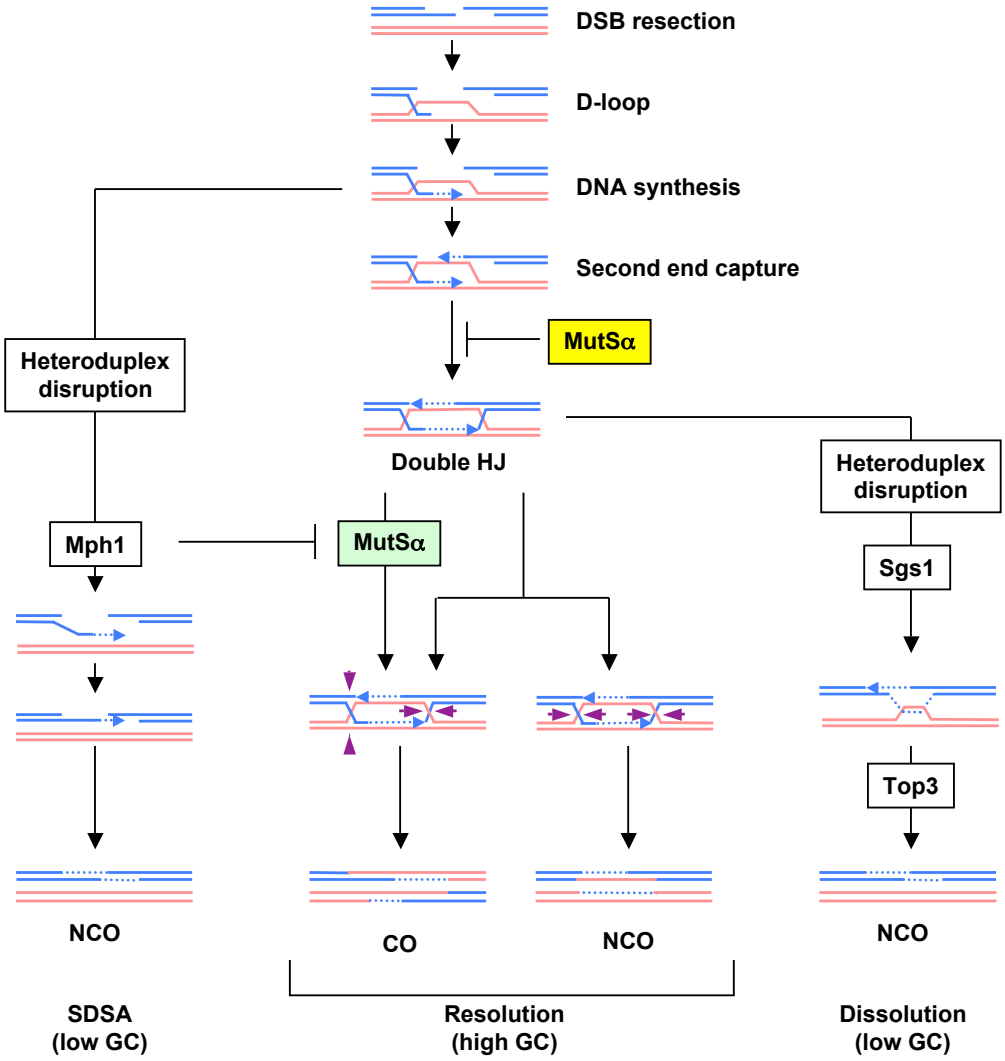


Figure 3.11 Schematic diagram showing the outcomes of different homologous recombination repair pathways and the proposed steps in which Mph1, MutSα and Sgs1 act. During homeologous recombination repair, MutSα specifically suppresses the formation of COs by inhibiting dHJ formation (yellow box). However, during HR, MutSα-dependent COs are generated that do not require the MMR functions of MutSα and are suppressed by the actions of Mph1 (green box). Tracts of DNA synthesis are shown by dotted blue lines with arrowheads. The resolution of HJs in one of two orientations is shown by magenta arrowheads.

Chapter Four

4. Development of a system for the analysis of *in vivo* Holliday Junction resolution in *Saccharomyces cerevisiae*

4.1.Introduction

As described in Chapter one, HR is a multi-step repair pathway that involves DSB end-resection, strand invasion and thus D-loop formation, HJ formation, branch migration and resolution (Figure 1.1(i)). HR events such as D-loop formation or second end capture are potentially reversible and these intermediates can be diverted into alternative repair pathways. In contrast, HJ formation is a terminal process in HR, which is not reversible but can only be completed by resolving the HJ. HJ resolution in *E.coli* is carried out by the RuvC resolvase in a complex with RuvAB (Connolly et al., 1991; Dunderdale et al., 1991; West, 1997). However, an orthologue of RuvC is absent from eukaryotic genomes. Hence, the enzymes and the exact mechanism of HJ processing in eukaryotes remain largely unclear.

Biochemical reconstitution experiments of DNA repair pathways such as Base Excision Repair (BER), NER and MMR pathways using purified enzymes have led to a detailed understanding of the mechanisms of these pathways (Constantin et al., 2005; Dianov and Lindahl, 1994; Guzder et al., 1995; Lahue et al., 1989; Mu et al., 1995; Zhang et al., 2005). However, a complete biochemical reconstitution of the HR pathway has not yet been achieved, although biochemical studies have provided some mechanistic insights into the stages of HR leading up to the formation of HJ, for example strand invasion and D-loop formation (New et al., 1998; Sung and Robberson, 1995; Sung and Stratton, 1996). Early HR events such as DSB end resection and strand invasion can also be monitored *in vivo* using Southern analysis and PCR, respectively (Mimitou and Symington, 2008; Sugawara et al., 1995; Zhu et al., 2008). Several eukaryotic proteins have been shown *in vitro*

to cleave model HJs. However, the precise DNA structures these enzymes process *in vivo* remains to be determined.

The inability to specifically analyse HJ resolution *in vivo* led us to design a system in which we could directly analyse the late step of HR in a cellular context. The system comprises a DNA molecule containing a single HJ, which must be resolved for its propagation. The system allows us to specifically analyse HJ resolution without requiring the preceding steps of the HR pathway. We chose *S.cerevisiae* as the model organism with which to genetically analyse this novel *in vivo* HJ resolution assay.

4.2. Results

4.2.1. Development of a system for the analysis of *in vivo* HJ resolution in *S.cerevisiae*

In an attempt to specifically analyse HJ resolution *in vivo,* a system was developed in which the resolution of a synthetic HJ could be detected when introduced into *S.cerevisiae*. The system is outlined in Figure 4.1. The HJ-containing substrate comprises of two plasmids. Plasmid P1 contains the *MET17* auxotrophic marker, whereas plasmid P2 contains the *ADE2* auxotrophic marker and a yeast Autonomously Replicating Sequence (ARS) element. Plasmids P1 and P2 are linked by a single HJ to form a Joint-molecule (X-JM) (see below).

The HJ in X-JM can be resolved in one of two orientations. As is shown in Figure 4.1, if the HJ is resolved in the horizontal plane, X-JM will be resolved into its constituent P1 and P2 plasmids. However, if the HJ is resolved in the vertical plane, a P1-P2 dimer will be formed. The linking of the *MET17* marker and the *ARS* on the P1-P2 dimer allows the stable maintenance of the *MET17* marker. Such events can then be scored by transforming X-JM into *met17Δ* cells and selecting for methionine prototrophs. The efficiency of methionine prototroph formation following X-JM transformation is therefore used as an indicator of HJ resolution efficiency.

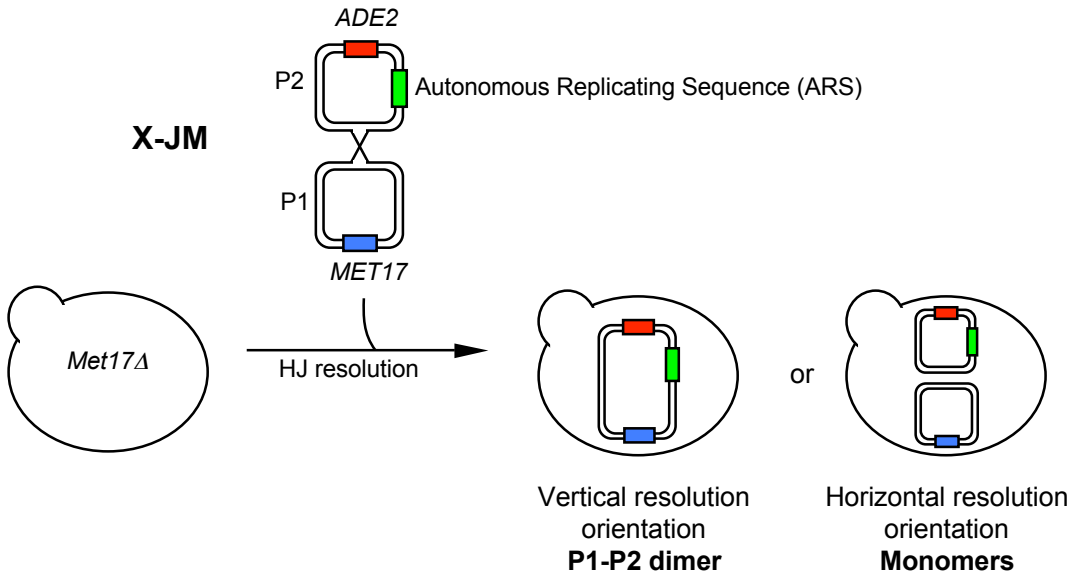


Figure 4.1 Schematic showing principle of system used for the analysis of HJ resolution *in vivo*. Following transformation of X-JM substrate into *met17Δ* cells, the selection of methionine prototrophs facilitates the detection of dimeric resolution products. Relevant markers and genotypes are indicated.

4.2.2. The design of the HJ-containing plasmid substrate, X-JM

X-JM was constructed *in vitro* according to the scheme shown in Figure 4.2. The first step of this scheme is to create single-stranded gaps of a defined sequence in P1 and P2 to generate P1-Gap and P2-Gap molecules, respectively. Oligonucleotides that are partially complementary to the single-stranded gaps are then annealed to form P1-Flap and P2-Flap molecules. The 3' flap of the annealing oligonucleotides of P2-Flap is complementary to the single-stranded gap in P1-Flap and *vice versa*. This allows P1 and P2 to be linked by base pairing, and to form a Joint-Molecule (X-JM) following ligation (Figure 4.2).

Plasmid P1 was generated by cloning a cassette, SHJ(1), into the BamHI site of plasmid pRS401, which contains the *MET17* auxotrophic marker but no ARS (Figure 4.3B). A related cassette, SHJ(2), was cloned into the BamHI site of pRS412, which contains the *ADE2* auxotrophic marker and an *ARS*, forming plasmid P2 (Figure 4.3B). SHJ(1) and SHJ(2) facilitate the formation of 60 and 55 nucleotide single strand gaps, respectively, using modified restriction enzymes that introduce single strand specific nicks within their respective restriction sites (NEB). SHJ(1) contains 6 recognition sites for BbvcI, separated by spacers of 4-5 nucleotides in length (Figure 4.3A). SHJ(2) is partially homologous to SHJ(1) in that they share identity in the first 35 nucleotides of the region that forms the single-stranded gap (Figure 4.3A). SHJ(2) thus has 3 BbvcI and 3 BsmI recognition sites (Figure 4.3A). The difference in 3' gap sequences between SHJ(1) and SHJ(2) facilitates the subsequent plasmids linking process (see below). The 5' sequence homology between SHJ(1) and SHJ(2) results in a homologous region of 45 basepairs in which the HJ formed between P1 and P2 can branch migrate in either

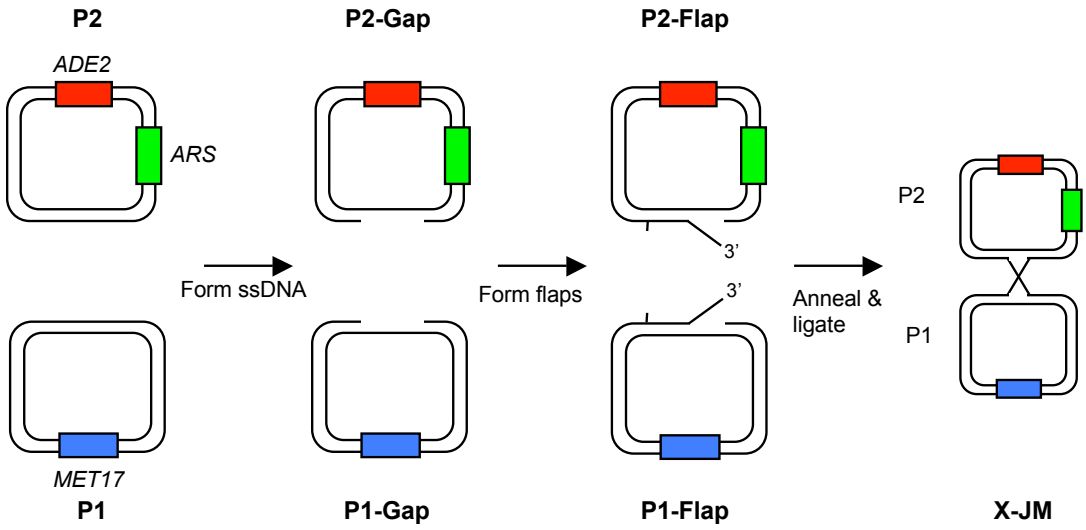


Figure 4.2 Schematic showing strategy for the production of the X-JM substrate containing a single HJ. Single-stranded gaps are produced on P1 and P2 plasmids, forming P1-Gap and P2-Gap, respectively. Partially complementary oligonucleotides are annealed to the single-stranded gap regions in P1-Gap and P2-Gap, forming P1-Flap and P2-Flap respectively. P1-Flap and P2-Flap are annealed together using the 3' complementarities of the annealing oligonucleotides to the gap on the other plasmid. Annealed products are ligated to form X-JM.

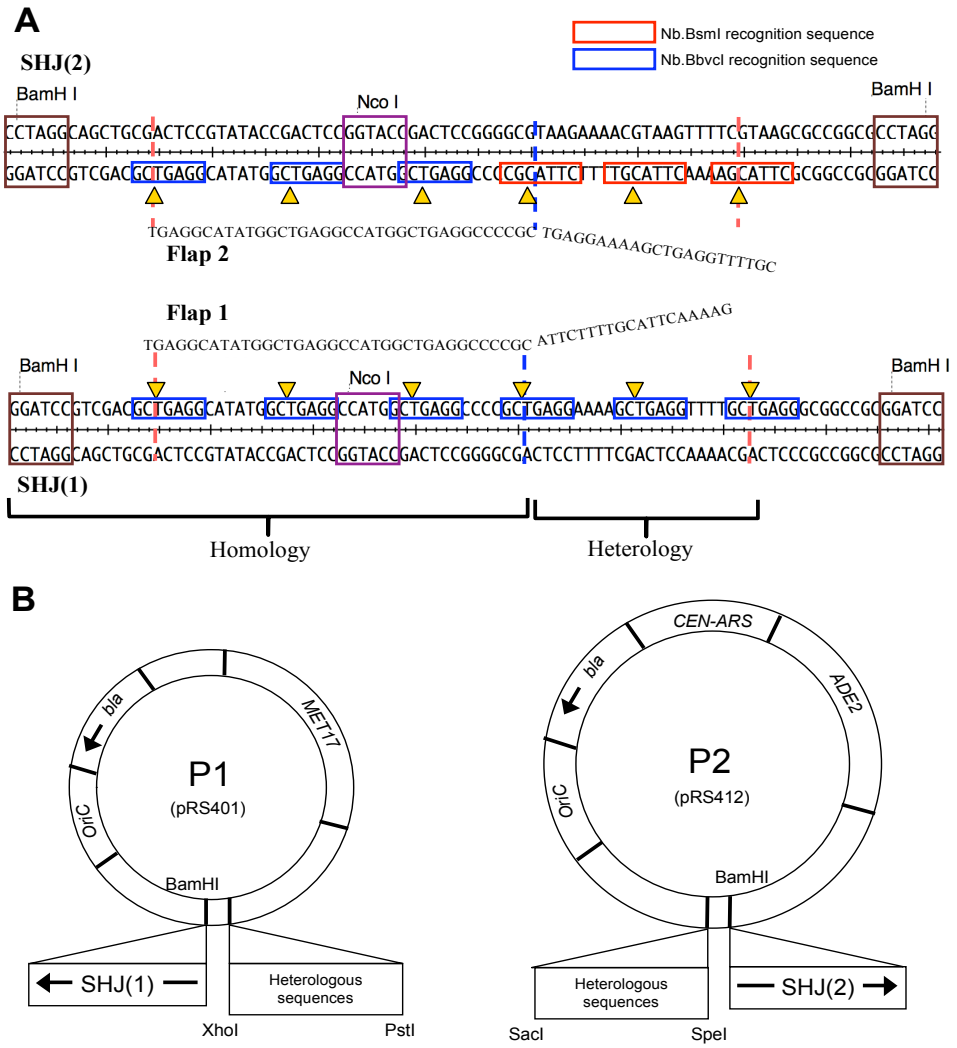


Figure 4.3. SHJ(1) and SHJ(2). (A) The DNA sequences of SHJ(1) and SHJ(2) cassettes. Sequences between the two red dashed lines are the gap regions. The blue and red rectangles show the recognition sites for two nicking enzymes, i.e. Nb.BbvcI and Nb.BsmI respectively. Yellow triangles show the point where the nicking enzymes incise on specific strands of SHJ(1) and SHJ(2). Flap1 and Flap2 oligonucleotides are annealed to the single-stranded gaps of SHJ(1) and SHJ(2). The 3' sequences of Flap1 and Flap2 are complementary to gaps of SHJ(2) and SHJ(1) respectively. These opposite complementarities allow SHJ(1) and SHJ(2) to be linked via base-pairing, creating a single HJ within the gap sites. (B) SHJ(1) and SHJ(2) are cloned into pRS401 and pRS412 respectively at BamHI sites in an opposite orientation with respect to the direction of transcription of the *bla* gene. Heterologous sequences amplified from pUC18 are inserted into the upstream regions of SHJ(1) and SHJ(2) to facilitate PCR analysis of HJ resolution products (see text).

direction. To enable PCR amplification of the sequences of SHJ(1) and SHJ(2) from the resolution products (see below), two ~500kb heterologous sequences from pUC18 were amplified by PCR and cloned into the XhoI/PstI and SacI/SpeI sites of pRS401 and pRS412, respectively (Figure 4.3B).

4.2.3. Construction of X-JM

P1-Gap and P2-Gap were generated by treating both P1 and P2 with Nb.BbvcI and P2 additionally with Nb.BsmI. Nb.BbvcI and Nb.BsmI make strand specific nicks at BbvcI and BsmI recognition sites, respectively. The nicks are separated by 10~13 nucleotides, such that each of the oligonucleotide fragments generated after nicking can readily be separated from the complementary strand by heating to 80°C. These free oligonucleotides were removed from the plasmid by purification using a Qiagen gel extraction column. To monitor the gapping efficiency we utilised a restriction site for NcoI which is located within the SHJ(1) and SHJ(2) sequences (Figure 4.3A). As shown on Figure 4.4A, P1 contains two NcoI sites. When both sites were cut, 3.6kb and 1.6kb fragments were generated (Figure 4.4B). After gapping, however, the NcoI site in the SHJ(1) gap region is no longer recognized due to the single-stranded nature of the gap region. P1-gap was only linearised by one NcoI restriction digestion outside the SHJ(1), forming a 5.2kb linear DNA fragment (Figure 4.4B, lane 4). More than 90% of the P1-gap substrate was cut at only one NcoI site, indicating a high efficiency of gapping. The monitoring of gapping efficiencies of SHJ(2) of P2 plasmid was also carried out using the NcoI sites positioned within SHJ(2) (data not shown).

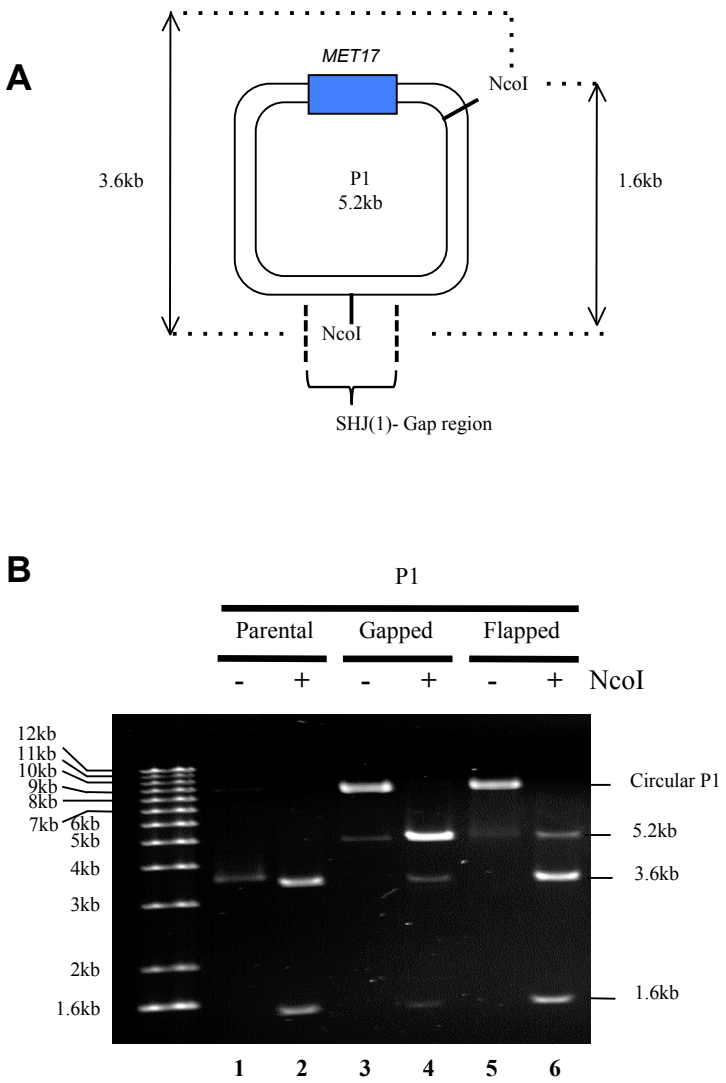


Figure 4.4 Verification of P1-Gap and P1-Flap. (A) The relative positions of NcoI sites and SHJ(1) region on P1 plasmid. (B) Confirmation of "gapping" and "flapping" efficiency on P1. Parental P1, P1-Gap and P1-Flap molecules were digested with NcoI and analysed by 0.7% TAE agarose gel electrophoresis.

To generate P1-Flap, a five fold molar excess of Flap1 oligonucleotide was incubated with P1-gap. The mixture was heated to 80ºC and allowed to cool down gradually in a thermo-stable container. Flap1 anneals to the SHJ(1) gap via a stretch of 35 nucleotides of complementary sequence at the 5' end and was ligated to SHJ(1) gap to form the P1-Flap molecule (Figure 4.3A). The 19 nucleotide sequence at the 3' end of the Flap1 oligonucleotide is not complementary to the SHJ(1) gap. Instead, the 3' end sequence is complementary to the 3' region of the SHJ(2) gap (Figure 4.3A).

To remove the excess Flap1 oligonucleotides that were not ligated to P1-gap, the P1-Flap molecule and the excessive Flap1 were heated to 80ºC. P1-Flap molecule was then purified from the mixture by binding to a Qiagen gel extraction column, whereas the short and single-stranded Flap1 oligonucleotides in excess were washed out from the column. As shown on lane 6 of figure 4.4B, annealing of Flap1 to the single-stranded gap on P1-gap reconstituted the NcoI site on SHJ(1) and P1-Flap was restricted to form the 3.6kb and 1.6kb fragments. P2-Flap was generated and analysed using the same approach as for the generation of P1-Flap.

The complementarity of the 3' flaps of P1-Flap and P2-Flap to SHJ (2) and SHJ (1) respectively allowed linking of P1 and P2 plasmids through base-pairing (Figure 4.3A and 4.5A). P1-Flap and P2-Flap were incubated together at 80ºC to remove any secondary structures. The mixture was then cooled down slowly to allow efficient base pairing of the flaps to the gaps on the other plasmid (Figure 4.5A). The mixture was subsequently ligated using T4 DNA ligase (NEB). Before loading onto 0.7% TAE agarose gel for purification, the ligation mixture was heated up to 80ºC to remove unligated X-JM intermediates. Figure 4.5B shows that when

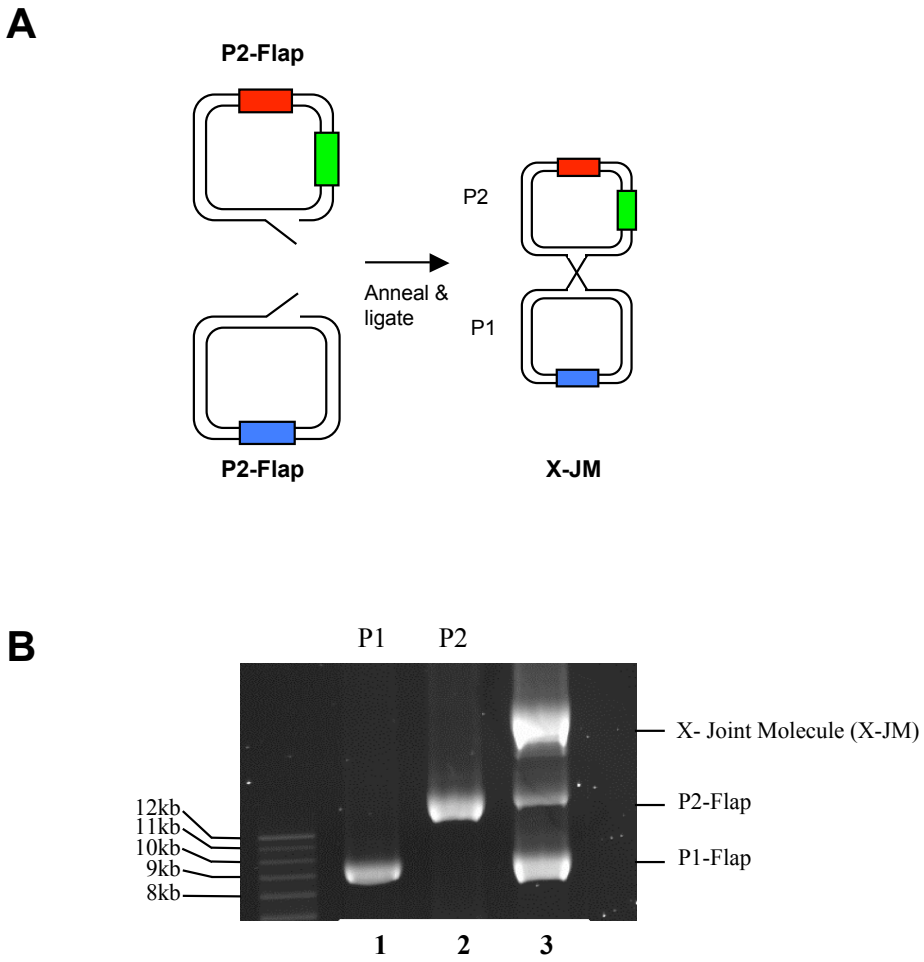


Figure 4.5 X-JM production. (A) Schematic showing the annealing and ligation of P1-Flap and P2-Flap to form X-JM. (B) Gel electrophoresis analysis of annealed and ligated mixture of P1-Flap and P2-Flap (lane 3). Markers: P1-Flap (lane1) and P2-Flap (lane2).

P1-flap and P2-flap were annealed and ligated, X-JM, which has a much reduced electrophoretic mobility, was formed. X-JM was purified from the excised agarose gel (0.7% w/v) using a Qiagen gel extraction kit. When the protocol was scaled up, all plasmid DNA and X-JM were purified from excised gel slices by electro-elution as described in the materials and methods section.

4.2.4. Confirmation of X-JM substrate

To confirm the structure of X-JM, the molecule was subjected to restriction digestion analysis. When X-JM was digested with BamHI, which excises SHJ(1) and SHJ(2) and thus the HJ (Figure 4.6A), the two predicted linear fragments of P1 (5.2kb) and P2 (6.4kb) were released (Figure 4.6B, lane 4). The two linear fragments existed in equimolar intensities, indicating that X-JM consists of P1 and P2 in a 1:1 ratio, consistent with the prediction that X-JM is composed of a single molecule of P1 linked to a single molecule of P2.

To further confirm the structure of X-JM, X-JM was digested with SnaBI and/or BbsI, which uniquely cut X-JM in its P1 or P2 components, respectively. When X-JM was digested with SnaBI, an α-structure was formed. This α-structure consisted of a circular P2 that was resistant to SnaBI digestion and two 1.5kb and 3.7kb fragments of P1 linked to circular P2 via a HJ (Figure 4.6B, lane 5). Similarly, digesting X-JM with BbsI that cuts once on P2 gave rise to an α-structure, in which P1 remained circular and P2 was cut into two 2.8kb and 3.6kb fragments (Figure 4.6B, lane 6). We predicted cutting X-JM with both BbsI and SnaBI would generate a χ-structure with four arms of 1.5kb, 2.8kb, 3.6kb and 3.7kb long. Indeed, a χ-structure was formed when X-JM was doubly digested with BbsI

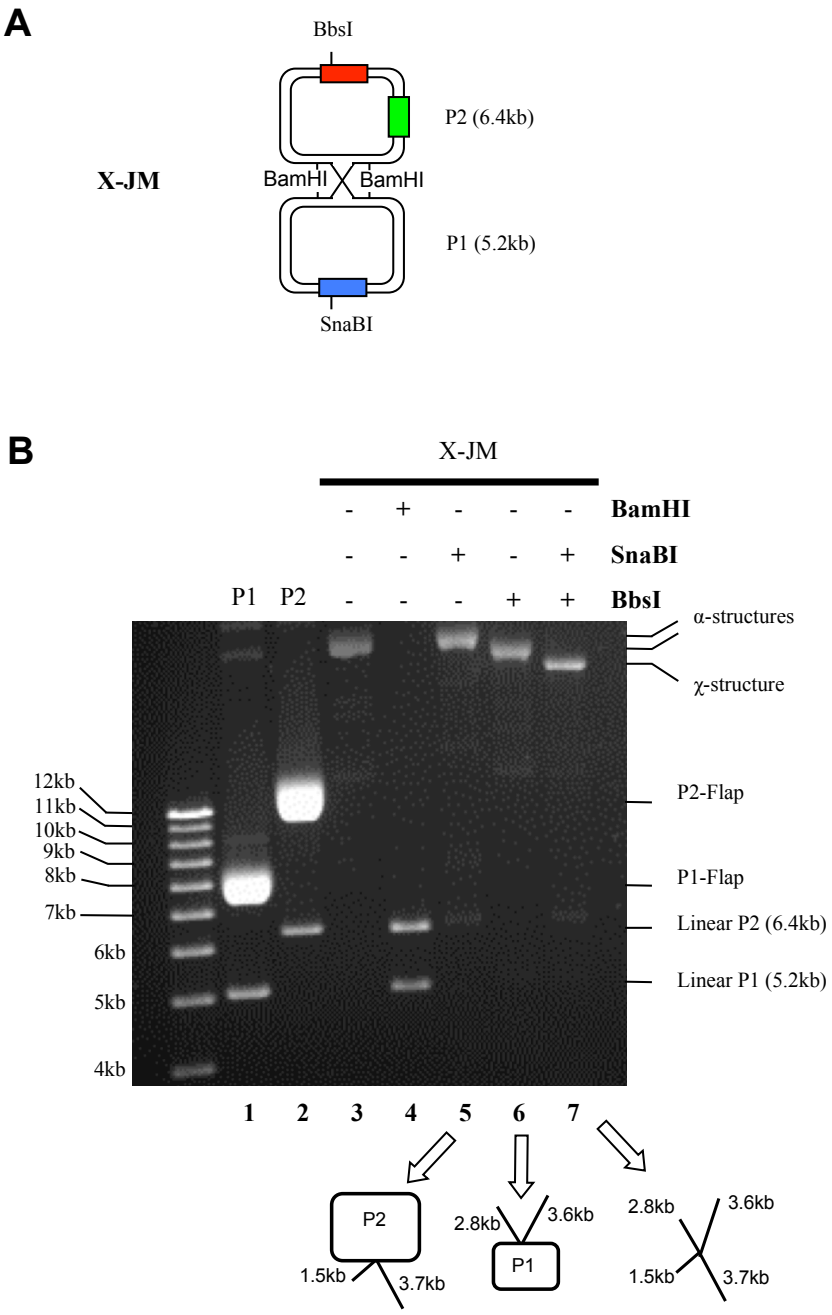


Figure 4.6 Restriction analysis of X-JM. (A) Diagram depicting the relative position of restriction sites on X-JM. (B) Gel electrophoresis analysis of X-JM. DNA has been digested with restriction enzymes as indicated. The diagrams below lane 5-7 indicate the predicted X-JM structure and the length of each linear DNA arm after restriction digestion.

and SnaBI (Figure 4.6B, lane 7). The χ-structure of X-JM had a greater electrophoretic mobility as compared to either of the two α-structures generated by SnaBI or BbsI digestion, as it does not possess a relaxed circular domain. Together these data are consistent with X-JM comprising P1 and P2 in a 1:1 ratio, and that they are linked by a HJ located between BamHI sites of SHJ(1) and SHJ(2).

To confirm the presence of a HJ that links P1 and P2, we treated X-JM with the HJ resolvase, RusA. RusA is a structure-specific nuclease that resolves specifically HJ intermediates in recombination and DNA repair (Mahdi et al., 1996). The resolution activity of RusA has been investigated using synthetic X-junctions with homologous cores. Since a junction lacking homology cannot be resolved by RusA (Chan et al., 1997), we predicted RusA should be able to resolve HJ in the X-JM because there is a 49bp of homology between SHJ(1) and SHJ(2) (Figure 4.7A). Treatment of X-JM with RusA resulted in the conversion of the molecule into three products. Two of these had electrophoretic mobilities consistent with circular P1 and P2 molecules whereas the largest RusA product had a mobility consistent with a circular dimer (Figure 4.7B). This was consistent with our prediction that RusA would cleave HJ in X-JM in one of two orientations, in which one resolution orientation would result in the formation of P1 and P2 monomers whereas the other would form a circular dimer (Figure 4.7A).

To confirm the nature of these products, RusA-mediated resolution products were digested with BbsI or SnaBI after RusA treatment. The § band in lane 4 of Figure 4.8A was predicted to be circular P2 and it was converted into linear P2 of 6.4kb after BbsI restriction digestion (Figure 4.8A, compare lane 4 and 5). The © band in lane 4 was also converted to a 5.2kb band upon digestion with SnaBI, consistent with the prediction that © was a circular P1 (Figure 4.8A, lane 6). We

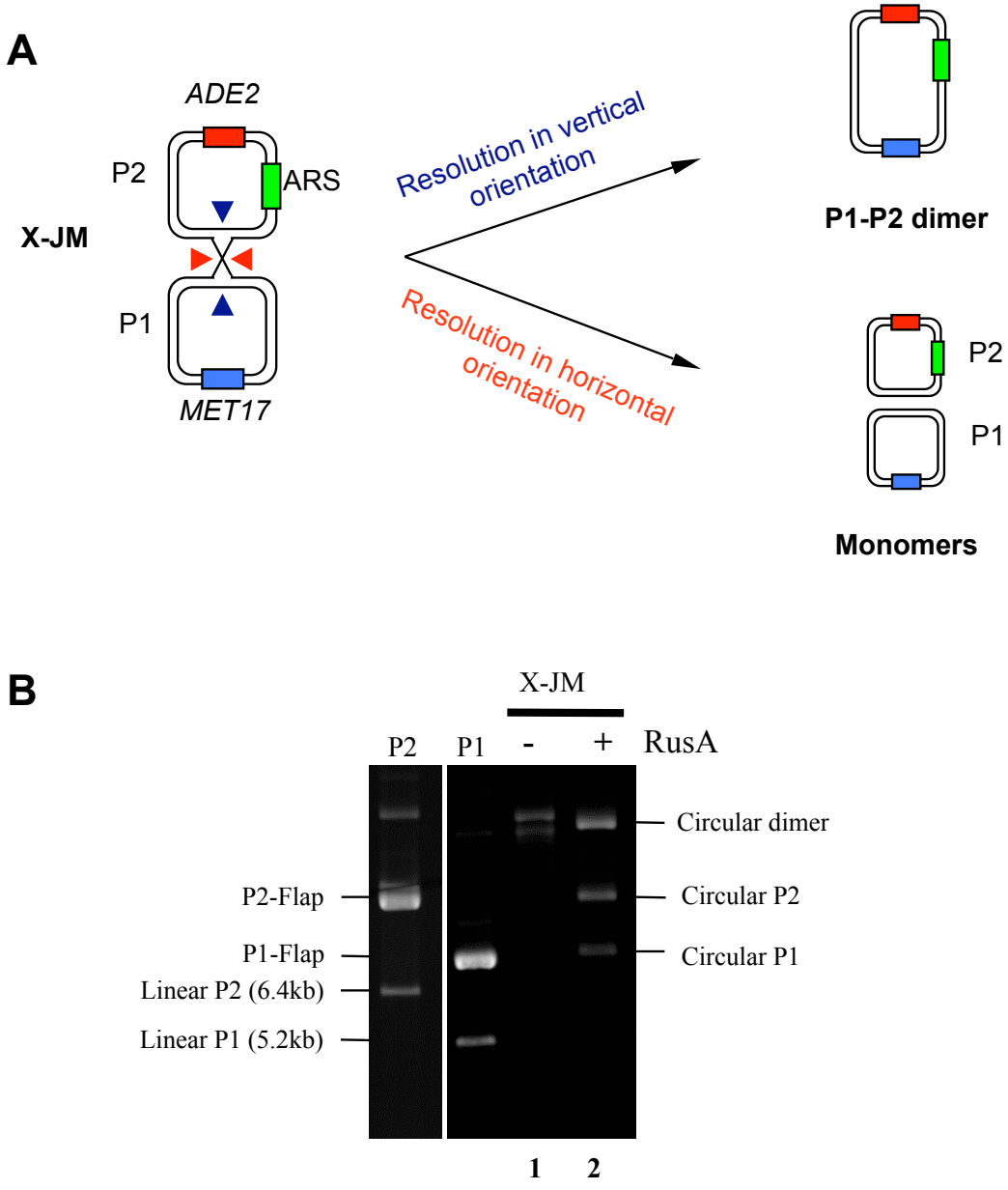


Figure 4.7 Cleavage of the HJ in X-JM by RusA resolvase. (A) Schematic showing two different outcomes of RusA resolution of the HJ in X-JM. (B) Gel electrophoresis analysis of X-JM before and after treatment with RusA HJ resolvase. Individual Flap molecules were included on gel as markers.

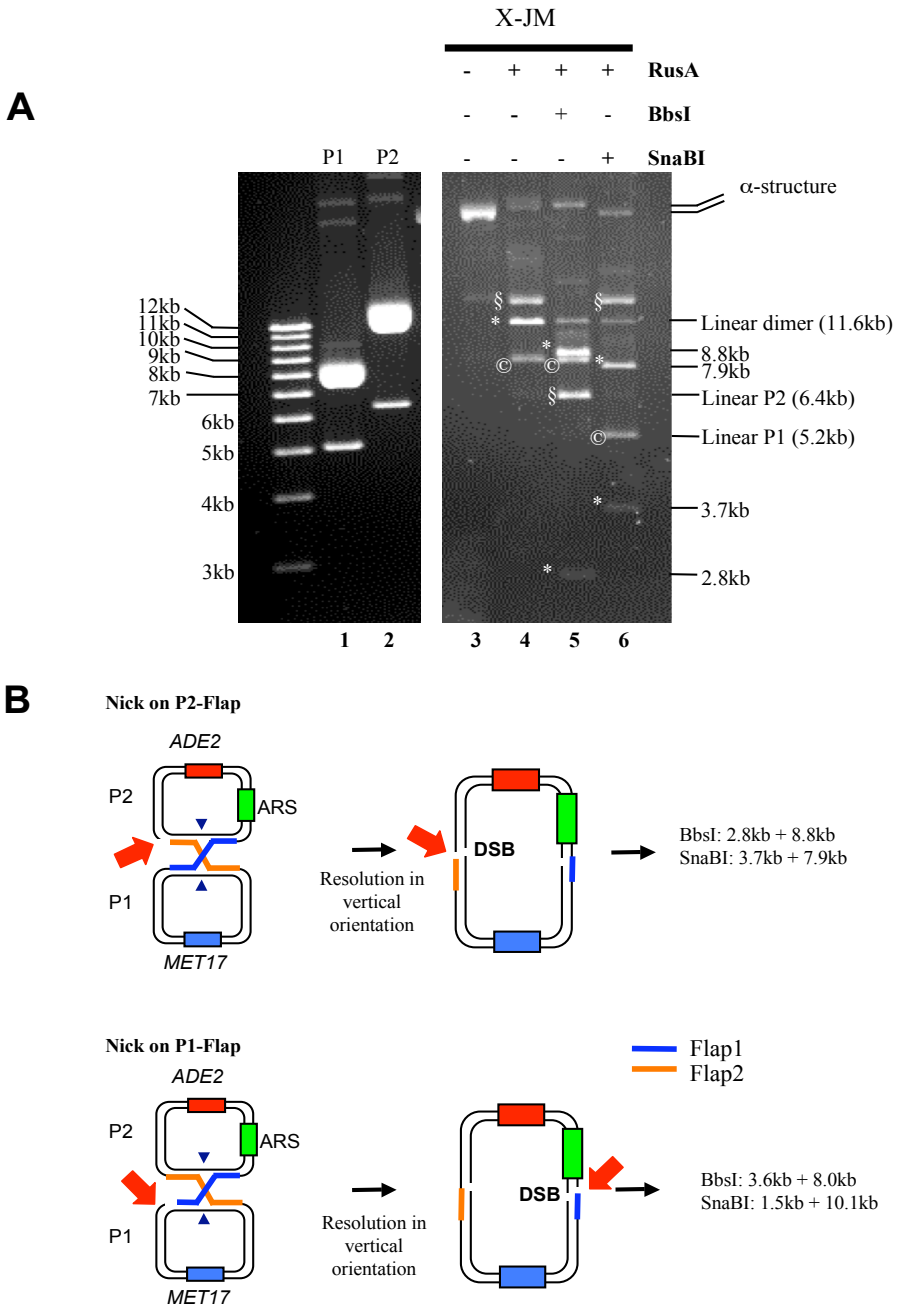


Figure 4.8 Analysis of X-JM resolution products generated by RusA treatment. (A) Gel electrophoresis analysis of resolution products of X-JM. X-JM, which was treated with RusA for 1 hour at 37°C, was subjected to restriction digestion as indicated. § and © represent P2 and P1 generated from X-JM post-RusA treament, respectively. DNA bands marked with asterisk were linear P1-P2 dimer formed after RusA treatment on X-JM. (B) Diagram depicting two possible outcome of RusA resolution on HJ that already has a nick/gap on P2-Flap (upper panel) or P1-Flap (lower panel).

also predicted that a circular dimer would be linearised if digested either with SnaBI or BbsI. This prediction was confirmed by observation of products having molecular weights consistent with the expected 11.6kb linear dimer (Figure 4.8A, lane 5 and 6). Products consistent with the apparent molecular weight of α-structures were also observed in lane 5 and 6 of Figure 4.8A after digestions with BbsI and SnaBI respectively post-RusA treatment. These were X-JM that had not been resolved by RusA proteins, and were restricted by BbsI or SnaBI in the subsequent reactions.

We also noticed a significant amount of linear dimer after RusA treatment and before SnaBI /BbsI restriction digestions (Figure 4.8A, * in Lane 4). This product was only detected in some of the X-JM preparations treated with RusA and therefore was unlikely to be the result of non-specific nuclease activity associated with RusA (compare lane 2 in Figure 4.7B with lane 4 in Figure 4.8A). It was more likely that a nick/gap was present on either the P1-Flap or P2-Flap components on a subset of X-JM molecules prior to RusA treatments. When this nicked-HJ is resolved by RusA in an orientation to form a dimer, the pre-existing nick together with the cleavage by RusA creates a DSB, thus generating a linear dimer molecule (Figure 4.8B). The nick/gap could be present on either P1-Flap or P2-Flap. The position of the nick determines the position of the DSB on the dimer plasmid after RusA resolution on X-JM (Figure 4.8B).

To map the position of nick/gap within the X-JM, the linear dimer formed by RusA resolution was digested with BbsI or SnaBI. We hypothesized that if the nick was present on Flap2, the linear dimer would be digested into 2.8kb and 8.8kb fragments by BbsI, or 3.7kb and 7.9kb fragments by SnaBI (Figure 4.8B, upper panel). Fragments of different sizes would be generated upon BbsI or SnaBI

digestions if the nick/gap were present on Flap1 (Figure 4.8B, bottom panel). After restriction digestions by BbsI or SnaBI, the * band in lane 4 (Figure 4.8A) was converted into two fragments (marked by *) in lane 5 and lane 6 of Figure 4.8A respectively, with DNA fragment sizes that were consistent with the prediction depicted in the upper panel of Figure 4.8B. This data suggested that a nick/break was present on Flap2 of the X-JM preparation shown in Figure 4.8B, prior to RusA-mediated HJ resolution. This is probably due to incomplete ligation of Flap2 to the gap of P1-Flap. RusA digestion was then subsequently used to confirm the complete ligation of individual X-JM preparations.

To summarize, we have established a protocol to synthesize a synthetic HJ-containing plasmid-based molecule, the composition and structure of which has been verified by restriction digestion and RusA-mediated HJ resolution.

4.2.5. *In vivo* HJ resolution of X-JM in *S.cerevisiae*

Having established the structure of X-JM we investigated if the HJ in X-JM could be resolved *in vivo* when transformed into yeast by selecting for resolution events that give rise to dimer and thus methionine prototrophs. Both genetic and molecular approaches were used to establish if the HJ in X-JM could be resolved *in vivo*.

As shown in Figure 4.9B, the transformation efficiency of X-JM is approximately 10^2 colonies forming units (cfu)/μg X-JM substrate. X-JM transformation efficiency is 100-1000 fold lower than that of a control circular plasmid. This is consistent with the prediction that X-JM does not readily provide methionine prototrophy upon transformation unless HJ on X-JM is resolved to form

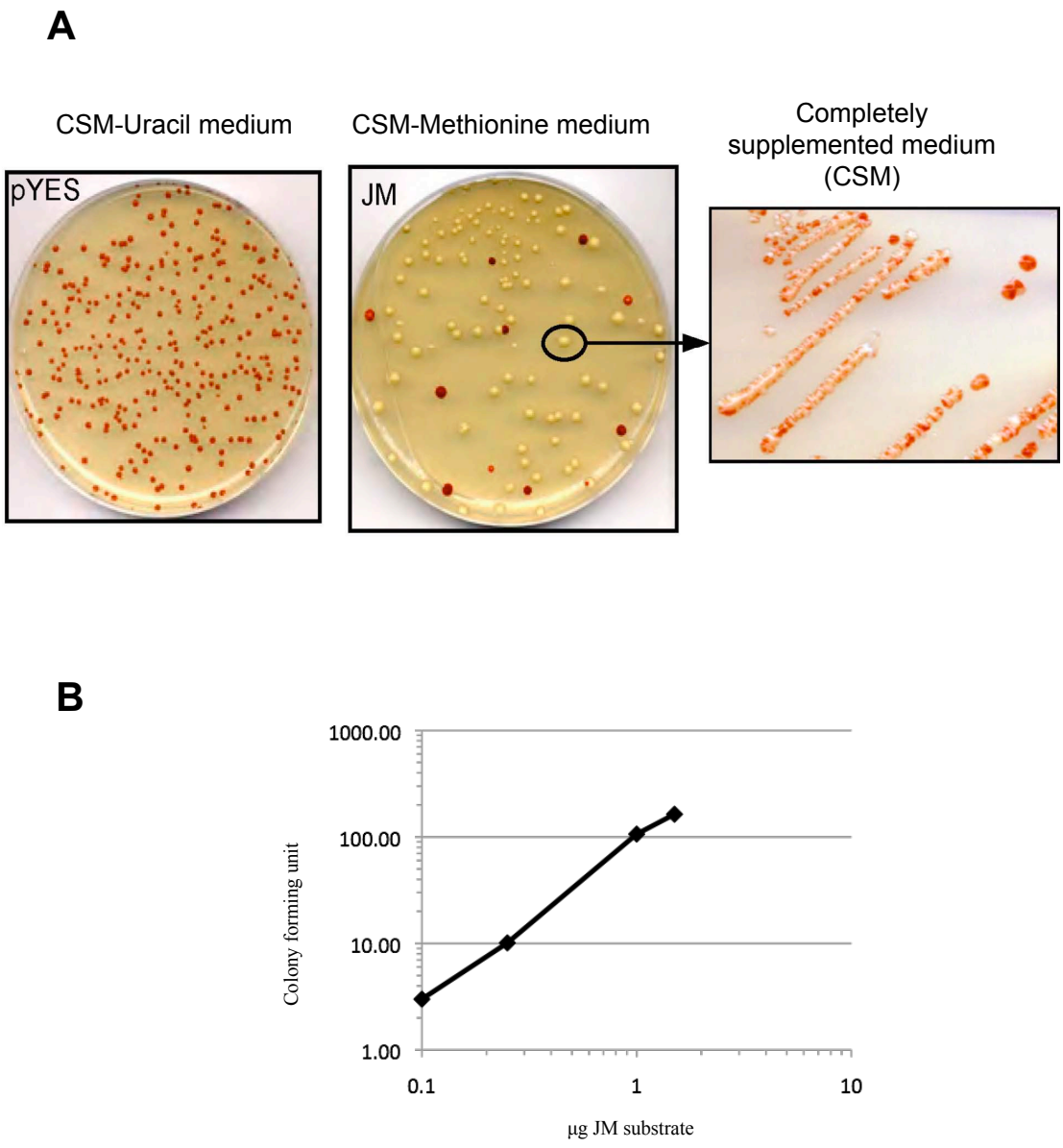


Figure 4.9. *In vivo* X-JM resolution in *met17Δade2Δ* cells. (A) BY4741 wild type cells were transformed with either with a control plasmid, pYES or X-JM, and transformants selected on medium lacking uracil or methionine, respectively, as indicated. Individual colonies of white X-JM transformants were streaked onto non-selective medium (black arrow) to visualise loss of the *ADE2* marker. (B) Quantification of methionine prototroph transformants with varying amounts of X-JM.

a P1-P2 dimer. To confirm that methionine prototrophs arose as a result of P1-P2 dimer formation, we exploited the *ADE2* auxotrophic marker on the P2 component of X-JM. We predicted that all methionine prototrophs should possess intact P2 and thus a functional *ADE2* marker. To confirm the *ADE2* and *MET17* markers were linked following X-JM resolution X-JM was transformed into *met17Δade2Δ* cells and the cells were assessed by the *ADE2* status of methionine prototrophs. 90% of the methionine prototrophs selected after X-JM transformation displayed a white phenotype in *met17Δade2Δ* cells (Figure 4.9A). This indicates that *MET17* and *ADE2* markers are genetically linked after HJ resolution following X-JM transformation, consistent with the prediction of HJ resolution described in Figure 4.1. Approximately 10% of the X-JM transformants displayed red phenotypes despite being methionine prototrophs, suggesting that these might be results of aberrantly processed products that have inactivated *ADE2* gene (Figure 4.9A and see below).

The *ADE2* marker was further exploited to confirm that the linked *MET17* and *ADE2* markers were episomally maintained rather than integrated into the yeast genome. White methionine prototroph colonies from X-JM transformations were therefore grown on non-selective/complete growth media. We predicted that following multiple generation of growth on complete media, some daughter cells would lose the P1-P2 dimer by unequal segregation, and thus lose both *MET17* and *ADE2* markers. Figure 4.9 showed that red sectoring occurred when the white colonies from X-JM transformation were grown on non-selective media. This indicated that the *ADE2* marker was maintained episomally, consistent with the formation of a P1-P2 dimer. Red cells arising through growth on non-selective medium fail to grow on media lacking methionine (data not shown). This is

consistent with our prediction that *MET17* and *ADE2* markers are physically linked after HJ resolution of X-JM and that P1-P2 dimer is episomally maintained in yeast rather than integrated into the genome.

4.2.6. Physical Analysis of X-JM Resolution Products

Having confirmed genetically that X-JM can be resolved *in vivo* into a P1-P2 dimer, X-JM resolution products were physically analysed. X-JM resolution products were recovered from yeast cells by glass-bead genomic preparation protocols as described in the materials and methods chapter. The genomic preparations of individual clones were subjected to Southern analysis.

Figure 4.10A shows the expected P1-P2 dimer resolution product and the predicted sizes of fragments generated by BamHI digestions. Figure 4.10A shows the Southern analysis of five independent X-JM resolution products. A 691bp DraI restriction fragment that is common to both P1 and P2 was used as a ^{32}P-labelled probe (P1/P2 probe). Uncut resolution products ran as two distinct species (Figure 4.10A, lanes 1,3, 5, 7 and 9). One possibility is that the two species were topological isomers that have different electrophoretic mobilities. As predicted BamHI digestion resulted in the conversion of both these species into linear P1 and P2. The P1 and P2 fragments were present in equimolar amounts consistent with the predicted structure of the P1-P2 dimer (Figure 4.10B, lanes 2, 4, 6, 8 and 10).

To confirm that the two bands generated by BamHI digestion were P1 and P2 respectively (Figure 4.10B), a P1-specific probe was used to analyse the Southern blot of the resolution products of X-JM (Figure 4.11). A 435kb NcoI-HindIII fragment from the *MET17* marker of P1 was used as a probe (Figure

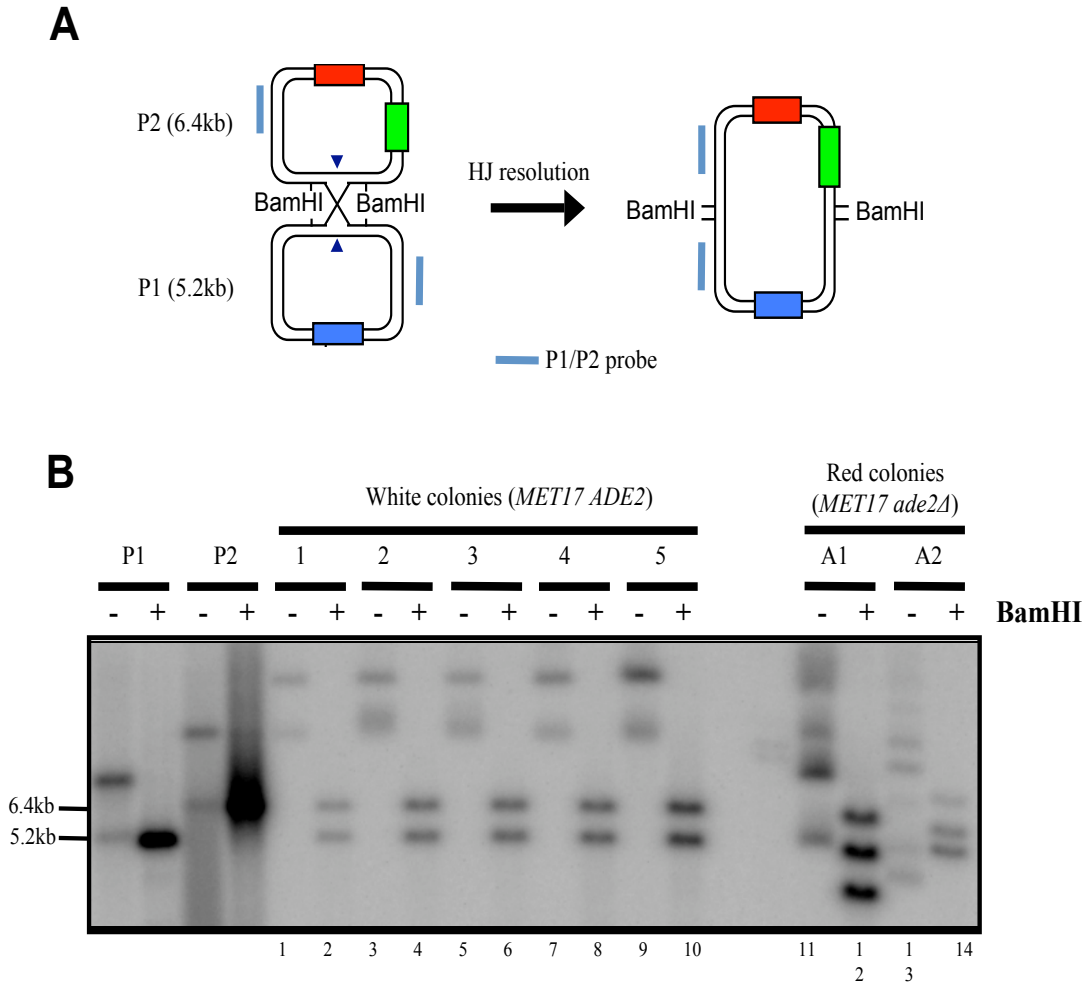


Figure 4.10. Physical analysis of X-JM resolution products. (A) Diagram depicting the relative position of BamHI sites and the P1/P2 probe (blue line). Predicted DNA fragments sizes following BamHI digestion on X-JM was shown. (B) Southern blot analysis of genomic DNA from five independent *MET17 ADE2* X-JM transformants and two *MET17 ade2Δ* digested with BamHI.

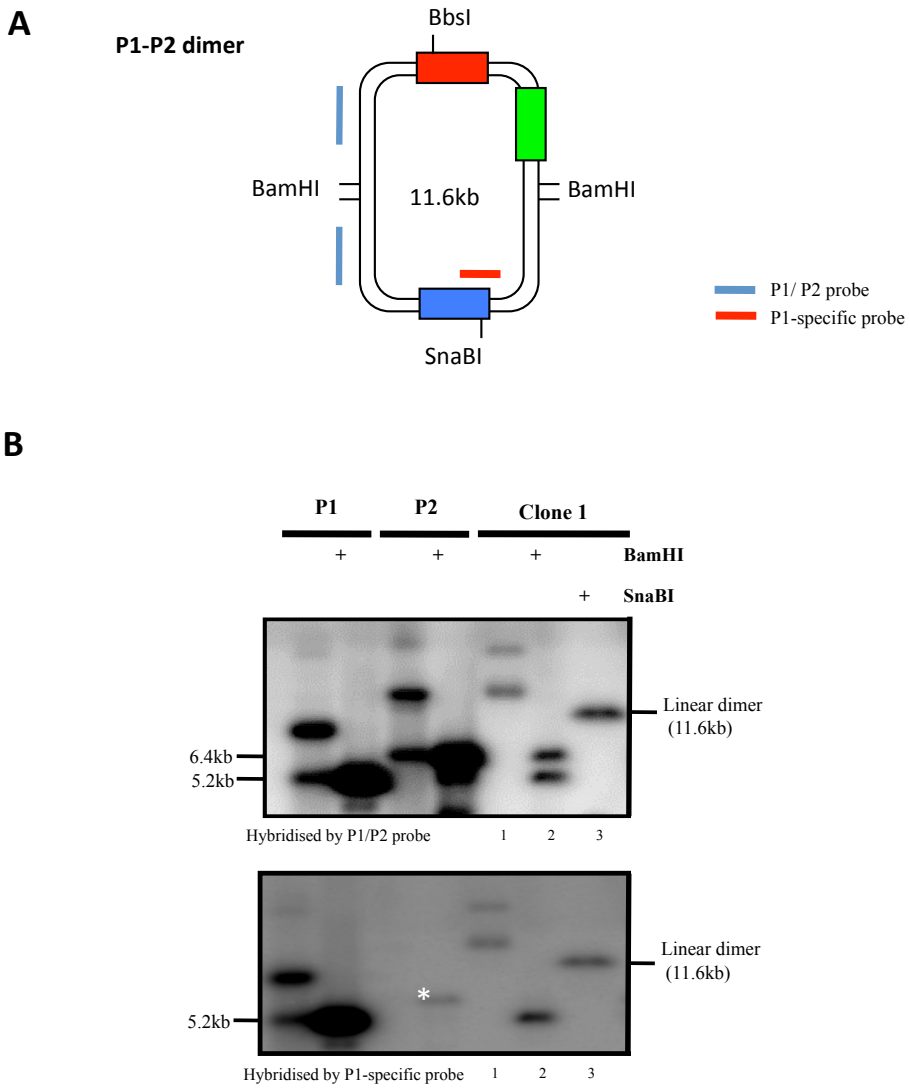


Figure 4.11 Detection of P1 fragment using P1-specific probe. (A) Diagram showing the P1-P2 dimer and the position to which P1/P2 and P1-specific probe hybridise. (B) Southern blot analysis of a randomly chosen white transformants digested with the indicated restriction enzymes. P1 and P2 plasmids were digested with the indicated restriction enzymes and run as markers. The blot in top panel was hybridised with the P1/P2 probe. The same blot was then stripped and re-probed by the P1-specific probe. The white asterisk indicates some residual radioactivity in the linear P2 position, due to the incomplete stripping of the P1/P2 probe.

4.11A). Both the P1-specific probe and P1/P2 probe hybridised to the uncut resolution product and linear fragment generated by SnaBI restriction digestion (Figure 4.11B, lanes 1 and 3 of both panels). As predicted, the P1/P2 probe also hybridised to both DNA fragments generated by BamHI-digested X-JM resolution product (Figure 4.11B, lanes 2 in upper panel). In contrast, the P1-specific probe only hybridised to the 5.2kb band of the BamHI-digested fragments (Figure 4.11B, lane 2 in lower panel). This confirms that the BamHI-digested fragment that runs as a 5.2kb fragment is the P1 plasmid.

Less than 10% of the methionine prototrophs following X-JM transformation show an *ade2Δ* phenotype (Figure 4.9). We predicted that the X-JM resolution products of these methionine prototrophs would have rearranged P2 sequences in the resolution product that renders the *ADE2* marker inactive. Consistent with this hypothesis, products recovered from these red colonies have different electrophoretic mobilities to the expected P1-P2 dimer (Figure 4.10B, compare lanes 11 and 13 with lane 9). BamHI digestion of these resolution products also generated linear fragments that did not correspond to the predicted sizes of P1-P2 dimer (Figure 4.10B, compare lanes 12 and 14 with lane 10). This indicates that methionine prototrophs with an *ade2Δ* phenotype arise as a result of gross rearrangements of X-JM following transformation into yeast.

4.2.7. P1-P2 dimer was generated by resolution of HJ in X-JM rather than inter-plasmid recombination

P1 and P2 plasmids are ~70% homologous. Therefore, an alternative explanation for the formation of P1-P2 dimer following X-JM transformation is that

the P1-P2 dimer arises through *de novo* recombination between contaminating amounts of P1 and P2 plasmid that might be present in X-JM preparations, rather than HJ resolution of X-JM (Figure 4.12). To eliminate this possibility, the hypothetical P1-P2 dimer was constructed by HR in yeast. To do this, plasmids P2 and P1 were sequentially transformed into BY4741 wild type cells, respectively. Both auxotrophic markers on P1 and P2 were selected for during transformation of P1. Since plasmid P1 contains no origin of replication, we predicted that P1 and P2 would recombine to form the "recombinant" form of P1-P2 dimer. Although this recombinant P1-P2 dimer is identical in size to the dimer predicted to arise from the resolution of X-JM, the P1 and P2 components are in opposite orientations in each of the two dimer molecules (Figure 4.12A). Southern blot analysis was used to compare the structure of the recombinant P1-P2 dimers with the products generated by X-JM transformation.

As predicted, BamHI digestion converted both P1-P2 recombinant and X-JM resolution dimers into linear P1 and P2 (Figure 4.10B, compare lanes 2, 6 and 10 in both panels). BbsI digestion produces a 11.6kb linear DNA fragment from both P1-P2 recombination and resolution dimers (Figure 4.10B, compare lanes 3, 7 and 11 in both panels). We predicted that upon BbsI and SnaBI double digestion, the P1/P2 probe should detect a single 6.3kb DNA fragment from digestion of the P1-P2 resolution dimer, whereas the probe should detect two DNA fragments of 4.5kb and 7.1kb following digestion of the P1-P2 recombination dimer (Figure 4.12A). Consistent with our hypothesis, one 6.3kb fragment was detected when P1-P2 resolution dimer were digested with BbsI and SnaBI (Figure 4.12B, lanes 4, 8 and 12 in upper panel). In contrast, two fragments consistent with the predicted lengths of 4.5kb and 7.1kb were produced by digesting P1-P2 recombination dimers

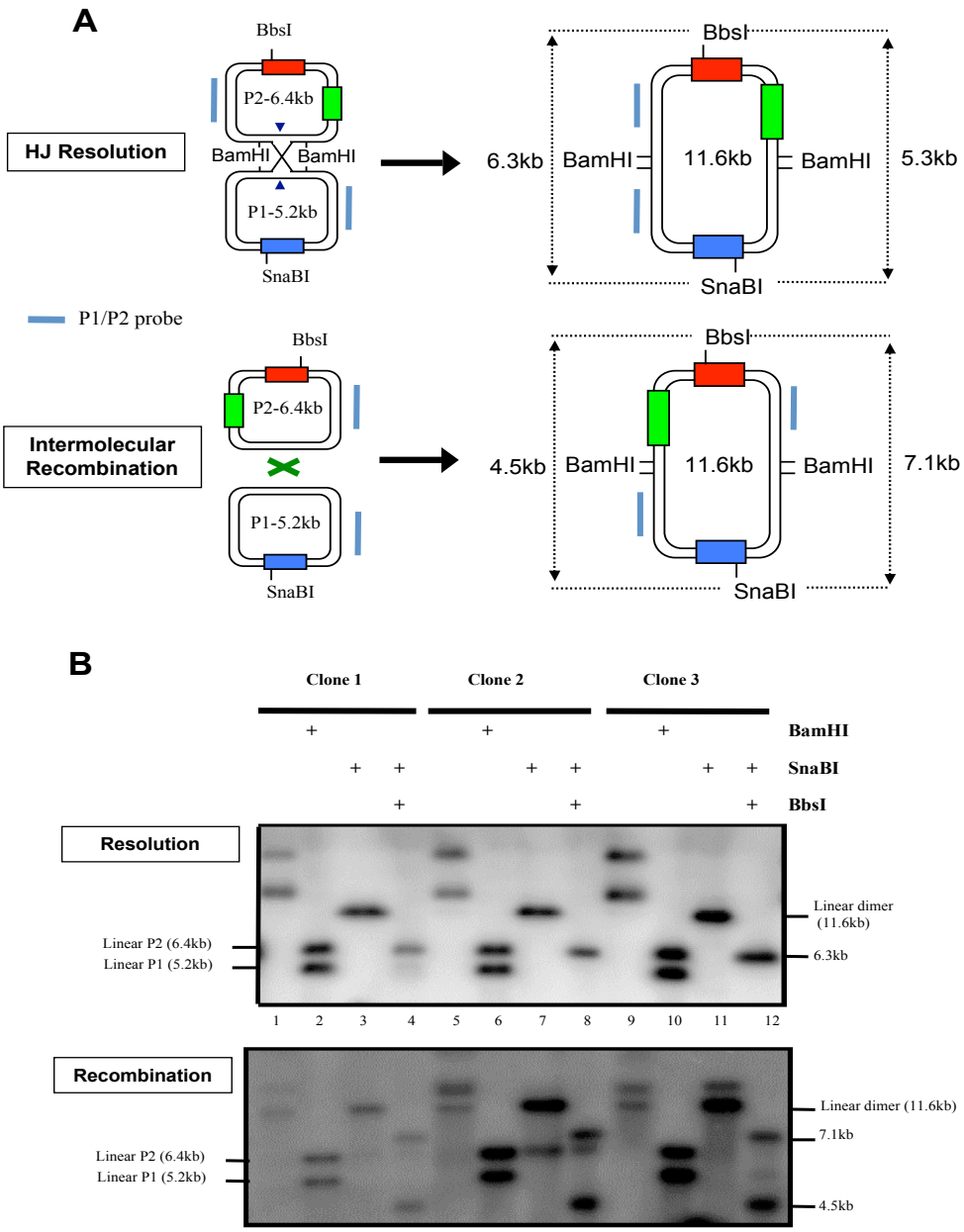


Figure 4.12 Comparison of X-JM resolution dimer and P1-P2 recombinant dimer. (A) Schematic depicting how P1-P2 dimer can be generated via HJ resolution of HJ on X-JM or *de novo* recombination between P1 and P2 plasmids. (B) Southern blot analysis of genomic DNA extracted from X-JM transformants (upper panel) and P1-P2 recombinant (lower panel) digested with restriction enzymes as indicated. (see texts for further details).

with BbsI and SnaBI (Figure 4.12B, lanes 4, 8 and 12 in lower panel). These results confirmed that the products recovered from yeast transformed with X-JM were generated exclusively through HJ resolution and not *de novo* recombination between P1 and P2 monomers.

4.2.8. Sequence Analysis of X-JM Resolution Products

Having established that X-JM transformants arose by a process consistent with HJ resolution as opposed to *de novo* recombination between P1 and P2, we went on to analyse the fidelity by which the HJ in X-JM was resolved *in vivo*. To do this, we amplified the SHJ regions on X-JM in which resolution was predicted to occur from the resolution products by PCR and carried out analysis by DNA sequencing (Figure 4.13A). SHJ(1) and SHJ(2) were designed such that the HJ forms within a 49bp of homologous sequence (Figure 4.3A). The HJ can thus potentially branch migrate freely in either direction within this homologous region.

We observed that 68.5% of all resolution products displayed no mutations in either of the SHJ regions, implying an accurate and potentially symmetrical HJ resolution event of the HJ in X-JM (Fig. 4.13C). Two of the 132 resolution products analyzed displayed evidence of a GC event, in which 24 and 29 nucleotide sequences , respectively, of one of the arms of the HJ was transferred to another non-reciprocally (Fig. 4.13C). We also observed a specific 33bp deletion event on one side of the HJ in 30% of resolution products (Fig. 4.13C). The deletion occurred in the homology/heterology boundary of Flap 2, as shown by the green rectangle marked in Figure 4.13A. The alignments of the PCR sequences of 33bp deletion regions are shown in Figure 4.13B. How the deletion event was generated

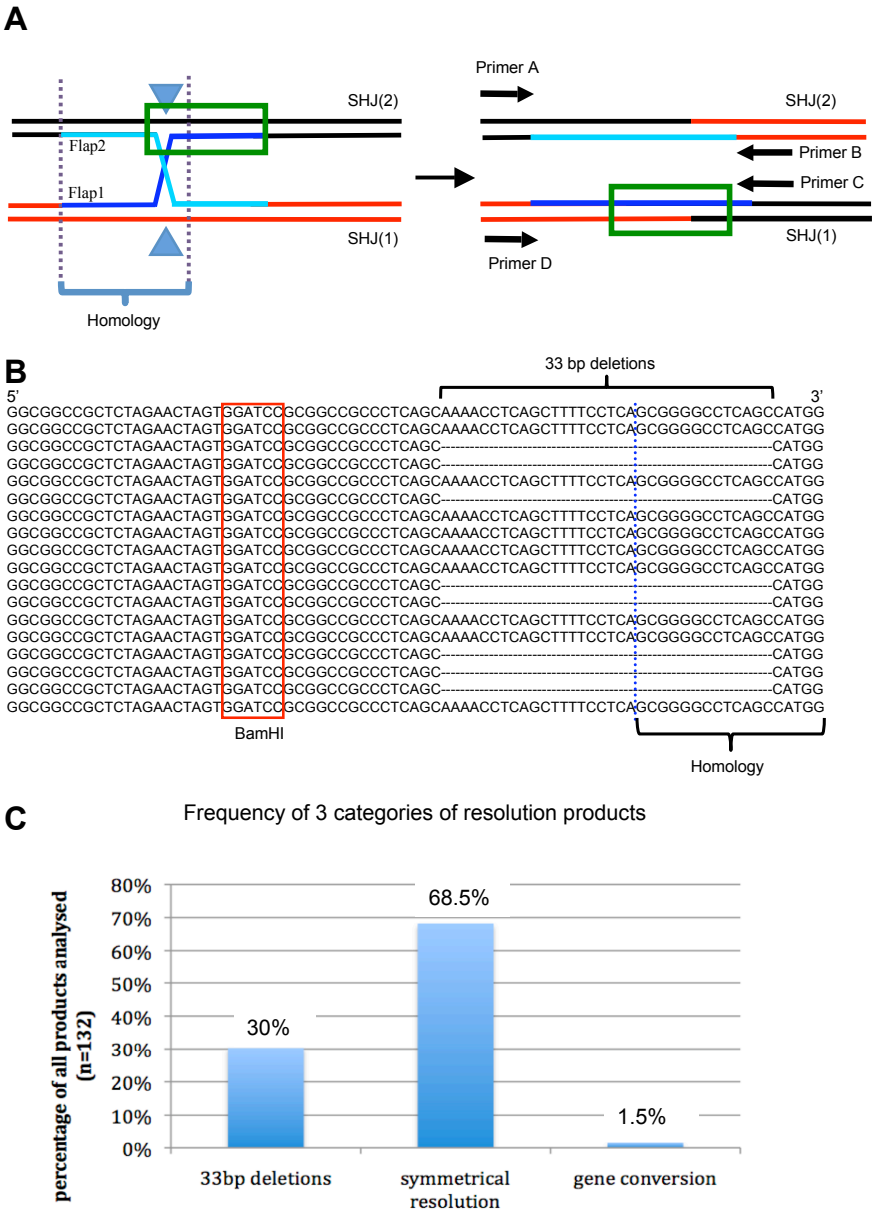


Figure 4.13. Sequence analysis of X-JM resolution products. (A) Diagram depicting the single HJ in X-JM and the resolution products generated following strand-specific incisions indicated by the blue arrowheads. The green rectangle indicates the position of the 33 bp deletion revealed by sequence analysis (see below). Primers A, B, C and D were used to amplify SHJ sequences from resolution products for sequencing. (B) Alignment of 18 sequencing results. Red rectangle indicates the BamHI recognition sites. The position of a 33bp deletion found in 30% of resolution event spans the homology/heterology boundaries. (C) Frequency of accurate resolution, GC and 33bp deletion events detected by SHJ sequence analysis among 132 independent X-JM transformants.

is not fully understood. Nevertheless, the accurate maintenance of SHJ sequences as shown in ~70% of the resolution products suggest that X-JM was resolved *in vivo* by a high-fidelity HJ resolution mechanism in *S.cerevisiae*.

4.3. Discussion

The canonical HR-mediated DSB repair model involves multiple, sequential events, which begins with DSB end resection, strand invasion, DNA synthesis, second-end capture, HJ branch migration and HJ resolution. As described in the introduction, the early steps of DSB repair pathway such as end-resection and strand invasion, in eukaryotes, have been extensively studied and this has resulted in detailed knowledge about the roles of several enzymes responsible for these processes. In contrast, much less is known about proteins involved in the later stages of eukaryotic DSB repair such as HJ resolution. HJ resolution is an essential process unique to HR and requires structural-specific nucleases known as resolvases to cleave a specific pair of DNA strands at HJ to generate either CO or NCO products (Figure 1.3(i)).

Here, we report the development of an *in vivo* HJ resolution assay in *S.cerevisiae*, which provides a direct and quantitative measurement of *in vivo* HJ resolution efficiency. We have engineered a synthetic HJ molecule by linking two plasmids by a single HJ. The structure of the Joint-molecule, X-JM, has been verified by restriction digestion analysis. More importantly, the single HJ engineered between the plasmids could be recognized and resolved by the prokaryotic RusA endonuclease, a HJ resolvase encoded by a cryptic prophage gene in the *E.coli* genome, which can resolve oligo-based model HJs (Chan et al., 1998; Mahdi et al., 1996). When transformed into *met17Δ* cells, the HJ on X-JM must be resolved to form a plasmid linking the ARS to the *MET17* auxotrophic marker. This will enable stable maintenance of the resolved X-JM and confer methionine prototrophy to *met17Δ* cells. Therefore, the transformation efficiency of X-JM

allows a quantitative measurement of the efficiency of HJ resolution in X-JM *in vivo*.

Using a combination of genetic and physical analyses, 90% of the methionine prototrophs following X-JM transformation were shown to contain the predicted P1-P2 dimer generated as a result of HJ resolution in X-JM. Approximately 10% of the X-JM transformed methionine prototrophs arose through a gross rearrangement of the X-JM molecule resulting in a non-functional *ADE2* allele (Figure 4.9). These products likely represent aberrant processing of the HJ in X-JM or some secondary recombination event, which led to the inactivation of *ADE2* auxotrophic marker on P2 plasmid. It was also shown that the resolution products of X-JM were generated specifically through HJ resolution, rather than *de novo* recombination between the two constituent plasmids, P1 and P2.

At the DNA sequence level 68.5% of resolution products displayed no mutations. This implies that the majority of the resolution products arise in an error-free process. Two out of 132 resolution products contained a short-patch GC event. This short-patch GC event suggests the HJ had migrated across the homology/heterology boundary of the HJ, resulting in the formation of heteroduplex DNA and its subsequent repair by MMR pathway. The repair of the heteroduplex by MMR machinery thus gives rise to GC.

In summary, we have demonstrated the proof of principle that a synthetic HJ introduced into yeast can be resolved. However the yield and quality of X-JM preparation were found to be highly variable. These inconsistencies, together with the facts that ~30% of X-JM transformants appeared to have arisen by a mechanism that did not resemble canonical HJ resolution and involved a specific 33bp deletion, prompted us to adapt an alternative approach to generate X-JM.

Chapter Five

5. The analysis of putative Holliday Junction Resolvases in *Saccharomyces cerevisiae*

5.1.Introduction

In chapter 4, a system was designed to analyse HJ resolution *in vivo* directly without involving the preceding steps of HR-mediated DSB repair. This set of pilot experiments confirmed the feasibility of such a system and demonstrated that synthetic HJ-containing plasmids can be resolved with high fidelity *in vivo*. However, the yield and more importantly the quality of X-JM preparations was found to be highly variable. This was partly due to the multi-step nature of the procedure to generate X-JM. To overcome these caveats, a more robust method for the synthesis of a plasmid-borne HJ substrate was sought. To do this, the XerC/D site-specific recombination system found in prokaryotic organisms was utilized to create an HJ-containing plasmid in *E.coli*. This chapter will describe the establishment and validation of such a system and its use in the genetic analysis of HJ resolution in *S.cerevisiae*.

5.2. Results

5.2.1. Exploitation of XerC/D site-specific recombination to generate a synthetic HJ for introduction into *S.cerevisiae*

XerC/D site-specific recombination is essential for the stable inheritance of multi-copy plasmids and efficient segregation of the *E.coli* chromosome or plasmids during cell division (Blakely et al., 1991; Summers and Sherratt, 1984). HR between replicating or newly replicated chromosomes can result in the formation of chromosomal dimers, preventing segregation of newly replicated chromosomes into daughter cells as the host cell divides (Summers and Sherratt, 1984). To resolve these dimeric molecules, XerC/D site-specific recombination is utilized to monomerize the multimers by acting on specific consensus sequences such as *cer* in ColE1 (Blakely et al., 1993; Colloms et al., 1990; Stirling et al., 1989; Stirling et al., 1988a; Stirling et al., 1988b; Summers et al., 1985). XerC and XerD, together with two accessory proteins ArgR and PepA, are necessary to mediate XerC/D site-specific recombination (Colloms et al., 1996; McCulloch et al., 1994). XerC/D-mediated recombination proceeds by sequential exchanges of two pairs of strands, a mechanism similar to that catalysed by members of the lambda integrase family of recombinase (Hoess et al., 1987; Hsu and Landy, 1984; Meyer-Leon et al., 1988; Stark et al., 1992). McCulloch and co-workers reported the construction of an *E.coli* strain (RM40) in which the expression of XerC can be tightly regulated by a *lac* promoter *in vivo* (McCulloch et al., 1994). They studied the effect of XerC/D-mediated recombination at two direct repeats of *cer* sequences on a plasmid. The analysis of the products demonstrated the production of a HJ that

was created by the exchange of a specific pair of DNA strains within the *cer* sites (McCulloch et al., 1994). More importantly, it was discovered that the HJ structures generated by XerC/D system accumulate rather than being processed subsequently to form monomers. This unique feature of XerC/D-mediated recombination specifically on *cer* sequences, in which HJ intermediates accumulate, made this an attractive system to exploit for the synthesis of a synthetic HJ substrate.

To create an HJ-containing plasmid substrate, two direct repeats of *cer* sequences were cloned into an *E.coli-S.cerevisiae* shuttle vector containing appropriate markers, forming JM (Figure 5.2 and refer to materials and methods for JM cloning strategy). The two *cer* sequences were positioned in the JM plasmid such that they separate CEN-ARS and the *MET17* auxotrophic marker from the *HIS3* marker (Figure 5.2). This is done to ensure that when the HJ forms between the *cer* sequences, the HJ will separate CEN-ARS/*MET17* and *HIS3* markers into two distinct circular domains (Figure 5.1 and 5.2A). By inducing XerC/D-mediated site-specific recombination between the two *cer* sequences in RM40 cells (McCulloch et al., 1994), a HJ-containing plasmid substrate, which we refer to as JM-HJ, can be synthesized *in vivo*. Similar to X-JM in chapter 4, the purified JM-HJ can be transformed into *S.cerevisiae* and resolved into selectable products (Figure 5.1).

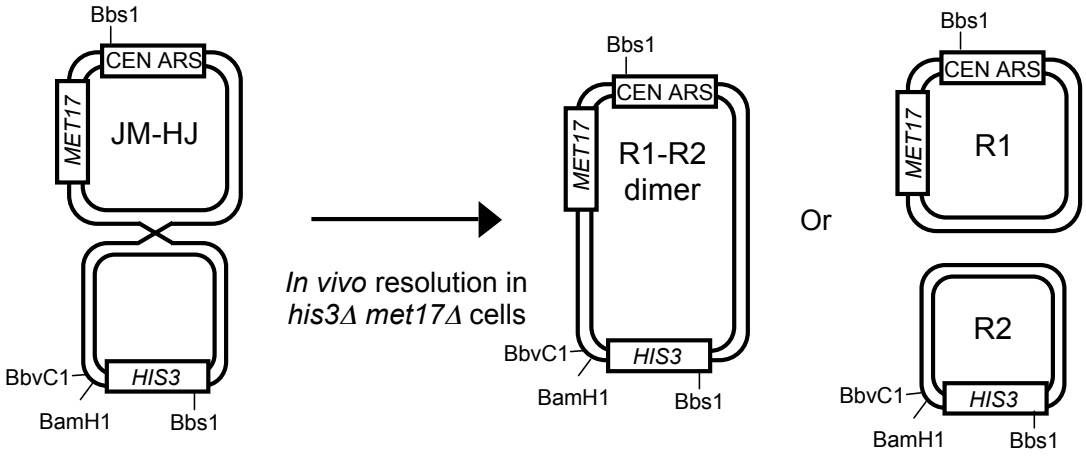


Figure 5.1 System to directly analyse HJ resolution *in vivo.* Depiction of system used to analyse HJ resolution *in vivo*. Resolution of the HJ in JM-HJ into an R1-R2 dimer is detected as methionine and histidine prototrophs that arise following JM-HJ transformation into *S.cerevisiae.* HJ Resolution to form R1 and R2 monomers separate ARS from *HIS3* marker, thus do not provide methionine and histidine prototrophy to the cells.

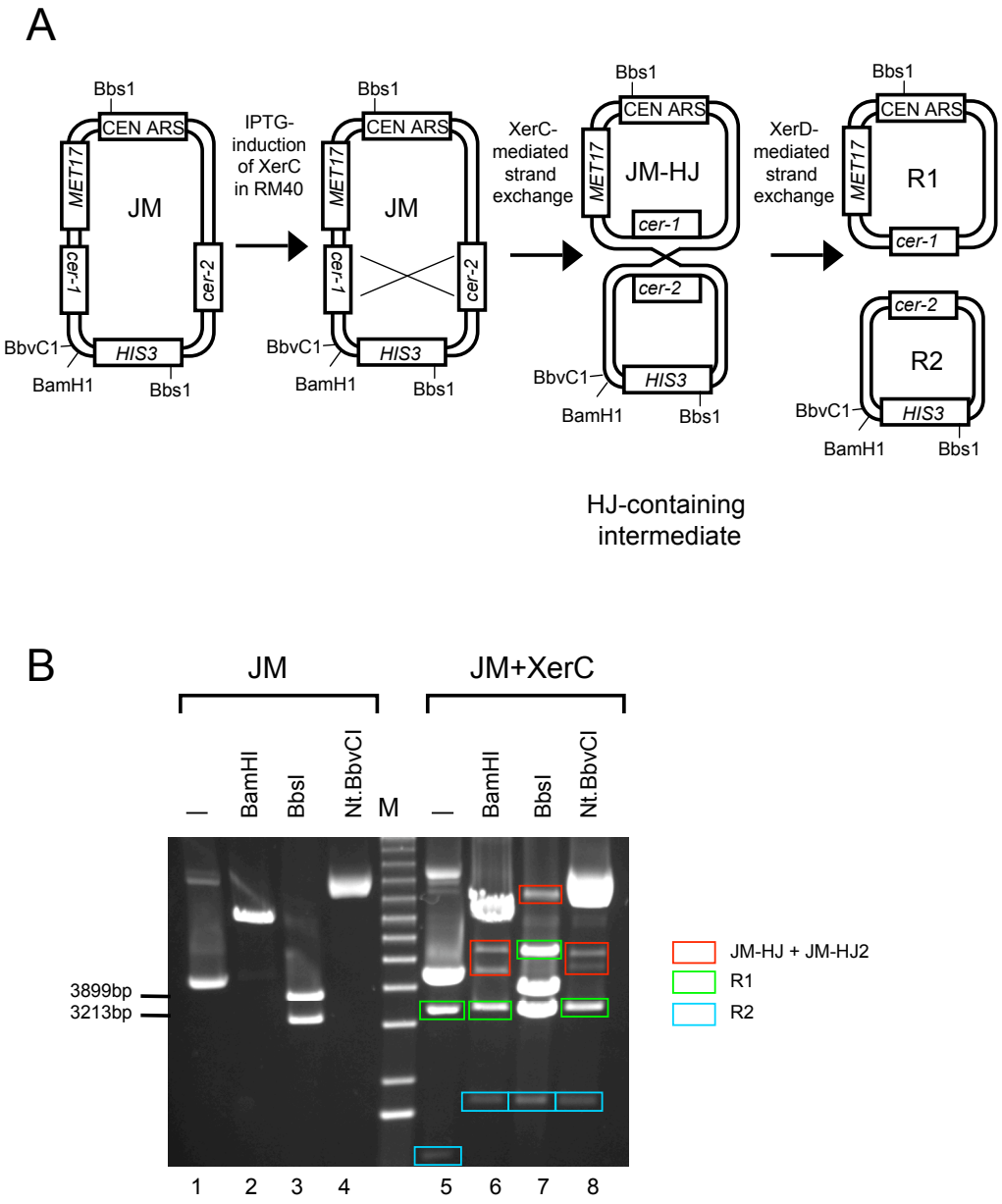


Figure 5.2 XerC/D site-specific recombination system and the induction of JM-HJ. (A) Schematic diagram showing the mechanism of XerC/D site-specific recombination system. XerC catalyses first strand exchange between the direct *cer* repeats to form HJ-containing intermediate. XerD catalyses second strand exchange of the HJ to monomerize the plasmid. (B) Gel electrophoresis analysis of plasmids prepared from RM40 cells carrying JM, which have or have not been subjected to XerC induction, as indicated. DNA has been digested with restriction enzymes as indicated. Species that arise following XerC induction have been boxed, as indicated.

5.2.2. Induction of JM-HJ

To generate the JM-HJ molecule, JM was transformed into RM40 cells that contain *xerC* under the control of the lac promoter (Figure 5.2A). *xerC* expression was induced for 2h in a 5l log-phase culture of RM40/JM by the addition of 1mM IPTG. Induction of *xer*-mediated intra-molecular recombination between the two *cer* sites generates two circular products, R1 and R2 (Figures 5.2B, compare lane 1 and 5). However, JM-HJ is indistinguishable from JM in the total plasmid preparation because JM-HJ and JM are identical in mass (Figure 5.2A and 5.2B, compare lane 1 and 5). To confirm the presence of JM-HJ, the *xerC*-induced plasmid preparations were analysed by restriction digestion.

When digested with BamHI, JM was converted into a linear molecule (Figure 5.2B, lane 2). In the *xerC*-induced plasmid preparations, BamHI digestion resulted in the formation of two new species that run at slightly above the position of the supercoiled JM (Figure 5.2B, red box in lane 6). The fact that these two new species have greater electrophoretic mobilities than the BamHI-digested linear JM indicates that they are most probably α structures that are partially supercoiled, since only the R2 component of JM-HJ is digested with BamHI, while the R1 domain remains intact and supercoiled. As predicted, the R2 plasmid that forms as a result of site-specific recombination was also linearised by BamHI digestion, whereas the R1 plasmid was resistant to BamHI digestion (Figure 5.2B, blue and green boxes in lane 6). BbsI digestion converts JM into 3899 and 3213bp fragments (Figure 5.2B, lane 3). In contrast, JM-HJs were converted into a single species that migrates slightly slower than the linear JM (Figure 5.2B, red box in lane 7). This is consistent with the predicted electrophoretic mobility of a χ structure that forms

when both R1 and R2 domains on JM-HJ are digested with BbsI (Figure 5.2A). As predicted, R1 and R2 plasmids were both linearised by BbsI digestion (Figure 5.2B, green and blue boxes in lane 7). Nt.BbvCI enzyme (NEB) creates a single-strand nick on the BbvCI recognition sites on JM, thus forming an open-circular JM plasmid (Figure 5.2B, lane 4). In contrast, upon Nt.BbvCI digestion of the R2 domain of JM-HJ, two species that have greater electrophoretic mobilities than the linear JM but slightly reduced electrophoretic mobilities than the supercoiled JM were formed (Figure 5.2B, red box in lane 8). This is consistent with the notion the two species are partially supercoiled, in which the R1 domain remains supercoiled even after the R2 domain is relaxed by Nt.BbvCI nicking enzymes.

Taken together, the data indicates that the formation of α and χ structures when *xerC*-induced plasmid preparations are digested with BamHI and BbsI, respectively, confirms that two HJ-containing species are generated following *xerC* induction. These data also demonstrate that the partially supercoiled JM-HJ formed as a result of Nt.BbvCI treatment has distinct R1 and R2 domains that are topologically independent, consistent with the observations reported in McCulloch et al. (McCulloch et al., 1994).

5.2.3. Purification of JM-HJ

To purify JM-HJ from the mix of molecules generated by XerC induction, we followed the scheme in Figure 5.3. As shown in lane 8 in Figure 5.2, the yield of the two JM-HJ species was low, relative to the relaxed circular JM. The level of accumulation of the HJ-containing molecules could not be increased by altering the *xerC* induction conditions such as increasing the duration of induction or the IPTG

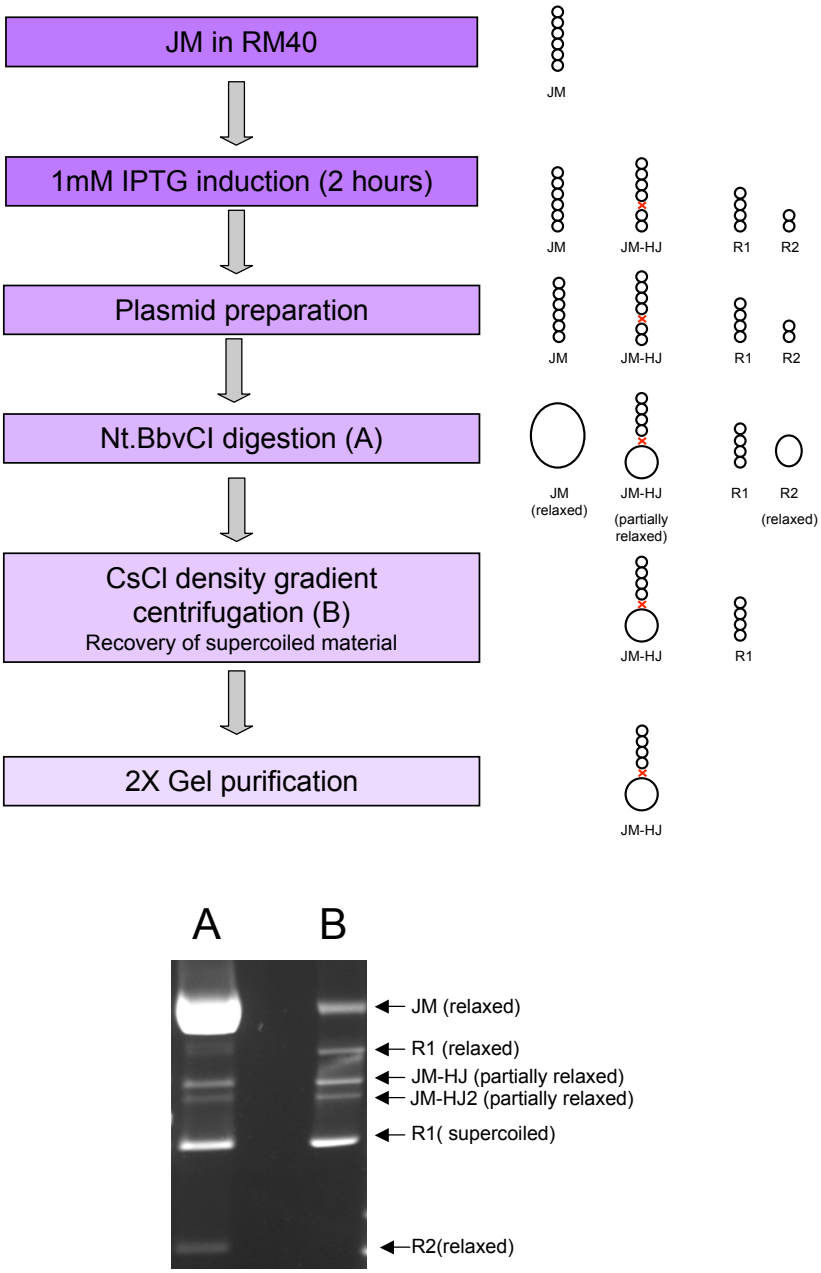


Figure 5.3 Purification of JM-HJ. Upper panel: Flow diagram outlining process for the purification of JM-HJ. Molecules expected to be enriched at each step are shown to the right (although R2 does not contain an origin of replication, R2 is still present since the period of XerC induction is too short for the circular R2 to be lost from the population). The HJ in JM-HJ is depicted in red. Lower panel: Agarose gel electrophoresis of DNA from steps (A) and (B) shows the enrichment of JM-HJ following CsCl density gradient centrifugation.

concentration (data not shown). The low yield of JM-HJ molecules precluded the purification of JM-HJ by conventional gel purification since the JM-HJ preparation were invariably contaminated with parental JM molecules. To overcome this problem, plasmid preparations were enriched for JM-HJ by exploiting the fact that after Nt.BbvcI digestion, the R1 domain of JM-HJ remains supercoiled whereas JM, which has no HJ, is completely relaxed. JM-HJ and JM following digestion with Nt.BbvCI could then be separated in a CsCl density gradient by virtue of the supercoiled domain in JM-HJ. As predicted, both HJ-containing molecules were enriched following CsCl density gradient centrifugation, confirming that these species contain supercoiled domains (Figure 5.3). Both molecules following this enrichment step were subjected to two rounds of gel purification in a 0.7% TAE agarose gel. Herein we refer to the purified upper and lower species containing partially supercoiled HJ as JM-HJ and JM-HJ2, respectively.

5.2.4. Verification of the Structure of JM-HJ Molecules

Southern blot analysis, using the *cer* sequence as a probe, was used to confirm the structures of JM-HJ and JM-HJ2 (Figure 5.4A). Purified JM-HJ appeared as two species following gel electrophoresis (Figure 5.4B, lane 7). The lower species is the partially relaxed molecule in which the R1 domain remains supercoiled, whereas the upper species corresponds to a fully relaxed molecule in which both R1 and R2 domains are relaxed. The spontaneous nicking of the R1 domains probably occurs during the agarose gel purification steps of the scheme shown in Figure 5.3. The electrophoretic mobilities of both forms of JM-HJ were slightly different to the supercoiled and relaxed forms of JM, consistent with the presence of a HJ in JM-HJ

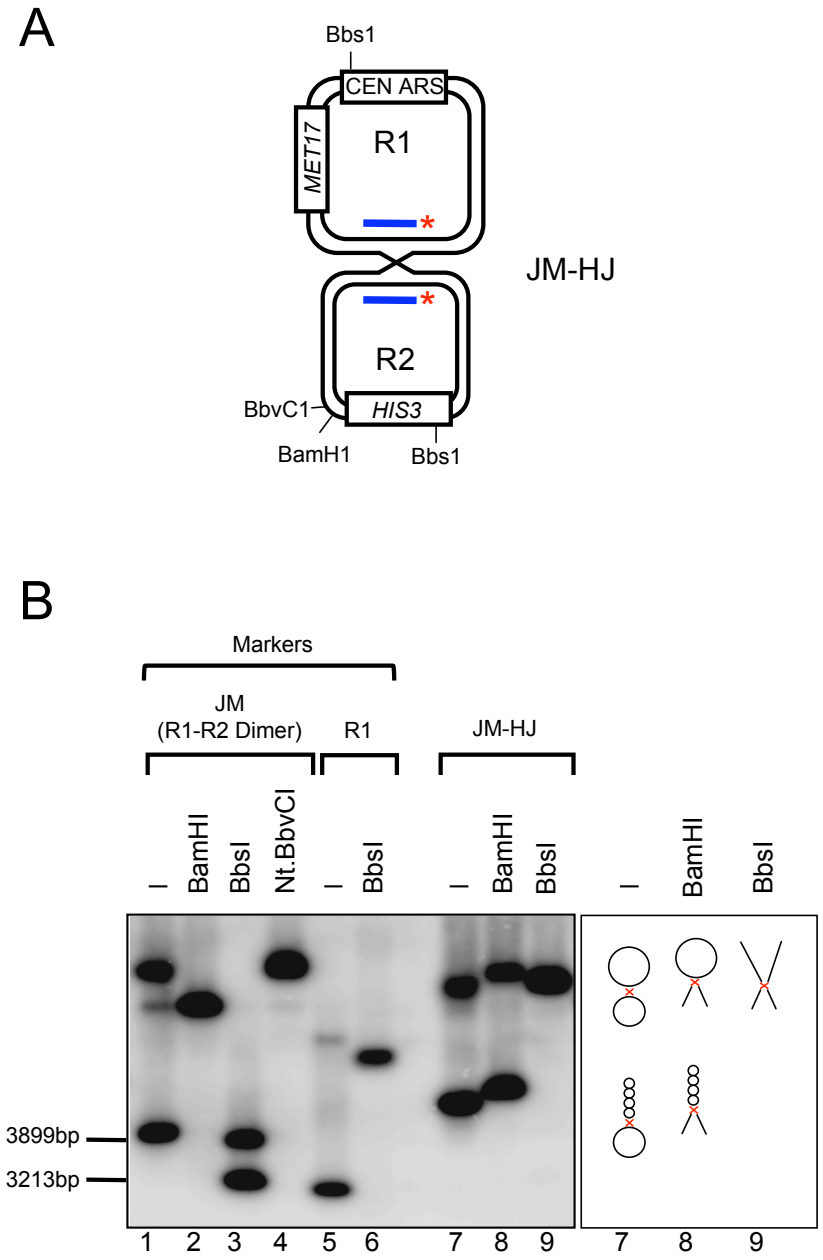


Figure 5.4 Analysis of JM-HJ. (A) Schematics of JM-HJ with positions of relevant restriction sites, auxotrophic markers and ARS. Blue line with red asterisk represents the ~200bp *cer* sequences used as the probe for Southern blot analysis. (B) Left panel: Southern blot analysis of purified JM, R1 and JM-HJ digested with various enzymes as indicated. Right panel: Representations of JM-HJ molecules present in lanes 7, 8 and 9 of the Southern blot as indicated. The HJ in JM-HJ is shown in red.

(Figure 5.4B, compare lane 1 and 7). When the R2 domain of JM-HJ was linearised by BamHI, the electrophoretic mobilities of the two JM-HJ species became retarded, consistent with the formation of an α structure (Figure 5.4B, lane 8). Linearisation of both R1 and R2 domains by BbsI converted both forms of JM-HJ into a single species that had an electrophoretic mobility consistent with a χ-structure (Figure 5.4B, lane 9).

BamHI or BbsI digestion of the parental JM molecule generated either linear JM (7112bp) or fragments of 3899 and 3213 bp, respectively, as predicted (Figure 5.4B, lanes 2 and 3). There was no evidence of these JM-derived fragments in the JM-HJ digestion products indicating that the JM-HJ preparation was free of any contaminating parental JM (Figure 5.4B, compare lanes 2 and 3 with lanes 8 and 9, respectively). Similarly, there was no evidence of any contaminating R1 in the JM-HJ products (Figure 5.4B, compare lanes 6 and 9). It is important to note the absence of any contaminating JM in the JM-HJ preparations since JM is indistinguishable from dimeric products of JM-HJ resolution and thus could give rise to false positive resolution events.

JM-HJ2 (Figures 5.2B and 5.3) was also gel purified and analysed by Southern blot. Like JM-HJ, JM-HJ2 also appeared as two species following gel electrophoresis, indicative of the nicking of R1 domains during gel purification (Figure 5.5B, red boxes in lane 4). JM-HJ2 could be converted into α and χ structures, which run at positions identical to α and χ structures derived from JM-HJ, upon BamHI and BbsI restriction digestions, respectively (Figure 5.5B, red boxes in lane 5 and 6). This confirms that JM-HJ2 also comprises a single HJ linking the two *cer* direct repeats. However, the purified JM-HJ2 was often contaminated with

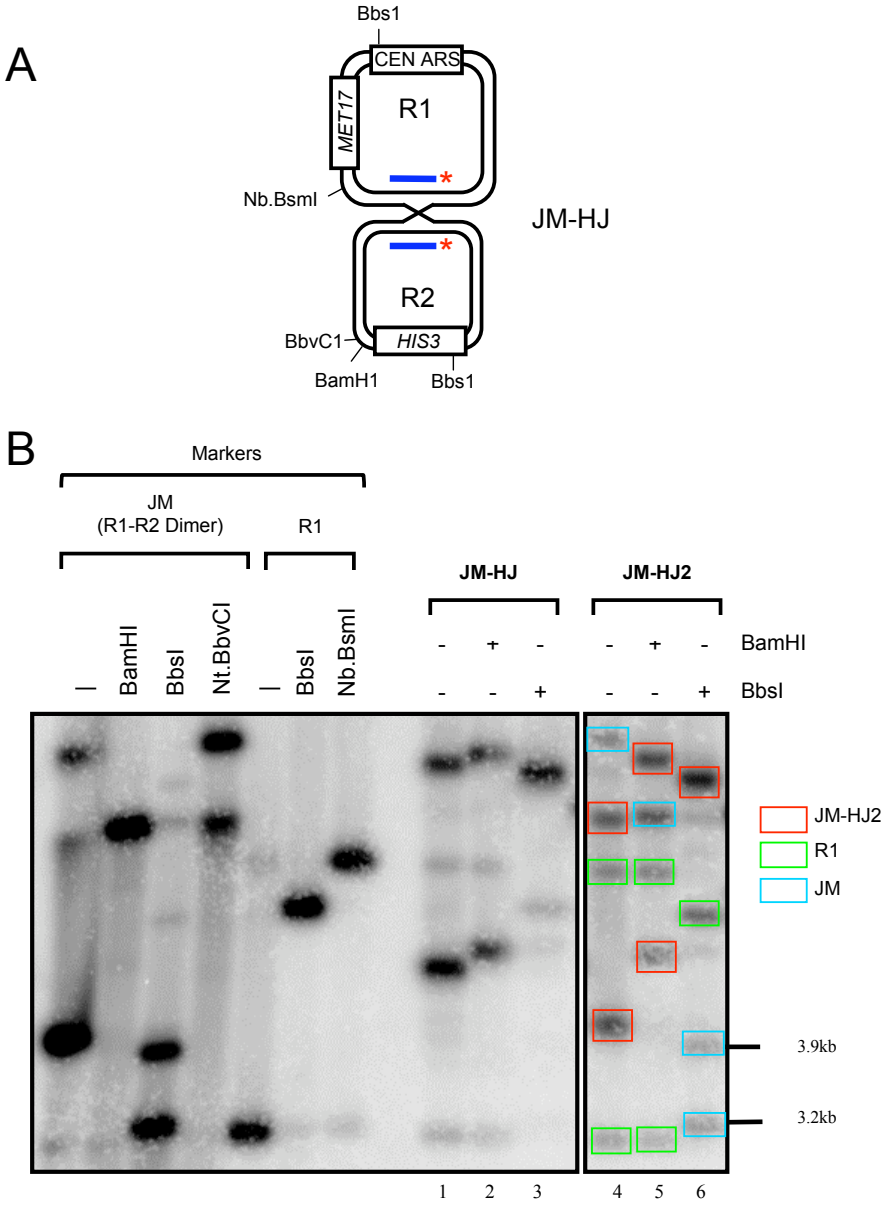


Figure 5.5 Analysis of JM-HJ and JM-HJ2. (A) Schematics of JM-HJ with positions of relevant restriction sites, auxotrophic markers and ARS. Blue line with red asterisk represents the ~200bp *cer* sequences used as the probe for Southern blot analysis. (B) Left panel: Southern blot analysis of purified JM, R1 and JM-HJ digested with various enzymes as indicated. Right panel: Southern blot analysis of JM-HJ2 digested with various enzymes as indicated. JM-HJ2, R1, parental JM and the restriction fragments derived from these molecules have been boxed, as indicated. The JM-HJ preparation used in this figure had only been subjected to one round of gel purification and thus still contains trace amounts of supercoiled and relaxed R1 plasmid.

open/supercoiled R1 and parental JM (Figure 5.5B, blue and green boxes in lane 4-6). JM-HJ2 was therefore not analysed further.

5.2.5. JM-HJ is Resolved by Bacterial HJ Resolvase, RusA

Further verification of the structure of JM-HJ was sought by treating JM-HJ with the HJ resolvase, RusA, which would be predicted to resolve the HJ in JM-HJ to form either an R1-R2 dimer or R1 and R2 monomers (Figure 5.6A). Indeed, treatment of JM-HJ with RusA resulted in 86% of the substrate being converted into either dimeric R1-R2 or monomeric R1 and R2 circular molecules (Figure 5.6B and 5.6C). There was a resolution bias towards the formation of monomeric R1 and R2, which is consistent with the finding that RusA resolves χ-structures with a bias towards one specific orientation (Figure 5.6C) (Sharples et al., 2004). Approximately 14% of the RusA generated products were linear which comprised of R1-R2 dimers, indicating that RusA resulted in a DSB (Figure 5.6B and 5.6C). These are likely to be aberrant resolution events in which three strands at the junction must have been nicked giving rise to a linear product. Overall, these data confirm the presence of a single HJ in JM-HJ, which can be resolved *in vitro* by a known HJ resolvase.

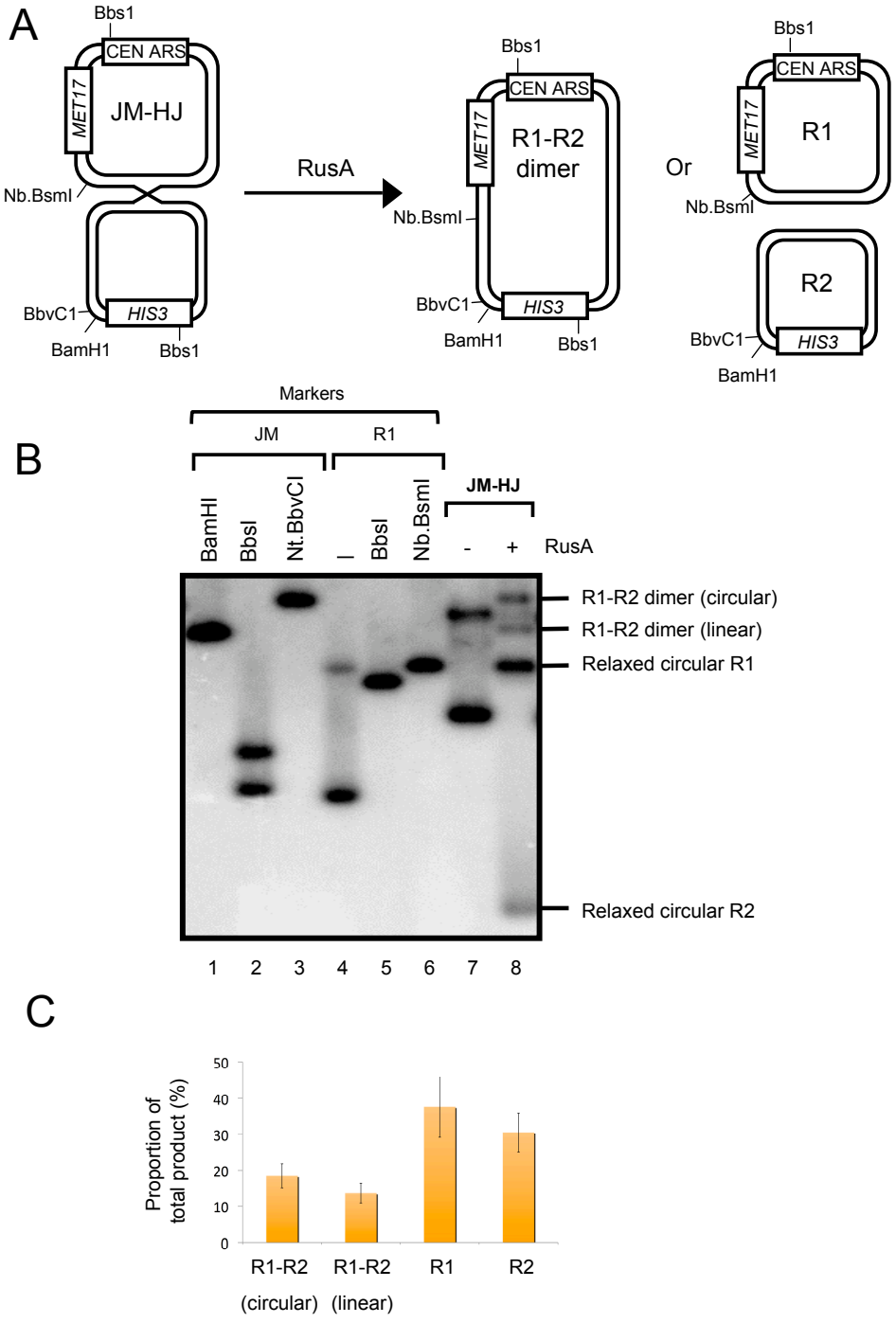


Figure 5.6 Resolution of JM-HJ by RusA resolvase. (A) Schematic diagram showing the two possible outcome of RusA resolution of HJ in JM-HJ. (B) Southern analysis of JM and R1 digested with various enzymes as indicated, and purified JM-HJ digested with RusA. (C) Quantification of products following treatment of JM-HJ with RusA. Bars are mean +/- S.D. from four independent experiments.

5.2.6. *In vivo* Resolution of HJ on JM-HJ

Having confirmed the structure of JM-HJ, it was transformed into *S. cerevisiae* to determine if yeast cells could resolve the HJ of JM-HJ *in vivo*. To monitor the *in vivo* resolution of JM-HJ, transformants of JM-HJ were screened for histidine and methionine prototrophy to select for resolution events giving rise to R1-R2 dimers (Figure 5.1). The transformation efficiency of JM-HJ ranged from 10^2-10^3 cfu per μg JM-HJ substrate, which is slightly higher than the transformation efficiency of X-JM described in Chapter 4. This suggests that either the greater integrity or the partially supercoiled nature of JM-HJ might facilitate the resolution of JM-HJ *in vivo*. However, the transformation efficiency of JM-HJ is still 1-2 orders of magnitude lower than the transformation efficiency of a circular control plasmid pRS415, which had a transformation efficiency of 10^4-10^5 cfu/μg substrate. We reasoned that the presence of the HJ was responsible for the low transformation efficiency of JM-HJ. To test this hypothesis, we resolved the HJ in JM-HJ using RusA resolvase prior to transformation into *met17Δ his3Δ* cells. As predicted, RusA-treated JM-HJ transformed 12 times more efficiently than untreated JM-HJ (Figure 5.7A). Moreover, if selecting for methionine prototrophs in which all resolution outcomes, i.e. both R1-R2 dimer and R1 monomer are selected, RusA-treated JM-HJ has a 20 times greater transformation efficiency than untreated JM-HJ (Figure 5.7B).

It was next investigated if the transformation efficiency of JM-HJ could also be increased by over-expressing RusA *in vivo*. Prior to JM-HJ transformation, wild type RusA or an active site mutant (D70N) (Bolt et al., 1999), in which HJ resolution activity is abolished, were individually over-expressed in wild type cells by galactose

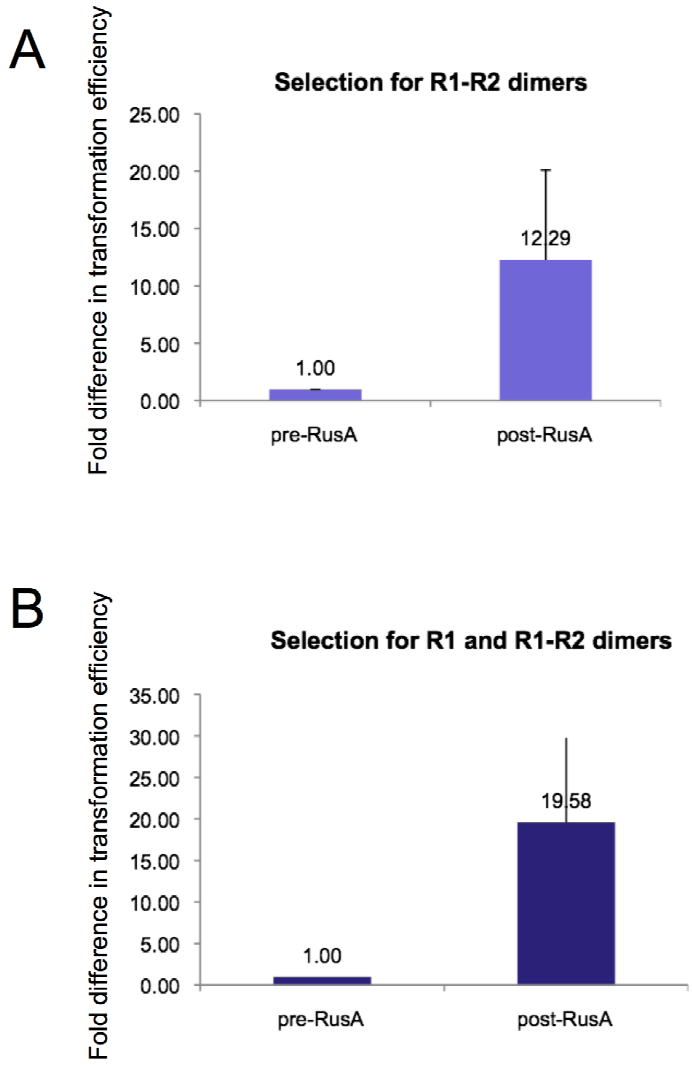


Figure 5.7. Effects of *in vitro* HJ resolution by RusA resolvase prior to transformation in *S.cerevisiae*. (A) Fold difference in HJ resolution efficiency if JM-HJ is pre-treated with RusA for 1hour at 37°C prior to transformation into wild type strain. Methionine and histidine prototrophs (R1-R2 dimers only) were selected following transformation. (B) Identical to (A) except methionine prototrophs (R1 and R1-R2 dimer resolution products) were selected following transformation. Bars are mean +/- S.D. from at least three independent experiments.

induction of the respective genes cloned into the pYES plasmid vector. JM-HJ was co-transformed with a control plasmid, pRS415 that contains a selectable *LEU2* marker, in order that resolution efficiencies could be normalized against inter-sample variations in transformation efficiencies. Methionine and histidine prototrophs were selected following JM-HJ transformation. It was predicted that the over-expression of RusA would result in a higher overall HJ resolution efficiency. However, HJ resolution efficiency in the cells in which RusA was over-expressed was about 50% of the wild type control containing the empty pYES vector (Figure 5.8). This reduction was attributed to the nuclease activity of RusA because over-expression of nuclease-dead RusA (D70N) did not reduce the HJ resolution efficiency of the cells (Figure 5.8). This suggests that although RusA can resolve the HJ in JM-HJ *in vitro*, RusA, when over-expressed *in vivo* can process JM-HJ but does so aberrantly giving rise to non-selectable products.

Overall, these data indicate that the HJ in JM-HJ suppresses the transformation efficiency of JM-HJ and that RusA can resolve the HJ in JM-HJ *in vitro* into either a dimer or two circular products that transform efficiently into yeast cells.

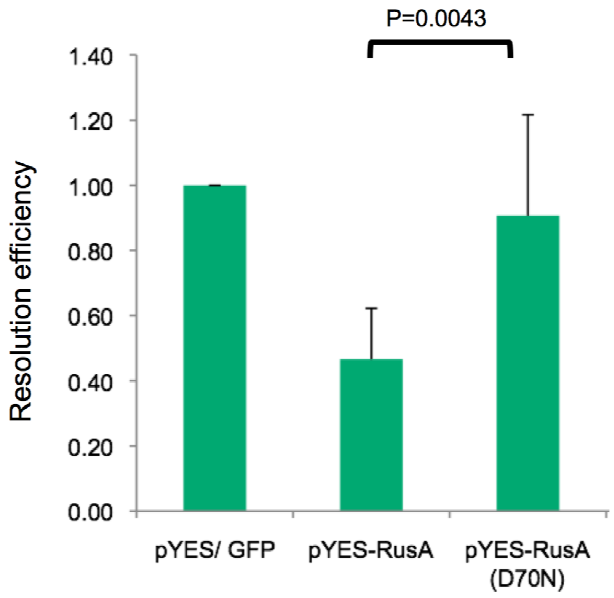


Figure 5.8 Effects of *in vivo* over-expression of RusA resolvases on HJ resolution efficiency. HJ resolution efficiency of wild type strains with over-expressed RusA and RusA(D70N) compared to wild type strain with a pYES control plasmid. JM-HJ was transformed into the yeast cells after 3 hours of induction using 1% galactose. Bars are mean +/- S.D. from at least three independent experiments. P-values were calculated using Student's *t*-test.

5.2.7. Analysis of JM-HJ resolution products

To confirm that the methionine and histidine prototrophs arose as a result of HJ resolution of JM-HJ, the resolution products were recovered from the wild type cells and subjected to Southern blot analysis, using *cer* sequence as a probe. Plasmids recovered from the wild type cells following JM-HJ transformation had the predicted structure of a circular dimeric R1-R2 plasmid (Figure 5.9A), confirming that resolution of the HJ in JM-HJ had occurred as opposed to, say, JM-HJ undergoing some aberrant rearrangement event or the *HIS3* and *MET17* markers ectopically integrating into the genome.

Resolution of the HJ in JM-HJ must occur within the *cer* sequences since the *cer* repeats in JM are flanked by heterologous sequences that prevent the HJ in JM-HJ branch migrating outside these sequences (Figure 5.2A). However, if HJ resolution occurs close to the homologous/heterelogous boundaries, it is possible that GC may arise. Similarly, if the HJ is not cleaved symmetrically, a product with DNA flaps or gaps will be generated, from which subsequent repair may potentially give rise to GC or other form of mutations. Since Mus81-Eme1 has been shown to resolve model HJs asymmetrically, in contrast to Yen1/GEN1 or the human SLX1-SLX4 complex, the analysis of HJ resolution fidelity may shed light on the potential HJ resolution mechanisms that generate the R1-R2 dimers. Therefore, both *cer* sequences in the R1-R2 dimers recovered from 15 independent JM-HJ wild type transformants were amplified by PCR and sequenced (Figure 5.9B). One of these products contained a mutation in the form of a dinucleotide GG-AA substitution. This mutation however was located 34bp upstream of *cer2* making it unlikely that it arose as a result of

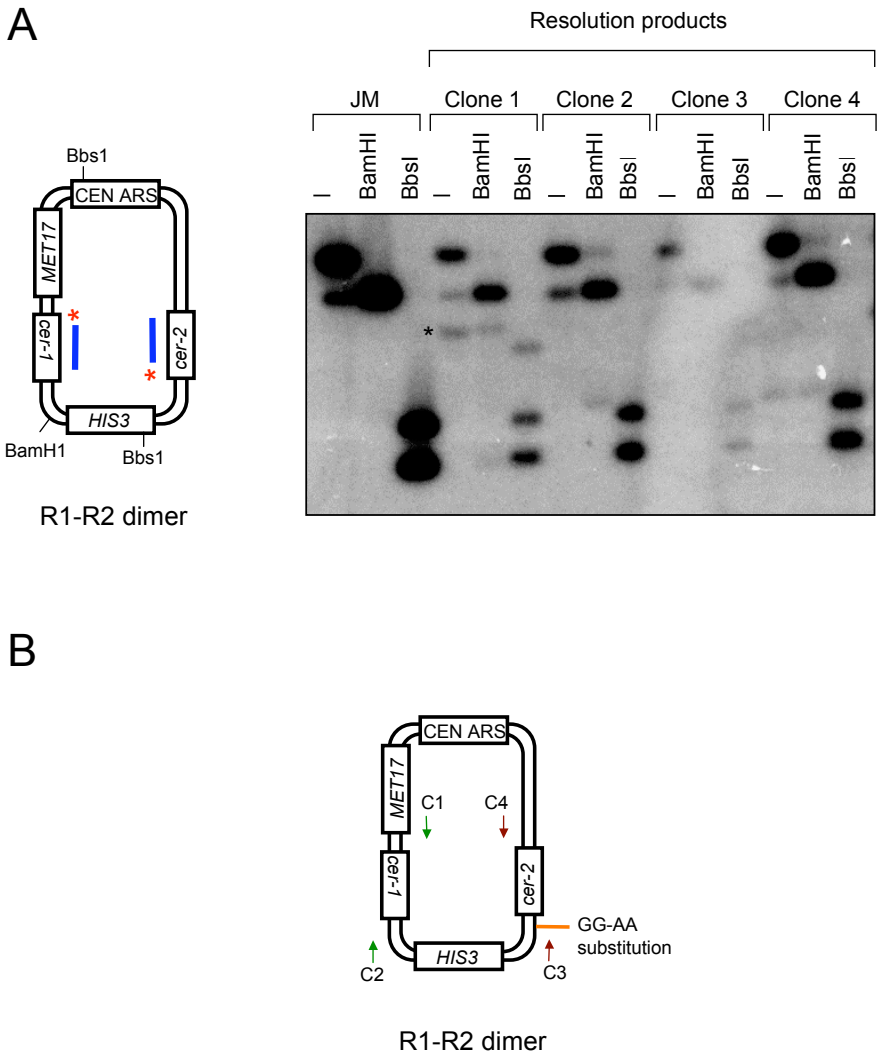


Figure 5.9 R1-R2 dimers can be detected as products of JM-HJ resolution. (A) Left panel: schematic of predicted R1-R2 dimer with positions of relevant restriction sites. Blue line with red asterisk represents the ~200bp *cer* sequences used as the probe for Southern blot analysis. Right panel: Southern analysis of purified JM and genomic DNA from 4 independent *MET17 HIS3* clones arising from JM-HJ transformation digested with various enzymes as indicated. Asterisk indicates monomeric R1 that most likely arose through a post-JM-HJ resolution event mediated through *cer*-mediated intra-molecular recombination of the R1-R2 dimer product. (B) C1/C2 and C3/C4 primer pairs were used to amplify the cer-1 and cer-2 sequences from the resolution products recovered from *MET17 HIS3* prototrophs arising from JM-HJ transformation. A GG-AA substitution that is 34bp upstream of the cer-2 sequence was observed in one of the *MET17 HIS3* clones analysed.

aberrant HJ resolution (Figure 5.9B). The remaining 14 resolution products did not demonstrate any GC or mutations. The fact that the resolution products of JM-HJ did not display any deletions as observed with resolution products of X-JM (as described in Chapter 4) suggests that the 33bp deletions associated with X-JM resolution might be an artefact of the X-JM substrate rather than having any physiological relevance. Overall, these data indicate that the HJ in JM-HJ can be resolved *in vivo* to generate R1-R2 dimers and, moreover, is done so in a faithful manner preserving the nucleotide sequence.

5.2.8. Analysis of the ability of putative HJ resolvase mutants to resolve JM-HJ *in vivo*

As described in Chapter 1, several *S.cerevisiae* proteins have been implicated in the HJ resolution of HR. Yen1, Mus81-Mms4, Slx1-Slx4 and Rad1-Rad10 have all been shown *in vitro* to cleave model HJs. However, the substrate these enzymes process *in vivo* remains to be determined. Therefore, it was next investigated if mutants in these putative HJ resolvases are defective in resolving the HJ in JM-HJ. The pRS415 control plasmid was co-transformed with JM-HJ to normalize resolution efficiencies against inter-sample variations in transformation efficiencies. Hence the potential differences in HJ resolution efficiencies in different genetic backgrounds could be quantified. As shown in Figure 5.10, *yen1Δ, mus81Δ, slx1Δ, slx4Δ* and *rad1Δ* single mutant cells retain JM-HJ resolution activities comparable to that of wild type cells, indicating that no single nuclease was solely responsible for resolution of JM-HJ. It was therefore investigated if these nucleases might act redundantly with each other to resolve JM-HJ. To do this, the HJ resolution efficiencies of the cells carrying

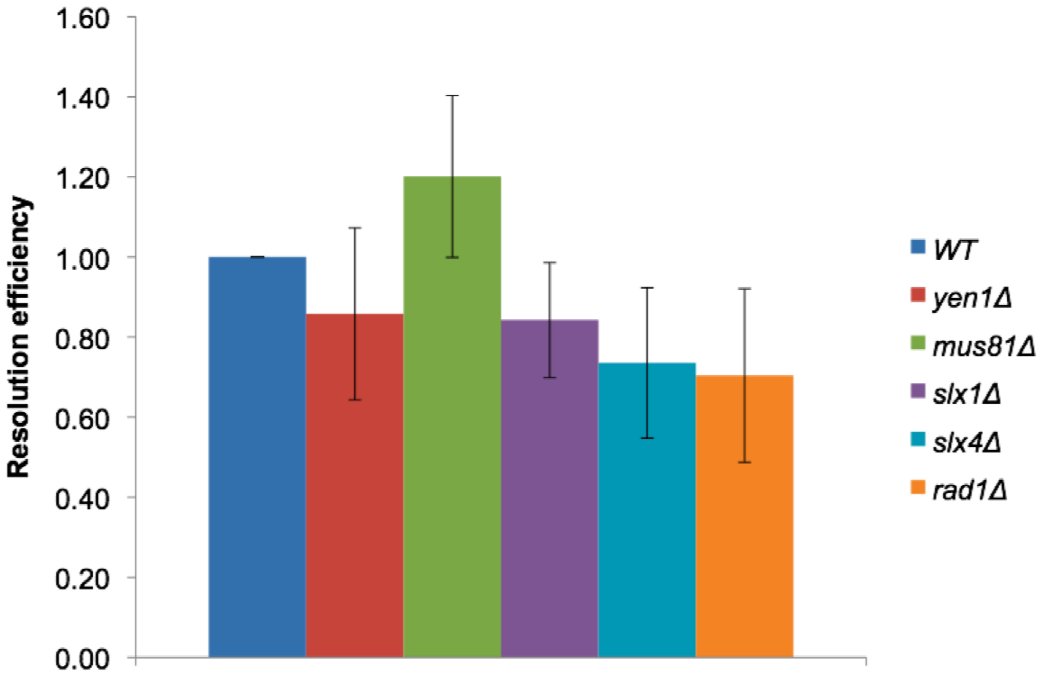


Figure 5.10 The resolution efficiencies of JM-HJ in cells carrying single mutation in putative HJ resolvase genes. Resolution efficiencies of JM-HJ in various strain backgrounds as indicated. Bars are means +/- S.D. from at least three independent experiments.

double mutations in these nucleases were analyzed. Interestingly, in contrast to wild type cells, loss of Yen1 in a *mus81Δ* background resulted in an approximately two-fold decrease in JM-HJ resolution efficiency (Figure 5.11A). Loss of Mus81 alone did not reduce JM-HJ resolution efficiency indicating that Mus81 and Yen1 therefore possess redundant, overlapping functions in the resolution of the HJ in JM-HJ. This overlapping function is specific to Mus81 and Yen1, but not to other nucleases because the loss of Yen1 from *slx1Δ*, *rad1Δ* or *slx4Δ* mutant backgrounds did not result in any significant changes in JM-HJ resolution efficiency (Figure 5.11B, C, D). Moreover, *mus81Δ rad1Δ* and *mus81Δ slx4Δ* mutant cells were still able to resolve JM-HJ with wild type efficiencies, reinforcing the specificity of the genetic interaction between Mus81 and Yen1 in resolving JM-HJ (Figure 5.11E and F).

Although Mus81 and Yen1 have been shown to resolve model HJ *in vitro*, the over-lapping roles of the two proteins in our *in vivo* assay may not necessarily involve the nucleolytic activities of the Mus81 and Yen1. The proteins may instead be required as a "HJ sensor" that recognises HJs and play the role as a recruiter for other nucleases to resolve HJs. To address this question, mutant forms of Mus81 and Yen1 were tested to determine if the nucleolytic activity of each protein is absolutely required for the *in vivo* resolution of HJ on JM-HJ. Mutations that result in the substitution of amino acid residues that are essential for the nuclease activities of Yen1 and Mus81 were introduced into the endogenous *YEN1* and *MUS81* genes, respectively. The resulting alleles were termed $mus81^{DD}$, which contained substitutions D414A and D415A, and $yen1^{EE}$, which contained substitutions E193A and E195A. As predicted, cells carrying either $mus81^{DD}$ or $yen1^{EE}$ alleles had resolution efficiencies comparable to that of wild-type cells (Figure 5.12). However $mus81^{DD}$ $yen1^{EE}$ cells were as defective as *mus81Δ yen1Δ* double mutant cells in

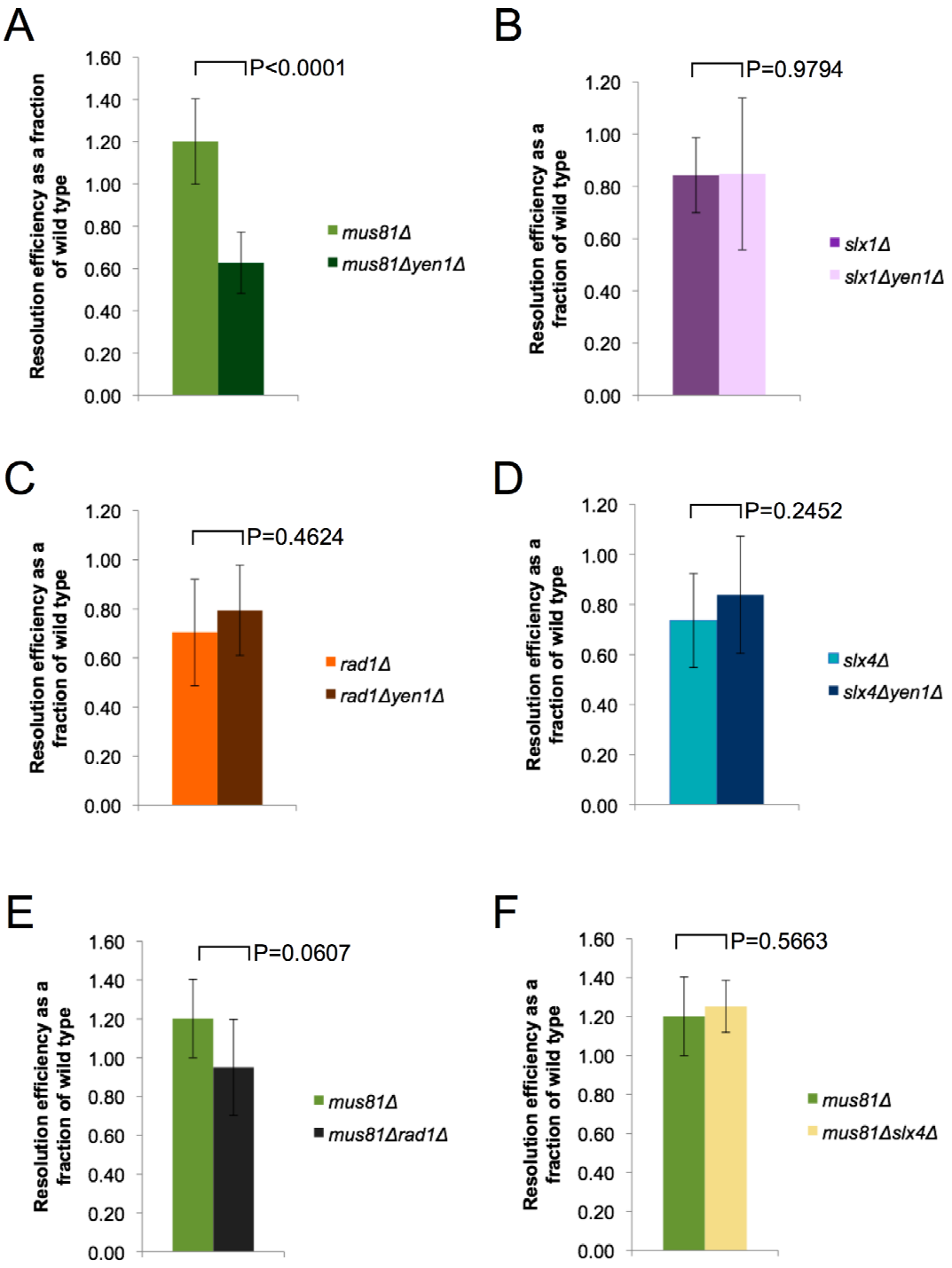


Figure 5.11 Yen1 and Mus81 act redundantly to resolve JM-HJ *in vivo*. (A-F) Resolution efficiencies of JM-HJ in various single and double mutant backgrounds as indicated. Bars are means +/- S.D. from at least three independent experiments. P-values were calculated using Student's *t*-test.

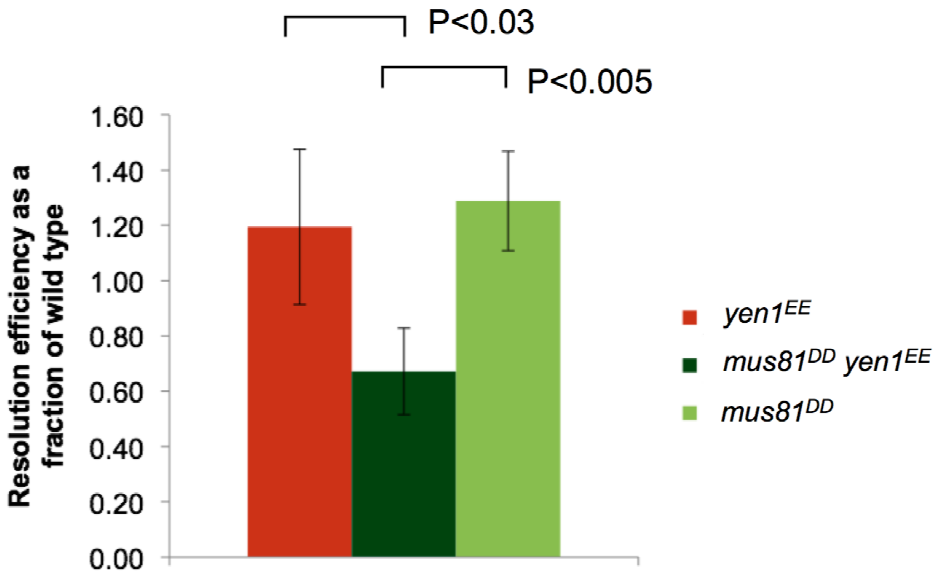


Figure 5.12 The endonuclease activities of Mus81 and Yen1 are essential for the resolution of JM-HJ *in vivo*. Resolution efficiencies of JM-HJ in various strain backgrounds as indicated. Bars are means +/- S.D. from at least three independent experiments. P-values were calculated using Student's *t*-test.

resolving JM-HJ confirming that the resolution defect in *mus81Δ yen1Δ* double mutant cells is directly attributed to the loss of the endonuclease activities of these proteins. Overall, these data indicate that JM-HJ resolution *in vivo* partially requires the nuclease activities of Mus81 and Yen1, which act in a redundant manner.

5.2.9. Yen1 and Mus81 are required for replication fork restart

Next the biological relevance of this novel interaction between Mus81 and Yen1, outside the context of JM-HJ resolution, was investigated. A central role for HR is the repair of DSB introduced by IR such as γ-rays. Consistent with previous observations, *mus81Δ* cells are not sensitive to γ-radiation up to 200-Gy (Figure 5.13A) (Osman and Whitby, 2007). Similarly, Yen1 was also not required for the repair of DSBs generated by IR (Figure 5.13A). Loss of both Yen1 and Mus81 did not result in a significant sensitivity to IR up to 200-Gy, indicating the overlapping functions of Yen1 and Mus81 required for JM-HJ resolution are not required for the repair of DSBs induced by IR (Figure 5.13A). However, it was noted that *mus81Δ yen1Δ* double mutant cells have a slightly slower growth rate than wild type and single mutant *yen1Δ* and *mus81Δ* cells. This is consistent with the findings in Blanco et al. that showed *mus81Δ yen1Δ* mutant cells have a prolonged cell cycle (Blanco et al., 2010).

As discussed in chapter 1, HR also plays an important role in the repair of damaged replication forks that have encountered lesions in the DNA by facilitating break-induced replication (BIR). Unlike IR-induced DSBs that are two-ended, which can be repaired by SDSA or dHJ dissolution that do not require HJ resolution, the BIR pathway restores replication forks from a one-ended DSB. The result of re-initiating replication via recombination is the formation of a HJ that cannot be

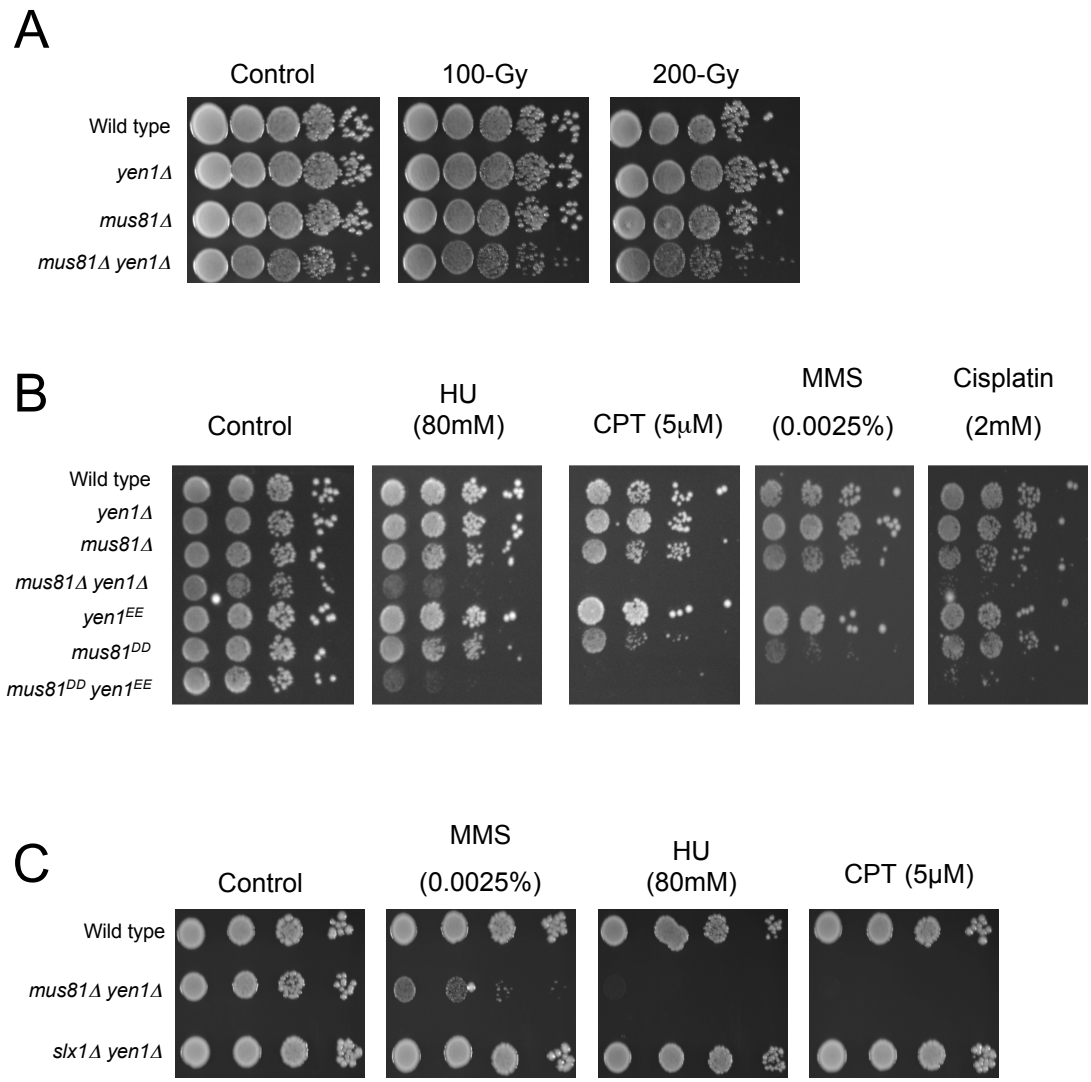


Figure 5.13 Yen1 and Mus81 are required for replication fork repair. (A-C) DNA damaging IR and drug sensitivity assays on various strains as indicated.

subjected to the SDSA or dissolution pathways, but must be resolved by HJ resolution, in order that the sister chromatids can properly segregate during mitosis. It was reasoned therefore that if the defect in JM-HJ transformation in the absence of Mus81 and Yen1 was due to a defect in HJ resolution, then in the absence of both nucleases, cells might be expected to have defects in the repair of lesions that initiate BIR. A variety of agents were used to perturb replication that might be expected to generate DSBs and thus initiate BIR. All these agents perturb replication but through different mechanisms. Hydroxyurea (HU) inhibits the activity of nucleotide reductase and induces replication fork stalling by depletion of the dNTP pool. MMS produces bulky lesions on DNA, which can interfere with the progression for replication forks. CPT is a topoisomerase poison that binds to topoI and DNA complexes, thus stabilizing the complex and resulting in the formation of ssDNA breaks by preventing DNA ligation. Replication fork reaching ssDNA breaks are converted to DNA DSBs (Pommier, 2006). Cisplatin generates DNA adducts that may be converted into DNA intra- and inter-strand crosslinks which prevent DNA strand separation for replisome progression (Dronkert and Kanaar, 2001). As has previously been found, *mus81Δ* and *mus81*^{DD} mutants show mild sensitivity to HU, CPT, MMS and cisplatin at the doses used in this study (Figure 5.13B). In contrast, neither the *yen1Δ* nor *yen1*^{EE} cells were sensitive to any of these agents. However, *mus81Δ yen1Δ* double mutant cells as well as the *mus81*^{DD} *yen1*^{EE} cells were hypersensitive to all replication inhibitors (Figure 5.13B). Consistently, *slx1Δ yen1Δ* mutant cells that resolve JM-HJ with wild type efficiency are also proficient in the repair of replication fork damage, as evidenced by the tolerance of the mutants to MMS, HU and CPT (Figure 5.13C). Taken together, these findings suggest that Yen1 and Mus81 endonuclease activities are essential for

replication fork repair, and presumably for the resolution of HJ intermediates formed during replication fork restart.

5.2.10. Analysis of Yen1 and Mus81-independent HJ Resolution Activity

JM-HJ is resolved with a high fidelity in wild type cells since no mutation in the nucleotide sequences of the HJ-containing regions was detected. While Yen1 and Mus81 are responsible for ~40% of the resolution events of JM-HJ, it is possible that some of the residual resolution events in *mus81Δ yen1Δ* cells occur as a result of compensatory pathways that may act with a lower fidelity. The fidelity of resolution of JM-HJ in the absence of Yen1 and Mus81 was therefore examined by analysing the *cer* sequences of R1-R2 dimers from 20 independent resolution events from *mus81Δ yen1Δ* double mutant cells. No mutations were found in any of the isolates indicating that in the absence of Mus81 and Yen1, JM-HJ is still resolved with high fidelity.

Since Rad1-Rad10 and Slx1-Slx4 complex have overlapping substrate specificities with Mus81 and Yen1, Rad1 and Slx4 were examined for their potential roles in the residual HJ resolution activity that persists in *mus81Δ yen1Δ* double mutant cells. However *mus81Δ yen1Δ rad1Δ* and *mus81Δ yen1Δ slx4Δ* cells were no more defective in JM-HJ resolution than the *mus81Δ yen1Δ* double mutant cells (Figure 5.14A). Surprisingly, in *mus81Δ yen1Δ slx1Δ* mutant background, the cells are able to resolve JM-HJ with an efficiency that is intermediate between *mus81Δ* and *mus81Δ yen1Δ* mutant cells (Figure 5.14A). This unexpected observation prompted us to investigate if the suppressive effect of *SLX1* mutation on *mus81Δ yen1Δ* cells translates into the suppression of MMS sensitivity of *mus81Δ yen1Δ* mutant cells. However, loss of Slx1 does not suppress the MMS sensitivity of *mus81Δ yen1Δ*

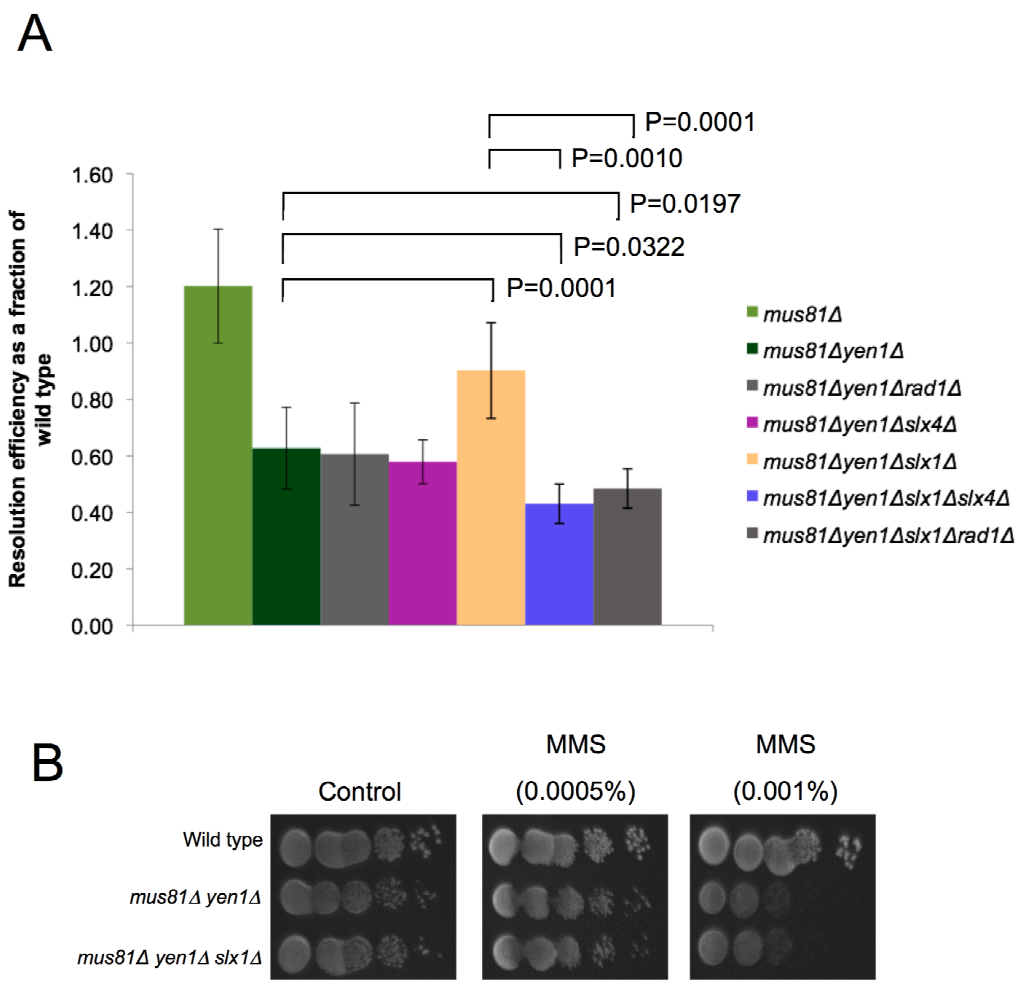


Figure 5.14 *SLX1* mutation suppresses JM-HJ resolution deficiency, but not MMS sensitivity of *mus81Δ yen1Δ* mutant cells. (A-B) Resolution efficiencies of JM-HJ in various strain backgrounds as indicated. Bars are means +/- S.D. from at least three independent experiments. P-values were calculated using Student's *t*-test. (B) MMS sensitivity assay on various strains as indicated.

mutant cells, as evidenced by the fact that *mus81Δ yen1Δ slx1Δ* mutant cells are as sensitive to MMS as the *mus81Δ yen1Δ* cells (Figure 5.14B). Therefore this suggests that the suppressive activity of *slx1Δ* is specific to our *in vivo* JM-HJ resolution assay. As described in Chapter 1, Slx4 has other roles in the maintenance of genome stability, independently of Slx1. For instance, Slx4, together with Rad1-Rad10 complex, acts to remove the 3' non-homologous DNA flap structures arise during SSA-mediated DSB repair (Flott et al., 2007; Li et al., 2008; Lyndaker et al., 2008). Therefore, this led us to hypothesize that Slx4 and Rad1 may be required for the suppressive effect of Slx1 mutations on the *mus81Δ yen1Δ* double mutation background. When *SLX4* is mutated in a *mus81Δ yen1Δ slx1Δ* mutant background, the cells have a two-fold decrease in HJ resolution efficiency as compared to *mus81Δ yen1Δ slx1Δ* triple mutant cells (Figure 5.14A). A similar observation is made when *RAD1* gene is mutated in the *mus81Δ yen1Δ slx1Δ* mutant background (Figure 5.14A). Furthermore, *mus81Δ yen1Δ slx1Δ slx4Δ* and *mus81Δ yen1Δ slx1Δ rad1Δ* quadruple mutants were found to resolve JM-HJs less efficiently than *mus81Δ yen1Δ* double mutant cells (Figure 5.14A). The effect of *slx4Δ* or *rad1Δ* is only observed in a *mus81Δ yen1Δ slx1Δ* mutant background, but not in a *mus81Δ yen1Δ* background. Therefore this is consistent with the notion that Slx1 suppresses the nuclease activity of Slx4-Rad1 complex in JM-HJ resolution *in vivo*, in the absence of Mus81 and Yen1.

Moreover, *mus81Δ yen1Δ slx1Δ slx4Δ* and *mus81Δ yen1Δ slx1Δ rad1Δ* quadruple mutant cells retain only ~40-50% of the HJ resolution activity of a wild type cell (Figure 5.14A). This suggests that a cell still has alternative resolvase(s) or other mechanisms to resolve the HJ of JM-HJ independently of Yen1, Mus81, Slx1, Slx4 and Rad1 proteins.

5.3. Discussion

Building on the pilot experiments described in Chapter 4, a new strategy for the synthesis of HJ-containing plasmid-borne substrate has been developed. The JM-HJ substrate, which is generated by XerC/D site-specific recombination system, was used to reveal the overlapping functions of Yen1 and Mus81 in HJ resolution and the repair of replication fork damage.

Like the X-JM substrate described in Chapter 4, JM-HJ transforms into yeast cells with 1-2 orders of magnitude lower than control plasmids because of the presence of a HJ. Contradictory to our prediction, the over-expression of RusA resolvase *in vivo* did not result in an increase in HJ resolution efficiency. Instead, RusA over-expression resulted in a reduction in the resolution efficiency of JM-HJ in wild type cells. Moreover, over-expression of nuclease-deficient RusA (D70N) did not reduce the HJ resolution efficiency suggesting that the reduction in HJ resolution efficiency caused by wild type RusA is dependent upon its nuclease activity (Figure 5.9). Although RusA has a high specificity for HJs, RusA can in fact cleave other branched DNA structures such as a replication fork or 3' flap structures, albeit with lower efficiency *in vitro* (Bolt and Lloyd, 2002). Therefore, it is possible that RusA over-expressed in yeast resolves HJ on JM-HJ aberrantly to generate non-selectable cleavage products. An example of this aberrant/unpredicted resolution activity of RusA is evidenced in Figure 5.6B, in which ~15% of the JM-HJ was linearised by RusA.

Using this *in vivo* HJ resolution system, Mus81 and Yen1 were shown to share redundant, over-lapping roles in resolving the HJ on JM-HJ. This redundant role is dependent on the endonuclease activities of both enzymes because cells carrying both endonuclease-deficient Mus81 and Yen1 were also unable to resolve JM-HJ as

efficiently as the single mutants or wild type cells. *In vitro*, Mus81 and Yen1 have been shown to have distinct substrate specificities. Yen1 can efficiently cleave intact model HJs in a manner similar to bacterial RuvC resolvase (Ip et al., 2008). On the contrary, biochemical studies showed that purified Mus81-Mms4 complex displays poor activity towards HJs but has a preference for branched structures that contain nicks or gaps at the junction (Kaliraman et al., 2001). However, recent observations suggest that Mus81 can also perform symmetrical resolution of an intact HJ structure in the form of a cruciform structure, generated *in vivo* by the extrusion of plasmid-borne palindromes (Cote and Lewis, 2008; Taylor and McGowan, 2008). The fact that the cruciform structures only forms on supercoiled plasmids indicates that the plasmids, and thus the HJs on this plasmid are intact and do not contain breaks/nicks. The latter observations are consistent with our findings that Mus81 can indeed recognise and process an intact, plasmid-borne HJ on a JM-HJ substrate in a similar manner to Yen1.

The resistance of the *mus81Δ yen1Δ* double mutant cells to IR indicates that Mus81 and Yen1 are not absolutely essential for the repair of two-ended DSBs presumably because two-ended DSBs are predominantly repaired by SDSA or dissolution pathways that do not require HJ resolution (Figure 5.15). This is consistent with the notion that HJ resolution-dependent HR pathway is suppressed during mitotic recombination due to its potential to generate deleterious CO products (see Chapter 3).

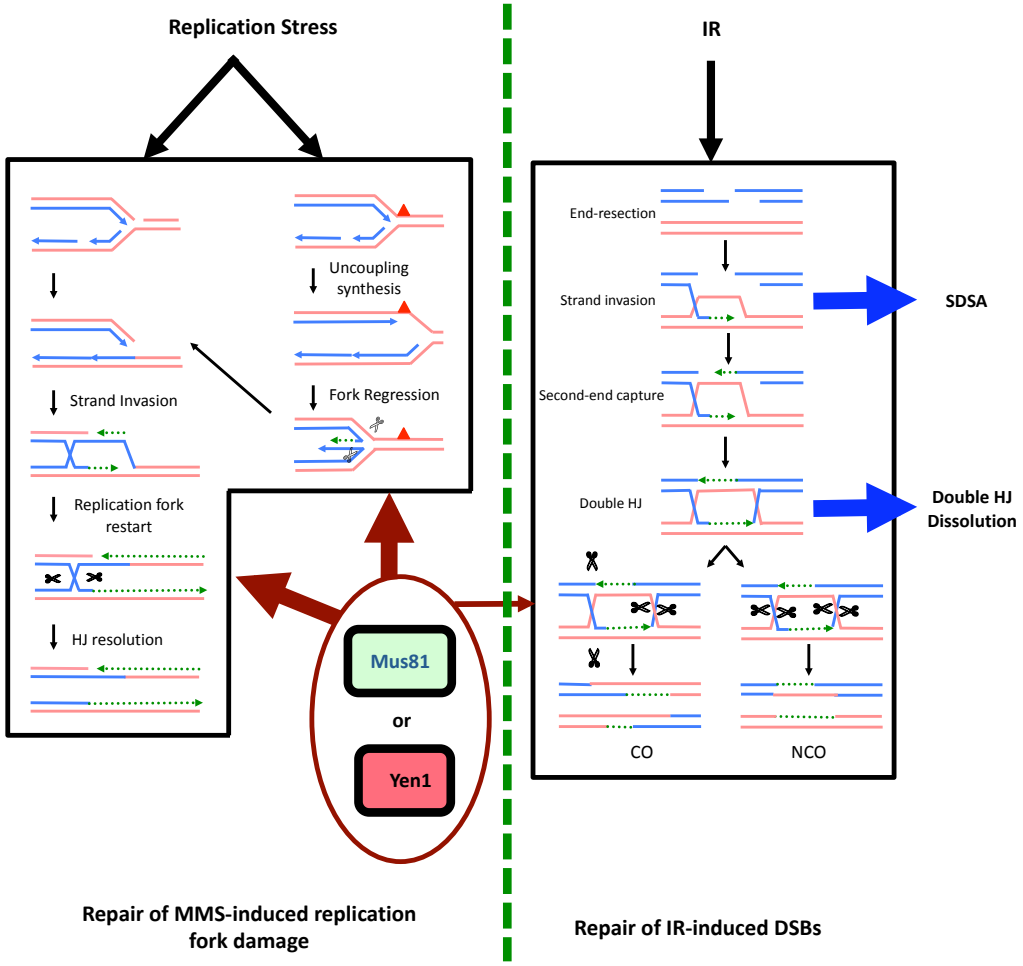


Figure 5.15 The roles of Yen1 and Mus81 in the repair of damaged replication forks. The restart of stalled/collapsed replication forks result in the formation of HJ intermediates, which can be resolved by the redundant activities of Mus81 and Yen1 (thick red arrows). IR-induced DSBs are repaired predominantly by SDSA and dHJ dissolution pathways (blue arrows), and are therefore less dependent upon the resolvase activities of Mus81 and Yen1 (thin red arrow).

Mus81 has been shown to be essential for the repair of stalled/collapsed replication forks (Doe et al., 2002). The sensitivity of *mus81Δ* mutant *S.pombe* cells to replication fork-stalling agents can be suppressed by the over-expression of RusA resolvase, an observation which led to the proposal that Mus81 may act on the HJ structures formed by fork regression (Doe et al., 2002). In contrast, *yen1Δ* mutant cells do not have any phenotype that indicates any deficiency in DNA repair. However, in the absence of both Mus81 and Yen1, the cells become more sensitive to replication stress than either of the single mutants or wild type cells. The endonuclease activities of Mus81 and Yen1 are essential for the resolution of HJs derived from the repair of stalled replication forks, as evidenced by the synthetic sickness of *mus81Δ yen1Δ* and $mus81^{DD}$ $yen1^{EE}$ double mutant cells when exposed to replication stress. The results from our *in vivo* HJ resolution study and the drug sensitivity tests are consistent with our proposal that both Mus81 and Yen1 are responsible for the resolution of HJs that arise from fork regression or BIR-mediated replication fork restart mechanisms (Figure 5.15). The functional over-lap between Mus81 and Yen1 found in our study is in agreement with the recent findings that expression of GEN1 and Yen1 can complement *mus81Δ* phenotypes in *S.pombe* and *S.cerevisiae*, respectively (Blanco et al., 2010; Lorenz et al., 2009). The slow growth phenotypes of *mus81Δ yen1Δ* found in this study is also consistent with the findings in Blanco et al. (Blanco et al., 2010).

Despite a significant reduction in HJ resolution activity, *mus81Δ yen1Δ* double mutant cells can still resolve JM-HJ with high fidelity. This suggests the presence of Mus81 and Yen1-independent HJ resolution pathway(s) in *S.cerevisiae*. In the search for endonucleases that are responsible for the residual HJ resolution activity observed in *mus81Δ yen1Δ* cells, *SLX1* mutation was shown to suppress the HJ resolution

deficiency of *mus81Δ yen1Δ* double mutant cells. This indicates that in the absence of Mus81 and Yen1, Slx1 nuclease prevents/inhibits the resolution of JM-HJ into R1-R2 dimers. Moreover, the suppression effect of *SLX1* mutation is dependent on Slx4 and Rad1, as shown by the two-fold reduction in HJ resolution efficiency in *mus81Δ yen1Δ slx1Δ slx4Δ* and *mus81Δ yen1Δ slx1Δ rad1Δ* quadruple mutants when compared to *mus81Δ yen1Δ slx1Δ* triple mutants. This observation suggests that in the absence of Mus81, Yen1 and Slx1, gene products of *SLX4* and *RAD1* can resolve HJ on JM-HJ.

Human SLX4 has been shown to interact with XPF (Rad1 in yeast) via the MLR domain (Fekairi et al., 2009) (Figure 1.7). Despite the lack of an MLR domain in Slx4, Slx4 has also been found to physically and functionally interact with Rad1, for the removal of 3' non-homologous tails during SSA repair and for GC when the DSB is flanked by non-homologous sequences that lead to 3' non-homologous tails (Flott et al., 2007; Li et al., 2008; Lyndaker et al., 2008). Therefore, the physical interaction between Slx4 and Rad1 is also consistent with our proposal that they can resolve HJ on JM-HJ, in the absence of Mus81 and Yen1. In the context of HJ resolution, Slx4 may be acting as a HJ sensor that loads Rad1-Rad10 onto the HJ. Alternatively, it is possible that Slx4 assists Rad1-Rad10 cleavage activity by denaturing/deforming the HJ substrate to one that is preferred by Rad1-Rad10 complex, for example a bubble/flap-like structure. Since Slx1-Slx4 and Rad1-Rad10 complexes have already been purified from *S.cerevisiae*, these hypotheses could be tested directly *in vitro* using either a synthetic oligo-based HJ substrate or our plasmid-borne JM-HJ substrate.

How does Slx1 suppress HJ resolution defects of *mus81Δ yen1Δ* double mutant? One possibility is that Slx1 sequesters Slx4, thereby preventing it from

interacting with Rad1 and forming a complex that can potentially catalyze HJ resolution (Figure 5.16). This model is consistent with the findings that the mutations in either *SLX4* or *RAD1* gene in a *mus81Δ yen1Δ slx1Δ* mutant background reduce the *in vivo* HJ resolution efficiencies to a similar extent (Figure 5.14B). It will be of interest to determine if the abilities of Slx1 and Rad1 to interact with Slx4 are mutually exclusive.

Contrary to our observation using the *in vivo* HJ resolution assay, the suppressive effect of *SLX1* mutation on HJ resolution defects of *mus81Δ yen1Δ* mutant was not observed in the MMS sensitivity assays (Figure 5.14C). *mus81Δ yen1Δ slx1Δ* mutant cells appear to be as sensitive as *mus81Δ yen1Δ* mutant cells to MMS (Figure 5.14C). One suggestion to explain this observation is that the Slx4/Rad1-dependent HJ resolution pathway revealed in the JM-HJ resolution assay may only be activated in a pathological *mus81Δ yen1Δ slx1Δ* mutant background. Alternatively, the discrepancy between the effect of losing Slx1 in JM-HJ resolution and MMS sensitivity assays may be related to the sensitivity the two assays. The *in vivo* HJ resolution assay detects the resolution of a single HJ on JM-HJ, whereas MMS will cause, in an individual cell, multiple forks to stall or collapse. Therefore unless the loss of *SLX1* causes absolute suppression in a *mus81Δ yen1Δ* background, the MMS dose used here may still result in an unsustainable and thus lethal number of stalled forks.

In conclusion, using our *in vivo* HJ resolution system, Mus81 and Yen1 have been shown to be the predominant HJ resolvases *in vivo,* which are essential for the repair of stalled replication forks. In contrast, IR-induced DSBs are not dependent on Mus81 and Yen1, consistent with the notion that DSBs are predominantly processed using SDSA and dHJ dissolution pathways, rather than through HJ resolution.

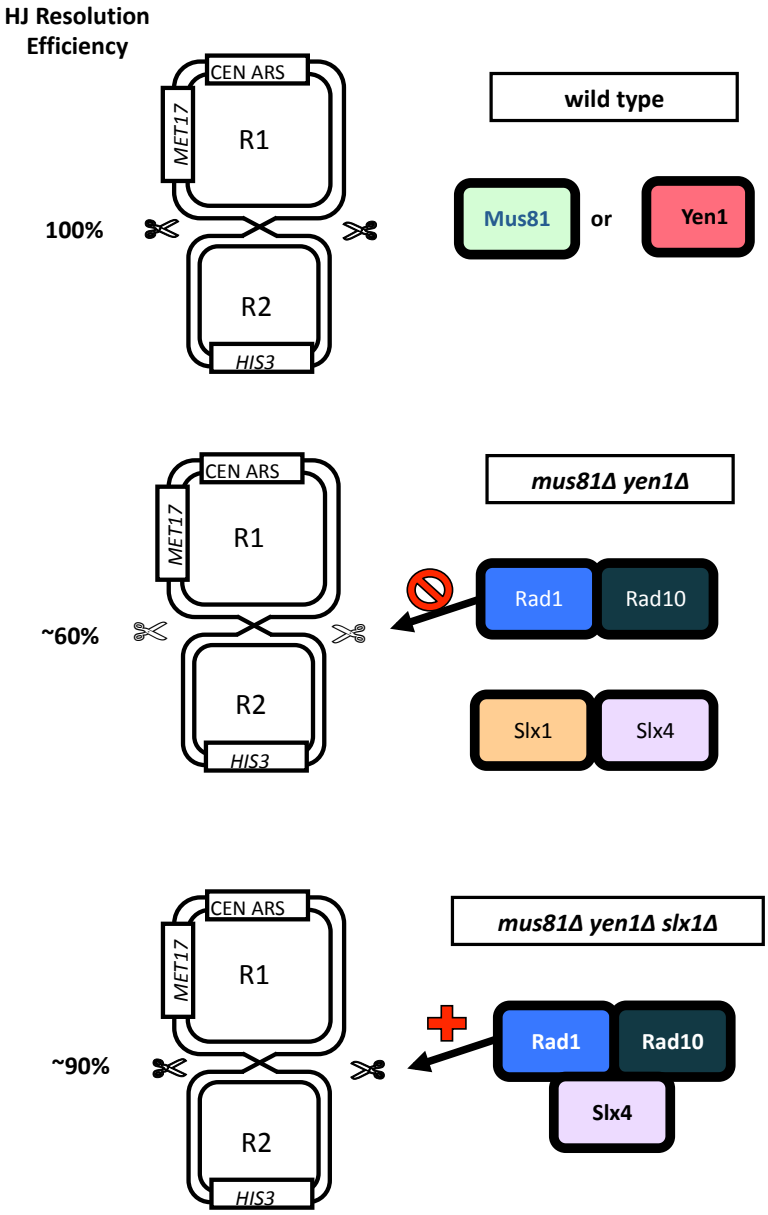


Figure 5.16 Mus81- and Yen1-independent JM-HJ resolution events. Mus81 and Yen1 act redundantly to resolve HJ of JM-HJ in wild type cells. In the absence of Mus81 and Yen1, Rad1-Rad10 complex does not resolve JM-HJ since Slx4 is sequestered by Slx1 through Slx1-Slx4 complex formation. In a *mus81Δ yen1Δ slx1Δ* background, Slx4 can act in a complex with Rad1-Rad10 to resolve HJ on JM-HJ. The HJ resolution efficiency of each genotype is displayed as percentage, as shown in Figure 5.14A.

In the absence of Mus81 and Yen1, HJ resolution is highly dependent on the Slx4-Rad1 interaction, which is antagonized by Slx1 (Figure 5.16). However additional resolvase(s) that act in parallel with Mus81, Yen1, Slx4 and Rad1 appear to exist, at least in *S.cerevisiae*. The findings from this study demonstrate that our *in vivo* HJ resolution system can discriminate between nucleases that have similar biochemical activities *in vitro*. This system thus paves the way to identify those additional resolvases(s) that can specifically resolve HJs *in vivo.*

Chapter Six

6. General Discussion

6. General Discussion

HR is a vital DNA metabolic process that is highly conserved across the three domains of life. As discussed in Chapter 1, HR is a multi-step pathway that involves DSB end-resection, strand invasion, DNA synthesis and HJ resolution. The resolution of HJs can result in the formation of either NCOs or COs (Figure 1.3 (i)). COs between homologous chromosomes may result in LOH for genes centromere-distal to the CO point as the sister chromatids of each homologous chromosomes are randomly segregated at mitosis. CO formation between non-sister chromatids poses a great risk to genome integrity of the cell and can result in the formation of GCR including chromosomal deletions, inversions and translocations (Krogh and Symington, 2004; Paques and Haber, 1999). Therefore, HR is perceived as a double-edged sword, which can preserve genomic stability when regulated accurately whereas promoting genomic instability if it is executed excessively or in an untimely manner.

CO formation during mitotic HR is actively suppressed by several helicases including Mph1, Sgs1 and Srs2. In the current study, the CO suppression function of Mph1 was shown to be closely associated with MutSα, the mismatch recognition complex of the MMR pathway. We have revealed a novel role of MutSα in promoting CO formation during HR-mediated DSB repair, independently of its MMR function. Mph1 was found to have two distinct functional interactions with MutSα in the regulation of CO formation. During recombination repair between completely homologous sequences, Mph1 suppresses COs that are generated in a MutSα-dependent manner. In contrast, Mph1, together with Sgs1, suppresses CO formation in a MutSα-dependent manner during homeologous recombination.

Furthermore, the analysis of DSB repair products supports the notion that Mph1 and Sgs1 suppresses CO formation using different pathways: Mph1 promotes SDSA pathways using its D-loop dissociation function whereas Sgs1 catalyses dHJ dissolution to generate specifically NCOs.

Mph1 is conserved in *S.pombe* and in humans, in which the orthologues are known as Fml1 and FANCM, respectively (Whitby, 2010). Similar to Mph1, both Fml1 and FANCM have been shown to dissociate synthetic D-loop structures *in vitro* through their helicase/translocase activities (Gari et al., 2008a; Sun et al., 2008). Also, *FANCM* deficient cells in both murine and chicken DT40 cell lines display elevated levels of spontaneous SCEs, indicative of an anti-CO role played by *FANCM* (Bakker et al., 2009; Rosado et al., 2009). Mutations in *FANCM* lead to FA, which is characterised by short stature, skeletal anomalies, increased incidence of solid tumours and leukaemias, bone marrow failure and cellular sensitivity to DNA interstrand cross-linking (ICL) agents such as Mitomycin C (Moldovan and D'Andrea, 2009). Apart from *FANCM*, at least 12 other complementation groups for FA have been identified, caused by defects in distinct genes (*FANCA, FANCB, FANCC, BRCA2, FANCD2, FANCE, FANCF, FANCG, FANCI, FANCJ, FANCL* and *FANCN*) (Thompson, 2005; van de Vrugt et al., 2009). The FA pathway is thought to interact with other DNA repair pathways such as HR and NER (Moldovan and D'Andrea, 2009). Indeed, FANCJ has also been shown to interact with the MutLα complex of the MMR pathway, and this interaction is essential for the repair of ICL-induced damages (Peng et al., 2007). Another piece of evidence of crosstalk between the FA and MMR pathways is that the combined inactivation of *FANCD2* and *MLH1* in mice results in growth retardation and thus embryonic lethality (van de Vrugt et al., 2009). Judging by the conserved anti-CO function

between FANCM and Mph1, and the crosstalk between FA and MMR pathways, it will be of interest to investigate if the functional interactions between *S.cerevisiae* Mph1 and MutSα observed in this study are also conserved between FANCM and MutSα in higher eukaryotes.

The analysis of HR-mediated DSB repair in the current study was based on a plasmid gap repair assay, which is in many ways similar to a chromosome DSB repair assay. For instance, Bartsch et al. confirmed that plasmid-based repair assays generally recapitulate the genetic requirements, such as the requirements for Rad51 and Rad52, of DSB-initiated chromosomal recombination (Bartsch et al., 2000). The levels of elevation in CO frequency in the *fml1Δ* or *mph1Δ* backgrounds, as detected by plasmid-based gap repair and HO-induced chromosomal DSB repair assays, respectively, are also comparable, thus suggesting a high level of consistencies between the two assays (Prakash et al., 2009; Sun et al., 2008). Nevertheless, differences between the two systems have also been reported. In contrast to DSB-induced chromosomal repair assays, transformation-based plasmid gap repair assays occurs out of the context of normal DNA packaging. Sugawara et al. showed that different states of chromatinization can affect the requirement for *RAD51* during HR-mediated DSB repair (Sugawara et al., 1995). Homology length can also have differential effects in plasmid- and chromosomal-based DSB repair assays. In the case of a chromosome DSB repair assay, a minimal homology length of about 1.7kb is required for the physical detection of COs (Inbar et al., 2000). In contrast, in the plasmid break-repair assay used here, the plasmid substrate contains 800bp of homology which is sufficient to generate COs at a frequency of about 20% (Figure 3.2B). Even when one arm of homology is reduced to 57bp, giving a total homology length of 457bp, the CO frequency is 10% (data not shown).

Furthermore, the repair products generated by plasmid- and chromosome-based systems are also different in terms of their GC tract lengths and directionalities. GC tract lengths of the repaired products of plasmid gap repair assays are usually unidirectional and ~15% of these GCs are short (<53bp in length) (Cho et al., 1998; Sweetser et al., 1994), whereas chromosomal-based assays display more bidirectional GC tracts and the shortest tracts are at least 227bp in length (Nickoloff et al., 1999). Judging by the differential observations between the plasmid gap repair and a chromosome DSB repair assays, it will be important to confirm our results in the context of repair of a chromosome DSB.

In summary, Chapter 3 of my thesis has shown that Mph1, Sgs1 and MutSα act in concert to suppress genome rearrangement during ectopic HR repair. Mutations in the human homologues of Mph1, Msh2, Msh6 and Sgs1 (FANCM, hMSH2, hMSH6 and BLM, respectively) give rise to cancer-prone disorders that are associated with aberrant HR and genome instability (Bakker et al., 2009; Ellis et al., 1995; Fishel et al., 1993; Leach et al., 1993; Mosedale et al., 2005). Assuming that the functional interactions of Mph1 and MutSα in *S.cerevisiae* are conserved between FANCM and MutSα in humans, our findings, which were derived in haploid strains of *S. cerevisiae,* are likely to be relevant to human cells where the potential for ectopic recombination and thus the necessity to suppress CO formation will be greater given the diploid and repetitive nature of the human genome.

The latter parts of my thesis focus on the mechanism of HJ resolution, which is an obligatory step for CO formation (Figure 1.3(i)). In order to analyse the *in vivo* HJ resolution process more directly and quantitatively, a system involving the transformation of a plasmid-based HJ-containing substrate into yeast cells was developed. Two molecules that were constructed using distinct strategies

demonstrated the proof of principle that a synthetic HJ introduced into yeast could be resolved into a selectable product.

A further application of the *in vivo* HJ resolution system established in this study could be to investigate the factors that affect HJ resolution orientation. In our *in vivo* HJ resolution system, it is possible to determine the ratio of monomers: dimers generated from the resolution of JM-HJ by selecting for all resolution products (methionine prototrophy) or dimer products alone (methionine and histidine prototrophy) (Figure 5.1). Our preliminary analysis in wild type yeast cells showed that twice as much monomeric resolution product was generated than the dimeric one following transformation of JM-HJ, suggesting that JM-HJ resolution may occur with a bias in wild type yeast (data not shown).

There are several factors that can potentially influence the orientation of HJ resolution. For instance, HJ resolution orientation might be determined by the inherent bias of HJ resolvases. As described in Chapter 1, some resolvases display sequence specificities (Sharples et al., 1999). It will therefore be of interest to determine if single resolvase mutants, while displaying no quantitative defect in JM-HJ resolution, have altered monomer:dimer ratios. HJ binding factors could also affect the orientation of HJ resolution. In *E.coli*, it was shown that the orientation in which RuvB is loaded onto a HJ can determine the direction of branch migration and thus the resolution orientation of the HJ by RuvC (van Gool et al., 1999). This was supported by the observations of Cromie and Leach, who indirectly showed that RuvABC in *E.coli* resolves HJs in a biased manner *in vivo* to avoid CO formation (Cromie and Leach, 2000). Therefore, as described in Chapter 3, it is possible that in *S.cerevisiae*, MutSα, which can also bind to HJs, can effect a bias on HJ resolution orientation, in favour of CO formation during HR-mediated DSB

repair. It would also be of interest to determine if Sgs1 might also affect the orientation in which JM-HJ is resolved through its ability to bind and branch migrate HJs. DNA topology has also been shown to affect the orientation of HJ resolution (Zerbib et al., 1997). Zerbib et al. showed that RuvC and T7 endonuclease I resolved model HJs, which were partially supercoiled, with a specific orientation bias (Zerbib et al., 1997). The role of supercoiling on effecting HJ resolution orientation bias was confirmed by the fact that the model HJs were resolved equally in two orientations when all topological constraints were removed (Zerbib et al., 1997). Since the JM-HJ used in our preliminary investigations on HJ resolution bias is partially supercoiled, the HJ resolution bias that we observed might potentially be caused by the specific topology of JM-HJ. To investigate this possibility, the analysis of HJ resolution efficiency could be performed using JM-HJ molecules in which the supercoiling status of the R1 and R2 domains can be altered.

At least 40% of the HJ resolution activity of JM-HJ in wild type *S.cerevisiae* depends on both Mus81 and Yen1 endonucleases (Figure 5.11A). Furthermore, the deletion of Rad1, Slx1 and Slx4, which have been implicated in HJ resolution, only have a minimal effect on reducing the residual HJ resolution activity in the *mus81Δ yen1Δ* double mutant cells (Figure 5.14A). Therefore, this suggests that at least half of the resolution events occurring in a wild type cells are dependent upon additional HJ resolvases yet to be identified. An alternative explanation for the residual resolution activity in *mus81Δ yen1Δ* cells is that JM-HJ transformants may arise through other mechanisms. In our *in vivo* HJ resolution system, the formation of a dimeric molecule containing ARS and both selectable auxotrophic markers indicates a successful HJ resolution event (Figure 5.1). Hypothetically, such dimeric

molecules can also be generated by single-strand replication of the continuous, exchanged strand of JM-HJ (Figure 6.1A). Therefore, the resolution products of JM-HJ generated by this "single-strand replication" model could account for the residual "HJ resolution activity" in the *mus81Δ yen1Δ* double mutant cells. It is currently unknown if dimeric resolution products can indeed be generated using this mechanism. To test this hypothesis, JM-HJ can be modified as shown in Figure 6.1B, such that it contains a single bp mismatch and thus allows the fate of the two strands of JM-HJ to be monitored. If this modified JM-HJ substrate is transformed into a MMR deficient background (e.g. *msh2Δ*), a *bona fide* HJ resolution reaction will result in the formation of two populations of dimeric molecules differing only at the position of the mismatch, as the mismatched bases will segregate post-HJ resolution in a MMR-deficient background (Figure 6.1B). In contrast, if dimeric molecules are generated by a single-strand replication model, they will exclusively contain the sequence of the replicated strand (Figure 6.1B).

To generate a dimer resolution product via this "single-strand replication" model, the replication fork must be able to transverse the single HJ so that the whole plasmid can be replicated to completion. This will potentially uncouple leading and lagging strand DNA synthesis. In cells, a progressing replication fork may encounter a HJ if strand invasion occurs ahead of the replication fork (Figure 6.2). It is therefore of interest to determine whether a HJ can result in a stalled replication fork similar to fork encountering a DNA lesion, or whether a replication fork can transverse the single HJ and continue replicating. Hence, our JM-HJ substrate, which consists of an origin of replication and a single HJ, may potentially be a model substrate to investigate the outcome following collision of a replication fork with a HJ.

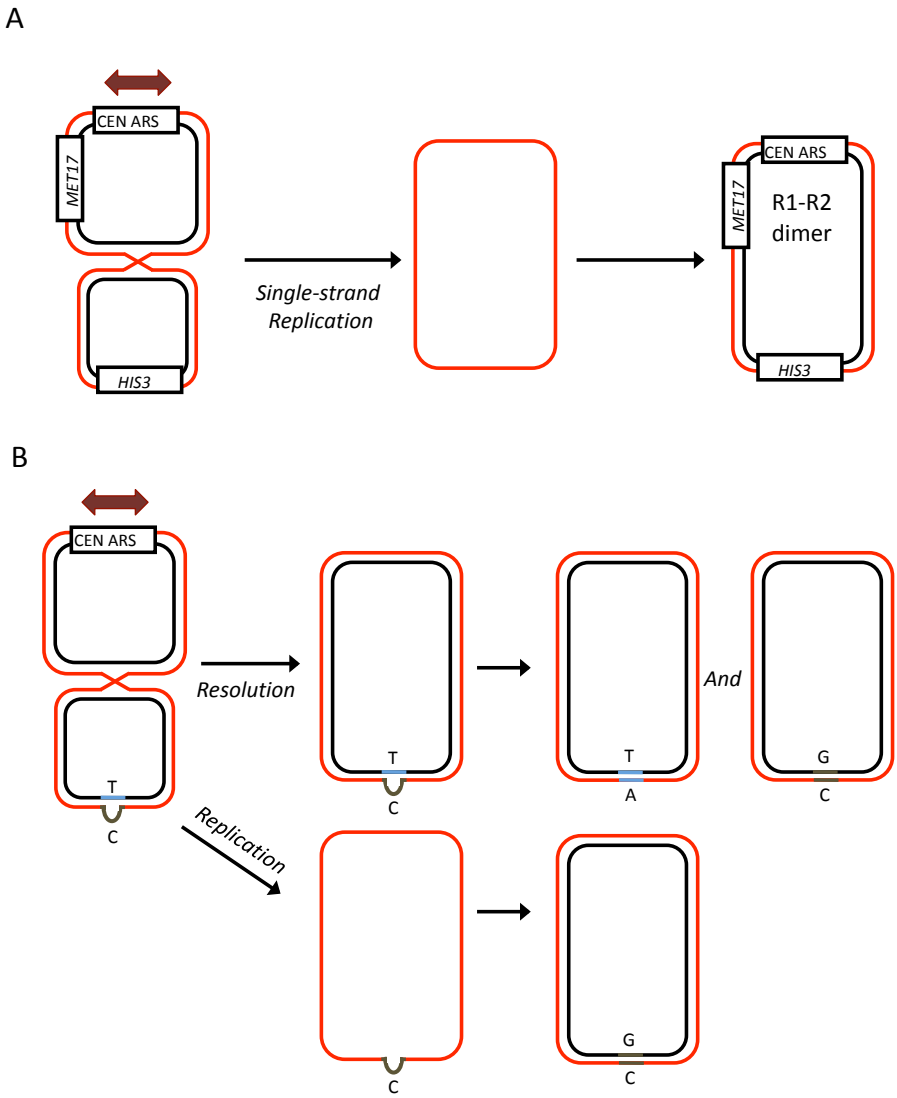


Figure 6.1 The generation of resolution products using "single-strand replication" model. (A) Dimeric resolution products can be generated through the single-strand replication of the continuous, exchanged strand of JM-HJ substrate from the CEN-ARS, providing that the replication fork can transverse the single HJ. (B) An experimental design to distinguish between genuine HJ resolution products and the dimeric product generated by the "single-strand replication" model. To distinguish between the two products, a single bp mismatch is incorporated into one domain of the JM-HJ substrate. This experiment needs to be carried out in an MMR-deficient background. If the resolution products are generated by genuine HJ resolution, two distinct resolution products differing at the single bp mismatch will be generated because in an MMR-deficient background, the single bp mismatch will not be repaired and is segregated into two molecules post-replication, via semi-conservative DNA replication. If the dimeric resolution products are generated by the "single-strand replication" model, only products containing the replicated strand will be detected.

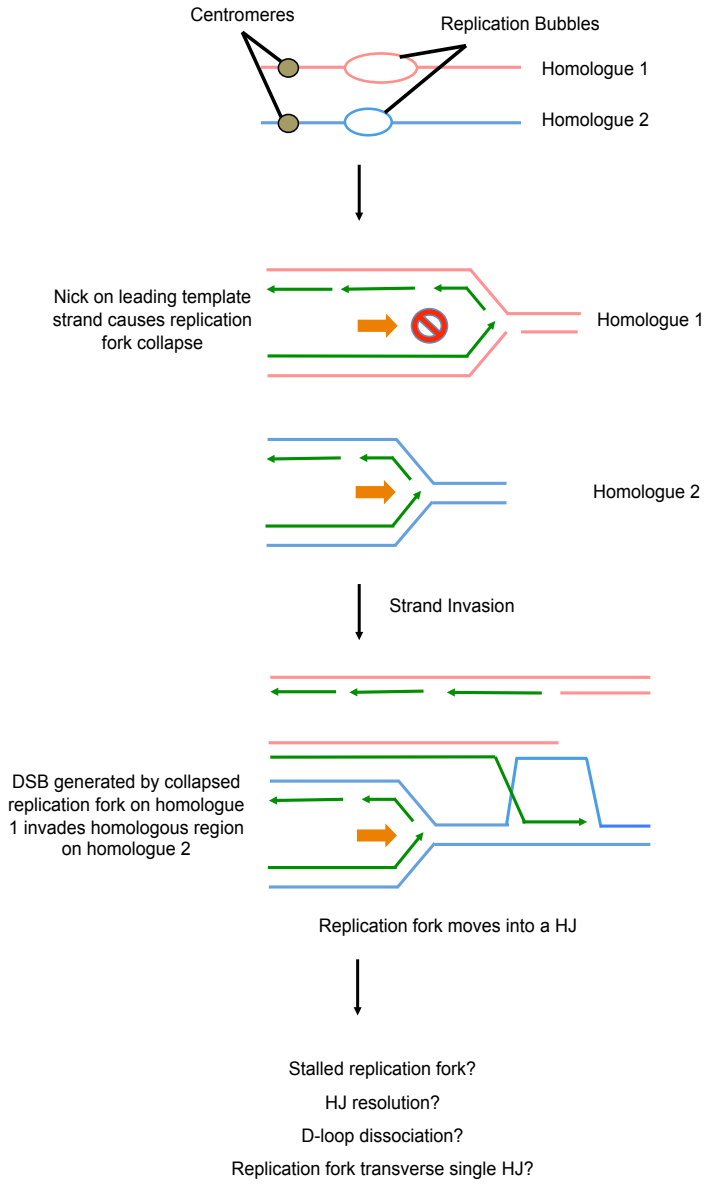


Figure 6.2 A scenario when a progressing replication fork collides with a HJ. The diagram depicts two replication bubbles progressing at different speeds on a pair of homologous chromosomes. If the faster replication fork collapses, for example when a nick is present on the leading strand template, a DSB is generated. This DSB can be used to reset a replication fork using BIR, by invading either into the sister chromatid or the homologous chromosomes. The strand invasion of the DSB into the homologous chromosome will produce a HJ ahead of the replication fork. The collision between the replication fork and the HJ may result in a stalled replication fork, which can be resumed if HJ resolution occurs or by D-loop dissociation prior to HJ formation. Alternatively, the replication fork may be able to transverse the single HJ and carry on replicating to the end of the chromosome.

In conclusion, Chapters 4 and 5 of this thesis demonstrated that two plasmid-based HJ substrates were constructed using two distinct approaches and can be used for the direct and quantitative analysis of *in vivo* HJ resolution in *S.cerevisiae*. We have also discussed other potential applications of these plasmid-based HJ substrates in the investigations on other aspects of HJ processing, for instance HJ resolution orientation bias and collision between a replication fork and a HJ. Using the JM-HJ substrate discussed in Chapter 5, we have revealed an over-lapping role of Mus81 and Yen1 in HJ resolution *in vivo*, which is essential for the repair of damaged replication forks but not for IR-induced DSBs. These findings are consistent with the notion that DSBs are repaired predominantly via SDSA or dissolution pathways, rather than via a pathway dependent upon HJ resolution. Since Mus81 and Yen1 are only responsible for ~40% of the HJ resolution activities in a wild type cell, this *in vivo* HJ resolution system will potentially facilitate the identification of additional HJ processing activities that act in parallel to these structure-specific nucleases.

Chapter Seven

7. Bibliography

7. Bibliography

Abdullah, M.F., Hoffmann, E.R., Cotton, V.E., and Borts, R.H. (2004). A role for the MutL homologue MLH2 in controlling heteroduplex formation and in regulating between two different crossover pathways in budding yeast. Cytogenet Genome Res *107*, 180-190.

Aboussekhra, A., Chanet, R., Adjiri, A., and Fabre, F. (1992). Semidominant suppressors of Srs2 helicase mutations of *Saccharomyces cerevisiae* map in the RAD51 gene, whose sequence predicts a protein with similarities to procaryotic RecA proteins. Mol Cell Biol *12*, 3224-3234.

Alani, E. (1996). The *Saccharomyces cerevisiae* Msh2 and Msh6 proteins form a complex that specifically binds to duplex oligonucleotides containing mismatched DNA base pairs. Mol Cell Biol *16*, 5604-5615.

Alani, E., Lee, S., Kane, M.F., Griffith, J., and Kolodner, R.D. (1997). *Saccharomyces cerevisiae* MSH2, a mispaired base recognition protein, also recognizes Holliday junctions in DNA. J Mol Biol *265*, 289-301.

Allers, T., and Lichten, M. (2001). Differential timing and control of noncrossover and crossover recombination during meiosis. Cell *106*, 47-57.

Amitani, I., Baskin, R.J., and Kowalczykowski, S.C. (2006). Visualization of Rad54, a chromatin remodeling protein, translocating on single DNA molecules. Mol Cell *23*, 143-148.

Andersen, S.L., Bergstralh, D.T., Kohl, K.P., LaRocque, J.R., Moore, C.B., and Sekelsky, J. (2009). Drosophila MUS312 and the vertebrate ortholog BTBD12 interact with DNA structure-specific endonucleases in DNA repair and recombination. Mol Cell *35*, 128-135.

Aravind, L., and Koonin, E.V. (2000). SAP - a putative DNA-binding motif involved in chromosomal organization. Trends Biochem Sci *25*, 112-114.

Atkinson, J., and McGlynn, P. (2009). Replication fork reversal and the maintenance of genome stability. Nucleic Acids Res *37*, 3475-3492.

Bailis, A.M., and Rothstein, R. (1990). A defect in mismatch repair in *Saccharomyces cerevisiae* stimulates ectopic recombination between homeologous genes by an excision repair dependent process. Genetics *126*, 535-547.

Bakker, S.T., van de Vrugt, H.J., Rooimans, M.A., Oostra, A.B., Steltenpool, J., Delzenne-Goette, E., van der Wal, A., van der Valk, M., Joenje, H., te Riele, H.*, et al.* (2009). Fancm-deficient mice reveal unique features of Fanconi anemia complementation group M. Hum Mol Genet *18*, 3484-3495.

Bardwell, A.J., Bardwell, L., Tomkinson, A.E., and Friedberg, E.C. (1994). Specific cleavage of model recombination and repair intermediates by the yeast Rad1-Rad10 DNA endonuclease. Science *265*, 2082-2085.

Bartsch, S., Kang, L.E., and Symington, L.S. (2000). RAD51 is required for the repair of plasmid double-stranded DNA gaps from either plasmid or chromosomal templates. Mol Cell Biol *20*, 1194-1205.

Basile, G., Aker, M., and Mortimer, R.K. (1992). Nucleotide sequence and transcriptional regulation of the yeast recombinational repair gene RAD51. Mol Cell Biol *12*, 3235-3246.

Bastin-Shanower, S.A., Fricke, W.M., Mullen, J.R., and Brill, S.J. (2003). The mechanism of Mus81-Mms4 cleavage site selection distinguishes it from the homologous endonuclease Rad1-Rad10. Mol Cell Biol *23*, 3487-3496.

Bell, L., and Byers, B. (1979). Occurrence of crossed strand-exchange forms in yeast DNA during meiosis. Proc Natl Acad Sci U S A *76*, 3445-3449.

Belmaaza, A., Milot, E., Villemure, J.F., and Chartrand, P. (1994). Interference of DNA sequence divergence with precise recombinational DNA repair in mammalian cells. EMBO J *13*, 5355-5360.

Benbow, R.M., Zuccarelli, A.J., and Sinsheimer, R.L. (1975). Recombinant DNA molecules of bacteriophage phi chi174. Proc Natl Acad Sci U S A *72*, 235-239.

Bennett, R.J., and West, S.C. (1995). Structural analysis of the RuvC-Holliday junction complex reveals an unfolded junction. J Mol Biol *252*, 213-226.

Bishop, D.K. (1994). RecA homologs Dmc1 and Rad51 interact to form multiple nuclear complexes prior to meiotic chromosome synapsis. Cell *79*, 1081-1092.

Blackwell, L.J., Bjornson, K.P., Allen, D.J., and Modrich, P. (2001). Distinct MutS DNA-binding modes that are differentially modulated by ATP binding and hydrolysis. J Biol Chem *276*, 34339-34347.

Blakely, G., Colloms, S., May, G., Burke, M., and Sherratt, D. (1991). Escherichia coli XerC recombinase is required for chromosomal segregation at cell division. New Biol *3*, 789-798.

Blakely, G., May, G., McCulloch, R., Arciszewska, L.K., Burke, M., Lovett, S.T., and Sherratt, D.J. (1993). Two related recombinases are required for site-specific recombination at dif and cer in E. coli K12. Cell *75*, 351-361.

Blanco, M.G., Matos, J., Rass, U., Ip, S.C., and West, S.C. Functional overlap between the structure-specific nucleases Yen1 and Mus81-Mms4 for DNA-damage repair in S. cerevisiae. DNA Repair (Amst).

Blastyak, A., Pinter, L., Unk, I., Prakash, L., Prakash, S., and Haracska, L. (2007). Yeast Rad5 protein required for postreplication repair has a DNA helicase activity specific for replication fork regression. Mol Cell *28*, 167-175.

Boddy, M.N., Gaillard, P.H., McDonald, W.H., Shanahan, P., Yates, J.R., 3rd, and Russell, P. (2001). Mus81-Eme1 are essential components of a Holliday junction resolvase. Cell *107*, 537-548.

Boddy, M.N., Lopez-Girona, A., Shanahan, P., Interthal, H., Heyer, W.D., and Russell, P. (2000). Damage tolerance protein Mus81 associates with the FHA1 domain of checkpoint kinase Cds1. Mol Cell Biol *20*, 8758-8766.

Bolt, E.L., and Lloyd, R.G. (2002). Substrate specificity of RusA resolvase reveals the DNA structures targeted by RuvAB and RecG in vivo. Mol Cell *10*, 187-198.

Bolt, E.L., Sharples, G.J., and Lloyd, R.G. (1999). Identification of three aspartic acid residues essential for catalysis by the RusA holliday junction resolvase. J Mol Biol *286*, 403-415.

Boulton, S.J., and Jackson, S.P. (1996). Identification of a *Saccharomyces cerevisiae* Ku80 homologue: roles in DNA double strand break rejoining and in telomeric maintenance. Nucleic Acids Res *24*, 4639-4648.

Bowers, J., Sokolsky, T., Quach, T., and Alani, E. (1999). A mutation in the MSH6 subunit of the *Saccharomyces cerevisiae* MSH2-MSH6 complex disrupts mismatch recognition. J Biol Chem *274*, 16115-16125.

Bowers, J., Tran, P.T., Liskay, R.M., and Alani, E. (2000). Analysis of yeast MSH2-MSH6 suggests that the initiation of mismatch repair can be separated into discrete steps. J Mol Biol *302*, 327-338.

Branzei, D., and Foiani, M. (2005). The DNA damage response during DNA replication. Curr Opin Cell Biol *17*, 568-575.

Bugreev, D.V., and Mazin, A.V. (2004). Ca2+ activates human homologous recombination protein Rad51 by modulating its ATPase activity. Proc Natl Acad Sci U S A *101*, 9988-9993.

Bugreev, D.V., Mazina, O.M., and Mazin, A.V. (2006). Rad54 protein promotes branch migration of Holliday junctions. Nature *442*, 590-593.

Bugreev, D.V., Yu, X., Egelman, E.H., and Mazin, A.V. (2007). Novel pro- and anti-recombination activities of the Bloom's syndrome helicase. Genes Dev *21*, 3085-3094.

Burke, D., Dawson, D., Stearns, T., and Cold Spring Harbor Laboratory. (2000). Methods in yeast genetics : a Cold Spring Harbor Laboratory course manual, 2000 edn (Plainview, N.Y., Cold Spring Harbor Laboratory Press).

Chan, S.N., Harris, L., Bolt, E.L., Whitby, M.C., and Lloyd, R.G. (1997). Sequence specificity and biochemical characterization of the RusA Holliday junction resolvase of *Escherichia coli*. J Biol Chem *272*, 14873-14882.

Chan, S.N., Vincent, S.D., and Lloyd, R.G. (1998). Recognition and manipulation of branched DNA by the RusA Holliday junction resolvase of *Escherichia coli.* Nucleic Acids Res *26*, 1560-1566.

Chen, W., and Jinks-Robertson, S. (1998). Mismatch repair proteins regulate heteroduplex formation during mitotic recombination in yeast. Mol Cell Biol *18*, 6525-6537.

Chen, W., and Jinks-Robertson, S. (1999). The role of the mismatch repair machinery in regulating mitotic and meiotic recombination between diverged sequences in yeast. Genetics *151*, 1299-1313.

Chen, X.B., Melchionna, R., Denis, C.M., Gaillard, P.H., Blasina, A., Van de Weyer, I., Boddy, M.N., Russell, P., Vialard, J., and McGowan, C.H. (2001). Human Mus81-associated endonuclease cleaves Holliday junctions in vitro. Mol Cell *8*, 1117-1127.

Cho, J.W., Khalsa, G.J., and Nickoloff, J.A. (1998). Gene-conversion tract directionality is influenced by the chromosome environment. Curr Genet *34*, 269-279.

Chu, S., DeRisi, J., Eisen, M., Mulholland, J., Botstein, D., Brown, P.O., and Herskowitz, I. (1998). The transcriptional program of sporulation in budding yeast. Science *282*, 699-705.

Ciccia, A., Constantinou, A., and West, S.C. (2003). Identification and characterization of the human mus81-eme1 endonuclease. J Biol Chem *278*, 25172-25178.

Ciccia, A., Ling, C., Coulthard, R., Yan, Z., Xue, Y., Meetei, A.R., Laghmani el, H., Joenje, H., McDonald, N., de Winter, J.P.*, et al.* (2007). Identification of FAAP24, a Fanconi anemia core complex protein that interacts with FANCM. Mol Cell *25*, 331-343.

Clegg, R.M., Murchie, A.I., and Lilley, D.M. (1994). The solution structure of the four-way DNA junction at low-salt conditions: a fluorescence resonance energy transfer analysis. Biophys J *66*, 99-109.

Colavito, S., Macris-Kiss, M., Seong, C., Gleeson, O., Greene, E.C., Klein, H.L., Krejci, L., and Sung, P. (2009). Functional significance of the Rad51-Srs2 complex in Rad51 presynaptic filament disruption. Nucleic Acids Res *37*, 6754-6764.

Colloms, S.D., McCulloch, R., Grant, K., Neilson, L., and Sherratt, D.J. (1996). Xer-mediated site-specific recombination *in vitro*. EMBO J *15*, 1172-1181.

Colloms, S.D., Sykora, P., Szatmari, G., and Sherratt, D.J. (1990). Recombination at ColE1 *cer* requires the *Escherichia coli xerC* gene product, a member of the lambda integrase family of site-specific recombinases. J Bacteriol *172*, 6973-6980.

Connolly, B., Parsons, C.A., Benson, F.E., Dunderdale, H.J., Sharples, G.J., Lloyd, R.G., and West, S.C. (1991). Resolution of Holliday junctions *in vitro* requires the *Escherichia coli ruvC* gene product. Proc Natl Acad Sci U S A *88*, 6063-6067.

Constantin, N., Dzantiev, L., Kadyrov, F.A., and Modrich, P. (2005). Human mismatch repair: reconstitution of a nick-directed bidirectional reaction. J Biol Chem *280*, 39752-39761.

Constantinou, A., Chen, X.B., McGowan, C.H., and West, S.C. (2002). Holliday junction resolution in human cells: two junction endonucleases with distinct substrate specificities. EMBO J *21*, 5577-5585.

Constantinou, A., Davies, A.A., and West, S.C. (2001). Branch migration and Holliday junction resolution catalyzed by activities from mammalian cells. Cell *104*, 259-268.

Cote, A.G., and Lewis, S.M. (2008). Mus81-dependent double-strand DNA breaks at *in vivo*-generated cruciform structures in *S. cerevisiae.* Mol Cell *31*, 800-812.

Cox, M.M., Goodman, M.F., Kreuzer, K.N., Sherratt, D.J., Sandler, S.J., and Marians, K.J. (2000). The importance of repairing stalled replication forks. Nature *404*, 37-41.

Cromie, G.A., and Leach, D.R. (2000). Control of crossing over. Mol Cell *6*, 815-826.

Datta, A., Adjiri, A., New, L., Crouse, G.F., and Jinks Robertson, S. (1996). Mitotic crossovers between diverged sequences are regulated by mismatch repair proteins in *Saccaromyces cerevisiae*. Mol Cell Biol *16*, 1085-1093.

Datta, A., Hendrix, M., Lipsitch, M., and Jinks-Robertson, S. (1997). Dual roles for DNA sequence identity and the mismatch repair system in the regulation of mitotic crossing-over in yeast. Proc Natl Acad Sci U S A *94*, 9757-9762.

Davies, A.A., Friedberg, E.C., Tomkinson, A.E., Wood, R.D., and West, S.C. (1995). Role of the Rad1 and Rad10 proteins in nucleotide excision repair and recombination. J Biol Chem *270*, 24638-24641.

Davis, A.P., and Symington, L.S. (2004). RAD51-dependent break-induced replication in yeast. Mol Cell Biol *24*, 2344-2351.

de Laat, W.L., Jaspers, N.G., and Hoeijmakers, J.H. (1999). Molecular mechanism of nucleotide excision repair. Genes Dev *13*, 768-785.

de los Santos, T., Hunter, N., Lee, C., Larkin, B., Loidl, J., and Hollingsworth, N.M. (2003). The Mus81/Mms4 endonuclease acts independently of double-Holliday junction resolution to promote a distinct subset of crossovers during meiosis in budding yeast. Genetics *164*, 81-94.

de los Santos, T., Loidl, J., Larkin, B., and Hollingsworth, N.M. (2001). A role for MMS4 in the processing of recombination intermediates during meiosis in *Saccharomyces cerevisiae.* Genetics *159*, 1511-1525.

Dianov, G., and Lindahl, T. (1994). Reconstitution of the DNA base excision-repair pathway. Curr Biol *4*, 1069-1076.

Doe, C.L., Ahn, J.S., Dixon, J., and Whitby, M.C. (2002). Mus81-Eme1 and Rqh1 involvement in processing stalled and collapsed replication forks. J Biol Chem *277*, 32753-32759.

Dronkert, M.L., and Kanaar, R. (2001). Repair of DNA interstrand cross-links. Mutat Res *486*, 217-247.

Duckett, D.R., Murchie, A.I., Diekmann, S., von Kitzing, E., Kemper, B., and Lilley, D.M. (1988). The structure of the Holliday junction, and its resolution. Cell *55*, 79-89.

Dunderdale, H.J., Benson, F.E., Parsons, C.A., Sharples, G.J., Lloyd, R.G., and West, S.C. (1991). Formation and resolution of recombination intermediates by *E. coli* RecA and RuvC proteins. Nature *354*, 506-510.

Eggleston, A.K., and West, S.C. (2000). Cleavage of holliday junctions by the Escherichia coli RuvABC complex. J Biol Chem *275*, 26467-26476.

Ehmsen, K.T., and Heyer, W.D. (2008). Saccharomyces cerevisiae Mus81-Mms4 is a catalytic, DNA structure-selective endonuclease. Nucleic Acids Res *36*, 2182-2195.

Eichman, B.F., Vargason, J.M., Mooers, B.H., and Ho, P.S. (2000). The Holliday junction in an inverted repeat DNA sequence: sequence effects on the structure of four-way junctions. Proc Natl Acad Sci U S A *97*, 3971-3976.

Elborough, K.M., and West, S.C. (1990). Resolution of synthetic Holliday junctions in DNA by an endonuclease activity from calf thymus. EMBO J *9*, 2931-2936.

Elliott, B., Richardson, C., and Jasin, M. (2005). Chromosomal translocation mechanisms at intronic alu elements in mammalian cells. Mol Cell *17*, 885-894.

Ellis, N.A., Groden, J., Ye, T.Z., Straughen, J., Lennon, D.J., Ciocci, S., Proytcheva, M., and German, J. (1995). The Bloom's syndrome gene product is homologous to RecQ helicases. Cell *83*, 655-666.

Engels, W.R., Johnson-Schlitz, D.M., Eggleston, W.B., and Sved, J. (1990). High-frequency P element loss in *Drosophila* is homolog dependent. Cell *62*, 515-525.

Entian, K.D., Schuster, T., Hegemann, J.H., Becher, D., Feldmann, H., Guldener, U., Gotz, R., Hansen, M., Hollenberg, C.P., Jansen, G.*, et al.* (1999). Functional analysis of 150 deletion mutants in *Saccharomyces cerevisiae* by a systematic approach. Mol Gen Genet *262*, 683-702.

Essers, J., Houtsmuller, A.B., van Veelen, L., Paulusma, C., Nigg, A.L., Pastink, A., Vermeulen, W., Hoeijmakers, J.H., and Kanaar, R. (2002). Nuclear dynamics of RAD52 group homologous recombination proteins in response to DNA damage. EMBO J *21*, 2030-2037.

Fabisiewicz, A., and Worth, L., Jr. (2001). *Escherichia coli* MutS,L modulate RuvAB-dependent branch migration between diverged DNA. J Biol Chem *276*, 9413-9420.

Fabre, F., Chan, A., Heyer, W.D., and Gangloff, S. (2002). Alternate pathways involving Sgs1/Top3, Mus81/ Mms4, and Srs2 prevent formation of toxic recombination intermediates from single-stranded gaps created by DNA replication. Proc Natl Acad Sci U S A *99*, 16887-16892.

Fekairi, S., Scaglione, S., Chahwan, C., Taylor, E.R., Tissier, A., Coulon, S., Dong, M.Q., Ruse, C., Yates, J.R., 3rd, Russell, P.*, et al.* (2009). Human SLX4 is a

Holliday junction resolvase subunit that binds multiple DNA repair/recombination endonucleases. Cell *138*, 78-89.

Ferguson, D.O., and Holloman, W.K. (1996). Recombinational repair of gaps in DNA is asymmetric in *Ustilago maydis* and can be explained by a migrating D-loop model. Proc Natl Acad Sci U S A *93*, 5419-5424.

Fishel, R., Lescoe, M.K., Rao, M.R., Copeland, N.G., Jenkins, N.A., Garber, J., Kane, M., and Kolodner, R. (1993). The human mutator gene homolog MSH2 and its association with hereditary nonpolyposis colon cancer. Cell *75*, 1027-1038.

Fishman-Lobell, J., Rudin, N., and Haber, J.E. (1992). Two alternative pathways of double-strand break repair that are kinetically separable and independently modulated. Mol Cell Biol *12*, 1292-1303.

Flott, S., Alabert, C., Toh, G.W., Toth, R., Sugawara, N., Campbell, D.G., Haber, J.E., Pasero, P., and Rouse, J. (2007). Phosphorylation of Slx4 by Mec1 and Tel1 regulates the single-strand annealing mode of DNA repair in budding yeast. Mol Cell Biol *27*, 6433-6445.

Fricke, W.M., Bastin-Shanower, S.A., and Brill, S.J. (2005). Substrate specificity of the *Saccharomyces cerevisiae* Mus81-Mms4 endonuclease. DNA Repair (Amst) *4*, 243-251.

Fricke, W.M., and Brill, S.J. (2003). Slx1-Slx4 is a second structure-specific endonuclease functionally redundant with Sgs1-Top3. Genes Dev *17*, 1768-1778.

Gaillard, P.H., Noguchi, E., Shanahan, P., and Russell, P. (2003). The endogenous Mus81-Eme1 complex resolves Holliday junctions by a nick and counternick mechanism. Mol Cell *12*, 747-759.

Gangloff, S., Soustelle, C., and Fabre, F. (2000). Homologous recombination is responsible for cell death in the absence of the Sgs1 and Srs2 helicases. Nat Genet *25*, 192-194.

Garcia, A.D., Aravind, L., Koonin, E.V., and Moss, B. (2000). Bacterial-type DNA holliday junction resolvases in eukaryotic viruses. Proc Natl Acad Sci U S A *97*, 8926-8931.

Gari, K., Decaillet, C., Delannoy, M., Wu, L., and Constantinou, A. (2008a). Remodeling of DNA replication structures by the branch point translocase FANCM. Proc Natl Acad Sci U S A *105*, 16107-16112.

Gari, K., Decaillet, C., Stasiak, A.Z., Stasiak, A., and Constantinou, A. (2008b). The Fanconi anemia protein FANCM can promote branch migration of Holliday junctions and replication forks. Mol Cell *29*, 141-148.

Garvik, B., Carson, M., and Hartwell, L. (1995). Single-stranded DNA arising at telomeres in cdc13 mutants may constitute a specific signal for the RAD9 checkpoint. Mol Cell Biol *15*, 6128-6138.

Gavin, A.C., Bosche, M., Krause, R., Grandi, P., Marzioch, M., Bauer, A., Schultz, J., Rick, J.M., Michon, A.M., Cruciat, C.M*., et al.* (2002). Functional organization of the yeast proteome by systematic analysis of protein complexes. Nature *415*, 141-147.

Gilbertson, L.A., and Stahl, F.W. (1996). A test of the double-strand break repair model for meiotic recombination in *Saccharomyces cerevisiae*. Genetics *144*, 27-41.

Giraud-Panis, M.J., and Lilley, D.M. (1998). Structural recognition and distortion by the DNA junction-resolving enzyme RusA. J Mol Biol *278*, 117-133.

Gloor, G.B., Nassif, N.A., Johnson-Schlitz, D.M., Preston, C.R., and Engels, W.R. (1991). Targeted gene replacement in *Drosophila* via P element-induced gap repair. Science *253*, 1110-1117.

Goldfarb, T., and Alani, E. (2005). Distinct roles for the *Saccharomyces cerevisiae* mismatch repair proteins in heteroduplex rejection, mismatch repair and nonhomologous tail removal. Genetics *169*, 563-574.

Gradia, S., Acharya, S., and Fishel, R. (1997). The human mismatch recognition complex hMSH2-hMSH6 functions as a novel molecular switch. Cell *91*, 995-1005.

Guzder, S.N., Habraken, Y., Sung, P., Prakash, L., and Prakash, S. (1995). Reconstitution of yeast nucleotide excision repair with purified Rad proteins, replication protein A, and transcription factor TFIIH. J Biol Chem *270*, 12973-12976.

Haber, J.E., and Heyer, W.D. (2001). The fuss about Mus81. Cell *107*, 551-554.

Habraken, Y., Sung, P., Prakash, L., and Prakash, S. (1994). Holliday junction cleavage by yeast Rad1 protein. Nature *371*, 531-534.

Habraken, Y., Sung, P., Prakash, L., and Prakash, S. (1996). Binding of insertion/deletion DNA mismatches by the heterodimer of yeast mismatch repair proteins MSH2 and MSH3. Curr Biol *6*, 1185-1187.

Hackett, J.A., and Greider, C.W. (2003). End resection initiates genomic instability in the absence of telomerase. Mol Cell Biol *23*, 8450-8461.

Hanada, K., Budzowska, M., Davies, S.L., van Drunen, E., Onizawa, H., Beverloo, H.B., Maas, A., Essers, J., Hickson, I.D., and Kanaar, R. (2007). The structure-specific endonuclease Mus81 contributes to replication restart by generating double-strand DNA breaks. Nat Struct Mol Biol *14*, 1096-1104.

Hanada, K., Budzowska, M., Modesti, M., Maas, A., Wyman, C., Essers, J., and Kanaar, R. (2006). The structure-specific endonuclease Mus81-Eme1 promotes conversion of interstrand DNA crosslinks into double-strands breaks. EMBO J *25*, 4921-4932.

Harfe, B.D., and Jinks-Robertson, S. (2000). DNA mismatch repair and genetic instability. Annu Rev Genet *34*, 359-399.

Hastings, P.J. (1988). Recombination in the eukaryotic nucleus. Bioessays *9*, 61-64.

Heller, R.C., and Marians, K.J. (2006). Replication fork reactivation downstream of a blocked nascent leading strand. Nature *439*, 557-562.

Heyer, W.D., Ehmsen, K.T., and Solinger, J.A. (2003). Holliday junctions in the eukaryotic nucleus: resolution in sight? Trends Biochem Sci *28*, 548-557.

Hickson, I.D. (2003). RecQ helicases: caretakers of the genome. Nat Rev Cancer *3*, 169-178.

Higuchi, K., Katayama, T., Iwai, S., Hidaka, M., Horiuchi, T., and Maki, H. (2003). Fate of DNA replication fork encountering a single DNA lesion during oriC plasmid DNA replication *in vitro*. Genes Cells *8*, 437-449.

Hoege, C., Pfander, B., Moldovan, G.L., Pyrowolakis, G., and Jentsch, S. (2002). RAD6-dependent DNA repair is linked to modification of PCNA by ubiquitin and SUMO. Nature *419*, 135-141.

Hoess, R., Wierzbicki, A., and Abremski, K. (1987). Isolation and characterization of intermediates in site-specific recombination. Proc Natl Acad Sci U S A *84*, 6840-6844.

Hoffmann, E.R., and Borts, R.H. (2004). Meiotic recombination intermediates and mismatch repair proteins. Cytogenet Genome Res *107*, 232-248.

Hoffmann, E.R., Shcherbakova, P.V., Kunkel, T.A., and Borts, R.H. (2003). MLH1 mutations differentially affect meiotic functions in *Saccharomyces cerevisiae*. Genetics *163*, 515-526.

Holliday, R. (1964). a mechanism for gene conversion in fungi. genetical research *5*, 282-304.

Hollingsworth, N.M., Ponte, L., and Halsey, C. (1995). MSH5, a novel MutS homolog, facilitates meiotic reciprocal recombination between homologs in *Saccharomyces cerevisiae* but not mismatch repair. Genes Dev *9*, 1728-1739.

Hsia, K.T., Millar, M.R., King, S., Selfridge, J., Redhead, N.J., Melton, D.W., and Saunders, P.T. (2003). DNA repair gene Ercc1 is essential for normal spermatogenesis and oogenesis and for functional integrity of germ cell DNA in the mouse. Development *130*, 369-378.

Hsu, P.L., and Landy, A. (1984). Resolution of synthetic att-site Holliday structures by the integrase protein of bacteriophage lambda. Nature *311*, 721-726.

Hu, P., Beresten, S.F., van Brabant, A.J., Ye, T.Z., Pandolfi, P.P., Johnson, F.B., Guarente, L., and Ellis, N.A. (2001). Evidence for BLM and Topoisomerase IIIalpha interaction in genomic stability. Hum Mol Genet *10*, 1287-1298.

Hu, Y., Raynard, S., Sehorn, M.G., Lu, X., Bussen, W., Zheng, L., Stark, J.M., Barnes, E.L., Chi, P., Janscak, P.*, et al.* (2007). RECQL5/Recql5 helicase regulates homologous recombination and suppresses tumor formation via disruption of Rad51 presynaptic filaments. Genes Dev *21*, 3073-3084.

Hyde, H., Davies, A.A., Benson, F.E., and West, S.C. (1994). Resolution of recombination intermediates by a mammalian activity functionally analogous to *Escherichia coli* RuvC resolvase. J Biol Chem *269*, 5202-5209.

Inbar, O., Liefshitz, B., Bitan, G., and Kupiec, M. (2000). The relationship between homology length and crossing over during the repair of a broken chromosome. J Biol Chem *275*, 30833-30838.

Interthal, H., and Heyer, W.D. (2000). MUS81 encodes a novel helix-hairpin-helix protein involved in the response to UV- and methylation-induced DNA damage in *Saccharomyces cerevisiae*. Mol Gen Genet *263*, 812-827.

Ip, S.C., Rass, U., Blanco, M.G., Flynn, H.R., Skehel, J.M., and West, S.C. (2008). Identification of Holliday junction resolvases from humans and yeast. Nature *456*, 357-361.

Ira, G., Malkova, A., Liberi, G., Foiani, M., and Haber, J.E. (2003). Srs2 and Sgs1-Top3 suppress crossovers during double-strand break repair in yeast. Cell *115*, 401-411.

Ivanov, E.L., and Haber, J.E. (1995). RAD1 and RAD10, but not other excision repair genes, are required for double-strand break-induced recombination in *Saccharomyces cerevisiae*. Mol Cell Biol *15*, 2245-2251.

Iwasaki, H., Takahagi, M., Nakata, A., and Shinagawa, H. (1992). *Escherichia coli* RuvA and RuvB proteins specifically interact with Holliday junctions and promote branch migration. Genes Dev *6*, 2214-2220.

Iwasaki, H., Takahagi, M., Shiba, T., Nakata, A., and Shinagawa, H. (1991). *Escherichia coli* RuvC protein is an endonuclease that resolves the Holliday structure. EMBO J *10*, 4381-4389.

Jessop, L., and Lichten, M. (2008). Mus81/Mms4 endonuclease and Sgs1 helicase collaborate to ensure proper recombination intermediate metabolism during meiosis. Mol Cell *31*, 313-323.

Jiang, J., Bai, L., Surtees, J.A., Gemici, Z., Wang, M.D., and Alani, E. (2005). Detection of high-affinity and sliding clamp modes for MSH2-MSH6 by single-molecule unzipping force analysis. Mol Cell *20*, 771-781.

Johnson, R.E., Prakash, S., and Prakash, L. (1994). Yeast DNA repair protein RAD5 that promotes instability of simple repetitive sequences is a DNA-dependent ATPase. J Biol Chem *269*, 28259-28262.

Joyce, E.F., Tanneti, S.N., and McKim, K.S. (2009). *Drosophila* hold'em is required for a subset of meiotic crossovers and interacts with the dna repair endonuclease complex subunits MEI-9 and ERCC1. Genetics *181*, 335-340.

Junop, M.S., Obmolova, G., Rausch, K., Hsieh, P., and Yang, W. (2001). Composite active site of an ABC ATPase: MutS uses ATP to verify mismatch recognition and authorize DNA repair. Mol Cell *7*, 1-12.

Kaliraman, V., Mullen, J.R., Fricke, W.M., Bastin-Shanower, S.A., and Brill, S.J. (2001). Functional overlap between Sgs1-Top3 and the Mms4-Mus81 endonuclease. Genes Dev *15*, 2730-2740.

Kanagaraj, R., Saydam, N., Garcia, P.L., Zheng, L., and Janscak, P. (2006). Human RECQ5beta helicase promotes strand exchange on synthetic DNA structures resembling a stalled replication fork. Nucleic Acids Res *34*, 5217-5231.

Karow, J.K., Constantinou, A., Li, J.L., West, S.C., and Hickson, I.D. (2000). The Bloom's syndrome gene product promotes branch migration of holliday junctions. Proc Natl Acad Sci U S A *97*, 6504-6508.

Kearney, H.M., Kirkpatrick, D.T., Gerton, J.L., and Petes, T.D. (2001). Meiotic recombination involving heterozygous large insertions in *Saccharomyces cerevisiae*: formation and repair of large, unpaired DNA loops. Genetics *158*, 1457-1476.

Keeney, S. (2001). Mechanism and control of meiotic recombination initiation. Curr Top Dev Biol *52*, 1-53.

Kemper, B., and Brown, D.T. (1976). Function of gene 49 of bacteriophage T4. II. Analysis of intracellular development and the structure of very fast-sedimenting DNA. J Virol *18*, 1000-1015.

Kijas, A.W., Studamire, B., and Alani, E. (2003). Msh2 separation of function mutations confer defects in the initiation steps of mismatch repair. J Mol Biol *331*, 123-138.

Kleff, S., Kemper, B., and Sternglanz, R. (1992). Identification and characterization of yeast mutants and the gene for a cruciform cutting endonuclease. EMBO J *11*, 699-704.

Komori, K., Sakae, S., Shinagawa, H., Morikawa, K., and Ishino, Y. (1999). A Holliday junction resolvase from *Pyrococcus furiosus*: functional similarity to *Escherichia coli* RuvC provides evidence for conserved mechanism of homologous recombination in Bacteria, Eukarya, and Archaea. Proc Natl Acad Sci U S A *96*, 8873-8878.

Kowalczykowski, S.C. (2000). Initiation of genetic recombination and recombination-dependent replication. Trends Biochem Sci *25*, 156-165.

Krejci, L., Chen, L., Van Komen, S., Sung, P., and Tomkinson, A. (2003a). Mending the break: two DNA double-strand break repair machines in eukaryotes. Prog Nucleic Acid Res Mol Biol *74*, 159-201.

Krejci, L., Macris, M., Li, Y., Van Komen, S., Villemain, J., Ellenberger, T., Klein, H., and Sung, P. (2004). Role of ATP hydrolysis in the antirecombinase

function of *Saccharomyces cerevisiae* Srs2 protein. J Biol Chem *279*, 23193-23199.

Krejci, L., Van Komen, S., Li, Y., Villemain, J., Reddy, M.S., Klein, H., Ellenberger, T., and Sung, P. (2003b). DNA helicase Srs2 disrupts the Rad51 presynaptic filament. Nature *423*, 305-309.

Kreuzer, K.N., Saunders, M., Weislo, L.J., and Kreuzer, H.W. (1995). Recombination-dependent DNA replication stimulated by double-strand breaks in bacteriophage T4. J Bacteriol *177*, 6844-6853.

Krogh, B.O., and Symington, L.S. (2004). Recombination proteins in yeast. Annu Rev Genet *38*, 233-271.

Kuzminov, A. (1999). Recombinational repair of DNA damage in *Escherichia coli* and bacteriophage lambda. Microbiol Mol Biol Rev *63*, 751-813, table of contents.

Kvaratskhelia, M., and White, M.F. (2000). Two Holliday junction resolving enzymes in *Sulfolobus solfataricus*. J Mol Biol *297*, 923-932.

Lahue, R.S., Au, K.G., and Modrich, P. (1989). DNA mismatch correction in a defined system. Science *245*, 160-164.

Lamb, N.E., Sherman, S.L., and Hassold, T.J. (2005). Effect of meiotic recombination on the production of aneuploid gametes in humans. Cytogenet Genome Res *111*, 250-255.

Le, S., Moore, J.K., Haber, J.E., and Greider, C.W. (1999). RAD50 and RAD51 define two pathways that collaborate to maintain telomeres in the absence of telomerase. Genetics *152*, 143-152.

Leach, F.S., Nicolaides, N.C., Papadopoulos, N., Liu, B., Jen, J., Parsons, R., Peltomaki, P., Sistonen, P., Aaltonen, L.A., Nystrom-Lahti, M*., et al.* (1993). Mutations of a mutS homolog in hereditary nonpolyposis colorectal cancer. Cell *75*, 1215-1225.

Lee, S.D., Surtees, J.A., and Alani, E. (2007). *Saccharomyces cerevisiae* MSH2-MSH3 and MSH2-MSH6 complexes display distinct requirements for DNA binding domain I in mismatch recognition. J Mol Biol *366*, 53-66.

Li, F., Dong, J., Pan, X., Oum, J.H., Boeke, J.D., and Lee, S.E. (2008). Microarray-based genetic screen defines SAW1, a gene required for Rad1/Rad10-dependent processing of recombination intermediates. Mol Cell *30*, 325-335.

Liang, F., Han, M., Romanienko, P.J., and Jasin, M. (1998). Homology-directed repair is a major double-strand break repair pathway in mammalian cells. Proc Natl Acad Sci U S A *95*, 5172-5177.

Lieber, M.R., Ma, Y., Pannicke, U., and Schwarz, K. (2003). Mechanism and regulation of human non-homologous DNA end-joining. Nat Rev Mol Cell Biol *4*, 712-720.

Lilley, D.M., and White, M.F. (2001). The junction-resolving enzymes. Nat Rev Mol Cell Biol *2*, 433-443.

Lin, F.L., Sperle, K., and Sternberg, N. (1984). Model for homologous recombination during transfer of DNA into mouse L cells: role for DNA ends in the recombination process. Mol Cell Biol *4*, 1020-1034.

Liu, Y., Masson, J.Y., Shah, R., O'Regan, P., and West, S.C. (2004). RAD51C is required for Holliday junction processing in mammalian cells. Science *303*, 243-246.

Llorente, B., Smith, C.E., and Symington, L.S. (2008). Break-induced replication: what is it and what is it for? Cell Cycle *7*, 859-864.

Lo, Y.C., Paffett, K.S., Amit, O., Clikeman, J.A., Sterk, R., Brenneman, M.A., and Nickoloff, J.A. (2006). Sgs1 regulates gene conversion tract lengths and crossovers independently of its helicase activity. Mol Cell Biol *26*, 4086-4094.

Lockshon, D., Zweifel, S.G., Freeman-Cook, L.L., Lorimer, H.E., Brewer, B.J., and Fangman, W.L. (1995). A role for recombination junctions in the segregation of mitochondrial DNA in yeast. Cell *81*, 947-955.

Lorenz, A., West, S.C., and Whitby, M.C. (2009). The human Holliday junction resolvase GEN1 rescues the meiotic phenotype of a *Schizosaccharomyces pombe* mus81 mutant. Nucleic Acids Res.

Lorenz, A., and Whitby, M.C. (2006). Crossover promotion and prevention. Biochem Soc Trans *34*, 537-541.

Lundblad, V., and Blackburn, E.H. (1993). An alternative pathway for yeast telomere maintenance rescues est1- senescence. Cell *73*, 347-360.

Lydeard, J.R., Jain, S., Yamaguchi, M., and Haber, J.E. (2007). Break-induced replication and telomerase-independent telomere maintenance require Pol32. Nature *448*, 820-823.

Lyndaker, A.M., Goldfarb, T., and Alani, E. (2008). Mutants defective in Rad1-Rad10-Slx4 exhibit a unique pattern of viability during mating-type switching in *Saccharomyces cerevisiae*. Genetics *179*, 1807-1821.

Lynn, A., Soucek, R., and Borner, G.V. (2007). ZMM proteins during meiosis: crossover artists at work. Chromosome Res *15*, 591-605.

Machwe, A., Xiao, L., Groden, J., and Orren, D.K. (2006). The Werner and Bloom syndrome proteins catalyze regression of a model replication fork. Biochemistry *45*, 13939-13946.

Machwe, A., Xiao, L., Lloyd, R.G., Bolt, E., and Orren, D.K. (2007). Replication fork regression *in vitro* by the Werner syndrome protein (WRN): holliday junction formation, the effect of leading arm structure and a potential role for WRN exonuclease activity. Nucleic Acids Res *35*, 5729-5747.

Macris, M.A., and Sung, P. (2005). Multifaceted role of the *Saccharomyces cerevisiae* Srs2 helicase in homologous recombination regulation. Biochem Soc Trans *33*, 1447-1450.

Mahdi, A.A., Sharples, G.J., Mandal, T.N., and Lloyd, R.G. (1996). Holliday junction resolvases encoded by homologous rusA genes in *Escherichia coli* K-12 and phage 82. J Mol Biol *257*, 561-573.

Malkova, A., Ivanov, E.L., and Haber, J.E. (1996). Double-strand break repair in the absence of RAD51 in yeast: a possible role for break-induced DNA replication. Proc Natl Acad Sci U S A *93*, 7131-7136.

Malkova, A., Naylor, M.L., Yamaguchi, M., Ira, G., and Haber, J.E. (2005). RAD51-dependent break-induced replication differs in kinetics and checkpoint responses from RAD51-mediated gene conversion. Mol Cell Biol *25*, 933-944.

Mandal, T.N., Mahdi, A.A., Sharples, G.J., and Lloyd, R.G. (1993). Resolution of Holliday intermediates in recombination and DNA repair: indirect suppression of ruvA, ruvB, and ruvC mutations. J Bacteriol *175*, 4325-4334.

Mankouri, H.W., Craig, T.J., and Morgan, A. (2002). SGS1 is a multicopy suppressor of srs2: functional overlap between DNA helicases. Nucleic Acids Res *30*, 1103-1113.

Marians, K.J. (2000). Replication and recombination intersect. Curr Opin Genet Dev *10*, 151-156.

Marsischky, G.T., Lee, S., Griffith, J., and Kolodner, R.D. (1999). '*Saccharomyces cerevisiae* MSH2/6 complex interacts with Holliday junctions and facilitates their cleavage by phage resolution enzymes. J Biol Chem *274*, 7200-7206.

McCulloch, R., Coggins, L.W., Colloms, S.D., and Sherratt, D.J. (1994). Xer-mediated site-specific recombination at *cer* generates Holliday junctions in vivo. EMBO J *13*, 1844-1855.

McGill, C., Shafer, B., and Strathern, J. (1989). Coconversion of flanking sequences with homothallic switching. Cell *57*, 459-467.

McGlynn, P., and Lloyd, R.G. (2000). Modulation of RNA polymerase by (p)ppGpp reveals a RecG-dependent mechanism for replication fork progression. Cell *101*, 35-45.

McGlynn, P., and Lloyd, R.G. (2001). Rescue of stalled replication forks by RecG: simultaneous translocation on the leading and lagging strand templates supports an active DNA unwinding model of fork reversal and Holliday junction formation. Proc Natl Acad Sci U S A *98*, 8227-8234.

McGlynn, P., Lloyd, R.G., and Marians, K.J. (2001). Formation of Holliday junctions by regression of nascent DNA in intermediates containing stalled replication forks: RecG stimulates regression even when the DNA is negatively supercoiled. Proc Natl Acad Sci U S A *98*, 8235-8240.

McInerney, P., and O'Donnell, M. (2004). Functional uncoupling of twin polymerases: mechanism of polymerase dissociation from a lagging-strand block. J Biol Chem *279*, 21543-21551.

McKim, K.S., Jang, J.K., and Manheim, E.A. (2002). Meiotic recombination and chromosome segregation in *Drosophila* females. Annu Rev Genet *36*, 205-232.

Meselson, M.S., and Radding, C.M. (1975). A general model for genetic recombination. Proc Natl Acad Sci U S A *72*, 358-361.

Mets, D.G., and Meyer, B.J. (2009). Condensins regulate meiotic DNA break distribution, thus crossover frequency, by controlling chromosome structure. Cell *139*, 73-86.

Meyer-Leon, L., Huang, L.C., Umlauf, S.W., Cox, M.M., and Inman, R.B. (1988). Holliday intermediates and reaction by-products in FLP protein-promoted site-specific recombination. Mol Cell Biol *8*, 3784-3796.

Michel, B., Flores, M.J., Viguera, E., Grompone, G., Seigneur, M., and Bidnenko, V. (2001). Rescue of arrested replication forks by homologous recombination. Proc Natl Acad Sci U S A *98*, 8181-8188.

Miller, R.D., Prakash, L., and Prakash, S. (1982). Genetic control of excision of *Saccharomyces cerevisiae* interstrand DNA cross-links induced by psoralen plus near-UV light. Mol Cell Biol *2*, 939-948.

Milne, G.T., Jin, S., Shannon, K.B., and Weaver, D.T. (1996). Mutations in two Ku homologs define a DNA end-joining repair pathway in *Saccharomyces cerevisiae*. Mol Cell Biol *16*, 4189-4198.

Mimitou, E.P., and Symington, L.S. (2008). Sae2, Exo1 and Sgs1 collaborate in DNA double-strand break processing. Nature *455*, 770-774.

Mimitou, E.P., and Symington, L.S. (2009). Nucleases and helicases take center stage in homologous recombination. Trends Biochem Sci *34*, 264-272.

Miyazaki, T., Bressan, D.A., Shinohara, M., Haber, J.E., and Shinohara, A. (2004). In vivo assembly and disassembly of Rad51 and Rad52 complexes during double-strand break repair. EMBO J *23*, 939-949.

Mizuuchi, K., Kemper, B., Hays, J., and Weisberg, R.A. (1982). T4 endonuclease VII cleaves holliday structures. Cell *29*, 357-365.

Moldovan, G.L., and D'Andrea, A.D. (2009). How the fanconi anemia pathway guards the genome. Annu Rev Genet *43*, 223-249.

Morrow, D.M., Connelly, C., and Hieter, P. (1997). "Break copy" duplication: a model for chromosome fragment formation in *Saccharomyces cerevisiae.* Genetics *147*, 371-382.

Mortensen, U.H., Bendixen, C., Sunjevaric, I., and Rothstein, R. (1996). DNA strand annealing is promoted by the yeast Rad52 protein. Proc Natl Acad Sci U S A *93*, 10729-10734.

Mosedale, G., Niedzwiedz, W., Alpi, A., Perrina, F., Pereira-Leal, J.B., Johnson, M., Langevin, F., Pace, P., and Patel, K.J. (2005). The vertebrate Hef ortholog is a component of the Fanconi anemia tumor-suppressor pathway. Nat Struct Mol Biol *12*, 763-771.

Mu, D., Park, C.H., Matsunaga, T., Hsu, D.S., Reardon, J.T., and Sancar, A. (1995). Reconstitution of human DNA repair excision nuclease in a highly defined system. J Biol Chem *270*, 2415-2418.

Mullen, J.R., Kaliraman, V., Ibrahim, S.S., and Brill, S.J. (2001). Requirement for three novel protein complexes in the absence of the Sgs1 DNA helicase in *Saccharomyces cerevisiae*. Genetics *157*, 103-118.

Munoz, I.M., Hain, K., Declais, A.C., Gardiner, M., Toh, G.W., Sanchez-Pulido, L., Heuckmann, J.M., Toth, R., Macartney, T., Eppink, B., *et al.* (2009). Coordination of structure-specific nucleases by human SLX4/BTBD12 is required for DNA repair. Mol Cell *35*, 116-127.

Myung, K., Chen, C., and Kolodner, R.D. (2001). Multiple pathways cooperate in the suppression of genome instability in *Saccharomyces cerevisiae*. Nature *411*, 1073-1076.

Nasmyth, K.A. (1982). Molecular genetics of yeast mating type. Annu Rev Genet *16*, 439-500.

Nassif, N., Penney, J., Pal, S., Engels, W.R., and Gloor, G.B. (1994). Efficient copying of nonhomologous sequences from ectopic sites via P-element-induced gap repair. Mol Cell Biol *14*, 1613-1625.

Nelson, H.H., Sweetser, D.B., and Nickoloff, J.A. (1996). Effects of terminal nonhomology and homeology on double-strand-break-induced gene conversion tract directionality. Mol Cell Biol *16*, 2951-2957.

New, J.H., Sugiyama, T., Zaitseva, E., and Kowalczykowski, S.C. (1998). Rad52 protein stimulates DNA strand exchange by Rad51 and replication protein A. Nature *391*, 407-410.

Nicholson, A., Fabbri, R.M., Reeves, J.W., and Crouse, G.F. (2006). The effects of mismatch repair and RAD1 genes on interchromosomal crossover recombination in *Saccharomyces cerevisiae*. Genetics *173*, 647-659.

Nickoloff, J.A., Sweetser, D.B., Clikeman, J.A., Khalsa, G.J., and Wheeler, S.L. (1999). Multiple heterologies increase mitotic double-strand break-induced allelic gene conversion tract lengths in yeast. Genetics *153*, 665-679.

Niedernhofer, L.J., Essers, J., Weeda, G., Beverloo, B., de Wit, J., Muijtjens, M., Odijk, H., Hoeijmakers, J.H., and Kanaar, R. (2001). The structure-specific

endonuclease Ercc1-Xpf is required for targeted gene replacement in embryonic stem cells. EMBO J *20*, 6540-6549.

Nowakowski, J., Shim, P.J., Prasad, G.S., Stout, C.D., and Joyce, G.F. (1999). Crystal structure of an 82-nucleotide RNA-DNA complex formed by the 10-23 DNA enzyme. Nat Struct Biol *6*, 151-156.

Ogawa, T., Yu, X., Shinohara, A., and Egelman, E.H. (1993). Similarity of the yeast RAD51 filament to the bacterial RecA filament. Science *259*, 1896-1899.

Oh, S.D., Lao, J.P., Taylor, A.F., Smith, G.R., and Hunter, N. (2008). RecQ helicase, Sgs1, and XPF family endonuclease, Mus81-Mms4, resolve aberrant joint molecules during meiotic recombination. Mol Cell *31*, 324-336.

Oram, M., Keeley, A., and Tsaneva, I. (1998). Holliday junction resolvase in *Schizosaccharomyces pombe* has identical endonuclease activity to the CCE1 homologue YDC2. Nucleic Acids Res *26*, 594-601.

Orr-Weaver, T.L., and Szostak, J.W. (1983). Yeast recombination: the association between double-strand gap repair and crossing-over. Proc Natl Acad Sci U S A *80*, 4417-4421.

Orr-Weaver, T.L., Szostak, J.W., and Rothstein, R.J. (1981). Yeast transformation: a model system for the study of recombination. Proc Natl Acad Sci U S A *78*, 6354-6358.

Orr-Weaver, T.L., Szostak, J.W., and Rothstein, R.J. (1983). Genetic applications of yeast transformation with linear and gapped plasmids. Methods Enzymol *101*, 228-245.

Ortiz-Lombardia, M., Gonzalez, A., Eritja, R., Aymami, J., Azorin, F., and Coll, M. (1999). Crystal structure of a DNA Holliday junction. Nat Struct Biol *6*, 913-917.

Osman, F., Dixon, J., Doe, C.L., and Whitby, M.C. (2003). Generating crossovers by resolution of nicked Holliday junctions: a role for Mus81-Eme1 in meiosis. Mol Cell *12*, 761-774.

Osman, F., and Whitby, M.C. (2007). Exploring the roles of Mus81-Eme1/Mms4 at perturbed replication forks. DNA Repair (Amst) *6*, 1004-1017.

Otsuji, N., Iyehara, H., and Hideshima, Y. (1974). Isolation and characterization of an *Escherichia coli* ruv mutant which forms nonseptate filaments after low doses of ultraviolet light irradiation. J Bacteriol *117*, 337-344.

Owen, B.A., Yang, Z., Lai, M., Gajec, M., Badger, J.D., 2nd, Hayes, J.J., Edelmann, W., Kucherlapati, R., Wilson, T.M., and McMurray, C.T. (2005). (CAG)(n)-hairpin DNA binds to Msh2-Msh3 and changes properties of mismatch recognition. Nat Struct Mol Biol *12*, 663-670.

Pages, V., and Fuchs, R.P. (2003). Uncoupling of leading- and lagging-strand DNA replication during lesion bypass in vivo. Science *300*, 1300-1303.

Panyutin, I.G., Biswas, I., and Hsieh, P. (1995). A pivotal role for the structure of the Holliday junction in DNA branch migration. EMBO J *14*, 1819-1826.

Panyutin, I.G., and Hsieh, P. (1993). Formation of a single base mismatch impedes spontaneous DNA branch migration. J Mol Biol *230*, 413-424.

Panyutin, I.G., and Hsieh, P. (1994). The kinetics of spontaneous DNA branch migration. Proc Natl Acad Sci U S A *91*, 2021-2025.

Paques, F., and Haber, J.E. (1999). Multiple pathways of recombination induced by double-strand breaks in *Saccharomyces cerevisiae*. Microbiol Mol Biol Rev *63*, 349-404.

Paques, F., Leung, W.Y., and Haber, J.E. (1998). Expansions and contractions in a tandem repeat induced by double-strand break repair. Mol Cell Biol *18*, 2045-2054.

Parsons, C.A., Stasiak, A., Bennett, R.J., and West, S.C. (1995). Structure of a multisubunit complex that promotes DNA branch migration. Nature *374*, 375-378.

Parsons, C.A., Tsaneva, I., Lloyd, R.G., and West, S.C. (1992). Interaction of *Escherichia coli* RuvA and RuvB proteins with synthetic Holliday junctions. Proc Natl Acad Sci U S A *89*, 5452-5456.

Parsons, C.A., and West, S.C. (1993). Formation of a RuvAB-Holliday junction complex *in vitro*. J Mol Biol *232*, 397-405.

Peng, M., Litman, R., Xie, J., Sharma, S., Brosh, R.M., Jr., and Cantor, S.B. (2007). The FANCJ/MutLalpha interaction is required for correction of the cross-link response in FA-J cells. EMBO J *26*, 3238-3249.

Perry, J., Kleckner, N., and Borner, G.V. (2005). Bioinformatic analyses implicate the collaborating meiotic crossover/chiasma proteins Zip2, Zip3, and Spo22/Zip4 in ubiquitin labeling. Proc Natl Acad Sci U S A *102*, 17594-17599.

Petukhova, G., Stratton, S., and Sung, P. (1998). Catalysis of homologous DNA pairing by yeast Rad51 and Rad54 proteins. Nature *393*, 91-94.

Pfander, B., Moldovan, G.L., Sacher, M., Hoege, C., and Jentsch, S. (2005). SUMO-modified PCNA recruits Srs2 to prevent recombination during S phase. Nature *436*, 428-433.

Pommier, Y. (2006). Topoisomerase I inhibitors: camptothecins and beyond. Nat Rev Cancer *6*, 789-802.

Porter, S.E., White, M.A., and Petes, T.D. (1993). Genetic evidence that the meiotic recombination hotspot at the HIS4 locus of *Saccharomyces cerevisiae* does not represent a site for a symmetrically processed double-strand break. Genetics *134*, 5-19.

Potter, H., and Dressler, D. (1979). DNA recombination: *in vivo* and *in vitro* studies. Cold Spring Harb Symp Quant Biol. 43 Pt2: 969-85.

Prakash, L., and Prakash, S. (1977). Isolation and characterization of MMS-sensitive mutants of *Saccharomyces cerevisiae*. Genetics *86*, 33-55.

Prakash, R., Krejci, L., Van Komen, S., Anke Schurer, K., Kramer, W., and Sung, P. (2005). *Saccharomyces cerevisiae* MPH1 gene, required for homologous recombination-mediated mutation avoidance, encodes a 3' to 5' DNA helicase. J Biol Chem *280*, 7854-7860.

Prakash, R., Satory, D., Dray, E., Papusha, A., Scheller, J., Kramer, W., Krejci, L., Klein, H., Haber, J.E., Sung, P.*, et al.* (2009). Yeast Mph1 helicase dissociates Rad51-made D-loops: implications for crossover control in mitotic recombination. Genes Dev *23*, 67-79.

Putnam, C.D., Hayes, T.K., and Kolodner, R.D. (2009). Specific pathways prevent duplication-mediated genome rearrangements. Nature *460*, 984-989.

Ralf, C., Hickson, I.D., and Wu, L. (2006). The Bloom's syndrome helicase can promote the regression of a model replication fork. J Biol Chem *281*, 22839-22846.

Raynard, S., Bussen, W., and Sung, P. (2006). A double Holliday junction dissolvasome comprising BLM, topoisomerase IIIalpha, and BLAP75. J Biol Chem *281*, 13861-13864.

Rich, T., Allen, R.L., and Wyllie, A.H. (2000). Defying death after DNA damage. Nature *407*, 777-783.

Rizki, A., and Lundblad, V. (2001). Defects in mismatch repair promote telomerase-independent proliferation. Nature *411*, 713-716.

Roberts, T.M., Kobor, M.S., Bastin-Shanower, S.A., Ii, M., Horte, S.A., Gin, J.W., Emili, A., Rine, J., Brill, S.J., and Brown, G.W. (2006). Slx4 regulates DNA damage checkpoint-dependent phosphorylation of the BRCT domain protein Rtt107/Esc4. Mol Biol Cell *17*, 539-548.

Rockmill, B., Voelkel-Meiman, K., and Roeder, G.S. (2006). Centromere-proximal crossovers are associated with precocious separation of sister chromatids during meiosis in *Saccharomyces cerevisiae*. Genetics *174*, 1745-1754.

Rong, L., and Klein, H.L. (1993). Purification and characterization of the SRS2 DNA helicase of the yeast *Saccharomyces cerevisiae*. J Biol Chem *268*, 1252-1259.

Rosado, I.V., Niedzwiedz, W., Alpi, A.F., and Patel, K.J. (2009). The Walker B motif in avian FANCM is required to limit sister chromatid exchanges but is dispensable for DNA crosslink repair. Nucleic Acids Res *37*, 4360-4370.

Ross-Macdonald, P., and Roeder, G.S. (1994). Mutation of a meiosis-specific MutS homolog decreases crossing over but not mismatch correction. Cell *79*, 1069-1080.

Rothstein, R., Michel, B., and Gangloff, S. (2000). Replication fork pausing and recombination or "gimme a break". Genes Dev *14*, 1-10.

Rouse, J. (2004). Esc4p, a new target of Mec1p (ATR), promotes resumption of DNA synthesis after DNA damage. EMBO J *23*, 1188-1197.

Rouse, J. (2009). Control of genome stability by SLX protein complexes. Biochem Soc Trans *37*, 495-510.

Saparbaev, M., Prakash, L., and Prakash, S. (1996). Requirement of mismatch repair genes MSH2 and MSH3 in the RAD1-RAD10 pathway of mitotic recombination in *Saccharomyces cerevisiae*. Genetics *142*, 727-736.

Scheller, J., Schurer, A., Rudolph, C., Hettwer, S., and Kramer, W. (2000). MPH1, a yeast gene encoding a DEAH protein, plays a role in protection of the genome from spontaneous and chemically induced damage. Genetics *155*, 1069-1081.

Schiestl, R.H., and Prakash, S. (1988). RAD1, an excision repair gene of *Saccharomyces cerevisiae*, is also involved in recombination. Mol Cell Biol *8*, 3619-3626.

Schiestl, R.H., and Prakash, S. (1990). RAD10, an excision repair gene of *Saccharomyces cerevisiae*, is involved in the RAD1 pathway of mitotic recombination. Mol Cell Biol *10*, 2485-2491.

Schofield, M.J., and Hsieh, P. (2003). DNA mismatch repair: molecular mechanisms and biological function. Annu Rev Microbiol *57*, 579-608.

Schofield, M.J., Lilley, D.M., and White, M.F. (1998). Dissection of the sequence specificity of the Holliday junction endonuclease CCE1. Biochemistry *37*, 7733-7740.

Schurer, K.A., Rudolph, C., Ulrich, H.D., and Kramer, W. (2004). Yeast MPH1 gene functions in an error-free DNA damage bypass pathway that requires genes from Homologous recombination, but not from postreplicative repair. Genetics *166*, 1673-1686.

Selva, E.M., New, L., Crouse, G.F., and Lahue, R.S. (1995). Mismatch correction acts as a barrier to homeologous recombination in *Saccharomyces cerevisiae*. Genetics *139*, 1175-1188.

Seong, C., Colavito, S., Kwon, Y., Sung, P., and Krejci, L. (2009). Regulation of Rad51 recombinase presynaptic filament assembly via interactions with the Rad52 mediator and the Srs2 anti-recombinase. J Biol Chem *284*, 24363-24371.

Shah, R., Bennett, R.J., and West, S.C. (1994). Activation of RuvC Holliday junction resolvase *in vitro*. Nucleic Acids Res *22*, 2490-2497.

Sharples, G.J. (2001). The X philes: structure-specific endonucleases that resolve Holliday junctions. Mol Microbiol *39*, 823-834.

Sharples, G.J., Benson, F.E., Illing, G.T., and Lloyd, R.G. (1990). Molecular and functional analysis of the ruv region of *Escherichia coli* K-12 reveals three genes involved in DNA repair and recombination. Mol Gen Genet *221*, 219-226.

Sharples, G.J., Curtis, F.A., McGlynn, P., and Bolt, E.L. (2004). Holliday junction binding and resolution by the Rap structure-specific endonuclease of phage lambda. J Mol Biol *340*, 739-751.

Sharples, G.J., Ingleston, S.M., and Lloyd, R.G. (1999). Holliday junction processing in bacteria: insights from the evolutionary conservation of RuvABC, RecG, and RusA. J Bacteriol *181*, 5543-5550.

Shinohara, A., Ogawa, H., and Ogawa, T. (1992). Rad51 protein involved in repair and recombination in *S. cerevisiae* is a RecA-like protein. Cell *69*, 457-470.

Silberman, R., and Kupiec, M. (1994). Plasmid-mediated induction of recombination in yeast. Genetics *137*, 41-48.

Smith, G.R., Boddy, M.N., Shanahan, P., and Russell, P. (2003). Fission yeast Mus81.Eme1 Holliday junction resolvase is required for meiotic crossing over but not for gene conversion. Genetics *165*, 2289-2293.

Snowden, T., Acharya, S., Butz, C., Berardini, M., and Fishel, R. (2004). hMSH4-hMSH5 recognizes Holliday Junctions and forms a meiosis-specific sliding clamp that embraces homologous chromosomes. Mol Cell *15*, 437-451.

Song, B., and Sung, P. (2000). Functional interactions among yeast Rad51 recombinase, Rad52 mediator, and replication protein A in DNA strand exchange. J Biol Chem *275*, 15895-15904.

Soulas-Sprauel, P., Rivera-Munoz, P., Malivert, L., Le Guyader, G., Abramowski, V., Revy, P., and de Villartay, J.P. (2007). V(D)J and immunoglobulin class switch recombinations: a paradigm to study the regulation of DNA end-joining. Oncogene *26*, 7780-7791.

Stark, W.M., Boocock, M.R., and Sherratt, D.J. (1992). Catalysis by site-specific recombinases. Trends Genet *8*, 432-439.

Stasiak, A., Tsaneva, I.R., West, S.C., Benson, C.J., Yu, X., and Egelman, E.H. (1994). The *Escherichia coli* RuvB branch migration protein forms double hexameric rings around DNA. Proc Natl Acad Sci U S A *91*, 7618-7622.

Stelter, P., and Ulrich, H.D. (2003). Control of spontaneous and damage-induced mutagenesis by SUMO and ubiquitin conjugation. Nature *425*, 188-191.

Stirling, C.J., Colloms, S.D., Collins, J.F., Szatmari, G., and Sherratt, D.J. (1989). xerB, an *Escherichia coli* gene required for plasmid ColE1 site-specific recombination, is identical to pepA, encoding aminopeptidase A, a protein with substantial similarity to bovine lens leucine aminopeptidase. EMBO J *8*, 1623-1627.

Stirling, C.J., Stewart, G., and Sherratt, D.J. (1988a). Multicopy plasmid stability in *Escherichia coli* requires host-encoded functions that lead to plasmid site-specific recombination. Mol Gen Genet *214*, 80-84.

Stirling, C.J., Szatmari, G., Stewart, G., Smith, M.C., and Sherratt, D.J. (1988b). The arginine repressor is essential for plasmid-stabilizing site-specific recombination at the ColE1 cer locus. EMBO J *7*, 4389-4395.

Storici, F., and Resnick, M.A. (2006). The *delitto perfetto* approach to *in vivo* site-directed mutagenesis and chromosome rearrangements with synthetic oligonucleotides in yeast. Methods Enzymol *409*, 329-345.

Sugawara, N., Goldfarb, T., Studamire, B., Alani, E., and Haber, J.E. (2004). Heteroduplex rejection during single-strand annealing requires Sgs1 helicase and mismatch repair proteins Msh2 and Msh6 but not Pms1. Proc Natl Acad Sci U S A *101*, 9315-9320.

Sugawara, N., and Haber, J.E. (1992). Characterization of double-strand break-induced recombination: homology requirements and single-stranded DNA formation. Mol Cell Biol *12*, 563-575.

Sugawara, N., Ivanov, E.L., Fishman-Lobell, J., Ray, B.L., Wu, X., and Haber, J.E. (1995). DNA structure-dependent requirements for yeast RAD genes in gene conversion. Nature *373*, 84-86.

Sugawara, N., Paques, F., Colaiacovo, M., and Haber, J.E. (1997). Role of *Saccharomyces cerevisiae* Msh2 and Msh3 repair proteins in double-strand break-induced recombination. Proc Natl Acad Sci U S A *94*, 9214-9219.

Sugawara, N., Wang, X., and Haber, J.E. (2003). *In vivo* roles of Rad52, Rad54, and Rad55 proteins in Rad51-mediated recombination. Mol Cell *12*, 209-219.

Sugiyama, T., Kantake, N., Wu, Y., and Kowalczykowski, S.C. (2006). Rad52-mediated DNA annealing after Rad51-mediated DNA strand exchange promotes second ssDNA capture. EMBO J *25*, 5539-5548.

Sugiyama, T., and Kowalczykowski, S.C. (2002). Rad52 protein associates with replication protein A (RPA)-single-stranded DNA to accelerate Rad51-mediated displacement of RPA and presynaptic complex formation. J Biol Chem *277*, 31663-31672.

Summers, D., Yaish, S., Archer, J., and Sherratt, D. (1985). Multimer resolution systems of ColE1 and ColK: localisation of the crossover site. Mol Gen Genet *201*, 334-338.

Summers, D.K., and Sherratt, D.J. (1984). Multimerization of high copy number plasmids causes instability: CoIE1 encodes a determinant essential for plasmid monomerization and stability. Cell *36*, 1097-1103.

Sun, H., Treco, D., and Szostak, J.W. (1991). Extensive 3'-overhanging, single-stranded DNA associated with the meiosis-specific double-strand breaks at the ARG4 recombination initiation site. Cell *64*, 1155-1161.

Sun, W., Nandi, S., Osman, F., Ahn, J.S., Jakovleska, J., Lorenz, A., and Whitby, M.C. (2008). The FANCM ortholog Fml1 promotes recombination at stalled replication forks and limits crossing over during DNA double-strand break repair. Mol Cell *32*, 118-128.

Sung, P. (1997a). Function of yeast Rad52 protein as a mediator between replication protein A and the Rad51 recombinase. J Biol Chem *272*, 28194-28197.

Sung, P. (1997b). Yeast Rad55 and Rad57 proteins form a heterodimer that functions with replication protein A to promote DNA strand exchange by Rad51 recombinase. Genes Dev *11*, 1111-1121.

Sung, P., Krejci, L., Van Komen, S., and Sehorn, M.G. (2003). Rad51 recombinase and recombination mediators. J Biol Chem *278*, 42729-42732.

Sung, P., and Robberson, D.L. (1995). DNA strand exchange mediated by a RAD51-ssDNA nucleoprotein filament with polarity opposite to that of RecA. Cell *82*, 453-461.

Sung, P., and Stratton, S.A. (1996). Yeast Rad51 recombinase mediates polar DNA strand exchange in the absence of ATP hydrolysis. J Biol Chem *271*, 27983-27986.

Surtees, J.A., Argueso, J.L., and Alani, E. (2004). Mismatch repair proteins: key regulators of genetic recombination. Cytogenet Genome Res *107*, 146-159.

Svendsen, J.M., Smogorzewska, A., Sowa, M.E., O'Connell, B.C., Gygi, S.P., Elledge, S.J., and Harper, J.W. (2009). Mammalian BTBD12/SLX4 assembles a Holliday junction resolvase and is required for DNA repair. Cell *138*, 63-77.

Sweetser, D.B., Hough, H., Whelden, J.F., Arbuckle, M., and Nickoloff, J.A. (1994). Fine-resolution mapping of spontaneous and double-strand break-induced gene conversion tracts in *Saccharomyces cerevisiae* reveals reversible mitotic conversion polarity. Mol Cell Biol *14*, 3863-3875.

Symington, L.S. (2002). Role of RAD52 epistasis group genes in homologous recombination and double-strand break repair. Microbiol Mol Biol Rev *66*, 630-670, table of contents.

Symington, L.S., Kang, L.E., and Moreau, S. (2000). Alteration of gene conversion tract length and associated crossing over during plasmid gap repair in nuclease-deficient strains of *Saccharomyces cerevisiae*. Nucleic Acids Res *28*, 4649-4656.

Szostak, J.W., Orr-Weaver, T.L., Rothstein, R.J., and Stahl, F.W. (1983). The double-strand-break repair model for recombination. Cell *33*, 25-35.

Taylor, E.R., and McGowan, C.H. (2008). Cleavage mechanism of human Mus81-Eme1 acting on Holliday-junction structures. Proc Natl Acad Sci U S A *105*, 3757-3762.

Teng, S.C., Chang, J., McCowan, B., and Zakian, V.A. (2000). Telomerase-independent lengthening of yeast telomeres occurs by an abrupt Rad50p-dependent, Rif-inhibited recombinational process. Mol Cell *6*, 947-952.

Thaler, D.S., and Stahl, F.W. (1988). DNA double-chain breaks in recombination of phage lambda and of yeast. Annu Rev Genet *22*, 169-197.

Thompson, L.H. (2005). Unraveling the Fanconi anemia-DNA repair connection. Nat Genet *37*, 921-922.

Tong, A.H., and Boone, C. (2006). Synthetic genetic array analysis in *Saccharomyces cerevisiae*. Methods Mol Biol *313*, 171-192.

Umar, A., Risinger, J.I., Glaab, W.E., Tindall, K.R., Barrett, J.C., and Kunkel, T.A. (1998). Functional overlap in mismatch repair by human MSH3 and MSH6. Genetics *148*, 1637-1646.

van de Vrugt, H.J., Eaton, L., Hanlon Newell, A., Al-Dhalimy, M., Liskay, R.M., Olson, S.B., and Grompe, M. (2009). Embryonic lethality after combined inactivation of Fancd2 and Mlh1 in mice. Cancer Res *69*, 9431-9438.

van Gool, A.J., Hajibagheri, N.M., Stasiak, A., and West, S.C. (1999). Assembly of the *Escherichia coli* RuvABC resolvasome directs the orientation of holliday junction resolution. Genes Dev *13*, 1861-1870.

Van Komen, S., Reddy, M.S., Krejci, L., Klein, H., and Sung, P. (2003). ATPase and DNA helicase activities of the *Saccharomyces cerevisiae* anti-recombinase Srs2. J Biol Chem *278*, 44331-44337.

Vance, J.R., and Wilson, T.E. (2002). Yeast Tdp1 and Rad1-Rad10 function as redundant pathways for repairing Top1 replicative damage. Proc Natl Acad Sci U S A *99*, 13669-13674.

VanHulle, K., Lemoine, F.J., Narayanan, V., Downing, B., Hull, K., McCullough, C., Bellinger, M., Lobachev, K., Petes, T.D., and Malkova, A. (2007). Inverted DNA repeats channel repair of distant double-strand breaks into chromatid fusions and chromosomal rearrangements. Mol Cell Biol *27*, 2601-2614.

Veaute, X., Jeusset, J., Soustelle, C., Kowalczykowski, S.C., Le Cam, E., and Fabre, F. (2003). The Srs2 helicase prevents recombination by disrupting Rad51 nucleoprotein filaments. Nature *423*, 309-312.

Wang, T.F., Kleckner, N., and Hunter, N. (1999). Functional specificity of MutL homologs in yeast: evidence for three Mlh1-based heterocomplexes with distinct roles during meiosis in recombination and mismatch correction. Proc Natl Acad Sci U S A *96*, 13914-13919.

Wang, T.F., and Kung, W.M. (2002). Supercomplex formation between Mlh1-Mlh3 and Sgs1-Top3 heterocomplexes in meiotic yeast cells. Biochem Biophys Res Commun *296*, 949-953.

Wang, X., and Baumann, P. (2008). Chromosome fusions following telomere loss are mediated by single-strand annealing. Mol Cell *31*, 463-473.

Wang, X., and Haber, J.E. (2004). Role of *Saccharomyces* single-stranded DNA-binding protein RPA in the strand invasion step of double-strand break repair. PLoS Biol *2*, E21.

Wang, X., Ira, G., Tercero, J.A., Holmes, A.M., Diffley, J.F., and Haber, J.E. (2004). Role of DNA replication proteins in double-strand break-induced recombination in *Saccharomyces cerevisiae*. Mol Cell Biol *24*, 6891-6899.

Warren, J.J., Pohlhaus, T.J., Changela, A., Iyer, R.R., Modrich, P.L., and Beese, L.S. (2007). Structure of the human MutSalpha DNA lesion recognition complex. Mol Cell *26*, 579-592.

Welz-Voegele, C., and Jinks-Robertson, S. (2008). Sequence divergence impedes crossover more than noncrossover events during mitotic gap repair in yeast. Genetics *179*, 1251-1262.

West, S.C. (1995). Holliday junctions cleaved by Rad1? Nature *373*, 27-28.

West, S.C. (1997). Processing of recombination intermediates by the RuvABC proteins. Annu Rev Genet *31*, 213-244.

Whitby, M.C. The FANCM family of DNA helicases/translocases. DNA Repair (Amst) *9*, 224-236.

Whitby, M.C., and Dixon, J. (1997). A new Holliday junction resolving enzyme from *Schizosaccharomyces pombe* that is homologous to CCE1 from *Saccharomyces cerevisiae*. J Mol Biol *272*, 509-522.

Whitby, M.C., Osman, F., and Dixon, J. (2003). Cleavage of model replication forks by fission yeast Mus81-Eme1 and budding yeast Mus81-Mms4. J Biol Chem *278*, 6928-6935.

White, C.I., and Haber, J.E. (1990). Intermediates of recombination during mating type switching in *Saccharomyces cerevisiae*. EMBO J *9*, 663-673.

White, J.H., Lusnak, K., and Fogel, S. (1985). Mismatch-specific post-meiotic segregation frequency in yeast suggests a heteroduplex recombination intermediate. Nature *315*, 350-352.

Wilcox, D.R., and Prakash, L. (1981). Incision and postincision steps of pyrimidine dimer removal in excision-defective mutants of *Saccharomyces cerevisiae*. J Bacteriol *148*, 618-623.

Wolner, B., van Komen, S., Sung, P., and Peterson, C.L. (2003). Recruitment of the recombinational repair machinery to a DNA double-strand break in yeast. Mol Cell *12*, 221-232.

Wood, L.D., Parsons, D.W., Jones, S., Lin, J., Sjoblom, T., Leary, R.J., Shen, D., Boca, S.M., Barber, T., Ptak, J.*, et al.* (2007). The genomic landscapes of human breast and colorectal cancers. Science *318*, 1108-1113.

Worth, L., Jr., Clark, S., Radman, M., and Modrich, P. (1994). Mismatch repair proteins MutS and MutL inhibit RecA-catalyzed strand transfer between diverged DNAs. Proc Natl Acad Sci U S A *91*, 3238-3241.

Wu, L., Bachrati, C.Z., Ou, J., Xu, C., Yin, J., Chang, M., Wang, W., Li, L., Brown, G.W., and Hickson, I.D. (2006). BLAP75/RMI1 promotes the BLM-dependent dissolution of homologous recombination intermediates. Proc Natl Acad Sci U S A *103*, 4068-4073.

Wu, L., Davies, S.L., and Hickson, I.D. (2000). Roles of RecQ family helicases in the maintenance of genome stability. Cold Spring Harb Symp Quant Biol *65*, 573-581.

Wu, L., and Hickson, I.D. (2003). The Bloom's syndrome helicase suppresses crossing over during homologous recombination. Nature *426*, 870-874.

Xiao, W. (2006). Yeast protocols, 2nd edn (Totowa, N.J., Humana Press).

Zerbib, D., Colloms, S.D., Sherratt, D.J., and West, S.C. (1997). Effect of DNA topology on Holliday junction resolution by *Escherichia coli* RuvC and bacteriophage T7 endonuclease I. J Mol Biol *270*, 663-673.

Zhang, Y., Yuan, F., Presnell, S.R., Tian, K., Gao, Y., Tomkinson, A.E., Gu, L., and Li, G.M. (2005). Reconstitution of 5'-directed human mismatch repair in a purified system. Cell *122*, 693-705.

Zhu, Z., Chung, W.H., Shim, E.Y., Lee, S.E., and Ira, G. (2008). Sgs1 helicase and two nucleases Dna2 and Exo1 resect DNA double-strand break ends. Cell *134*, 981-994.

Chapter Eight

8. Appendix

A1:
GAGAGAGACGTCGATCGCCAACAAATACTACC

A2:
GAGAGAGACGTCGATCGCTTGCCTGTAACTTA

App. Figure 1. Primers for the cloning of pADE2(400/400) [Chapter 2.2.1.4]

Oligonucleotide	**Sequence**
primer A	TTGGGTACCGAGGAACGGCTGATACA
primer B	ACCTCGAGCGCATTCACCGCAGCAAA
primer C	CCAGCAGCCTGGATTTTTTCGGGGTAAGGTCTTTGCTGCGG TGAATGCGCTCGAGGTCGACCGTTTTAAGAGCT
primer D	TCTGCTCGCTCAAGTTGGATCCGCCGGCTGAGGGCTAGCTC AGGCGTACGGCTTAGGTCACACCGCATATGATCCGTCGAG TTCAAGAG
primer E	CCGGCGGATCCAACTTGAGCGAGCAGACAGAACGCTTGAG CCAGTTATACAGCGAGAACTGGAGATAAGAGAGGAACGG CTGATACAG
primer F	CGGGGTAAGGTCTTTGCTGCGGTGAATGCGCCAGCTTTTGT TCCCTTTAGTGAGGGCTGCATTAATGAATCGG

App. Figure 2. Primers for the cloning of JM [Chapter 2.2.1.6]

IROs for delitto perfetto

Oligo EE forward	TTATTAGACTTGATGAACATTTCATATGTAATCGCATGTGGGGcGGGAGc AGCCCAGTGTGTTTGGCTGCAAGTTTCTGGGGCTGTAGATTTC
Oligo EE reverse	GAAATCTACAGCCCCAGAAACTTGCAGCCAAACACACTGGGCTgCTCCC gCCCCACATGCGATTACATATGAAATGTTCATCAAGTCTAATAA
Oligo DD forward	TTGCAGTGTGTGCTCAACACCATAGTTGAAAGAAAAAGGCTAGcaGcaT TAGCTTTAAGTATAAGGGATAACAGGTTTATGGAGCAAAAA
Oligo DD reverse	TTTTTGCTCCATAAACCTGTTATCCCTTATACTTAAAGCTAAtgCtgCTAGC CTTTTTCTTTCAACTATGGTGTTGAGCACACACTGCAA

App. Figure 3. IROs used for the generation of *yen1*^{EE} and *mus81*^{DD} via *delitto perfetto* strategy [Chapter 2.2.2.2]

pADE2(400/400):

*cccgggggatcc*ATGTGCTAACGATTGAGATTGAGCATGTTGATGTTCCTACACTAAAGA
ATCTTCAAGTAAAACATCCCAAATTAAAAATTTACCCTTCTCCAGAAACAATCAGATT
GATACAAGACAAATATATTCAAAAAGAGCATTTAATCAAAAATGGTATAGCAGTTAC
CCAAAGTGTTCCTGTGGAACAAGCCAGTGAGACGTCCCTATTGAATGTTGGAAGAG
ATTTGGGTTTTCCATTCGTCTTGAAGTCGAGGACTTTGGCATACGATGGAAGAGGT
AACTTCGTTGTAAAGAATAAGGAAATGATTCCGGAAGCTTTGGAAGTACTGAAGGAT
CGTCCTTTGTACGCCGAAAAATGGGCACCATTTACTAAAGAATTAGCAGTCATGATT
GTGAGATCT**GTTAAC**GGTTTAGTGTTTTCTTACCCAATTGTAGAGACTATCCACAAG
GACAATATTTGTGACTTATGTTATGCGCCTGCTAGAGTTCCGGACTCCGTTCAACTT
AAGGCGAAGTTGTTGGCAGAAAATGCAATCAAATCTTTTCCCGGTTGTGGTATATTT
GGTGTGGAAATGTTCTATTTAGAAACAGGGGAATTGCTTATTAACGAAATTGCCCCA
AGGCCTCACAACTCTGGACATTATACCATTGATGCTTGCGTCACTTCTCAATTTGAA
GCTCATTTGAGATCAATATTGGATTTGCCAATGCCAAAGAATTTCACATCTTTCTCCA
CCATTACAACGAACGCCATTATGCTAAATGTTCTTGGAGACAAACATACAAAAGATA
AAGAGCTAGAA*ggatccactagt*

pADE2(1bp/mis):

*cccgggggatcc*ATGTGCTAACGATTGAGATTGAGCATGTTGATGTTCCTACACTAAAGA
ATCTTCAAGTAAAACAGCCCAAATTAAAAATTTACCCTTCTCCAGAAACAATCAGATT
GATACAAGACAAATATATTCAAAAAGAGCATTTGATCAAAAATGGTATAGCAGTTAC
CCAAAGTGTTCCTGTGGAACAAGCCAGTGAGGCGTCCCTATTGAATGTTGGAAGAG
ATTTGGGTTTTCCATTCGTCTTGAAGTCGAGGACTTTGGCATACGACGGAAGAGGT
AACTTCGTTGTAAAGAATAAGGAAATGATTCCGGAGGCTTTGGAAGTACTGAAGGAT
CGTCCTTTGTACGCCGAAAAATGGGCACCATTTACTAAAGAATTAGCAGTCATGATT
GTGAGATCT**GTTAAC**GGTTTAGTGTTTTCTTACCCAATTGTAGAGACTATCCACAAG
GACAATGTTTGTGACTTATGTTATGCGCCTGCTAGAGTTCCGGACTCCGTTCAACTT
GAGGCGAAGTTGTTGGCAGAAAATGCAATCAAATCTTTTCCCGGTTGTGTATATTTT
GGTGTGGAAATGTTCTATTTAGAAACAGGGGAATTGCTTATTAACGAAATTGCCCCA
GGGCCTCACAACTCTGGACATTATACCATTGATGCTTGCGTCACTTCTCAATTTGAA
GCTCATTTGAGATCAGTATTGGATTTGCCAATGCCAAAGAATTTCACATCTTTCTCCA
CCATTACAACGAACGCCATTATGCTAAATGTTCTTGGAGACAAACATACAAAAGATA
AAGAGCTAGAA*ggatccactagt*

App. Figure 4. Sequence (upper case) in plasmids pADE2(400/400) and pADE2(1bp/mis) used to target the endogenous *ADE2* locus. Plasmid sequences are in lower case and the BamHI, XmaI and SpeI sites used for cloning the *ADE2*-derived targeting sequences are italicized. Unique HpaI site used to linearise the repair substrates is in red and bold. Nucleotide differences between pADE2(1bp/mis) and the endogenous *ADE2* ORF are boxed in black. [Chapter 3]

N1:
TCACTATAGGGCGAATTGGGTA

N2:
TGTGTGGAATTGTGAGCGGA

C1:
ACGTATGATTGTTGAGGCAGCAAAC

C2:
CAGGCTTTACACTTTATGCTTCCGG

C3:
TCACTATAGGGCGAATTGGGTA

C4:
TTCACATTCCGCCATACTGG

App. Figure 5. Primers for sequence analysis of NCO and CO repair products in Chapter 3.2.7.

Primer A: AAGGGCGATCGGTGCG
Primer B: GGAAGGGCGATCGGTGC
Primer C: CGCAAACCGCCTCTCC
Primer D: AATGCAGCTGGCACGA

App. Figure 6. Primers for sequence analysis of X-JM resolution products in Chapter 4 (refer to Figure 4.13A).

C1	CGGTGCGGGCCTCTTCGCTA
C2	AGAGTGTACTAGAGGAGGCCAAGA
C3	AGCGAGCAGACAGAACG
C4	CTTTGAGTGAGCTGATACCGC

App. Figure 7. Primers for sequence analysis of JM-HJ resolution products in Chapter 5 (refer to Figure 5.9).

Publications

Tay, Y.D., Sidebotham, J.M., and Wu, L. Mph1 requires mismatch repair-independent and -dependent functions of MutSα to regulate crossover formation during homologous recombination repair. *Nucleic Acids Res 38*, 1889-1901.

Tay, Y.D., and Wu, L. Overlapping roles for Yen1 and Mus81 in cellular Holliday junction processing. *J Biol Chem 285*, 11427-11432.